

UNIVERSITAT POLITÈCNICA DE VALÈNCIA

**INSTITUTO INTERUNIVERSITARIO DE RECONOCIMIENTO
MOLECULAR Y DESARROLLO TECNOLÓGICO**



**Molecular probes and ruthenium (II) and
osmium(II) complexes for the chromo-
fluorogenic sensing of charged species and
carbon monoxide**

PhD. THESIS

Submitted by

Cristina Marín Hernández

PhD. Supervisors:

**Prof. Ramón Martínez Máñez
Dr. Félix Sancenón Galarza**

Valencia, October 2017



UNIVERSITAT
POLITÈCNICA
DE VALÈNCIA

RAMÓN MARTÍNEZ MÁÑEZ, PhD in Chemistry and Professor at the *Universitat Politècnica de València*, and FÉLIX SANCENÓN GALARZA, PhD in Chemistry and Lecturer at the *Universitat Politècnica de València*.

CERTIFY:

That the work ***“Molecular probes and ruthenium(II) and osmium(II) complexes for the chromo-fluorogenic sensing of charged species and carbon monoxide”*** has been developed by Cristina Marín Hernández under their supervision in the Instituto Interuniversitario de Reconocimiento Molecular y Desarrollo Tecnológico (IDM) of the *Universitat Politècnica de València*, as a Thesis Project in order to obtain the degree of PhD in Chemistry at the *Universitat Politècnica de València*.

Valencia, December 15th 2017.

Prof. Ramón Martínez Máñez

Dr. Félix Sancenón Galarza

*A mis padres,
por todo su cariño y apoyo*

“Lo único imposible es aquello que no intentas”

Acknowledgements

Agradecimientos

Cada vez que entro, se despierta una parte de mí que me vuelve a traer las sensaciones y los momentos que estuvieron allí. Durante el tiempo en el doctorado, no pensé que cada rincón se estaba llenando de detalles que se quedarían formando parte de mí, pero cuando ahora vuelvo a pasar por la puerta que entraba cada día a la universidad, a verme envuelta del césped por el que pasaba hasta llegar al laboratorio, a subir esas escaleras y a ver el tráfico de gente hacia el fluorímetro, o al rayos X... Me transporto allí. Yo seguía un hilo que simplemente parecía que me llevaba a poder escribir una tesis, pero en realidad, la parte más mágica que bordó, fue el dibujo de las sonrisas compartidas con quienes me fueron acompañando...

En primer lugar, me gustaría agradecer a mis directores de tesis todos sus consejos, ayuda y orientación; sin ellos, no habría podido hacer esta tesis. Gracias Ramón, por darme la oportunidad de hacer esta tesis en tu grupo y dejarme formar parte del mundo de la investigación. Y gracias a ti también Félix, por tu gran ayuda y apoyo en todo momento, por la dedicación que pones siempre y por preocuparte por mi trabajo desde que empecé.

In my PhD stay abroad, I discovered a charming city and different ways of researching. Thanks James for the opportunity of joining your group at the Imperial College of London and letting me experience that.

Acknowledgements

Gràcies també als que el món de la investigació ens ha fet coincidir i ens ha portat a apreciar els moments compartits, als que em van acollir i ajudar quan estava començant, o als que heu fet que el laboratori no sols fóra un espai on treballàvem. Heu fet que m'haja portat eixe record bonic dels moments de treball en aquesta tesi. M'ha encantat compartir laboratori, dinars, cafès, tertúlies, sopars i estones de desestrès amb vosaltres.

Por último, gracias a los que ya formabais parte de mi vida antes y habéis continuado durante esta etapa; también a los que he conocido y sé que seguiréis estando. Y en especial, a quienes me hacéis llegar día a día que estáis ahí siempre. Gracias porque me hacéis feliz y sois quienes me dais las ganas que tengo de hacer todo lo que hago. Es una suerte y me encanta teneros cerca de mí. Os quiero.

Resum

La present tesi doctoral titulada “Sondas moleculars i complexos de ruteni (II) i osmi (II) per a la detecció cromofluorogènica d’espècies carregades i monòxid de carboni” es centra en el desenvolupament de sensors químics moleculars. El treball realitzat es pot dividir en dues parts: (i) síntesi i caracterització de sondes moleculars multifuncionals per a la detecció òptica d’anions i cations metàl·lics i, (ii) preparació de complexos de ruteni (II) i osmi (II) per a la detecció cromofluorogènica de monòxid de carboni.

La primera família de sondes moleculars, a la qual es fa referència en el capítol 2, es basa en l’ús d’imidazoantraquinones com a subunitat indicadora. Emprant aquest fragment molecular es van preparar i caracteritzar quatre sondes (**2a-2d**). De tots els anions que es van assajar, només el fluorur és capaç d’induir l’aparició d’una banda d’absorció (la qual cosa es reflecteix en diferents canvis de color) i bandes d’emissió desplaçades cap al roig. Aquests canvis s’atribuïxen a la desprotonació del grup NH de l’anell d’imidazol induïda pel fluorur. També els cations Fe^{3+} , Al^{3+} i Cr^{3+} són capaços de produir desplaçaments moderats cap al blau de les bandes d’adsorció dels quatre receptors, així com una desactivació marcada de l’emissió a causa de la seua coordinació (amb els àtoms d’oxigen i nitrogen del cromòfor imidazoantraquinona).

El segon capítol també està dedicat a l’estudi del comportament de coordinació en presència d’anions i cations d’una segona família de sondes (**3a-3d**) basades en derivats d’imidazoquinolina. Novament l’anió fluorur promou la desprotonació d’aquests compostos, la qual cosa es reflecteix en l’aparició de bandes d’absorció i d’emissió desplaçades cap al roig. Quant a la resposta òptica en presència de cations metàl·lics és molt poc selectiva, observant-se canvis en les bandes UV-visible i una desactivació de les bandes d’emissió en presència de Hg^{2+} , Cu^{2+} , Co^{2+} , Fe^{3+} , Fe^{2+} , Zn^{2+} , Pb^{2+} , Cd^{2+} , Cr^{3+} i Al^{3+} .

Al capítol 3 es presenta la síntesi, caracterització i comportament cromofluorogènic en presència de monòxid de carboni de dos conjunts de complexos de ruteni (II) i osmi (II) que tenen a la seua esfera de coordinació els fluoròfors 2,1,3-benzotiadiazol (BTD) i 5-(3-tienil)-1,2,3-benzotiadiazol (TBTD). A la primera part d'aquest capítol es van preparar huit compostos amb el lligant BTD (**1-8**). Al banyoljar-les CO, les dissolucions de cloroform d'aquests complexos van mostrar notables canvis de color. A més, la seua emissió es va veure incrementada a causa de la coordinació dels complexos amb el CO i el desplaçament del fluoròfor BTD. D'altra banda, l'adsorció dels complexos en sílice va donar lloc a sòlids que van presentar importants canvis de color premetent la detecció de CO en fase gas a simple vista i amb alta selectivitat i sensibilitat.

El segon conjunt de complexos de ruteni (II) i osmi (II) conté el fluoròfor TBTD (**3-7**). Aquests també són capaços de detectar CO quan es troben dissolts en cloroform i adsorbits en sílice a través de canvis de color i fluorescència. D'altra banda, es van preparar dos nous complexos (**8 i 9**) funcionalitzats amb una cadena de polietilenglicol. Ambdós complexos són solubles en aigua i permeten la detecció de CO en aquest dissolvent altament competitiu. A més, els compostos **8** i **9** no són tòxics i es van emprar amb èxit en la detecció de CO en cèl·lules HeLa.

Resumen

La presente tesis doctoral titulada "Sondas moleculares y complejos de rutenio (II) y osmio (II) para la detección cromo-fluorogénica de especies cargadas y monóxido de carbono" se centra en el desarrollo de sensores químicos moleculares. El trabajo realizado se puede dividir en dos partes: (i) síntesis y caracterización de sondas moleculares multifuncionales para la detección óptica de aniones y cationes metálicos y, (ii) preparación de complejos de rutenio (II) y osmio (II) para la detección cromo-fluorogénica de monóxido de carbono.

La primera familia de sondas moleculares, a la cual se hace referencia en el capítulo 2, se basa en el uso de imidazoantraquinonas como subunidad indicadora. Empleando este fragmento molecular se prepararon y caracterizaron cuatro sondas (**2a-2d**). De todos los aniones que se ensayaron, sólo el fluoruro es capaz de inducir la aparición de una banda de absorción (lo cual se refleja en diferentes cambios de color) y bandas de emisión desplazadas hacia el rojo. Estos cambios se atribuyen a la desprotonación del grupo N-H del anillo de imidazol inducida por el fluoruro. También los cationes Fe^{3+} , Al^{3+} y Cr^{3+} son capaces de producir desplazamientos moderados hacia el azul de las bandas de absorción de los cuatro receptores, así como una desactivación marcada de la emisión a causa de su coordinación (con los átomos de oxígeno y nitrógeno del cromóforo imidazoantraquinona).

El segundo capítulo también está dedicado al estudio del comportamiento de coordinación frente a aniones y cationes de una segunda familia de sondas (**3a-3d**) basadas en derivados de imidazoquinolina. Nuevamente el anión fluoruro promueve la desprotonación de estos compuestos, lo cual se refleja en la aparición de bandas de absorción y de emisión desplazadas hacia el rojo. En cuanto a la respuesta óptica en presencia de cationes metálicos es muy poco selectiva, observándose cambios en las bandas UV-visible y una desactivación de

las bandas de emisión en presencia de Hg^{2+} , Cu^{2+} , Co^{2+} , Fe^{3+} , Fe^{2+} , Zn^{2+} , Pb^{2+} , Cd^{2+} , Cr^{3+} y Al^{3+} .

A lo largo del capítulo 3 se presenta la síntesis, caracterización y comportamiento cromo-fluorogénico frente al monóxido de carbono de dos conjuntos de complejos de rutenio (II) y osmio (II) que tienen en su esfera de coordinación los fluoróforos 2,1,3-benzotiadiazol (BTD) y 5-(3-tienil)-2,1,3-benzotiadiazol (TBTD). En la primera parte de este capítulo se prepararon ocho compuestos con el ligando BTD (**1-8**). Al burbujearles CO, las disoluciones de cloroformo de dichos complejos mostraron notables cambios de color. Además, su emisión se vio incrementada debido a la coordinación de los complejos con el CO y el desplazamiento del fluoróforo BTD. Por otro lado, la adsorción de los complejos en sílice dio lugar a sólidos que presentaron importantes cambios de color permitiendo la detección de CO en fase gas a simple vista y con alta selectividad y sensibilidad.

El segundo conjunto de complejos de rutenio (II) y osmio (II) contiene el fluoróforo TBTD (**3-7**). Éstos también son capaces de detectar CO cuando se encuentran disueltos en cloroformo y adsorbidos en sílice a través de cambios de color y fluorescencia. Por otra parte, se prepararon dos nuevos complejos (**8** y **9**) funcionalizados con una cadena de polietilenglicol. Ambos complejos son solubles en agua y permiten la detección de CO en este disolvente altamente competitivo. Además, los compuestos **8** y **9** no son tóxicos y se emplearon con éxito en la detección de CO en células HeLa.

Abstract

The present PhD thesis entitled “Molecular probes and ruthenium (II) and osmium (II) complexes for the chromo-fluorogenic sensing of charged species and carbon monoxide” is focused on the development of molecular chemosensors. More in detail, the work carried out is clearly divided into two independent parts: (i) the synthesis and characterization of multifunctional molecular probes for the optical detection of anions and metal cations and, (ii) the preparation of ruthenium (II) and osmium (II) complexes for the chromo-fluorogenic sensing of carbon monoxide.

The first family of molecular probes, reported in chapter 2, is based on the use of imidazoanthraquinone as signaling subunit. Using this molecular fragment four probes (**2a-2d**) are prepared and characterized. Of all the anions tested, only fluoride is able to induce the appearance of red-shifted absorption (reflected in marked color changes) and emission bands. These changes are ascribed to a fluoride-induced deprotonation of the N-H moiety of the imidazole ring. Also Fe^{3+} , Al^{3+} and Cr^{3+} were able to induce moderate blue-shifts of the absorption bands of the four receptors upon coordination (with the oxygen and nitrogen atoms of the imidazoanthraquinone chromophore) and marked emission quenching.

The second chapter is also devoted to study the coordination behavior toward anions and cations of a second family of probes (**3a-3d**) containing imidazoquinoline derivatives. Again, fluoride anion promoted the deprotonation on the probes that are reflected in the appearance of red-shifted absorption and emission bands. The optical response in the presence of metal cations is quite unselective and UV-visible shifts and emission quenchings are observed in the presence of Hg^{2+} , Cu^{2+} , Co^{2+} , Fe^{3+} , Fe^{2+} , Zn^{2+} , Pb^{2+} , Cd^{2+} , Cr^{3+} and Al^{3+} .

Chapter 3 presents the synthesis, characterization and chromo-fluorogenic behavior toward of carbon monoxide of two set of ruthenium (II) and osmium (II)

complexes bearing 2,1,3-benzothiadiazole (BTD) and 5-(3-thienyl)-2,1,3-benzothiadiazole (TBTD) fluorophores. Eight complexes functionalized with BTD ligand (**1-8**) are prepared in the first part of this chapter. Chloroform solutions of the complexes underwent remarkable color changes when CO is bubbled. Also, significant emission enhancements are observed due to coordination of CO and displacement of BTD fluorophore. Besides, the adsorption of the complexes on silica yielded solids that presented remarkable color changes that allowed a naked eye detection of CO in gas phase.

The second set of ruthenium (II) and osmium (II) complexes contains TBTD fluorophore (**3-7**). Also these complexes are able to detect CO in chloroform solution and in gas phase when adsorbed on silica through color and fluorescence changes. Moreover, two new complexes (**8** and **9**) containing a poly(ethylene) glycol chain are prepared. Both complexes are water soluble and allowed CO detection in this highly competitive solvent. Besides, **8** and **9** are non-toxic and are successfully used for CO detection in HeLa cells.

Abbreviations and Acronyms

BODIPY	Boron-dipyrromethene
BTB	2,1,3-benzothiadiazole
CCDC	Cambridge Crystallographic Data Centre
CD₃CN	Deuterated acetonitrile
CDCl₃	Deuterated chloroform
CIBER-BBN	Centro de Investigación Biomédica en Red en Bioingeniería, Biomateriales y Nanomedicina
CO	Carbon monoxide
COD	1,5-cyclooctadiene
COHb	Carboxyhemoglobin
CO₂	Carbon dioxide
CO-RMs	Carbon monoxide Releasing Molecules
CPCM	Conductor-like Polarizable Continuum Model
cpy	4-cyanopyridine
dmap	4-dimethylaminopyridine
DME	Dimethoxyethane
DMF	Dimethyl Formamide
DMSO	Dimethylsulfoxide
DNA	Deoxyribonucleic Acid
DPBS	Dulbecco's phosphate-buffered saline
Em	Emission
EPA	Environmental Protection Agency
EtOH	Ethanol
Ex	Excitation
FRET	Förster Resonance Energy Transfer
FT-IR	Fourier Transform Infrared Radiation
GSH	Glutathione
Hb	Hemoglobin
HeLa	Henrietta Lacks

HOMO	High Occupied Molecular Orbital
HRMS	High Resolution Mass Spectrometry
	Instituto Internacional de Reconocimiento Molecular y Desarrollo Tecnológico
IDM	
IR	Infrared
LMCT	Ligand-to-metal charge transfer
LOD	Limit Of Detection
LUMO	Low Unoccupied Molecular Orbital
MeCN	Methyl Cyanide (Acetonitrile)
Me₂Hpz	3,5-dimethylpyrazole
MLCT	Metal-to-Ligand Charge Transfer
MO	Molecular Orbital
Mp	Melting point
Nap	Napthalene
NDIR	Non-Dispersive Infrared Method
NMR	Nuclear Magnetic Resonance
NO	Nitric Oxide
PBS	Phosphate Buffered Saline
Ph	Phenyl groups
Phen	Phenanthrene
PM3	Parameterized Model Number 3
PNP-iPr	<i>N,N'</i> -bis(diisopropylphosphino)-2,6-diaminopyridine
ppb	Parts per billion
ppm	Parts per million
py	Pyridine
QqTOF	Quadrupole Time OF Flight
RMS	Root Mean Square
SI	Supporting Information
TBTD	5-(3-thienyl)-2,1,3-benzothiadiazole
TD-DFT	Time-dependent Density Functional Theory
TMPP	Tris(2,4,6-trimethoxyphenyl)phosphine

TWA	Time-Weighted Average
TZVP	Triple Zeta Valence Plus Polarization
UPV	Universitat Politècnica de València
UV-Vis	Ultraviolet – Visible
VOCs	Volatile Organic Compounds
ZnTPP	Zinc tetraphenylporphyrin

Table of Contents

1. General objectives.....	3
2. Sensors for anions and cations.....	7
2.1. Introduction	9
2.2. Objectives.....	31
2.3. Imidazoanthraquinone derivatives for the chromo-fluorogenic sensing of basic anions and trivalent metal cations	35
2.4. Synthesis and evaluation of the chromo-fluorogenic recognition ability of imidazoquinoline derivatives toward ions.....	87
2.5. Conclusions	119
3. CO Sensors	123
3.1. Introduction	125
3.2. Objectives.....	149
3.3. Ruthenium (II) and osmium (II) vinyl complexes as highly sensitive and selective chromogenic and fluorogenic probes for the sensing of carbon monoxide in air	153
3.4. Highly sensitive and selective molecular probes for chromo-fluorogenic sensing of carbon monoxide in air, aqueous solution and living cells	221
3.5. Conclusions	305
4. General conclusions	309

1. General objectives

This PhD thesis is focused on the design and synthesis of chromo-fluorogenic sensors for the sensitive and selective detection of anions, cations and carbon monoxide. Particularly our aims are:

- To prepare and evaluate new chromo-fluorogenic chemosensors that can selectively recognize anions and cations through colour and/or emission changes. The underlying idea is to implement, in one molecular scaffold, cation and anion binding sites in order to prepare multifunctional probes.
- To prepare and evaluate new chromo-fluorogenic ruthenium(II) and osmium(II) complexes for the selective detection, through colour and emission changes, of carbon monoxide both in solution (to evaluate its applicability for CO sensing in cells) and in air.

2. Sensors for anions and cations

2.1. Introduction

2.1.1. Supramolecular chemistry

A vast number of molecules of different sizes and shapes are known, ranging from the simple H₂ molecule to the infinitely more complex biological proteins and nucleic acids. We may therefore be tempted to believe that the structures and properties of these materials and compounds can be directly related to those of the individual molecules that comprise them in a straightforward way. Unfortunately, this is an incorrect concept. Deeply we understand the nature of individual molecules, this knowledge is not enough to explain the structures, functions and micro-macroscopic properties of molecular assemblies, which are derived as a result of organizing individual molecules. The discipline that provides us the tools to understand how simple molecules organize themselves to build-up more complex units is *Supramolecular Chemistry*.¹ Supramolecular Chemistry is often defined as “*chemistry beyond the molecules*” intended as chemistry beyond the covalent bond. Thus this new branch of chemistry deals mainly with how discrete molecules can cooperate through non-covalent interactions as hydrogen bonding, metal coordination, hydrophobic forces, van der Waals forces, π - π interactions and electrostatic effects, to generate unique nanostructured supermolecules that present different properties (often better) than the sum of the properties of each individual component.

Bearing in mind the infinite number of possibilities given by the noncovalent bond chemistry an organization of this new discipline should be useful; thus supramolecular chemistry can be divided in two main areas:

1. **Molecular recognition chemistry**, chemistry associated with a molecule recognizing a partner molecule, also defined as host-guest chemistry.
2. **Self-assembly chemistry**, chemistry of molecular assembly of many molecules.

¹ J. M. Lehn, *Angew. Chem.*, **1988**, *100*, 91.

The present chapter of this PhD thesis deals with molecular recognition chemistry in solution. For this reason, in the next paragraphs, the basis of molecular recognition chemistry will be discussed.

2.1.1.1. Molecular recognition chemistry

Through the supramolecular studies, nowadays we know that all biological functions are associated with a selective recognition between two or more molecules through specific interactions. This process is known as "molecular recognition". More specifically, the molecular recognition is considered the way that molecules can recognize each other to form complex structures through a privileged relationship resting on the mutual interest of interacting partners possessing special qualities. Usually, the interactions between these partners (host-guest) are of non-covalent nature (hydrogen bonding, metal coordination, hydrophobic forces, van der Waals forces and π - π interactions).²

The first model of molecular recognition is the lock-key principle suggested by Emil Fischer in 1894.³ In this model, an enzyme (host) can discriminate among different substrates (guests) through the specific geometric complementarity between host and guest. Thus, only one guest fit exactly into one host like only a key enter in a specific lock. Knowledge of this simple principle allowed explaining the enzymatic catalysis, the compression of many complex biological processes and setting up the foundation for the preparation and optimization of new synthetic hosts (receptors).⁴

A chemical receptor is a particular molecule designed and optimized for molecular recognition of a given substrate (see Figure 2.1.1). During the design of a receptor an extensive evaluation of the size, shape, geometry, charge, hydrophilic/lipophilic character and other physico-chemical characteristics of

² a) F. P. Schmidtchen, *Chem. Soc. Rev.*, **2010**, *39*, 3916; b) D. K. Smith, *J. Chem. Edu.*, **2005**, *82*, 393.

³ E. Fischer, *Ber. Dtsch. Chem. Ges.*, **1895**, *28*, 1429.

⁴ a) F. W. Lichtenthaler, *Angew. Chem.*, **1992**, *104*, 1577; b) D. E. Koshland, *Angew. Chem.*, **1995**, *33*, 2375.

guest-analyte is necessary in order to provide the best and largest amount of intermolecular forces between the host and the guest. In addition, an assessment of the environment in which molecular recognition takes place is very important when designing the chemical receptor due to the influence of intermolecular processes such as solvation and electrostatic interactions between receptor, medium and analyte.⁵

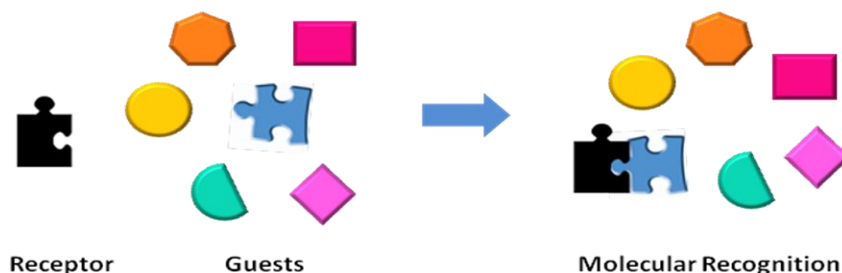


Figure 2.1.1. Scheme of molecular recognition event by a specific host-guest interaction.

Moreover, the effectiveness of a chemical receptor is associated to the degree of complementarity between host and guest, which promotes the action of one or more intermolecular forces during the recognition process. Furthermore, the receptor efficiency is determined by its ability to selectively recognize a specific guest, including the presence of other substrates with similar features. Therefore, it is intended that the receptor have more than one type of interaction with the analyte, such as biological receptors whose complexity and complementarity with certain substrates ensures the activation of biological processes in a consistent and very specific manner.⁶

The first studies with biological receptors were conducted by Villiers in 1891 with cyclodextrins.⁷ However, the skills of cyclodextrins as receptors were not

⁵ a) G. V. Oshovsky, D. N. Reinhoudt, W. Verboom, *Angew. Chem. Int. Ed.* **2007**, *46*, 2366;

b) S. Kubik, *Chem. Soc. Rev.*, **2010**, *39*, 3648.

⁶ L. A. Joyce, S. H. Shabbir, E. V. Anslyn, *Chem. Soc. Rev.*, **2010**, *39*, 3621.

⁷ A. Villiers *Compt. Rend. Fr. Acad. Sci.* **1891**, *112*, 435.

studied until 1935 when Pringsheim demonstrated their ability to form complexes with certain specific substrates.⁸ The first synthetic receptors were reported in 1960 by Lehn,⁹ Cram¹⁰ and Pedersen¹¹ who prepared crown ethers and cryptands capable of a specific molecular recognition of certain metal cations by coordination processes (Figure 2.1.2). Then, at the end of the same decade, the first anion receptors were also reported by Biallas¹² and by Simmons (Figure 2.1.3).¹³

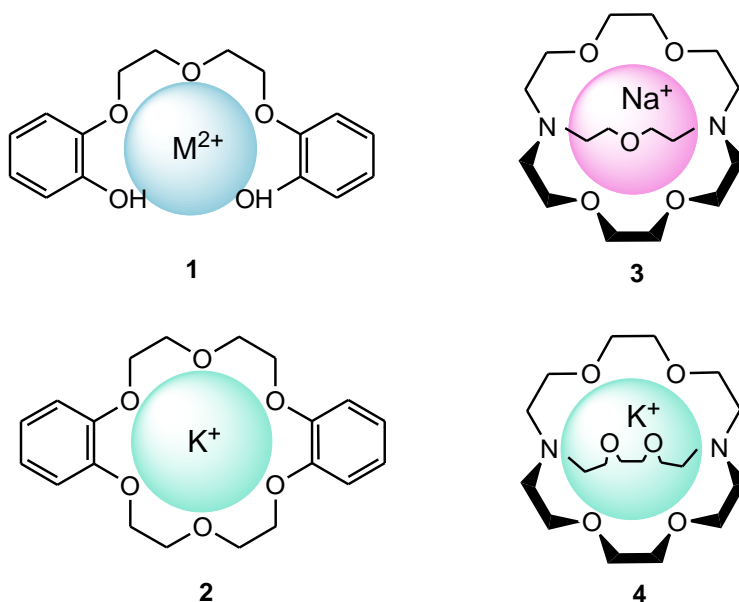


Figure 2.1.2. Metal complex based on crown ethers and cryptands. Left: Pedersen's complexes of divalent cations (1) and K⁺ (2) with crown ethers. Right: Structures of metal complex of Na⁺ (3) and K⁺ (4) with two of the first synthetic cryptands.

⁸ H. Pringsheim, *Chemistry of the Saccharides*, McGraw-Hill: New York, **1932**, 280.

⁹ a) J. M. Lehn, *Acc. Chem. Res.*, **1978**, *11*, 49; b) J. M. Lehn, *Pure Appl. Chem.*, **1978**, *50*, 9, 871.

¹⁰ D. J. Cram, *J. Am. Chem. Soc.* **1978**, *100*, 8190.

¹¹ a) C. J. Pedersen, *J. Am. Chem. Soc.* **1957**, *79*, 2295; b) C. J. Pedersen, *J. Am. Chem. Soc.* **1967**, *89*, 7017.

¹² D. F. Shriver, M. J. Biallas, *J. Am. Chem. Soc.*, **1967**, *89*, 1078.

¹³ C. H. Park, H. E. Simmons, *J. Am. Chem. Soc.*, **1968**, *90*, 2429.

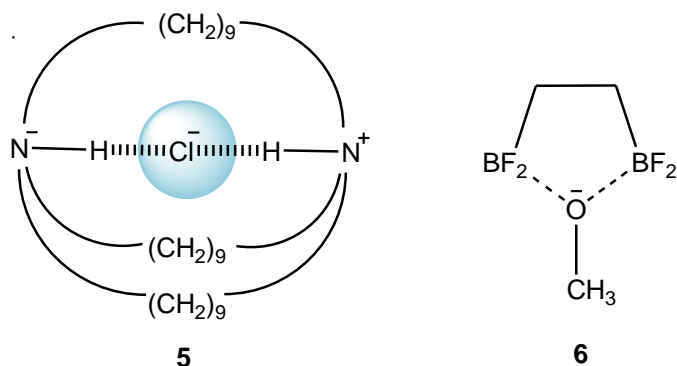


Figure 2.1.3. Representation of the first anion receptors. Left: chelated complex (**5**) formed between macrobicyclic amines and Cl^- anion, reported by Park and Simmons. Right: chelated complex (**6**) formed between bidentate 1,2-bis(difluoroboryl)ethane and methoxide anion, reported by Shriver and Biallas.

2.1.1.2. Molecular sensors

In the supramolecular chemistry field, receptors specifically designed for sensing purposes are generally called molecular sensors (or chemosensors).¹⁴ A chemosensor is a molecule that produces a detectable and easy-to-measure signal, revealing the presence of the guest, as a result of molecular recognition. Signals widely used to detect the presence of certain guest molecules are changes in color,¹⁵ fluorescence¹⁶ or modulations in electrochemical properties.¹⁷ In this sensing process, information at the molecular level, such as the presence or not of a certain guest in solution, is amplified to a macroscopic level; hence, sensing might open the door to the determination (qualitative or quantitative) of certain guests. In this sense, one interesting goal in the development of sensors deals with the synthesis of highly selective systems.¹⁸ Reversibility and fast response will

¹⁴ Ed. J. P. Desvergne, A. W. Czarnik, *Chemosensors for Ion and Molecule Recognition* NATO Asi Series, Series C., **1997**, Kluwer Academic Publishers.

¹⁵ a) H. G. Löhr, F. Vögtle, *Acc. Chem. Res.*, **1985**, , 65. b) M. Takagi, K. Ueno, *Top. Curr. Chem.*, **1984**, *121*, 39.

¹⁶ A. W. Czarnik, *Acc. Chem. Res.*, **1994**, *27*, 302.

¹⁷ a) P. D. Beer, *Chem. Commun.*, **1996**, 689. b) P. D. Beer, *Coord. Chem. Rev.*, **2000**, *205*, 131.

¹⁸ a) R. Martínez-Máñez, F. Sancenón, *Chem. Rev.*, **2003**, *103*, 4419. b) M. Moragues, R. Martínez-Máñez, F. Sancenón, *Chem. Soc. Rev.*, **2011**, *40*, 2593. c) L. E. Santos-Figueroa,

be also appealing features for an applicable sensor to be taken into account in its design.

A molecular chemical sensor is composed mainly by two units:

1. **Binding subunit**, is the unit responsible of the recognition of the analyte. The process of recognition depends on the host molecule characteristics. The binding subunit is designed in order to achieve a selective coordination via a suitable receptor-guest complementarity.
2. **Signalling subunit**, acts as a signal transducer and informs of the recognition process that occurs at molecular level through changes in a measurable macroscopic signal.

Among changes that could be observed, modulations in colour and fluorescence are especially appealing. While colorimetric sensors can be used to the naked eye detection of analytes, fluorogenic sensors have in general a high degree of sensitivity. Chromo-fluorogenic chemosensors are normally constructed by one of following approaches (see Figure 2.1.4):

1. **Binding site-signalling subunit approach**: The chemosensor is formed by “binding sites” and “signaling units” that are covalently linked. The coordination of the guest with the binding site changes physical properties of the signaling subunit giving rise to variations either in the color (chromogenic chemosensor) or in its fluorescence behavior (fluorogenic chemosensor).¹⁹
2. **The displacement approach**: This approach uses binding sites and signaling subunits forming a coordination complex (molecular ensemble),

M. Moragues, E. Climent, A. Agostini, R. Martínez-Máñez, F. Sancenón, *Chem. Soc. Rev.* **2013**, *42*, 3489.

¹⁹ R. A. Bissell, P. de Silva, H. Q. N. Gunaratne, P. L.M. Lynch, G. E. M. Maguire, K. R. A. S. Sandanayake, *Chem. Soc.Rev.*, **1992**, *21*, 187.

not covalently linked. This approach relies in a displacement reaction when the target molecule is coordinated with the binding site and the signaling subunit returns to the solution. A suitable signal is observed when the color or emission of the signaling subunit in the sensing ensemble is different than that present when it is free in solution.²⁰

3. **The “chemodosimeter” approach:** This is related with the use of specific irreversible reactions involving hosts and guests, which are coupled to a color or emission variations.²¹ If the chemical reaction is irreversible, the use of the term chemosensor cannot strictly be used and we will refer to these systems as chemodosimeters or chemoreactants.²²

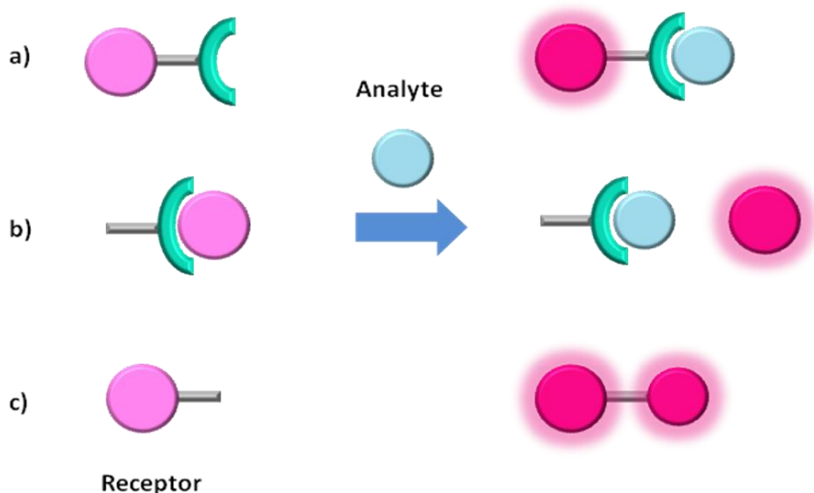


Figure 2.1.4. Representative scheme of the three main approaches used in the development of optical chemosensors. a) Binding site-signalling subunit; b) Displacement protocol; c) Chemodosimeter approach.

²⁰ a) S. L. Wiskur, H. Ait-Haddou, J. J. Lavigne, E. V. Anslyn, *Acc. Chem. Res.*, **2001**, *34*, 963.

b) B. T. Nguyen, E. V. Anslyn, *Coord. Chem. Rev.*, **2006**, *250*, 3118.

²¹ a) M.-Y. Chae, A. W. Czarnik, *J. Am. Chem. Soc.*, **1992**, *114*, 9704. b) V. Dujols, F. Ford, A. W. Czarnik, *J. Am. Chem. Soc.*, **1997**, *119*, 7386.

²² Z. Xu, X. Chen, H. N. Kim, J. Yoon, *Chem. Soc. Rev.*, **2010**, *39*, 127.

Next, several examples of chromo-fluorogenic sensors for cations and anions.

2.1.1.3. Chromo-fluorogenic sensors for cations

Of all the three approaches used for the synthesis of chromo-fluorogenic sensors for cations, the binding site-signaling subunit is, perhaps, the most employed. In this approach the binding site and the signaling subunits are linked together through a covalent bond or are both integrated in a superstructure. We will use this approach for the preparation of our chemosensors based on imidazoanthraquinone and imidazoquinoline heterocycles.

The first example of chromogenic chemosensors for metal cations was published by Dix and Vögtle in 1978.²³ The authors prepared receptor composed by a crown ether linked, through a covalent bond, with an azo dye (see structure **7** in Figure 2.1.5). The key point in chemosensor design is the incorporation of one of the nitrogen atoms of the azo dye inside the structure of the crown ether. Acetonitrile solutions of receptor **7** presented an absorption band centered at 477 nm that is the responsible of the orange color observed. Of all the cations tested, only Ba²⁺ was able to induce a remarkable hypsochromic shift of the visible band (from 477 to 357 nm) that was reflected in a color change from orange to yellow. The observed hypsochromic shift was ascribed to a coordination of Ba²⁺ cation with the crown ether. The interaction of this cation with the nitrogen atom of the azo dye located in the crown ether induced an increase in the HOMO/LUMO energy gap.

²³ J. P. Dix, F. Vögtle, *Angew. Chem. Int. Ed.*, **1978**, 17 857.

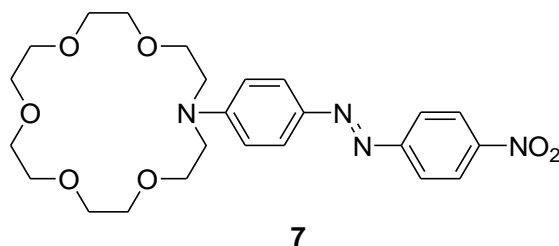


Figure 2.1.5. Chromogenic receptor bearing an azo dye for the selective recognition of Ba^{2+} cation.

Following the binding site-signaling subunit approach a myriad of chromo-fluorogenic cation sensors have been prepared. Most of them used common chromophores of fluorophores such as azo dyes, fluorescein derivatives, rhodamine derivatives, polycyclic aromatic hydrocarbons (naphthalene, anthracene, pyrene, perylene), dansyl derivatives, cyanine dyes, and so on. However, the use of anthraquinone and quinoline as signaling subunits has been less explored. At this respect, Kim and co-workers synthesized 9,10-anthraquinonecalix[4]crown **8** (see Figure 2.1.6) and studied its chromogenic behavior toward metal cations.²⁴ Acetonitrile solutions of chemosensor **8** showed the typical absorption of the anthraquinone chromophore centered at 380 nm. Of all the cations tested (Li^+ , Na^+ , K^+ , Rb^+ , Cs^+ , Ag^+ , Cd^{2+} , Mg^{2+} , Ca^{2+} , Sr^{2+} , Ba^{2+} , Zn^{2+} , Hg^{2+} , Pb^{2+} , Co^{2+} and Cu^{2+}) only Cu^{2+} induced the appearance of a new absorption band centered at 450 nm. Cu^{2+} forms an 1:1 stoichiometry complex with chemosensor **8** interacting with the oxygen of the polyether chains.

²⁴ H. J. Kim, S. H. Kim, J. H. Kim, L. N. Ahn, J. H. Lee, C. -H. Lee, J. S. Kim, *Tetrahedron Lett.*, **2009**, *50*, 2782.

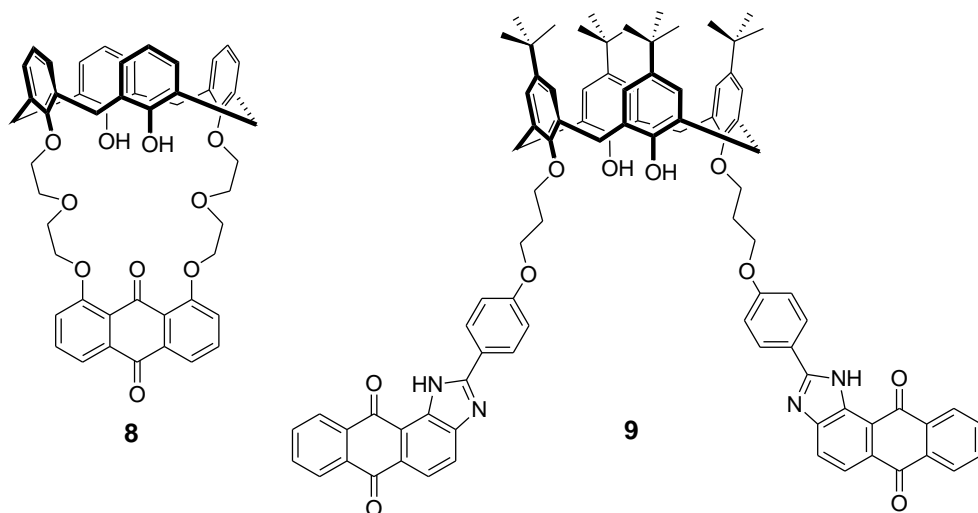


Figure 2.1.6. Chemical structure of anthraquinone-based chemosensors **8** and **9**.

Chawla and co-workers also prepared an anthraquinonoidal calix[4]arene for the selective recognition of Zn^{2+} cation (structure **9** in Figure 2.1.6).²⁵ Chloroform-acetonitrile 1:4 v/v solution of chemosensor **9** showed an emission band centered at 565 nm upon excitation at 420 nm that was ascribed to the imidzoanthraquinone fluorophore. Changes in the emission band were tested upon addition of Zn^{2+} , Pb^{2+} , Fe^{2+} , Hg^{2+} , Co^{2+} , Na^+ , Mn^{2+} , Li^+ , Ag^+ , Ni^{2+} and Cd^{2+} cations. Of all the cations tested, only Zn^{2+} induced a moderate quenching of the emission band ascribed to the formation of a 1:1 stoichiometry complex in which the cation interacted with the nitrogen atoms of the imidzoanthraquinone fluorophore.

Imidazonanthraquinone fluorophore has been also coupled to a terpyridine as cation binding site (see structure **10** in Figure 2.1.7).²⁶ Acetonitrile solution of **10** presented an intraligand charge transfer band at 404 nm and an intense emission band at 528 nm (upon excitation at the wavelength of the visible band). The spectral changes of acetonitrile solutions of **10** in the presence of Ni^{2+} , Zn^{2+} , Cu^{2+} ,

²⁵ H. M. Chawla, R. Shukla, S. Pandey, *Tetrahedron Lett.*, **2012**, 53, 2996.

²⁶ D. Mondal, M. Bar, D. Maity, S. Baitalik, *J. Phys. Chem. C*, **2015**, 119, 25429.

Al^{3+} , Co^{2+} , Cd^{2+} and Fe^{2+} were studied. Of all the cations tested, only Fe^{2+} induced the appearance of a new band centered at 576 nm that was reflected in a color change from pale yellow to deep violet. This new absorption was ascribed to a metal to ligand charge transfer band that was generated upon coordination of Fe^{2+} cation with the terpyridine subunit forming 2:1 ligand-cation stoichiometry complexes. In spite of this selectivity toward Fe^{2+} cation observed when using UV-visible measurements, an unselective response was found by fluorescence. At this respect, an emission quenching was observed with Ni^{2+} , Co^{2+} , Fe^{2+} and Cu^{2+} whereas Cd^{2+} , Al^{3+} and Zn^{2+} induced moderate enhancements.

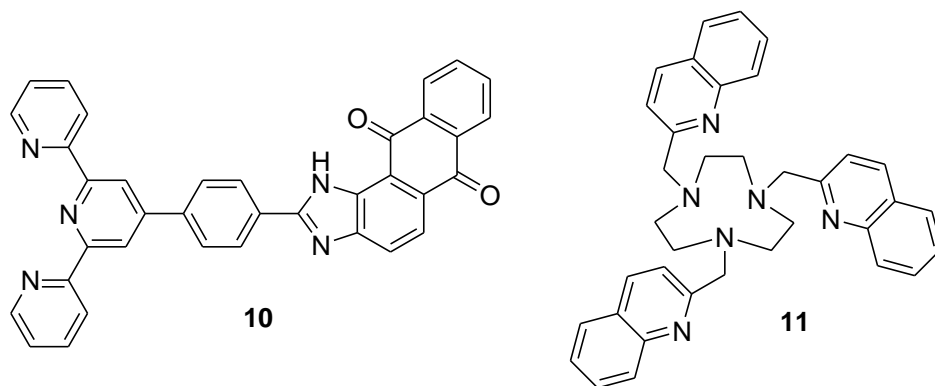


Figure 2.1.7. Structure of chemosensors **10** and **11**.

Quinoline is other chromophore/fluorophore that has been recently used for the development of molecular chemosensors for metal cations. At this respect, Lippolis and co-workers functionalized nitrogen-containing macrocycles with quinoline pendant (see structure **11** in Figure 2.1.7) arms and tested the emission behavior of the prepared chemosensors in the presence of Cu^{2+} , Zn^{2+} , Cd^{2+} , Hg^{2+} and Pb^{2+} transition metal cations.²⁷ Acetonitrile-water 1:1 v/v solution of chemosensor **11** presented a very weak emission band at 380 nm when excited at

²⁷ M. Mameli, M. C. Aragoni, M. Arca, M. Atzori, A. Bencini, C. Bazzicalupi, A. J. Blake, C. Caltagirone, F. A. Devillanova, A. Garau, M. B. Hursthouse, F. Isaia, V. Lippolis, B. Valtancoli, *Inorg. Chem.*, **2009**, *48*, 9236.

316 nm. This weak emission was ascribed to a photoinduced electron transfer process between the tertiary nitrogen atoms of the macrocycle and the quinoline fluorophores. Of all the cations tested, only Zn^{2+} induced a marked increase in the emission intensity ascribed to a preferential coordination with the nitrogen atoms of the macrocycle and subsequent inhibition of the photoinduced electron transfer process.

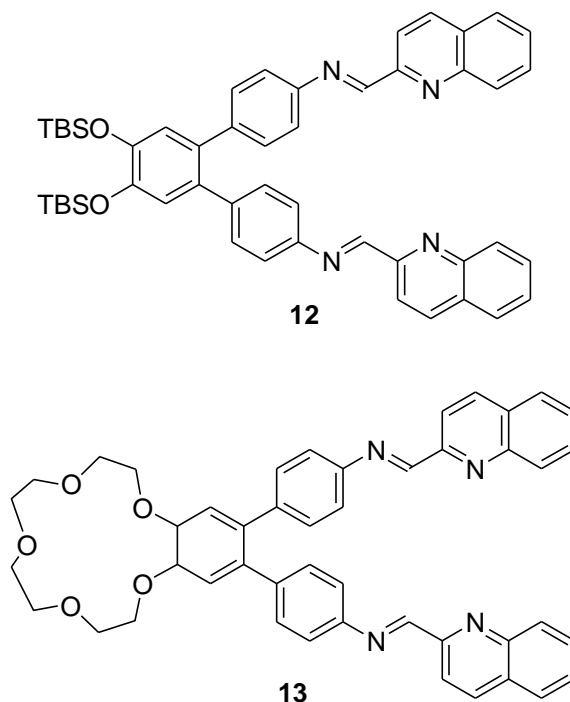


Figure 2.1.8. Chemical structure of the quinoline chemosensors **12** and **13** prepared by Bhalla and co-workers.

Bhalla and co-workers prepared chemosensors **12** and **13** and studied their emission behavior in the presence of selected metal cations (see Figure 2.1.8). THF solutions of both receptors showed an intense absorption band centered at 354 nm that suffers a bathochromic shift to 434 nm only in the presence of Hg^{2+} cation. This shift was reflected in a color change from colorless to yellow. This red shift of the visible band was ascribed to the coordination of Hg^{2+} with the imino

nitrogens leading to an intramolecular charge transfer from the quinoline moieties to the imino groups. Also, both receptors exhibited low emission bands at 415 nm in THF due to a photoinduced electron transfer from the imino nitrogen atoms to the excited quinoline fluorophore. Only Hg^{2+} addition induced marked emission intensity (and small redshifts) of both receptors due to the inhibition of the photoinduced electron transfer process upon cation coordination.

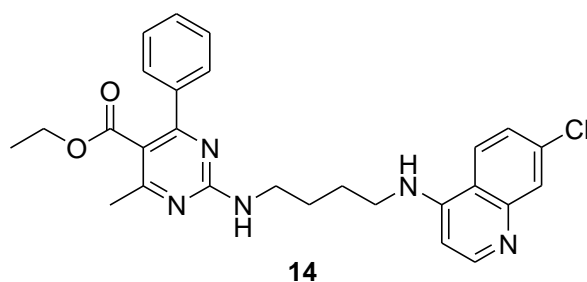


Figure 2.1.9. Chemical structure of quinoline-containing chemosensor **14**.

The quinoline-functionalized chemosensor **14** (see Figure 2.1.9) exhibit a broad emission band centered at 376 nm (excited at 330 nm) when dissolved in methanol.²⁸ The fluorogenic response of **14** was studied in the presence of Fe^{3+} , Fe^{2+} , Hg^{2+} , Ni^{2+} , Co^{2+} , Zn^{2+} , Cd^{2+} , Pb^{2+} , Mg^{2+} , Mn^{2+} , K^+ , Ag^+ , Ca^{2+} , Ba^{2+} , Cu^+ , Cu^{2+} , Na^+ and Cr^{3+} cations. Of all the cations tested, only addition of Fe^{3+} , Cu^{2+} and Hg^{2+} induced a marked quenching of the emission intensity of receptor **14**. Job's plots carried out with Fe^{3+} , Cu^{2+} and Hg^{2+} revealed the formation of 1:1 stoichiometry complexes. TD-DTF calculations suggested that coordination of the three metal cations with quinoline was the responsible of the observed quenching.

2.1.1.4. Chromo-fluorogenic sensors for anions

For the development of molecular sensors for anions the three main approaches have been extensively used. However, in the last years, the chemodosimeter approach was emerged as a preferential choose because most of the prepared sensors using this approach work in aqueous environment and the reactions that induced color and/or emission changes are highly selective. In

²⁸ P. Kaur, H. Kaur, K. Singh, *RSC Adv.*, **2013**, *3*, 64.

many of the published examples, deprotonation processes induced by basic anions (such as fluoride, cyanide and acetate) of acidic protons in the chemosensors were coupled with color and/or emission changes. The first examples of these chemosensors based on deprotonation processes were published by Fabbrizzi and co-workers.²⁹ In a pioneering work they prepared an urea containing receptor **15** (see Figure 2.1.10) and studied its chromogenic behavior in the presence of fluoride, acetate, benzoate, dihydrogen phosphate, nitrite, hydrogen sulfate and nitrate. At this respect, acetonitrile solutions of **15** presented an absorption band centered at 345 nm that was redshifted upon addition of fluoride, acetate, benzoate and dihydrogen phosphate. The most remarkable redshift was observed with fluoride (130 nm reflected in a color change from yellow to deep orange) whereas with the other anions tested moderate values (ca. 25 nm) were measured. The authors ascribed the remarkable shift obtained with fluoride to a deprotonation of the urea moiety in **15** whereas the other anions only yielded hydrogen bonded 1:1 stoichiometry complexes.

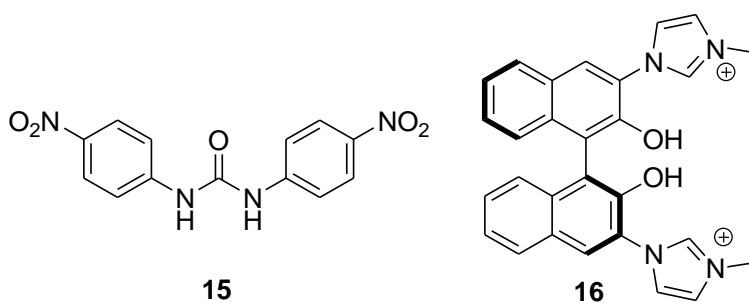


Figure 2.1.10. Chemical structures of receptors **15** and **16**.

Yu and co-workers prepared an imidazolium BINOL derivative that was able to detect chromo-fluorogenically fluoride and acetate anions.³⁰ At this respect,

²⁹ V. Amendola, D. Esteban-Gómez, L. Fabbrizzi, M. Licchelli, *Acc. Chem. Res.*, **2006**, *39*, 343.

³⁰ Q. -S. Lu, L. Dong, J. Zhang, J. Li, L. Jiang, Y. Huang, Q. Qin, C. -W. Hu, X. -Q. Yu, *Org. Lett.*, **2009**, *11*, 669.

acetonitrile-DMSO 9:1 v/v solutions of probe **16** (see Figure 2.1.10) presented an absorption band at 365 nm that was redshifted upon addition of fluoride (to 475 nm) and acetate (to 450 nm) anions. Also, the emission of the free receptor centered at ca. 450 nm was enhanced upon addition of both anions. The changes observed upon addition of acetate anions were ascribed to the formation of a hydrogen bonding complex with the C(2)-H units (located between the two nitrogen atoms) of the imidazolium subunits. Besides, the changes observed upon fluoride addition were ascribed to a deprotonation process of the C(2)-H units of the imidazolium subunits.

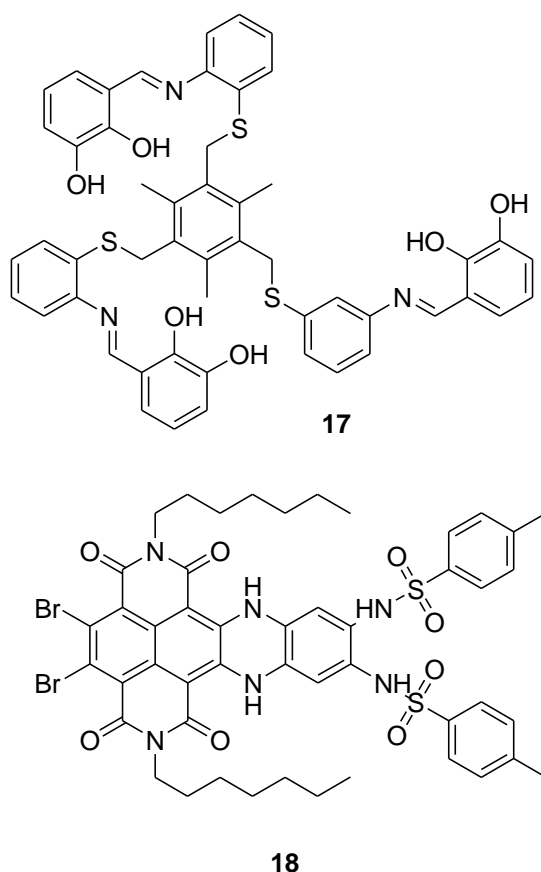


Figure 2.1.11. Chemical structures of molecular probes **17** and **18**.

DMSO solution of tripodal catechol-imine probe **17** (see Figure 2.1.11) showed three absorption bands centered at 274, 306 and 353 nm that remained

unchanged upon addition of chloride, bromide, iodide, nitrate, cyanide, perchlorate, acetate, hydrogen sulfate and dihydrogen phosphate anions.³¹ However, addition of fluoride induced the appearance of a new band centered at 433 nm that was the responsible of the observed color change (from colorless to bright yellow). The chromogenic changes observed were ascribed to a fluoride-induced deprotonation of the hydroxyl moieties in the catechol subunits.

Naphthaenedimindes were also used as signaling subunits for the preparation of chromo-fluorogenic sensors for anions.³² At this respect, Langford and co-workers prepared probe **18** (see Figure 2.1.11) and tested its chromo-fluorogenic behavior in chloroform. Solutions of probe **18** presented three absorption bands at 559, 609 and 696 nm (blue color) that were shifted to 570, 622 and 715 nm (green color) upon addition of fluoride anion. The other anions tested (chloride, bromide, iodide, hydrogen phosphate, acetate and hydrogen sulfate) induced negligible color changes. Also, the emission band of the free probe centered at 635 nm (excitation at 600 nm) suffered a marked quenching only in the presence of fluoride anion. The optical changes observed were ascribed again to a fluoride-induced deprotonation of the sulfonamide moieties presented in the structure of **18**.

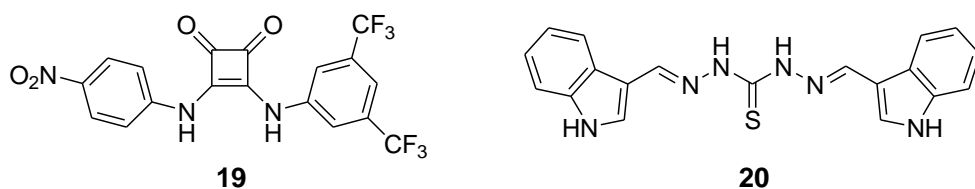


Figure 2.1.12. Anion probes **19** and **20**.

³¹ V. K. Bhardwaj, M. S. Hundal, G. Hundal, *Tetrahedron*, **2009**, *65*, 8556.

³² S. V. Bhosale, S. V. Bhosale, M. B. Kalyankar, S. J. Langford, *Org. Lett.*, **2009**, *11*, 5418.

Unsymmetrical squaramides (such probe **19** in Figure 2.1.12) were also used for the chromogenic sensing of fluoride and acetate anions.³³ Acetonitrile solutions of probe **19** showed an intense absorption at 377 nm that vanished and was substituted with another band centered at 475 nm upon addition of fluoride anion. These changes were reflected in the fact that the yellow color of the initial solution turned dark orange in the presence of fluoride. Nearly the same changes were observed upon addition of acetate anion but the redshifted band appeared at ca. 450 nm and the change in color was from colorless to orange. The authors ascribed the optical changes observed with both anions to deprotonations of the squaramide subunit in probe **19**.

Indole conjugated thiourea probes (see structure **20** in Figure 2.1.12) were described by Ghosh and Bose as chromogenic chemodosimeter for fluoride anion.³⁴ Solutions of probe **20** in acetonitrile-DMF 9.6:0.4 v/v presented an absorption band in the UV zone centered at 342 nm. Addition of chloride, bromide, iodide, acetate, nitrate and dihydrogen phosphate induced negligible changes in the UV band whereas remarkable shifts were observed with fluoride anion. At this respect, addition of 50 equivalents of fluoride induced the disappearance of the 342 nm band with the concomitant appearance of new absorptions at 522, 572 and 936 nm (reflected in a color change from colorless to deep violet). The authors ascribed the chromogenic changes observed to a fluoride-induced deprotonation of the NH indole and/or thiourea protons. The negative charge generated is delocalized over the entire molecule and the overall conjugation is the responsible of the NIR absorption observed.

³³ A. Rostami, A. Colin, X. Y. Li, M. G. Chudzinski, A. J. Lough, M. S. Taylor, *J. Org. Chem.*, **2010**, *75*, 3983.

³⁴ P. Bose, P. Ghosh, *Chem. Commun.*, **2010**, *46*, 2962.

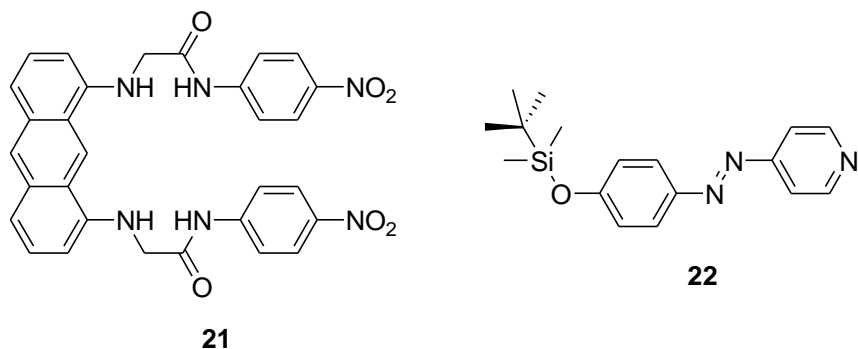


Figure 2.1.13. Anthracene (**21**) and pyridine azo dye (**22**) probes for the chromogenic detection of basic anions.

Kang and co-workers described an anthracene derivative functionalized with nitrophenyl groups for the chromogenic detection of pyrophosphate and fluoride anions.³⁵ At this respect, DMSO solutions of probe **21** (see Figure 2.1.13) showed an strong absorption in the UV zone centered at 331 nm that was shifted to longer wavelength upon addition of fluoride and pyrophosphate (at 446 nm for both anions). These changes were reflected in color modulation from colorless to yellow and were ascribed to an anion-induced deprotonation of the amide moieties.

Martínez-Máñez and co-workers prepared an azopyridine dye functionalized with a fluoride-sensitive *t*-butyl dimethyl silyl moiety (structure **22** in Figure 2.1.13) for the chromogenic sensing of this anion.³⁶ Acetonitrile-water 9:1 v/v solutions of probe **22** showed an absorption band at 350 nm that remained unchanged upon addition of chloride, acetate, benzoate, hydrogen sulfate, dihydrogen phosphate, cyanide, nitrate and carbonate. However, addition of fluoride induced the formation of an absorption band centered at 470 nm (color change from colorless to orange-red). The chromogenic behavior was ascribed to a fluoride-induced hydrolysis of the silyl ether moiety that generated a highly

³⁵ J. J. Park, Y. -H. Kim, C. Kim, J. Kang, *Tetrahedron Lett.*, **2011**, 52, 2759.

³⁶ A. Agostini, M. Milani, R. Martínez-Máñez, M. Licchelli, J. Soto, F. Sancenón, *Chem. As. J.*, **2012**, 7, 2040.

colored phenolate anion. Furthermore, the probe was grafted onto TLC silica foils that were used to detect fluoride in aqueous solution.

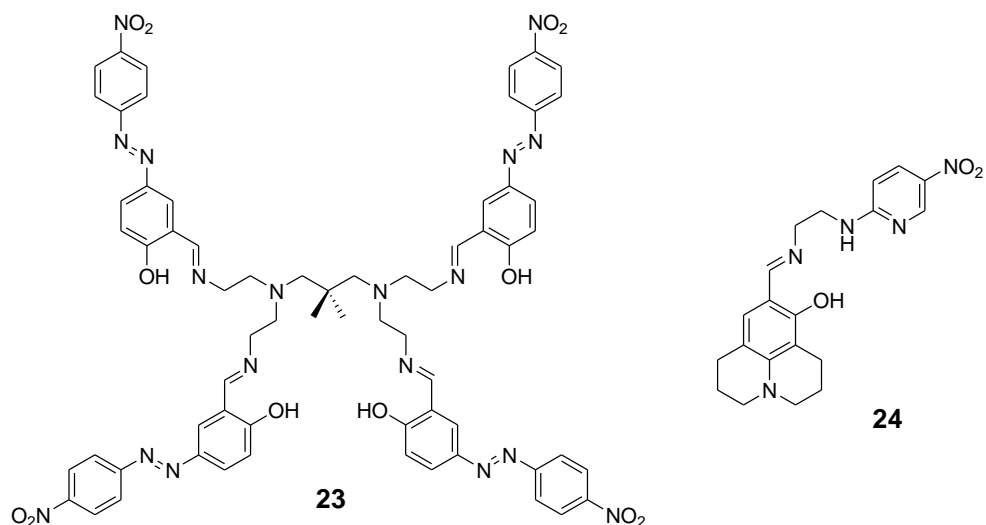


Figure 2.1.14. Structure of probes **23** and **24**.

Azo dyes containing acidic hydroxyl moieties were also used for the chromogenic detection of basic anions. At this respect, Khanmohammadi and co-workers synthesized probe **23** (see Figure 2.1.14) and tested its anion recognition abilities.³⁷ DMSO solutions of probe **23** presented an intense absorption band centered at 443 nm that was unchanged in the presence of chloride, bromide, nitrite, nitrate, hydrogen sulfate, iodide, perchlorate and azide anions. Addition of fluoride, acetate and dihydrogen phosphate induced the appearance of a new redshifted band centered at 549 nm. The intensity of the 549 band was clearly related with the basicity of the anions ($F^- > AcO^- > H_2PO_4^-$). A marked color change from yellow to blue was observed with fluoride anion that was ascribed to a deprotonation of the phenol moieties in the azo signaling subunits.

³⁷ K. Rezaeian, H. Khanmohammadi, *Spectrochim. Acta Part A*, **2014**, *133*, 31.

Finally, in a recent publication, Kim and co-workers used julolidine probe **24** (see Figure 2.1.14) for the chromogenic sensing of fluoride anion.³⁸ DMSO solutions of probe **24** showed an absorption band centered at 350 nm that was bathochromically shifted to 465 nm only in the presence of fluoride anion (change in color from colorless to orange). These changes were ascribed to a fluoride-induced deprotonation of the phenolic hydroxyl moiety. On the other hand, the other anions tested (cyanide, acetate, chloride, bromide, iodide, dihydrogen phosphate, benzoate, azide and thiocyanate) were unable to induce any noticeable change in the UV-vis spectra. Besides, this probe was able to selectively detect Cu²⁺ cation by color changes upon formation of a 1:1 stoichiometry complex.

³⁸ Y. W. Choi, J. J. Lee, G. R. You, S. Y. Lee, C. Kim, *RSC Adv.*, **2015**, *5*, 86463.

2.2. Objectives

Taking into account the growing interest in the development of efficient chemosensors for anions and cations, our objective is to prepare and evaluate new multianalyte sensors (by incorporating anion and cation binding sites into one organic scaffold) for the chromo-fluorogenic detection of anions and cations of environmental and biological interest. In particular, our aims are:

- To design and synthesize two families of chromo-fluorogenic probes based on imidazoanthraquinone and imidazoquinolines for anion and cation recognition.
- To characterize the new prepared probes by standard methods (NMR, HRMS, IR, UV/Vis and emission spectroscopy).
- To evaluate the sensibility and selectivity of the synthesized probes toward anions and cations of environmental and biological interest.

***2.3. Imidazoanthraquinone derivatives for
the chromo-fluorogenic sensing of basic
anions and trivalent metal cations***

Imidazoanthraquinones derivatives for the chromo-fluorogenic sensing of basic anions and trivalent metal cations

Cristina Marín-Hernández,^{a,b} Luis E. Santos-Figueroa,^{a,b} María E. Moragues,^{a,b} M. Manuela M. Raposo,^c Rosa M. F. Batista,^c Susana P. G. Costa,^c Teresa Pardo,^{a,b} Ramón Martínez-Máñez^{a,b} and Félix Sancenón^{a,b}*

^a *Centro de Reconocimiento Molecular y Desarrollo Tecnológico (IDM), Unidad Mixta Universidad de Valencia-Universidad Politécnica de Valencia. Camino de Vera s/n, 46022 Valencia, Spain.*

^b *CIBER de Bioingeniería, Biomateriales y Nanomedicina (CIBER-BBN).*

^c *Centro de Química, Universidade do Minho, Campus de Gualtar, 4710-057 Braga, Portugal.*

Published online: November 3, 2014

*(Reprinted with permission from
J. Org. Chem., 2014, 79, 10752–10761
Copyright © 2014 American Chemical Society)*

2.3.1. Abstract

Four imidazo-anthraquinone derivatives (**2a-d**) were synthesized, characterized and their coordination behaviour against selected anions and cations tested. Acetonitrile solutions of probes showed charge-transfer absorptions in the 407-465 nm range. The four probes emitted in the 533-571 nm interval. The recognition ability of **2a-d** was evaluated in the presence of F^- , Cl^- , Br^- , I^- , OCN^- , BzO^- , ClO_4^- , AcO^- , HSO_4^- , $H_2PO_4^-$ and CN^- . Only F^- , AcO^- and $H_2PO_4^-$ induced a new red-shifted absorption band that was attributed to a deprotonation process involving the amine moiety of the imidazole ring. Moreover, upon increasing quantities of F^- , AcO^- and $H_2PO_4^-$, it was induced moderate quenching in the emission of **2a-d** together with the appearance of a new red-shifted band. The UV-visible and emission behaviour of the four probes in the presence of Cu^{2+} , Co^{2+} , Mg^{2+} , Fe^{3+} , Ba^{2+} , Fe^{2+} , Ni^{2+} , Ca^{2+} , Zn^{2+} , Pb^{2+} , Cd^{2+} , Cr^{3+} , Al^{3+} , K^+ and Li^+ was also assessed. Only addition of Fe^{3+} , Cr^{3+} and Al^{3+} caused a new blue-shifted band in **2a-d** that was ascribed to a preferential coordination with the acceptor part of the probes. Moreover it was observed an important quenching of the emission which was ascribed to the interaction between these trivalent cations and **2a-d**.

2.3.2. Introduction

The design of new molecular probes to detect anions, cations and neutral species has gained primary significance in recent years due to the importance to detect certain target analytes in environmental and biological samples.¹ In this context, these probes transform probe-analyte interactions into a signal which allows analyte detection via optical or electrochemical changes.² Among these particular output signals optical responses are highly appealing due to the opportunity of using low-cost, extensively accessible instrumentation and they offer, in certain circumstances, the possibility of detecting target species “to-the-naked-eye”.³ Moreover, chromo-fluorogenic chemosensors displaying a displacement of the absorption or emission band are of importance for the development of ratiometric procedures.⁴ Optical detection probes for cations were developed before twenty years ago,⁵ whereas the anionic ones have only been investigated during recent years.⁶ In general anion sensing is more

challenging that cation detection. Comparing ions, anions usually show lower stability constants than metal cations and some of them display a complex pH-dependence, and varied shapes, that make the design of selective receptors for anions more difficult than for cationic species.⁷ However, despite these shortcomings, the design of anion probes has advanced and gained importance in recent years helped by the progress made in the comprehension about the formation of host-anion complexes and how this knowledge can be used for the design of selective anion receptors.⁸ The most widely approach to design probes is the use of the “binding site-signaling subunit” paradigm, in which the “binding site” is covalently connected to an optical “signaling subunit” in such a way that the interaction of certain species with the coordination site induces electronic modulations in the signaling unit, resulting in colour or emission changes.⁹ Inspired in these concepts authors have designed a number of probes for anions using in most cases well-known binding interactions such as hydrogen bonding and electrostatic forces.^{10, 11}

Imidazole derivatives have been shown to be effective in coordinating anions.¹² Besides, acidity of the NH protons affects the hydrogen-bonding ability of the imidazole group moiety. Its acidity can be modulated by the presence of easily delocalizable heteroaromatic rings, such as thiophene, pyrrole and furan, electronically connected to the imidazole group, as a way to enhance intramolecular electronic delocalization.¹³

On the other hand, trivalent metal cations played crucial roles in biological processes and their detection is a timely topic. For instance, iron is the most abundant transition metal in cellular systems. More specifically, Fe³⁺ cation is an essential element in the growth and development of living systems as well as in many biochemical processes at the cellular level¹⁴ and its deficiency is associated with several diseases (anemia, hemochromatosis, diabetes, Parkinson's and dysfunction of heart, pancreas, and liver).¹⁵ On the other hand, aluminum is the third element in earth and the most abundant metallic element. Aluminum is highly used in several commercial applications such as water treatment, food additives, medicines and metallic dispositives. Besides, some studies indicate that abnormal levels of aluminum ions in certain human

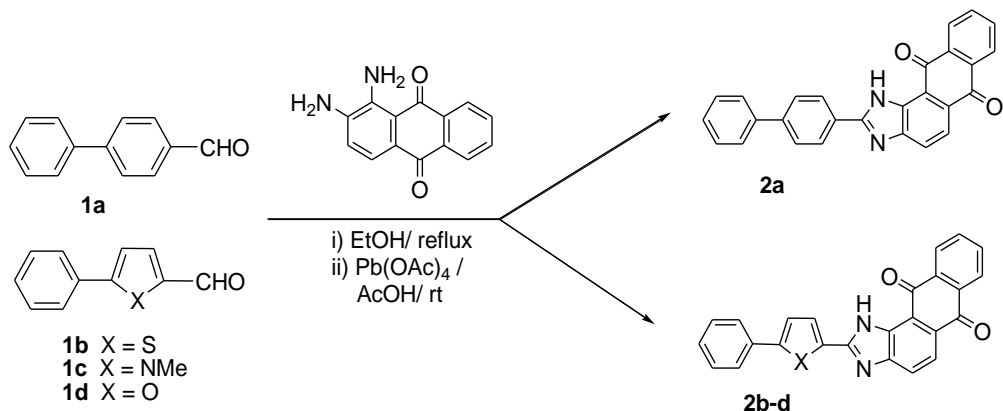
tissues and cells could induce Alzheimer's and Parkinson's diseases.¹⁶ Finally, Cr^{3+} cation is one of the most important nutrient in human and animal diet and plays a fundamental role in the metabolism of carbohydrates, proteins, lipids and nucleic acids.¹⁷ Their deficiency is associated to the development of diabetes and some cardiovascular diseases.¹⁸ Moreover, their use in metal industry has resulted in increased levels of chromium in the environment and today has come to be regarded as a pollution element.¹⁹

From a different point of view some anthraquinone derivatives have been recently reported as suitable systems for the colorimetric sensing of certain anions and have also been used for metal ion recognition.²⁰ Anthraquinones have been widely used in the manufacture of pigments,²¹ fibers and paper²² in textile industry²³ and to semiconductors in electronic industry.²⁴ More recently, anthraquinones have attracted increasing research interest by their bioactive properties and some of their derivatives have been reported to be used as antiviral,²⁵ antibacterial,²⁶ antiparasitic,²⁷ insecticidal,²⁸ fungicidal,²⁹ antimalarial³⁰ and anticancer.³¹

Taking into account the above mentioned facts, and our interest in the development of optical probes,³² we report herein the synthesis and characterization of a new family of imidazo-anthraquinone derivatives functionalized with aromatic and heterocyclic groups (i.e. biphenyl, *N*-methylpyrrole, thiophene and furan). The spectroscopic behavior of the designed probes in the presence of selected anions and cations was studied.

2.3.3. Results and discussion

Synthesis and characterization



Scheme 2.3.1. Synthesis of imidazo-anthraquinone receptors **2a-d**.

The formyl precursor **1c** was synthesized through Suzuki-Miyaura cross-coupling reaction of 1-methyl-2-(4,4,5,5-tetramethyl-1,3,2-dioxaborolan-2-yl)-1H-pyrrole with bromobenzene in dry DME with Pd(PPh₃)₄ as catalyst and Na₂CO₃, followed by Vilsmeier formylation. The new imidazo-anthraquinone derivatives **2a-d** with biphenyl, phenylthiophene, phenylpyrrole and phenylfuran substituents as π -conjugated groups were synthesized in moderate to good yields (32-71%). In a typical synthesis, aldehydes **1a-d** and 1,2-diaminoanthraquinone were heated for 15 h in ethanol at reflux using formic acid as catalyst, to yield the respective imines that were subsequently cyclized to the corresponding imidazo-anthraquinones **2a-d** in the presence of lead tetraacetate in acetic acid as solvent and at room temperature (see Scheme 2.3.1). For all reactions, the crudes were purified by column chromatography on silica with chloroform or through recrystallization with dichloromethane to finally give the pure compounds. The four **2a-d** receptors were characterized by ¹H, ¹³C NMR, and HRMS. The obtained data was in agreement with the expected structures (see Supporting Information and Experimental Section for details).

One of the most relevant characteristic in the ^1H NMR spectrum of this group of imidazo-anthraquinone derivatives was that corresponding to N-H protons of the imidazole heterocycle which appeared as singlets in downfield in the 12.74–13.38 ppm range. These values suggested the formation in solution of an intramolecular hydrogen bond between the NH of the imidazole ring and the neighboring quinone carbonyl group.³³

Spectroscopic characterization

Acetonitrile solutions of imidazo-anthraquinone derivatives **2a-d** presented a strong absorption ($\log \epsilon \approx 4.2$) in the 400-470 nm interval (see Table 2.3.1). The position of the visible absorption band in the receptors was clearly related to the electron donor strength of the aromatic or heterocycle system (pyrrole \gg furan $>$ thiophene $>$ benzene) used as π -bridge linked to the imidazo-anthraquinone moiety. In particular for **2a**, bearing a benzene π -bridge, the absorption band was centred at 407 nm. On changing the π -bridge to thiophene (**2b**) and furan (**2d**) the absorption maximum suffered a moderate bathochromic shifts to 435 and 441 nm respectively. Moreover when a *N*-methylpyrrole was used as π -bridge (**2c**) the probe displayed a significant bathochromic shift to 465 nm. Additionally, upon excitation in the corresponding wavelength maximum the four probes, a broad unstructured emission in the 540-580 nm region appeared (see Table 2.3.1).

The HOMO and LUMO differences in energy for probes **2a-d** were determined by quantum chemical studies at the semiempirical level using the PM3 model and with RMS gradient of 0.001. For the four receptors, the HOMO orbitals are mainly situated in the imidazole moiety and the heterocyclic rings (donor part of the molecule), whereas the LUMO orbitals are located in the anthraquinone moiety (acceptor fragment common to the four probes). These data indicated that the electronic transition between the HOMO and the LUMO has a charge-transfer character. As an example, Figure 2.3.1 shows the HOMO and LUMO orbitals for probe **2a**.

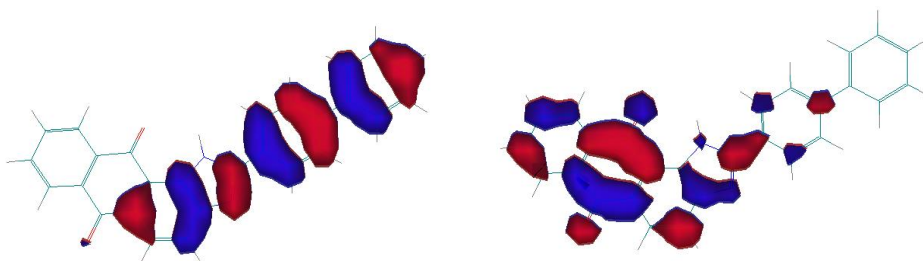


Figure 2.3.1. HOMO (left) and LUMO (right) orbitals for probe **2a**.

Spectroscopic behavior of **2a-d** in presence of anions

In a first step, the ability of receptors **2a-d** to detect anions was studied. In typical experiments, the UV-Vis spectrum of the probes was monitored in acetonitrile solutions at 25 °C in the presence of chosen anions with different sizes and shapes (*i.e.* F^- , Cl^- , Br^- , I^- , OCN^- , BzO^- , ClO_4^- , AcO^- , HSO_4^- , $H_2PO_4^-$ and CN^-). The chromogenic response observed with compounds **2a-d** was quite similar and in all cases only addition of F^- , AcO^- and $H_2PO_4^-$ anions induced colour changes that were especially visible to the naked eye in the presence of F^- anion. As an example, Figure 2.3.2 shows the colour modulations observed for **2a** probe upon addition of 10 eq. of selected anions.

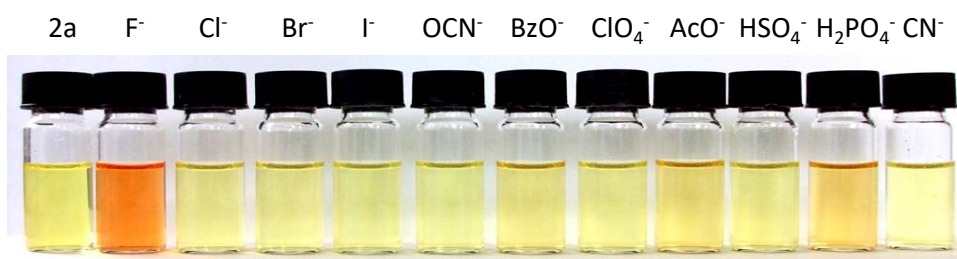


Figure 2.3.2. Colour changes observed for **2a** probe (1.0×10^{-4} mol dm^{-3} in acetonitrile) upon addition of 10 eq. of the selected anions.

As seen in Figure 2.3.2, acetonitrile solutions of probe **2a** were yellow and turned orange upon addition of F^- anion. Upon addition of AcO^- and $H_2PO_4^-$ anions, it was shown a moderate colour change from yellow to dark yellow. Other anions were unable to induce remarkable colour changes. A similar behaviour was observed for probes **2b**, **2c** and **2d**; i.e. clear colour modulations in the presence of F^- and only a moderate colour change in the presence of AcO^- and $H_2PO_4^-$ anions.

Once assessed the response found for **2a-d** probes toward anions, UV-visible changes in the presence of F^- , AcO^- and $H_2PO_4^-$ was studied more in detail. UV-visible titration profiles of probe **2b** with F^- and AcO^- anions are shown in Figure 2.3.3. Acetonitrile solutions of probe **2b** displayed an intense band at 435 nm that, upon addition of increasing quantities of F^- anion, decreased in intensity while a new red shifted band grew at 518 nm. In contrast the addition of AcO^- and $H_2PO_4^-$ anions induced only moderate changes in the UV-visible profiles of probe **2b**. As seen in Figure 2.3.3, addition of increasing amounts of AcO^- anion resulted in a hypochromic effect for the band at 435 nm together with the appearance of a broad shoulder centred at ca. 520 nm. Similar titration profiles were obtained for $H_2PO_4^-$ anion and **2b**.

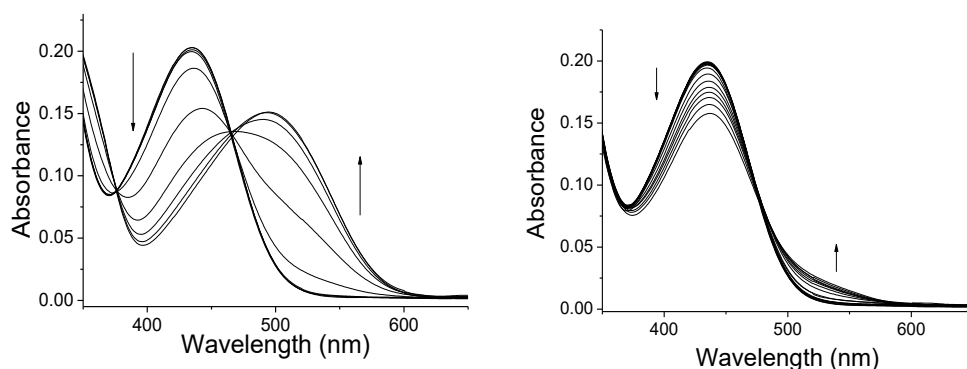


Figure 2.3.3. UV-Vis titration profiles of receptor **2b** (1.0×10^{-5} mol dm^{-3} in acetonitrile) obtained upon the addition of F^- (left) and AcO^- (right) anions.

UV-visible titration experiences carried out with probes **2a**, **2c** and **2d**

showed the same behaviour than that observed for **2b**, *i.e.* only the addition of F^- anion caused a remarkable decrease in the visible band of the receptor with a concomitant clear increase of a new red-shifted absorbance (see Supporting Information). Addition of AcO^- and $H_2PO_4^-$ anions to acetonitrile solutions of **2a**, **2c** and **2d** induced small changes in the UV-profiles, similar to those depicted in Figure 2.3.3 for **2b** (data not shown).

The fact that colour modulations in the four probes were induced by the addition of basic anions (F^- , AcO^- and $H_2PO_4^-$) pointed to a ground state proton shift as the mechanism for the chromogenic response observed.³⁴ In this scenario, addition of F^- anion would induce the deprotonation of the N-H moiety of the imidazo-anthraquinone fragment, which is common to all four probes. The mechanism of the chromogenic response was assessed with additional titration experiments carried out with probes **2a-d** and tetrabutylammonium hydroxide that showed an identical behaviour to that found in the presence of F^- anion (see Supporting Information). On the whole, the results were in agreement with the expectation that the deprotonation of a donor group in a push-pull system by an electron-rich anion would to induce a bathochromic shift of the absorption band. Indeed, other benzimidazole-, urea-, thiourea-, amide-, pyrrole-, benzimidazole- or thiosemicarbazone-containing probes have been reported to caused similar shifts upon addition of fluoride.³⁵ Besides, AcO^- and $H_2PO_4^-$ showed a less relevant response with the probes as expected because they are not as basic as F^- anion.³⁶ One striking feature of probes **2a-d** is their lack of response upon addition of the basic and nucleophilic CN^- anion. However this lack of response has also been described in other anthraquinone-containing probes.³⁷

The chromogenic behaviour of **2a-d** toward F^- was rather selective and for instance the intensity of the red shifted absorption band obtained upon addition of 10 eq. of this anion is identical to that obtained in mixtures containing 10 eq. fluoride and 10 eq. of Cl^- , Br^- , I^- , OCN^- , BzO^- , ClO_4^- , HSO_4^- and CN^- anions (see Figure 2.3.4). Besides, the limits of detection of **2a-d** for F^- were also determined from the corresponding titration profiles. The values obtained were quite similar for the four probes and around 10 μM .

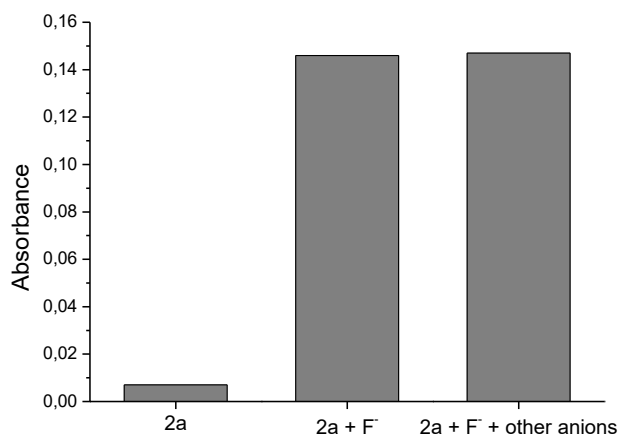


Figure 2.3.4. Absorbance of receptor **2a** (1.0×10^{-5} mol dm⁻³) at 479 nm alone, and upon the addition of 10 equiv. of F⁻ anion, and 10 equiv. of Br⁻, Cl⁻, I⁻, OCN⁻, BzO⁻, ClO₄⁻, HSO₄⁻ and CN⁻ anions in acetonitrile.

Once the UV-visible behaviour of **2a-d** probes was assessed, more detailed fluorogenic studies with F⁻ anion were carried out. F⁻ was selected because this was the anion that induced the most remarkable changes in the UV-visible of the four probes. Emission experiments were carried out in acetonitrile solutions in the presence of F⁻ and using as λ_{ex} the corresponding isosbestic point observed in the UV-visible titrations. The obtained response with the four probes was quite similar and, as an example, Figure 2.3.5 shows the emission changes for probe **2a** upon addition of increasing quantities of F⁻. As seen, probe **2a** showed a broad emission band at 544 nm ($\lambda_{\text{ex}} = 438$ nm) the intensity of which gradually decreased as the amount of F⁻ anion increased. Together with this quenching effect a progressive bathochromic shift of the fluorescence was observed (from 544 to 588 nm upon addition of 2 eq.) with an isoemissive point at 576 nm.

As a general trend, the remaining probes **2b-d** also showed a moderate bathochromic shift and a simultaneous partial quenching of their original emission band upon addition of increasing quantities of F⁻ anion. However, a more detailed look to the titration experiments indicated that, to induce the

same behaviour, bigger amounts of fluoride were necessary for receptor **2b**, **2c** and **2d** than for receptor **2a**. Emission data of the four probes alone and in the presence of F⁻ anion are shown in Table 2.3.1.

The emission changes observed for the four probes in the presence of F⁻ anion were quite similar to those observed for related derivatives.³⁸ For **2a-d** the quenching of the initial fluorescence band together with the appearance of the red-shifted emission was ascribed to a proton transfer process that yielded the deprotonated probes. This mechanism was proposed, for instance, by Han and co-workers for the interaction of fluoride with phenyl-1*H*-anthra(1,2-*d*)imidazole-6,11-dione; a probe closely related with **2a-d**.³⁹ The four probes alone are highly emissive. In the excited state, fluoride anion induced the loss of the proton of the N-H group and the formed HF binds, through the formation of a weak hydrogen bond, with the deprotonated receptor. This complex is not stable and, as a consequence, a deprotonation process takes place and the formed complex loses the HF molecule yielding the also emissive anionic form of the corresponding probe. The lifetimes of the hydrogen bonded complexes is too short and are not observed experimentally in the emission titration profiles. The negative charge generated upon the proton transfer process induced a new emission band that corresponds to the deprotonated form which emits at longer wavelength than the neutral probe.

The optical response of **2a-d** was also studied in mixed acetonitrile:water solutions. However it was found that addition of more than 2% of water to acetonitrile disabled the chromo-fluorogenic response observed upon addition of F⁻ anion. This could be ascribed to the fact that F⁻ has a high free energy of solvation (-465 kJ mol⁻¹) and, hence a strong affinity for coordinating water molecules rather than with the N-H moiety of the four probes. The formation of a dense water shell around fluoride anion decreased significantly its basicity and, as a consequence, the proton transfer process was disabled.

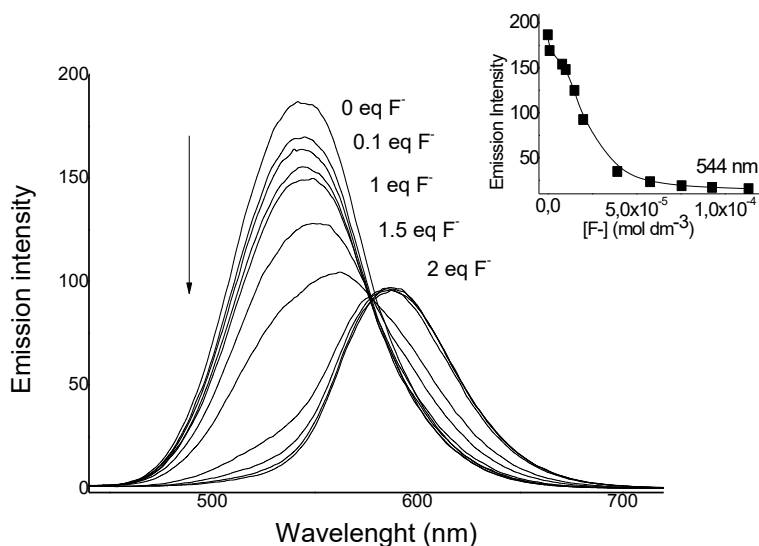


Figure 2.3.5. Emission spectra of probe **2a** ($1 \times 10^{-5} \text{ mol dm}^{-3}$) in acetonitrile upon addition of increasing quantities of F^- anion (excitation at 438 nm). The inset shows the change in the intensity of the 544 nm band upon addition of increasing quantities of F^- anion.

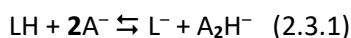
Table 2.3.1. Spectroscopic data for the interaction of **2a-d** with fluoride anion.

	Absorbance data				Fluorescence data				
	λ_{ab} LH (nm)	Log ϵ	$\lambda_{\text{ab}} \text{ L}^-$ (nm) ^a	$\Delta\lambda_{\text{ab}}$ (nm)	$\lambda_{\text{ex}} \text{ LH}$ (nm)	$\lambda_{\text{em}} \text{ LH}$ (nm)	$\lambda_{\text{em}} \text{ L}^-$ (nm) ^a	$\Delta\lambda_{\text{em}}$ (nm)	Stokes shift (cm^{-1})
2a	407	4.25	479	72	438	544	588	44	6188
2b	435	4.30	490	55	465	571	608	37	5506
2c	465	4.22	514	49	458	533	609	76	3123
2d	441	4.13	501	60	467	568	621	53	4658

^a Measured upon addition of 50 equivalents of fluoride anion

Determination of stability constants with anions and quantum mechanical studies

As stated above, basic anions (such as F^- , AcO^- and $H_2PO_4^-$) induced proton transfer processes in the probes **2a-d**. This proton transfer equilibrium is represented in equation 2.3.1 in which LH is the probe and A^- represents a basic anion such as fluoride.



To complete the characterization of the interaction among **2a-d** with anions the deprotonation process was studied, by the determination of the stability constants from UV-Vis spectroscopic titrations, using the HypSpec software.⁴⁰ The studies were performed using F^- because this was the anion that induced the more remarkable changes in the UV-visible (*vide ante*). The results are shown in Table 2.3.2.

Table 2.3.2. Logarithms of the stability constants measured for the interaction of probes **2a-d** with F^- anion.

Receptor	2a	2b	2c	2d
log K	4.208±0.006	3.308±0.007	3.819±0,071	3.381±0.071

The logarithms of the stability constants for probes **2b**, **2c** and **2d** in their interaction with F^- were rather similar and lower than $\log K = 4$. Moreover, when the π -bridge was a biphenyl system the acidity of the N-H moiety was enhanced (pK of 4.208). This observed enhancement was clearly related with the less electron donor character of the benzene ring, when compared with the pyrrole (**2c**), furan (**2d**) and thiophene (**2b**) heterocycles. In spite of this fact, the logarithms of the stability constants for the proton transfer reactions for probes **2a-d** are of the same order of magnitude and similar to those reported for related compounds.⁴¹

It has been reported that the hydrogen bond-donating or accepting ability of a molecule can be studied from quantum chemical calculations as a difference between the energy of the molecule and that of the deprotonated form.¹³ Calculations for probes **2a-d** (assuming that the N-H moiety of the four receptors was deprotonated) were carried out using a PM3 semi-empirical model and the results are shown in Table 2.3.3.

Table 2.3.3. Stabilization energy of the deprotonation for probes **2a-d**

Receptor	$E_{(LH)}$ (kcal/mol)	$E_{(L^-)}$ (kcal/mol)	$E_{(LH)} - E_{(L^-)}$ (kcal/mol)
2a	-5735.5	-5724.9	-10.6
2b	-5343.6	-5336.0	-7.6
2c	-5725.9	-5721.9	-4.0
2d	-5374.3	-5365.8	-8.5

Data in Table 2.3.3 indicated that the most acidic probe was **2a**. This was in agreement with the stability constants calculated above for the deprotonation process of the probes in the presence of fluoride. However for the remaining chemosensors there was not a clear correlation between the acidity predicted by quantum chemical calculations (*i.e.* **2d** > **2b** > **2c**) and that found from titration experiments (*i.e.* **2c** > **2d** > **2b**). This is most likely due to the different conditions in which the calculations were performed (gas for quantum calculations vs. acetonitrile solutions for stability constants).

Spectroscopic behaviour of **2a-d** with cations

Probes **2a-d** contain in their structures two oxygen and two nitrogen atoms that could be able to coordinate with transition metal cations.⁴² For this reason, the interaction of probes **2a-d** with selected cations (Cu^{2+} , Co^{2+} , Mg^{2+} , Fe^{3+} , Ba^{2+} , Fe^{2+} , Ni^{2+} , Ca^{2+} , Zn^{2+} , Pb^{2+} , Cd^{2+} , Cr^{3+} , Al^{3+} , K^+ and Li^+) in acetonitrile

was studied upon addition of 10 eq. of the corresponding cation. Only addition of trivalent cations (Fe^{3+} , Al^{3+} and Cr^{3+}) induced colour changes in the acetonitrile solutions of the four probes.

Once assessed the selective chromogenic response of **2a-d** to trivalent cations, more detailed studies of the four probes with Fe^{3+} , Al^{3+} and Cr^{3+} were performed via UV-visible titrations. As a general trend, addition of increasing amounts of these cations induced a progressive reduction in absorption of the visible band concomitant with the growth of a new blue-shifted band. As an example of this behaviour, Figure 2.3.6 shows the UV-visible titration profile of probe **2a** with Fe^{3+} cation. The absorption at 407 nm progressively decreased when increasing quantities of Fe^{3+} cation were added. At the same time, a new absorption band at 396 nm ($\Delta\lambda = 36$ nm) was formed. These changes were reflected in a colour modulation from yellow to colourless.

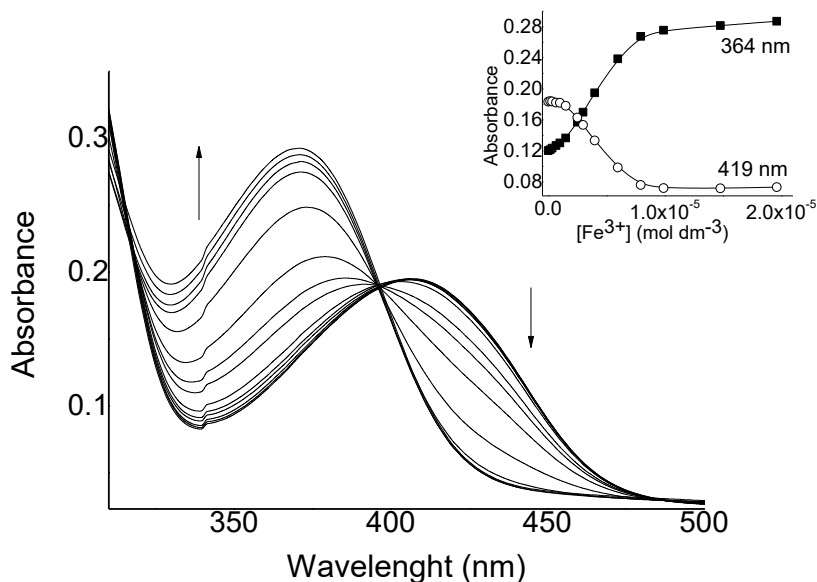


Figure 2.3.6. UV-visible titration of probe **2a** (1.0×10^{-5} mol dm^{-3}) with Fe^{3+} in acetonitrile. The inset shows the absorbance changes at 364 and 419 nm vs Fe^{3+} concentration.

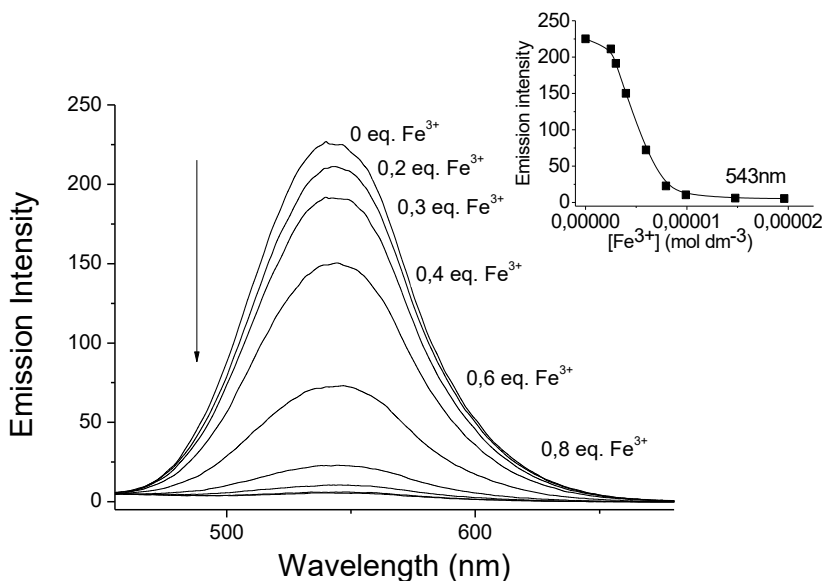


Figure 2.3.7. Emission spectra (excitation at 317 nm) of receptor **2a** (1.0×10^{-5} mol dm^{-3}) in acetonitrile upon addition of increasing quantities of Fe^{3+} cation. The inset shows the changes in the emission intensity at 543 nm vs Fe^{3+} concentration.

The emission behaviour of **2a-d** in the presence of trivalent cations was also studied. The four probes presented a very similar response upon addition of Fe^{3+} , Al^{3+} and Cr^{3+} cations, namely a marked emission quenching. As an example, Figure 2.3.7 shows the titration obtained for probe **2a** and Fe^{3+} cation. As seen, the emission at 543 nm ($\lambda_{\text{ex}} = 317$ nm) was progressively quenched upon addition of increasing amounts of Fe^{3+} . Changes in the UV-visible and emission of probes **2a-d** in the presence of trivalent cations are summarized in Table 2.3.4. Furthermore the limits of detection of the four probes toward trivalent metal cations were evaluated from fluorescence titration profiles. The values obtained were quite similar for all **2a-d** probes and are shown in Table 2.3.5.

Table 2.3.4. Spectroscopic data for probes **2a-d** with trivalent cations.

Receptor	Absorption Wavelength (nm)				Emission Wavelength (nm) ^a			
	LH	LH-Al ³⁺	LH-Cr ³⁺	LH-Fe ³⁺	LH	LH-Al ³⁺	LH-Cr ³⁺	LH-Fe ³⁺
2a	407	371	372	371	544	544	543	543
2b	435	410	410	410	571	559	562	563
2c	465	429	429	428	533	533	534	534
2d	441	419	419	419	580	558	556	555

^a Measured upon excitation at isosbestic point in the UV-vis titration.

Table 2.3.5. Limits of detection for **2a-d** probes to trivalent cations (μM) from emission titrations.

Receptor	Fe ³⁺	Al ³⁺	Cr ³⁺
2a	1.43	1.78	0.98
2b	2.10	2.46	3.10
2c	1.65	-	1.89
2d	1.81	1.35	1.85

The blue shift of the visible band of **2a-d** observed upon addition of trivalent cations was indicative of a preferential coordination with the donor part of the probes.⁴³ In fact the results are in agreement with the expectation that the interaction between an electron-acceptor cation and a donor group in a push-pull system will induce a blue shift. The common donor fragment in the four probes is the imidazo group and the results strongly suggested an interaction of the metal cations with this moiety.

¹H-NMR spectroscopic studies in the presence of cations

In order to study, in more depth, the coordination mode of probes **2a-d** with trivalent cations ¹H-NMR titration experiments were performed. For this

purpose we selected receptor **2a** and changes in $^1\text{H-NMR}$ spectra (in CD_3CN) upon addition of increasing quantities of Al^{3+} cation were studied.

The $^1\text{H-NMR}$ spectrum of **2a** in CD_3CN (see Figure 2.3.8 for proton assignment) showed the signals of the monosubstituted benzene ring centred at 7.45 (t, Ha), 7.53 (t, Hb) and 7.80 (d, Hc) ppm. Protons of the 1,4-disubstituted benzene ring appeared at 7.90 (m, Hd overlapped with Hi) and at 8.38 (He) ppm whereas protons of the anthraquinone moiety appeared at 7.90 (m, Hi overlapped with Hd), 8.13 (d, Hf), 8.21 (d, Hg) and 8.31 (dd, Hh) ppm. As a general trend, addition of Al^{3+} cation induced downfield shifts of the signals of probe **2a** (see Figure 2.3.8). Besides, the shifts of the proton resonances stopped upon addition of 1 eq. of Al^{3+} cation suggesting the formation of 1:1 (probe-cation) complexes.

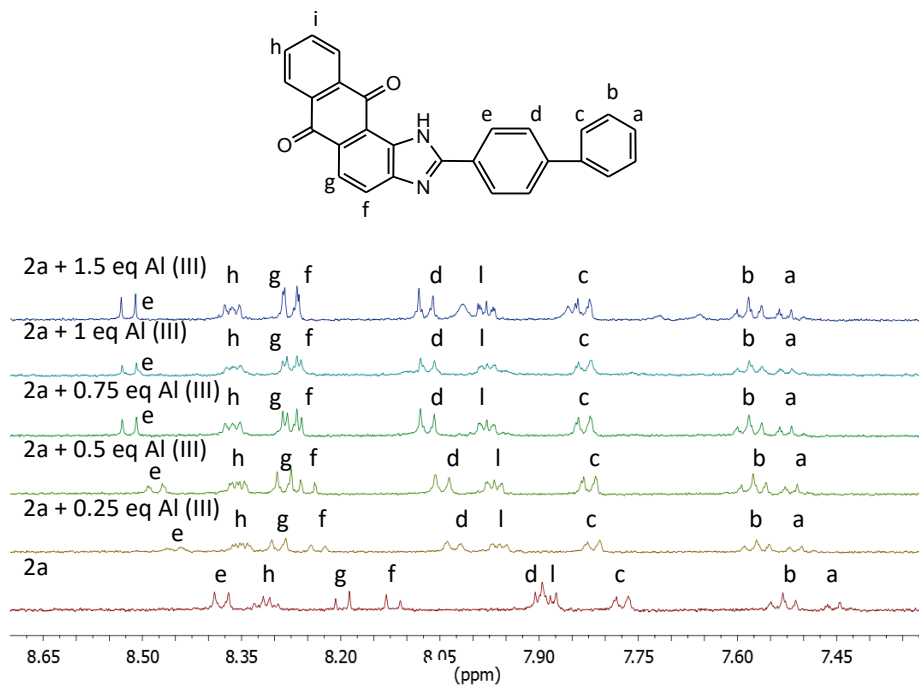


Figure 2.3.8. ^1H NMR spectra of probe **2a** in CD_3CN alone and in the presence of increasing quantities of Al^{3+} cation.

The more remarkable shifts observed upon Al^{3+} addition were those of protons Hd, Hf, Hg and He that are located in the 1,4-disubstituted benzene ring of the biphenyl system and in the anthraquinone aromatic ring fused with the imidazole heterocycle (see Figure 2.3.8). More in detail, the Hg signal shifted from 8.21 to 8.27 ppm, whereas Hf was displaced from 8.13 to 8.27 ppm. On the other hand the protons of the biphenyl group centred at 7.90 (Hd) and 8.38 (He) ppm shifted to 8.08 and 8.51 ppm respectively. These observed shifts are tentatively ascribed to a preferential coordination of Al^{3+} cation with one of the nitrogen atom of the imidazole ring.

Finally, the 1:1 stoichiometry of the complex formed between probes **2a-d** and Al^{3+} , Fe^{3+} and Cr^{3+} was assessed by the method of continuous variation (Job's plot). The probes for the interaction between **2a** and Fe^{3+} cation are shown in Figure 2.3.9. In all cases, the formation of 1:1 (probe-trivalent cation) complexes was confirmed.

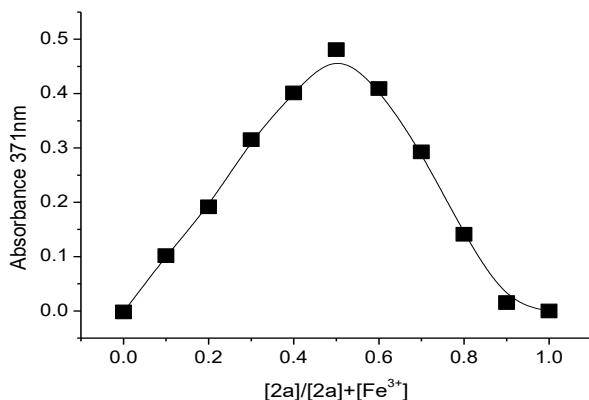


Figure 2.3.9. Job's plot for the complexation of **2a** with Fe^{3+} cation determined by UV–visible spectrophotometry in acetonitrile at 371 nm and $[\mathbf{2a}] + [\text{Fe}^{3+}] = 1.0 \times 10^{-3} \text{ mol dm}^{-3}$.

Stability constants with cations

To complete the characterization of the interaction between probes **2a-d** and cations, the corresponding stability constants for the formation of 1:1

complexes were determined from UV-visible spectroscopic titrations using the HypSpec software. The results are shown in Table 2.3.6. As seen, the stability constants determined for probes **2b**, **2c** and **2d** were of the same order of magnitude and were in the 3.74 - 4.52 range. Compared with these data, **2a** formed in general stronger complexes with values of the logarithms of the stability constants of 5.28, 4.80 and 4.49 for the coordination with Al^{3+} , Cr^{3+} and Fe^{3+} respectively. The fact that **2a** form stronger complexes with trivalent metal cations than that of **2b-d** may be tentatively ascribed to the presence of *N*-methylpyrrole, thiophene and furan heterocycles in **2b-d** that may inhibit, to some extent, the coordination with the trivalent cations.

Table 2.3.6. Logarithms of the stability constants calculated for the probes **2a-d** with trivalent cations (Al^{3+} , Cr^{3+} and Fe^{3+}) interactions.

	Al^{3+}	Cr^{3+}	Fe^{3+}
	$\text{LH} + \text{C}^{3+} \rightleftharpoons \text{LH}^- - \text{C}^{3+}$	$\text{LH} + \text{C}^{3+} \rightleftharpoons \text{LH}^- - \text{C}^{3+}$	$\text{LH} + \text{C}^{3+} \rightleftharpoons \text{LH}^- - \text{C}^{3+}$
2a	5.28 ± 0.02	4.80 ± 0.02	4.49 ± 0.02
2b	4.44 ± 0.04	3.74 ± 0.05	4.52 ± 0.03
2c	4.23 ± 0.04	4.34 ± 0.03	4.40 ± 0.03
2d	4.52 ± 0.04	4.19 ± 0.05	4.01 ± 0.07

2.3.4. Conclusion

A family of imidazo-anthraquinone probes (**2a-d**) was synthesized and characterized. Moreover, it was studied their interactions with ions via UV-visible, fluorescence and $^1\text{H-NMR}$ spectroscopy. Among the anions probed, F^- induced a clear deprotonation process of **2a-d** that was reflected in a red-shift of the absorption and in a moderate quenching of the emission intensities of the four probes. Other basic anions (AcO^- and H_2PO_4^-) induced moderated changes in the UV-visible and emission profiles of the probes. On the other hand, of all the cations tested, only Al^{3+} , Fe^{3+} and Cr^{3+} induced changes in the UV-visible and

fluorescence of **2a-d**. In particular, addition of trivalent cations to solutions of the four probes induced a remarkable blue shift of the absorption band and a partial quenching of the emission. The spectroscopic changes observed with Al^{3+} , Fe^{3+} and Cr^{3+} were ascribed to the formation of 1:1 (probe-cation) complexes. $^1\text{H-NMR}$ measurements suggested that trivalent cations coordinated with the donor part of the probes, i.e. the imidazole group. Receptors **2a-d** are rare dual probes able to be used as both anion (F^-) or cation (Al^{3+} , Fe^{3+} and Cr^{3+}) chemosensors.

2.3.5. Experimental section

Materials and methods:

General. TLC analyses were carried out on 0.25 mm thick precoated silica plates and spots were visualised under UV light. NMR spectra were obtained at an operating frequency of 300 or 400 MHz for ^1H and 75.4 MHz for ^{13}C using the solvent peak as internal reference at 25 °C. All chemical shifts are given in ppm using $\delta_{\text{H}} \text{Me}_4\text{Si} = 0$ ppm as reference and J values are given in Hz. Precursors **1a**, **1b**, **1d** and 1,2-diaminoanthraquinone are commercially available and were used as received.

Synthesis of formyl precursor **1c**

The synthesis of compound **1c** includes two steps: *i*) Suzuki-Miyaura cross-coupling to obtain the intermediate *1-methyl-2-phenyl-1H-pyrrole* followed by *ii*) Vilsmeier formylation to obtain the formyl precursor *1-methyl-5-phenyl-1H-pyrrole-2-carbaldehyde*.

i) Suzuki-Miyaura cross-coupling: To bromobenzene (0.112 g, 0.72 mmol) in DME (6 mL), 1-methyl-2-(4,4,5,5-tetramethyl-1,3,2-dioxaborolan-2-yl)-1H-pyrrole (0.193 g, 0.93 mmol, 1.3 equiv), $\text{Pd}(\text{PPh}_3)_4$ (0.050 g, 0.06 equiv.) and Na_2CO_3 2M (0.72 mL, 2 equiv) were added. The mixture was stirred at 80°C under an argon atmosphere during 15 hours until disappearance of the halide. The mixture was cooled to room temperature and a saturated solution of NaCl (10 mL) and ethyl acetate (30 mL) were added. The two phases were separated and the organic phase was extracted with ethyl acetate (3 x 20 mL), washed with water and then

with aqueous NaOH (10%), dried with anhydrous magnesium sulfate and evaporated to dryness. The obtained residue was purified by column chromatography, using mixtures of diethyl ether-light petroleum of increasing polarity and *1-methyl-2-phenyl-1H-pyrrole* was obtained as a yellow oil (0.085 g, 76%).

ii) Vilsmeier formylation: POCl₃ (0.079 mL, 1.20 mmol) was added to DMF (0.056 mL, 1.20 mmol) and the mixture was stirred for 15 min at 0 °C. *1-Methyl-2-phenyl-1H-pyrrole* (0.062 g, 0.39 mmol) dissolved in DMF (1 mL) was added dropwise with stirring. The mixture was heated for 2 h at 60 °C. The solution was then poured slowly into a saturated sodium acetate aqueous solution (5 mL) and stirred during 30 min. The organic layer was diluted with diethyl ether (20 mL), washed with saturated NaHCO₃ aqueous solution (10 mL), and dried with anhydrous MgSO₄. The organic extract was filtered, evaporated under reduced pressure and was purified by column chromatography, using mixtures of diethyl ether-light petroleum of increasing polarity, yielding *1-methyl-5-phenyl-1H-pyrrole-2-carbaldehyde* (**1c**) as colourless oil (0.073 g, 90%).⁴⁴ ¹H NMR (400 MHz, CDCl₃) δ = 6.31 (d, 1H, *J* = 4.0 Hz, H-4), 6.98 (d, 1H, *J* = 4.0 Hz, H-3), 7.40–7.47 (m, 5H, H-2', H-3', H-4', H-5' and H-6'), 9.59 (s, 1H, CHO) ppm.

General procedure for the synthesis of imidazoanthraquinones **2a-d**

i) Preparation of the imines: The aldehydes **1a-d** (0.20 mmol) and 1,2-diaminoanthraquinone (0.24 mmol) were dissolved separately in ethanol (4 mL/mmol). The ethanolic solution of aldehyde and formic acid (0.04 mL/mmol of aldehyde) was added to the solution of 1,2-diaminoanthraquinone heated at reflux. The reaction mixture was heated under reflux overnight.

ii) Cyclisation of the imines: After cooling, the ethanolic solution was evaporated and the crude imine was dissolved in a small volume of acetic acid (5 mL/mmol of imine). To this solution, lead tetraacetate was added (0.20 mmol) and the mixture was stirred overnight at room temperature. The mixture was poured into water (20 mL) and extracted with chloroform (2x50 mL). The organic layer was dried with magnesium sulphate and evaporated under reduced pressure

to give compounds **2a-d**, which were purified by column chromatography on silica with chloroform as eluent.

2-([1',1''-Biphenyl]-4'-yl)-1H-anthra[1,2-d]imidazole-6,11-dione (2a): Yellow solid (55 mg, 65%). Mp: 267–269 °C (269–270 °C).⁴⁵ ¹H NMR (400 MHz, DMSO-*d*₆) δ = 7.40–7.44 (m, 1H), 7.49–7.53 (m, 2H), 7.79 (dd, 2H, *J* = 8.4 and 1.2 Hz), 7.87 (d, 2H, *J* = 8.4 Hz), 7.91–7.95 (m, 2H), 8.07–8.14 (m, 2H), 8.19–8.24 (m, 2H), 8.52 (d, 2H, *J* = 8.0 Hz), 13.23 (s, 1H) ppm.

2-(5'-Phenylthiophen-2'-yl)-1H-anthra[1,2-d]imidazole-6,11-dione (2b): Orange solid (53 mg, 71%). Mp: 269–271 °C. ¹H NMR (300 MHz, DMSO-*d*₆) δ = 7.34–7.39 (m, 1H), 7.43–7.48 (m, 2H), 7.63 (d, 1H, *J* = 3.9 Hz), 7.74 (d, 2H, *J* = 7.2 Hz), 7.86–7.93 (m, 2H), 8.02 (s, 2H), 8.15–8.21 (m, 2H), 8.50 (d, 1H, *J* = 3.9 Hz), 13.38 (s, 1H) ppm. ¹³C NMR (75.4 MHz, DMSO-*d*₆) δ = 118.3, 121.2, 124.3, 125.2, 125.7, 126.2, 126.8, 127.9, 128.6, 129.3, 131.3, 131.6, 132.8, 132.9, 133.0, 133.1, 134.2, 134.4, 147.4, 149.2, 152.7, 182.2, 183.1 ppm. MS (FAB) *m/z* (%): 407 ([M+H]⁺, 25), 406 (M⁺, 9), 307 (33), 289 (17), 166 (13), 155 (30), 154 (100). HRMS: (FAB) *m/z* (%) for C₂₅H₁₅N₂O₂S; calcd 407.0854; found 407.0847.

2-(1'-Methyl-5'-phenyl-1H-pyrrol-2'-yl)-1H-anthra[1,2-d]imidazole-6,11-dione (2c): Dark red solid (24 mg, 32%). Mp: 246–248 °C. ¹H NMR (400 MHz, DMSO-*d*₆) δ = 4.08 (s, 3H), 6.39 (d, 1H, *J* = 4.0 Hz), 7.39–7.44 (m, 1H), 7.48–7.56 (m, 4H), 7.59 (d, 1H, *J* = 4.0 Hz), 7.88–7.93 (m, 2H), 8.04 (s, 2H), 8.19–8.24 (m, 2H), 12.74 (s, 1H) ppm. ¹³C NMR (100.6 MHz, DMSO-*d*₆) δ = 35.2, 109.8, 115.5, 117.7, 121.0, 123.3, 123.8, 126.2, 126.8, 127.3, 127.8, 128.7, 128.9, 131.9, 132.3, 133.1, 133.3, 134.2, 134.4, 140.2, 149.8, 152.3, 182.2, 183.2 ppm. HRMS: (FAB) *m/z* (%) for C₂₆H₁₇N₃O₂; calcd 403.1321; found 403.1307.

2-(5'-Phenylfuran-2'-yl)-1H-anthra[1,2-d]imidazole-6,11-dione (2d): Dark orange solid (38 mg, 33%). Mp: 250–252 °C. ¹H NMR (400 MHz, DMSO-*d*₆) δ = 7.22 (d, 1H, *J* = 4.0 Hz), 7.38 (t, 1H, *J* = 8.0 Hz), 7.50 (t, 2H, *J* = 8.0 Hz), 7.84 (d, 1H, *J* = 4.0 Hz), 7.87–7.89 (m, 2H), 7.94 (d, 2H, *J* = 8.0 Hz), 8.01–8.06 (m, 2H), 8.15–8.19 (m, 2H), 13.27 (s, 1H) ppm. ¹³C NMR (100.6 MHz, DMSO-*d*₆) δ = 108.5, 116.7, 118.5, 121.2, 124.3, 124.6, 126.2, 126.8, 128.0, 128.6, 129.0, 129.3, 132.4, 133.0, 133.1,

134.2, 134.5, 143.6, 149.1, 149.5, 155.7, 182.2, 183.1 ppm. HRMS: (FAB) m/z (%) for $C_{25}H_{14}N_2O_3$; calcd 390.1004; found 390.0986.

Physical measurements:

Stock solutions of the anions (F^- , Cl^- , Br^- , I^- , OCN^- , BzO^- , ClO_4^- , AcO^- , HSO_4^- , $H_2PO_4^-$ and CN^- as tetrabutylammonium salts) and cations ($Cu(ClO_4)_2 \cdot 6H_2O$, $Co(ClO_4)_2 \cdot 6H_2O$, $Mg(ClO_4)_2$, $Fe(ClO_4)_3 \cdot xH_2O$, $Ba(ClO_4)_2$, $Fe(ClO_4)_2 \cdot xH_2O$, $Ni(ClO_4)_2 \cdot 6H_2O$, $Ca(ClO_4)_2 \cdot 4H_2O$, $Zn(ClO_4)_2 \cdot 6H_2O$, $Pb(ClO_4)_2 \cdot xH_2O$, $Cd(ClO_4)_2 \cdot xH_2O$, $Cr(ClO_4)_3 \cdot 6H_2O$, $Al(ClO_4)_3 \cdot 9H_2O$, $KClO_4$ and $LiClO_4$) were prepared at 10^{-3} mol dm^{-3} in acetonitrile. The concentrations of ligands used in spectroscopy measurements were ca. 1×10^{-4} and 1×10^{-5} mol dm^{-3} . The quantity of anion solutions added did not exceed 10% of the volume of the compounds **2a-d** to avoid relevant changes in the total solution concentration. For the probes that required the addition of excess of ions (30 equiv.), corrections of the volume and concentration were made. The UV-Vis and fluorescence titrations were measured at room temperature (25 °C).

Theoretical studies:

Quantum chemical calculations were carried out in vacuum with Hyperchem V6.03 with a semi-empirical level (PM3, within restricted Hartree–Fock level). For optimization, it was used the Polar–Ribiere algorithm. The convergence limit and the RMS gradient were set to 0.01 kcal mol^{-1} . Stability constants, were calculated with the HypSpec Software V1.1.18 and using the data of the titration of receptors with target anions and cations.

2.3.6. Acknowledgements

We thank the Spanish Government (project MAT2012-38429-C04) for support. C. Marín-Hernández thanks the Spanish Ministry of Economy and Competitiveness for her grant. We also gratefully acknowledge financial support from Fundación Carolina and UPNFM-Honduras for a pre-doctoral grant to L. E. Santos-Figueroa and from Spanish Ministry of Science and

Innovation for a FPU grant to M. E. Moragues. Thanks are also given to the Fundação para a Ciência e Tecnologia (Portugal) and FEDER-COMPETE for financial support through the Centro de Química - Universidade do Minho, Project PEst-C/QUI/ UI0686/2013 (FCOMP-01-0124-FEDER-037302) and a Post-doctoral grant to R.M.F. Batista (SFRH/BPD/79333/2011).

2.3.7. Supporting information

Supporting information: ^1H NMR spectra of compounds **1c** and **2a**, ^1H and ^{13}C spectra of probes **2b**, **2c** and **2d**. UV-Vis and emission titration profiles. Cartesian coordinates of the optimized geometries. This material is available free of charge via the Internet at <http://pubs.acs.org/>.

2.3.8. References and footnotes

- 1 Kaur, K.; Saini, R.; Kumar, A.; Luxami, V.; Kaur, N.; Singh, P.; Kumar, S. *Coord. Chem. Rev.* **2012**, *256*, 1992-2028.
- 2 (a) Rurack, K. *Spectrochim. Acta, Part A* **2001**, *57A*, 2161-2195. (b) Lloris, J. M.; Martínez-Mañez, R.; Padilla-Tosta, M. E.; Pardo, T.; Soto, J.; Beer, P. D.; Cadman, J.; Smith, D. K. *J. Chem. Soc., Dalton Trans.* **1999**, *14*, 2359-2369.
- 3 Miyaji, H.; Sessler, J. L. *Angew. Chem. Int. Ed.* **2001**, *40*, 154-157.
- 4 (a) Yuan, L.; Lin, W.; Zheng, K.; Zhu, S. *Acc. Chem. Res.* **2013**, *46*, 1462-1473. (b) Doussineau, T.; Schulz, A.; Lapresta-Fernandez, A.; Moro, A.; Körsten, S.; Trupp, S.; Mohr, G. J. *Chem. Eur. J.* **2010**, *16*, 10290-10299. (c) Wang, S.; Li, N.; Pan, W.; Tang, B. *Trends Anal. Chem.* **2012**, *39*, 3-37.
- 5 See for example: (a) Kaur, N.; Kumar, S. *Tetrahedron* **2011**, *67*, 9233-9264. (b) Prodi, L.; Montalti, M.; Zaccheroni, N.; Dolci, L. S. *Top. Fluoresc. Spec.* **2005**, *9*, 1-57. (c) Fabbrizzi, L.; Poggi, A. *Chem. Soc. Rev.* **1995**, *24*, 197-202. (d) Okamoto, K.; Araki, Y.; Ito, O.; Fukuzumi, S. *J. Am. Chem. Soc.* **2004**, *126*, 56-57. (e) Okamoto, K.; Fukuzumi, S. *J. Am. Chem. Soc.* **2004**, *126*, 13922-13923.
- 6 (a) Suksai, C.; Tuntulani, T. *Chem. Soc. Rev.* **2003**, *32*, 192-202. (b) Snowden, T. S.; Ansyn, E. V. *Curr. Opin. Chem. Biol.* **1999**, *3*, 740-746. (c) Wiskur, S. L.; Ait-Haddou, H.; Lavigne, J. J.; Ansyn, E. V. *Acc. Chem. Res.* **2001**, *34*, 963-972. (d) Fukuzumi, S.; Ohkubo, K.; D'Souza, F.; Sessler, J. L. *Chem. Commun.* **2012**, *48*, 9801-9815.
- 7 Beer, P. D.; Gale, P. A. *Angew. Chem. Int. Ed.* **2001**, *40*, 486-516.

- 8 (a) Santos-Figueroa, L. E.; Moragues, M. E.; Climent, E.; Agostini, A.; Martínez-Máñez, R.; Sancenón, F. *Chem. Soc. Rev.* **2013**, *42*, 3489-3613. (b) Moragues, M. E.; Martínez-Máñez, R.; Sancenón, F. *Chem. Soc. Rev.* **2011**, *40*, 2593-2643.
- 9 Martínez-Máñez, R.; Sancenón, F. *Chem. Rev.* **2003**, *103*, 4419-4476.
- 10 (a) Schug, K. A.; Lindner, W. *Chem. Rev.* **2005**, *105*, 67-113. (b) Blondeau, P.; Segura, M.; Pérez-Fernández, R.; de Mendoza, J. *Chem. Soc. Rev.* **2007**, *36*, 198-210. (c) Gale, P. A.; García-Garrido, S. E.; Garric, J. *Chem. Soc. Rev.* **2008**, *37*, 151-190. (d) Steed, J. W. *Chem. Soc. Rev.* **2009**, *38*, 506-519.
- 11 (a) Dydio, P.; Lichosyt, D.; Jurczak, J. *Chem. Soc. Rev.* **2011**, *40*, 2971-2985. (b) Sessler, J. L.; Camiolo, S.; Gale, P. A. *Coord. Chem. Rev.* **2003**, *240*, 17-55. (c) Bondy, C. R.; Loeb, S. J. *Coord. Chem. Rev.* **2003**, *240*, 77-99. (d) Choi, K.; Hamilton, A. D. *Coord. Chem. Rev.* **2003**, *240*, 101-110.
- 12 (a) Yoon, J.; Kim, S. K.; Singh, N. J.; Kim, K. S. *Chem. Soc. Rev.* **2006**, *35*, 355-360. (b) Xu, Z.; Kim, S. K.; Yoon, J. *Chem. Soc. Rev.* **2010**, *39*, 1457-1466.
- 13 (a) Raposo, M. M. M.; García-Acosta, B.; Ábalos, T.; Calero, P.; Martínez-Máñez, R.; Ros-Lis, J. V.; Soto, J. *J. Org. Chem.* **2010**, *75*, 2922-2933. (b) Santos-Figueroa, L. E.; Moragues, M. E.; Raposo, M. M. M.; Batista, R. M. F.; Costa, S. P. G.; Ferreira, R. C. M.; Sancenón, F.; Martínez-Máñez, R.; Ros-Lis, J. V.; Soto, J. *Org. Biomol. Chem.* **2012**, *10*, 7418-7428.
- 14 Winter, W. E.; Bazydło, L. A.; Harris, N. S. *Lab. Med.* **2014**, *45*, 92-102.
- 15 von Haehling, S.; Anker, S. D. *Dtsch. Med. Wochenschr.* **2014**, *139*, 841-844.
- 16 (a) Perl, D.; Brody, A. *Science* **1980**, *208*, 297-299. (b) Belojevic, G.; Jakovljevic, B. *Srp. Arh. Celok. Lek.* **1998**, *126*, 283-289. (c) Perl, D.; Gajdusek, D.; Garruto, R.; Yanagihara, R.; Gibbs, C. *Science* **1982**, *217*, 1053-1055.
- 17 Mertz, W. *J. Nutr.* **1993**, *123*, 626-633.
- 18 Wallach, S. *J. Am. Coll. Nutr.* **1985**, *4*, 107-120.
- 19 Szczygiel, J.; Dyrek, K.; Kruczala, K.; Bidzinska, E.; Brozek-Mucha, Z.; Wenda, E.; Wieczorek, J.; Szymonska, J. *J. Phys. Chem. B* **2014**, *118*, 7100-7107.
- 20 (a) Langdon-Jones, E. E.; Pope, S. J. A. *Coord. Chem. Rev.* **2014**, *269*, 32-53. (b) Batista, R. M. F.; Costa, S. P. G.; Raposo, M. M. M. *Sensors Act. B Chem.* **2014**, *191*, 791-799. (c) Batista, R. M. F.; Oliveira, E.; Costa, S. P. G.; Lodeiro, C.; Raposo, M. M. M. *Supramol. Chem.* **2014**, *26*, 71-80. (d) Saini, R.; Kaur, N.; Kumar, S. *Tetrahedron* **2014**, *70*, 4285-4307.

- 21 (a) Stathopoulou, K.; Valianou, L.; Skaltsounis, A. –L.; Karapanagiotis, I.; Magiatis, P. *Anal. Chim. Acta* **2013**, *804*, 264-272. (b) Shindy, H. A. *Mini-Rev. Org. Chem.* **2012**, *9*, 361-373.
- 22 (a) De Almeida, D. P.; Gomide, J. L. *Papel* **2013**, *74*, 53-56. (b) Song, W.; Liu, J. *J. Chem. Pharm. Res.* **2013**, *5*, 1217-1221. (c) Alfaro, A.; López, F.; Pérez, A.; García, J. C.; Pelach, M. A.; Mutje, P. *Cell. Chem. Technol.* **2013**, *47*, 765-775.
- 23 (a) Chen, M.; Zhang, C.; Shen, Y.; Zu, G. *Adv. Mater. Res.* **2013**, *610-613*, 9-14. (b) Gomes, A. C.; Nunes, J. C.; Simoes, R. M. S. *J. Hazard. Mater.* **2010**, *178*, 57-65.
- 24 (a) Zhu, H.; Yang, Y.; Hyeon-Deuk, K.; Califano, M.; Song, N.; Wang, Y.; Zhang, W.; Prezhdo, O. V.; Lian, T. *Nano Lett.* **2014**, *14*, 1263-1269. (b) Rabache, V.; Chaste, J.; Petit, P.; Della Rocca, M. L.; Martin, P.; Lacroix, J. –C.; McCreery, R. L.; Lafarge, P. *J. Am. Chem. Soc.* **2013**, *135*, 10218-10221. (c) Darwish, N.; Díez-Pérez, I.; Da Silva, P.; Tao, N.; Gooding, J. J.; Paddon-Row, M. N. *Angew. Chem. Int. Ed.* **2012**, *51*, 3203-3206.
- 25 (a) Liu, Z.; Wei, F.; Chen, L. –J.; Xiong, H. –R.; Liu, Y. –Y.; Luo, F.; Hou, W.; Xiao, H.; Yang, Z. –Q. *Molecules* **2013**, *18*, 11842-11858. (b) Li, D.; Zhang, N.; Cao, Y.; Zhang, W.; Su, G.; Sun, Y.; Liu, Z.; Li, F.; Liang, D.; Liu, B.; Guo, M.; Fu, Y.; Zhang, X.; Yang, Z. *Eur. J. Pharm.* **2013**, *705*, 79-85.
- 26 (a) Claes, P.; Cappoen, D.; Uythethofken, C.; Jacobs, J.; Mertens, B.; Mathys, V.; Verschaeve, L.; Huygen, K.; De Kimpe, N. *Eur. J. Med. Chem.* **2014**, *77*, 409-421. (b) Yildiz, E.; Keles, M.; Kaya, A.; Dincer, S. *Chem. Sci. Trans.* **2013**, *2*, 547-555. (c) Kardong, D.; Upadhyaya, S.; Salkia, L. R. *J. Pharm. Res.* **2013**, *6*, 179-182.
- 27 Patil, A. G.; Joshi, K. A.; Patil, D. A.; Phatak, A. V.; Naresh, C. *Pharmacogn. J.* **2009**, *1*, 267-272.
- 28 (a) Ayo, R. G. *J. Med. Plants Res.* **2010**, *4*, 1339-1348. (b) Ee, G. L. C.; Ng, K. N. *As. J. Chem.* **2004**, *16*, 429-433.
- 29 (a) Shah, A.; Varma, O.; Patankar, S.; Kadam, V. *Curr. Bioact. Comp.* **2013**, *9*, 288-305. (b) Khamthong, N.; Rukachaisirikul, V.; Phongpaichit, S.; Preedanon, S.; Sakayaroj, J. *Tetrahedron* **2012**, *68*, 8245-8250.
- 30 (a) Abdissa, N.; Induli, M.; Akala, H. M.; Heydenreich, M.; Midiwo, J. O.; Ndakala, A.; Yenesew, A. *Phytochem. Lett.* **2013**, *6*, 241-245. (b) Choomuenwai, V.; Andrews, K. T.; Davis, R. A. *Bioorg. Med. Chem.* **2012**, *20*, 7167-7174.
- 31 (a) Shrestha, J. P.; Fosso, M. Y.; Bearss, J.; Chang, C. –W. T. *Eur. J. Med. Chem.* **2014**, *77*, 96-102. (b) Wei, W. –T.; Lin, S. –Z.; Liu, D. –L.; Wang, Z. –H. *Oncol. Rep.* **2013**, *30*, 2555-2562.

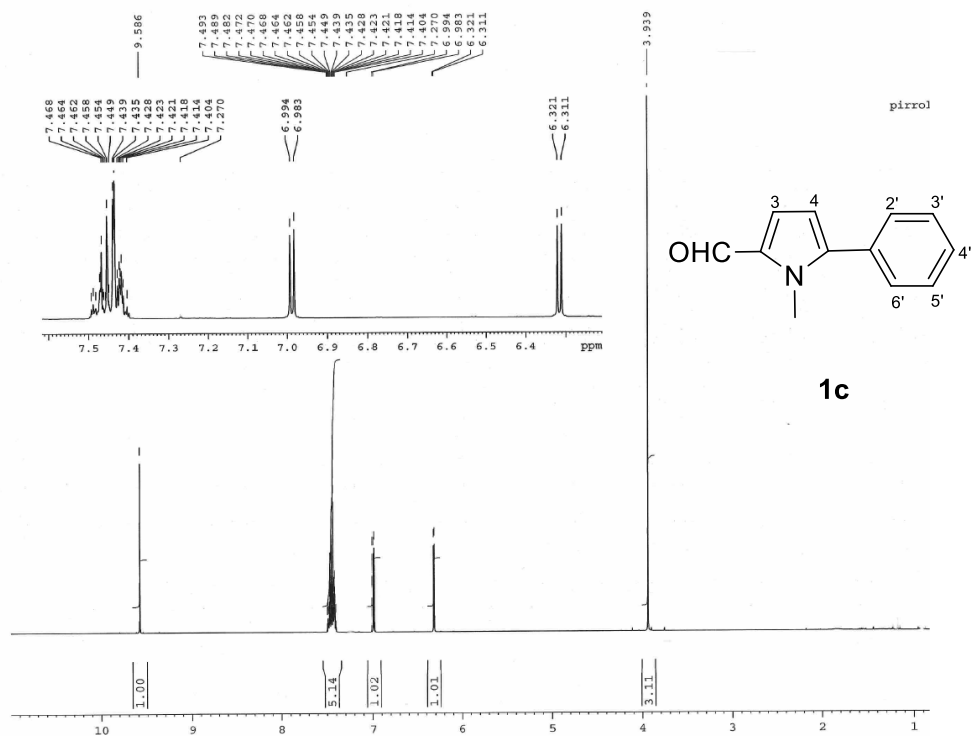
- 32 See for example: (a) Agostini, A.; Campos, I.; Milani, M.; Elsayed, S.; Pascual, L.; Martínez-Máñez, R.; Licchelli, M.; Sancenón, F. *Org. Biomol. Chem.* **2014**, *12*, 1871-1874. (b) Climent, E.; Mondragón, L.; Martínez-Máñez, R.; Sancenón, F.; Marcos, M. D.; Murguía, J. R.; Amorós, P.; Rurack, K.; Pérez-Payá, E. *Angew. Chem. Int. Ed.* **2013**, *52*, 8939-8942. (c) Santos-Figueroa, L. E.; Giménez, C.; Agostini, A.; Aznar, E.; Marcos, M. D.; Sancenón, F.; Martínez-Máñez, R.; Amorós, P. *Angew. Chem. Int. Ed.* **2013**, *52*, 13712-13716. (d) Climent, E.; Gröninger, D.; Hecht, M.; Walter, M. A.; Martínez-Máñez, R.; Weller, M. G.; Sancenón, F.; Amorós, P.; Rurack, K. *Chem. Eur. J.* **2013**, *19*, 4117-4122. (e) Moragues, M. E.; Esteban, J.; Ros-Lis, J. V.; Martínez-Máñez, R.; Marcos, M. D.; Martínez, M.; Soto, J.; Sancenón, F. *J. Am. Chem. Soc.* **2011**, *133*, 15762-15772. (f) Climent, E.; Marcos, M. D.; Martínez-Máñez, R.; Sancenón, F.; Soto, J.; Rurack, K.; Amorós, P. *Angew. Chem. Int. Ed.* **2009**, *48*, 8519-8522.
- 33 Saha, S.; Ghosh, A.; Mahato, P.; Mishra, S.; Mishra, S. K.; Suresh, E.; Das, S.; Das, A. *Org. Lett.* **2010**, *12*, 3406-3409.
- 34 Amendola, V.; Esteban-Gómez, D.; Fabbrizzi, L.; Licchelli, M. *Acc. Chem. Res.* **2006**, *39*, 343-353.
- 35 (a) Moragues, M. E.; Santos-Figueroa, L. E.; Ábalos, T.; Sancenón, F.; Martínez-Máñez, R. *Tetrahedron Lett.* **2012**, *53*, 5110-5113. (b) Batista, R. M. F.; Oliveira, E.; Costa, S. P. G.; Lodeiro, C.; Raposo, M. M. M. *Tetrahedron* **2011**, *67*, 7106-7113. (c) Santos-Figueroa, L. E.; Moragues, M. E.; Batista, R. M. F.; Costa, S. P. G.; Raposo, M. M. M.; Ferreira, R. C. M.; Sancenón, F.; Martínez-Máñez, R.; Ros-Lis, J. V.; Soto, J. *Tetrahedron* **2012**, *68*, 7179-7186. (d) Aldrey, A.; Núñez, C.; García, V.; Bastida, R.; Lodeiro, C.; Macías, A. *Tetrahedron* **2010**, *66*, 9223-9230. (e) Atta, A. K.; Ahn, I. -H.; Hong, A. -Y.; Heo, J.; Kim, C. K.; Cho, D. -G. *Tetrahedron Lett.* **2012**, *53*, 575-578. (f) Amendola, V.; Fabbrizzi, L.; Mosca, L.; Schmidtchen, F. -P. *Chem. Eur. J.* **2011**, *17*, 5972-5981. (g) Amendola, V.; Bergamaschi, G.; Boiocchi, M.; Fabbrizzi, L.; Milani, M. *Chem. Eur. J.* **2010**, *16*, 4368-4380.
- 36 Bordwell, F. G. *Acc. Chem. Res.* **1988**, *21*, 456-463. The pK_a of acetic and hydrofluoric acids in DMSO are 12.3 and 15.2, respectively. Taking into account this value, fluoride is a stronger base than acetate in organic solvents and the extension of the proton shift observed with the former anion is larger than the observed for the later.
- 37 Batista, R. M. F.; Oliveira, E.; Costa, S. P. G.; Lodeiro, C.; Raposo, M. M. M. *Org. Lett.* **2007**, *9*, 3201-3204.

- 38 Peng, X.; Wu, Y.; Fan, J.; Tian, M.; Han, K. *J. Org. Chem.* **2005**, *70*, 10524-10531.
- 39 Li, G. -Y.; Zhao, G. -J.; Liu, Y. -H.; Han, K. -L.; He, G. Z. *J. Comput. Chem.* **2010**, *31*, 1759-1765.
- 40 HyperChem 6.03 Molecular Modeling System, Hypercube Inc, Gainsville, Florida, USA.
- 41 (a) Kumari, N.; Jha, S.; Bhattacharya, S. *J. Org. Chem.* **2011**, *76*, 8215-8222. (b) Batista, R. M. F.; Costa, S. P. G.; Raposo, M. M. M. *J. Photochem. Photobiol. A* **2013**, *259*, 33-40.
- 42 (a) Chawla, H. M.; Shukla, R.; Shubha, P. *Tetrahedron Lett.* **2012**, *53*, 2996-2999. (b) Yang, H.; Zhou, Z. -G.; Xu, J.; Li, F. -Y.; Yi, T.; Huang, C. -H. *Tetrahedron* **2007**, *63*, 6732-6736. (c) Yoshida, K.; Mori, T.; Watanabe, S.; Kawai, H.; Nagamura, T. *J. Chem. Soc., Perkin Trans. 2* **1999**, 393-398.
- 43 Valeur, B.; Leray, I. *Coord. Chem. Rev.* **2000**, *205*, 3-40.
- 44 Carson, J. R.; Jetter, M. C.; Lee, J. S.; Youngman M. A. *U. S. Pat..Appl. Publ.* **2004**, US 20040192720 A1 20040930.
- 45 da Silva, E. N.; Guimaraes, T. T.; Menna-Barreto, R. R. S.; Pinto, M. D. F. R.; de Simone, C. A.; Pessoa, C.; Cavalcanti, B. C.; Sabino, J. R.; Andrade, C. K. Z.; Goulart, M. O. F.; de Castro, S. L.; Pinto, A. V. *Bioorg. Med. Chem.* **2010**, *18*, 3224-3230.

SUPPORTING INFORMATION

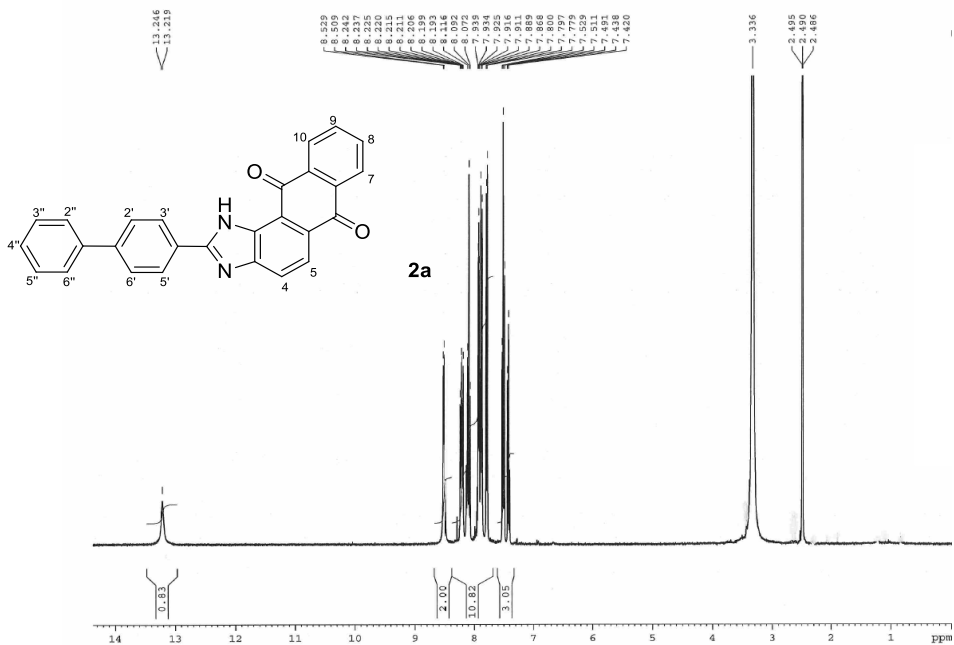
Imidazo Imidazoanthraquinones derivatives for the chromo-fluorogenic sensing of basic anions and trivalent metal cations

Cristina Marín-Hernández, Luis E. Santos-Figueroa, María E. Moragues, M. Manuela M. Raposo, Rosa M. F. Batista, Susana P. G. Costa, Teresa Pardo, Ramón Martínez-Máñez* and Félix Sancenón

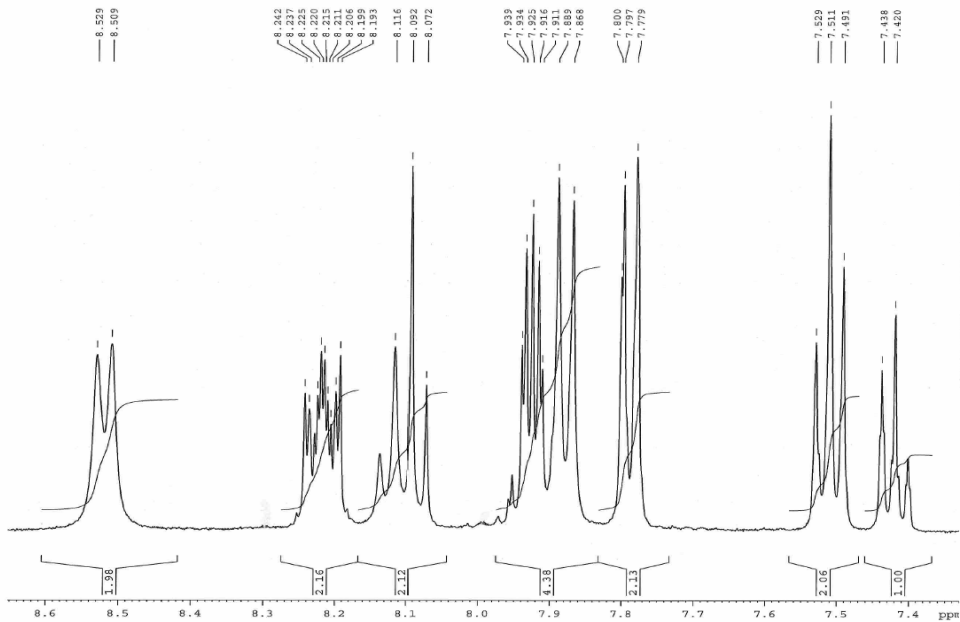
¹H spectra of compound 1c**¹H NMR and expansion of aromatic zone**

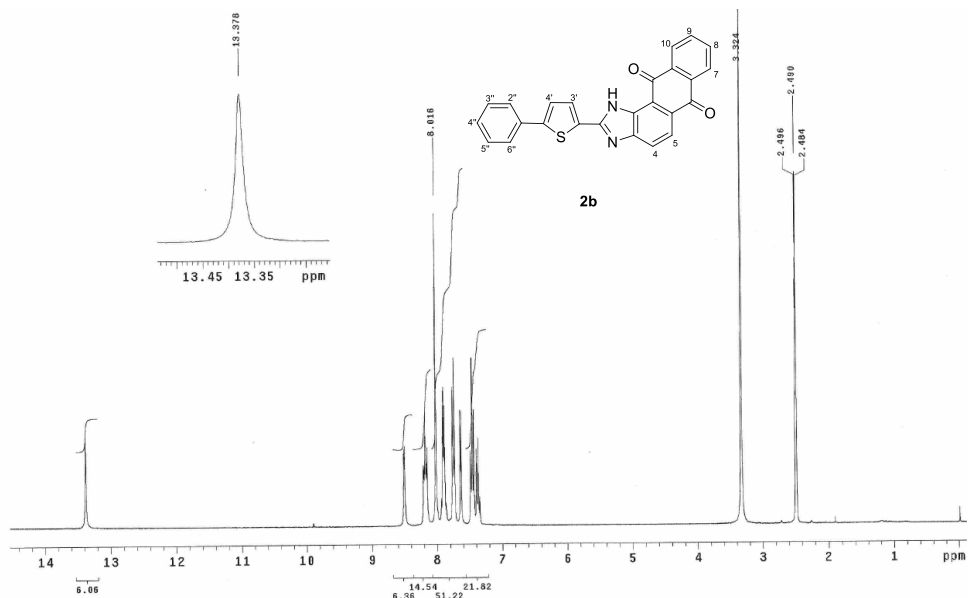
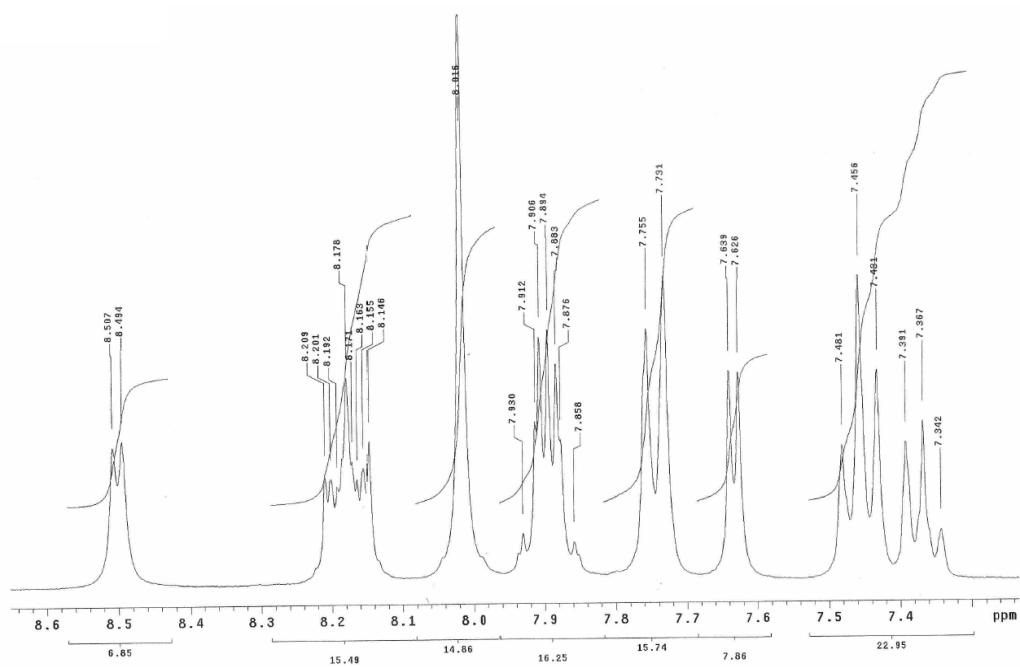
¹H spectra of compound 2a

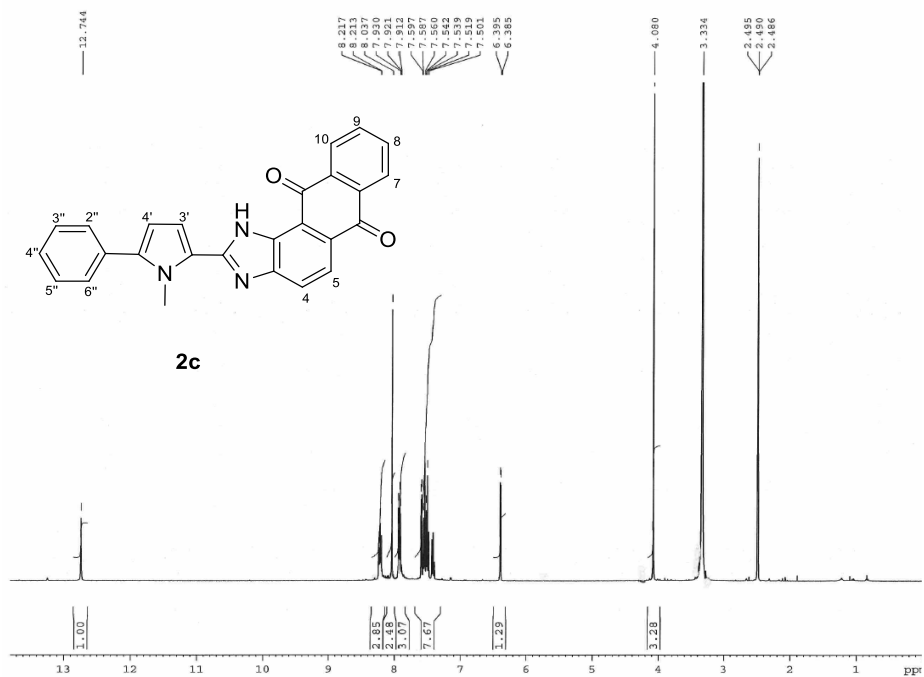
¹H NMR



Expansion of aromatic zone

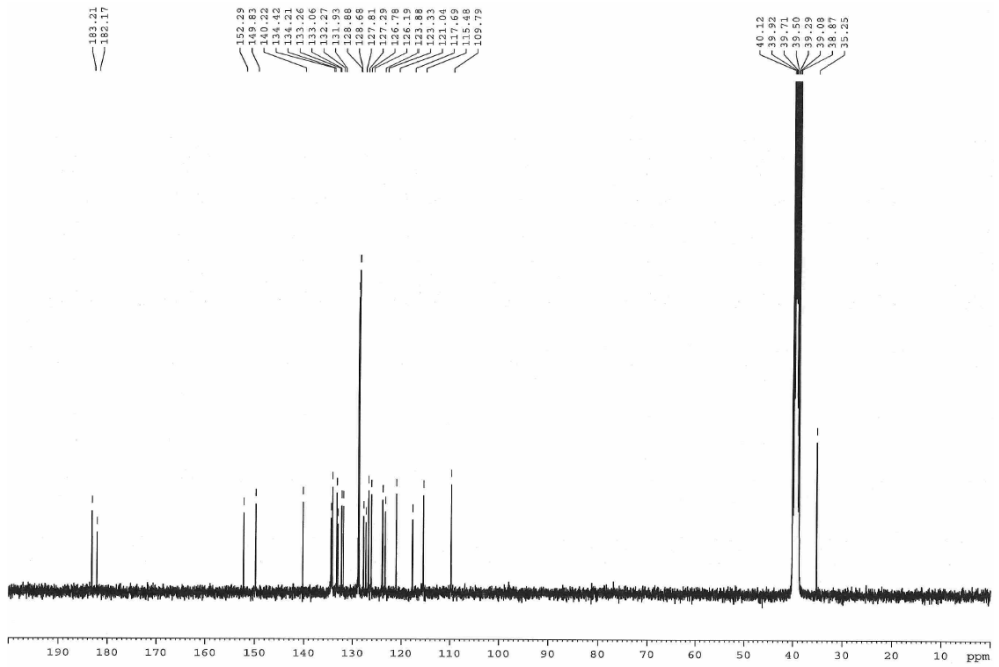


^1H and ^{13}C NMR spectra of compound 2b **^1H NMR****Expansion of aromatic zone**

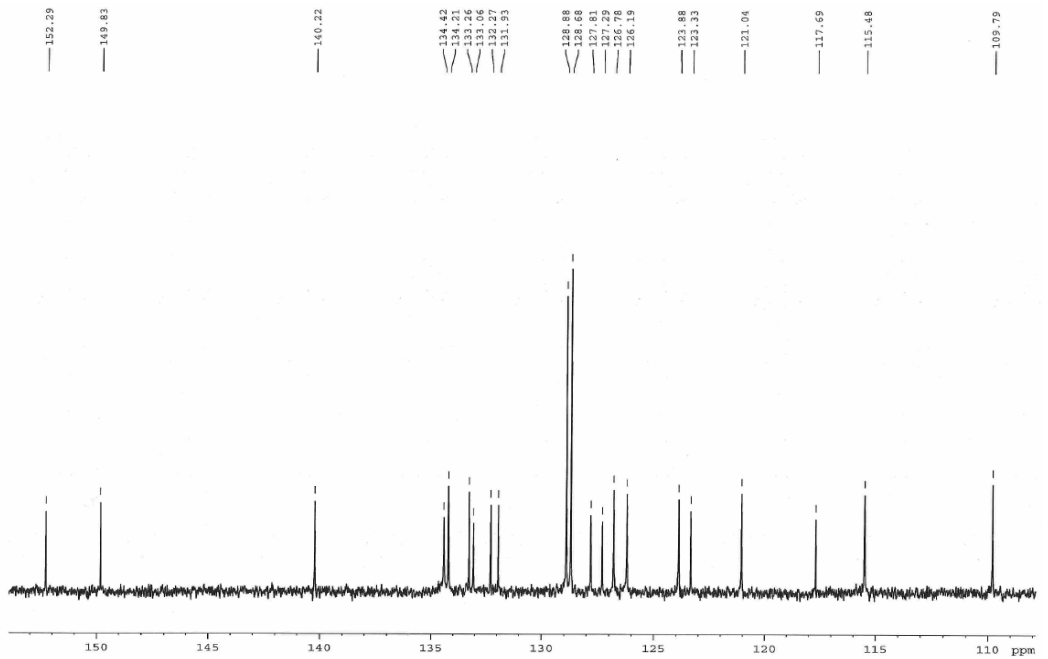
^1H and ^{13}C NMR spectra of compound **2c** ^1H NMR

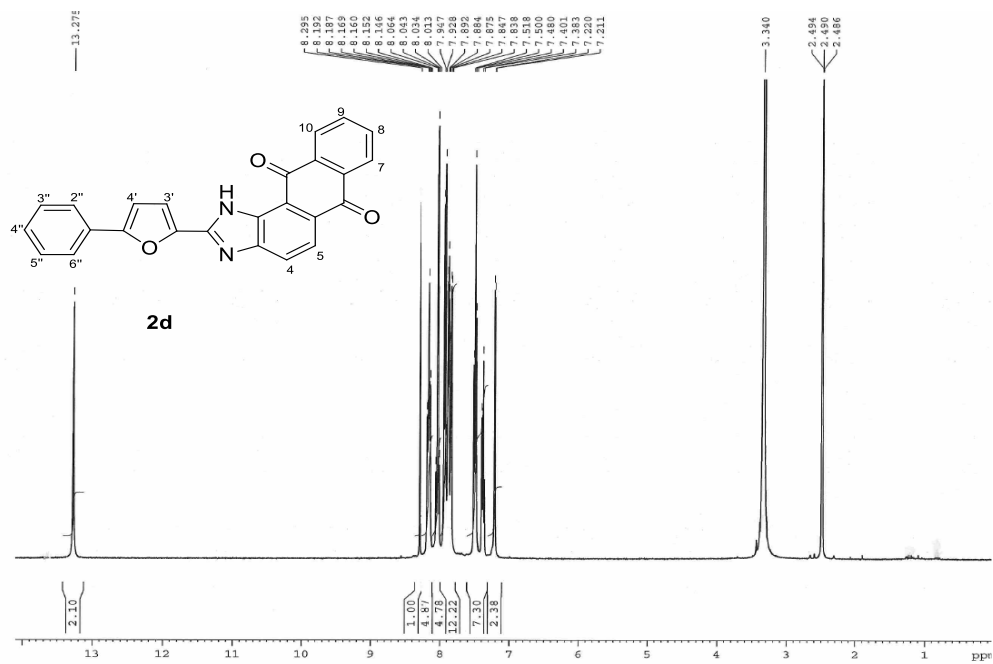
Chapter 2

¹³C NMR

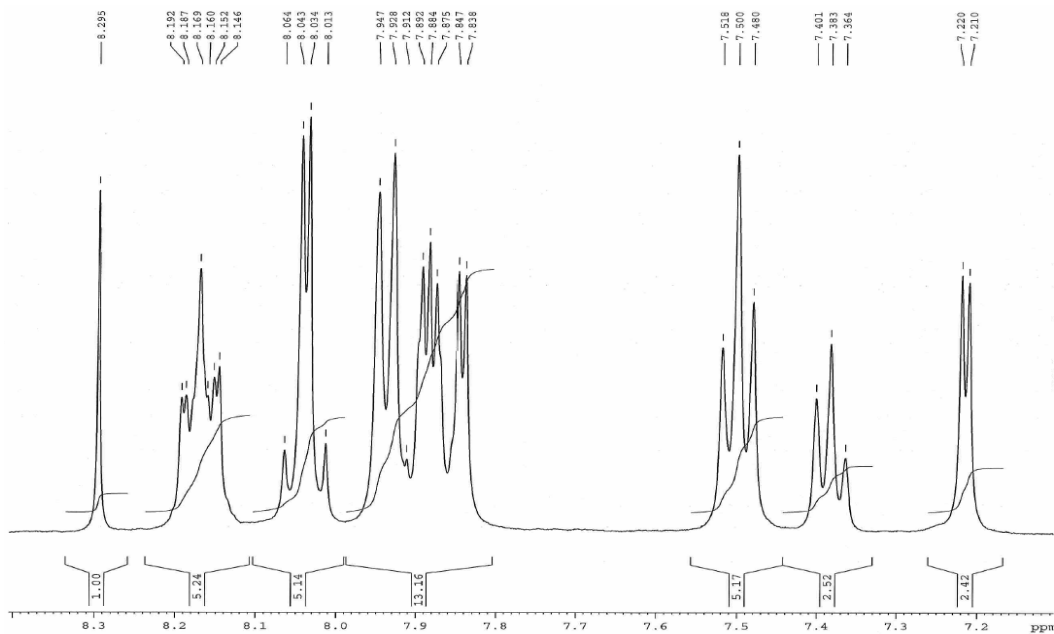


Expansion of aromatic zone



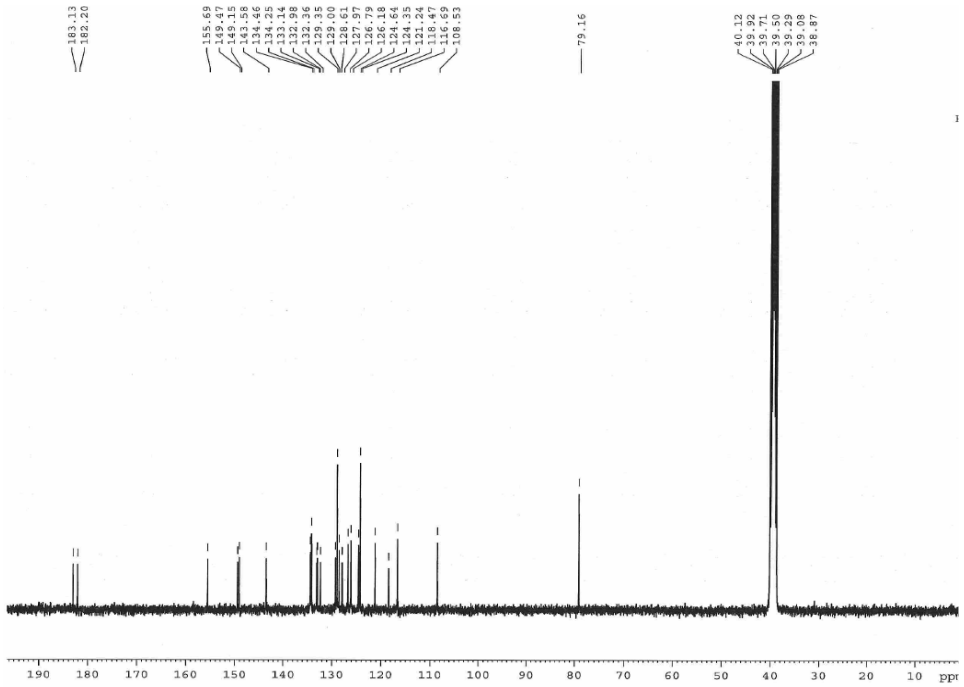
^1H and ^{13}C NMR spectra of compound **2d** ^1H NMR

Expansion of aromatic zone

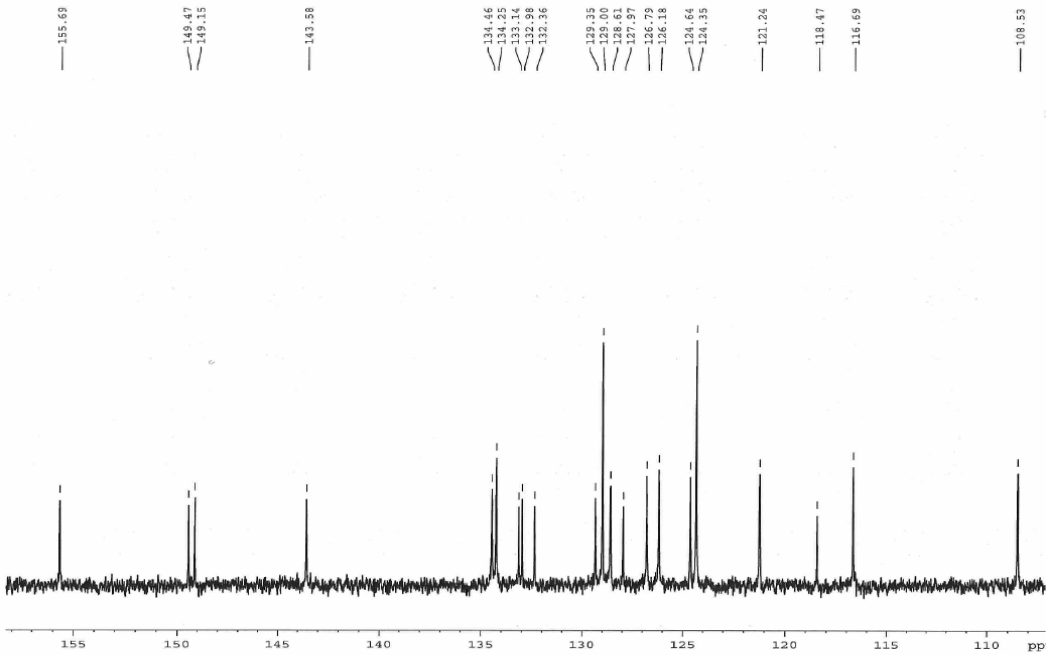


Chapter 2

^{13}C NMR



Expansion of aromatic zone



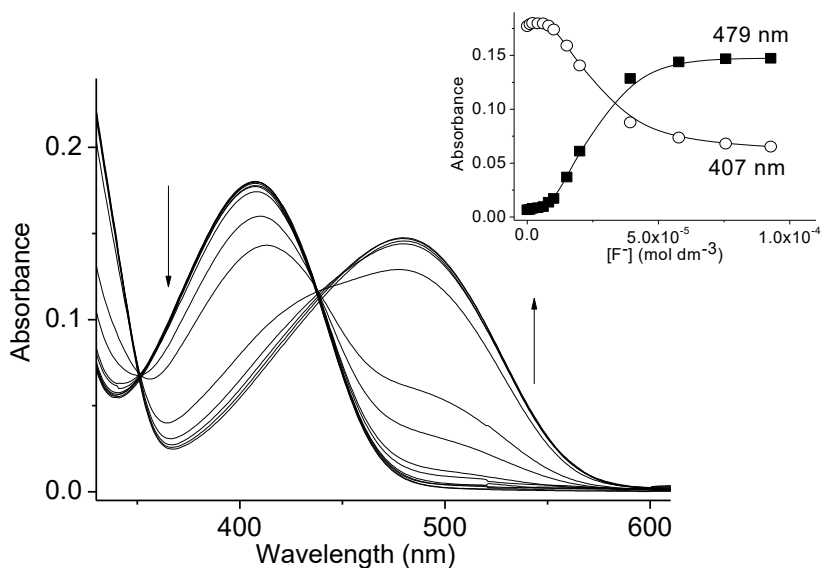


Figure SI-3.2.1. UV-Vis titration profiles of receptor **2a** (1.0×10^{-5} mol dm^{-3} in acetonitrile) obtained upon the addition of F^- anion.

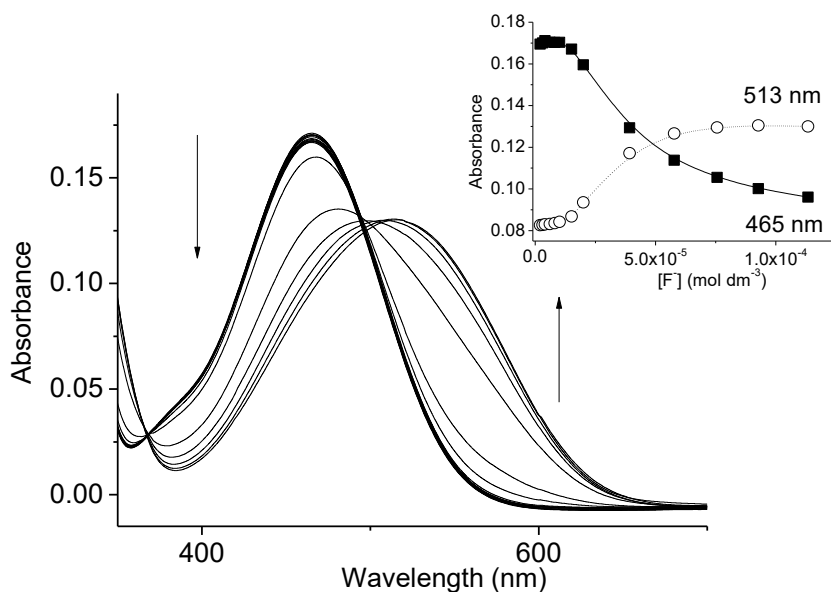


Figure SI-3.2.2. UV-Vis titration profiles of receptor **2c** (1.0×10^{-5} mol dm^{-3} in acetonitrile) obtained upon the addition of F^- anion.

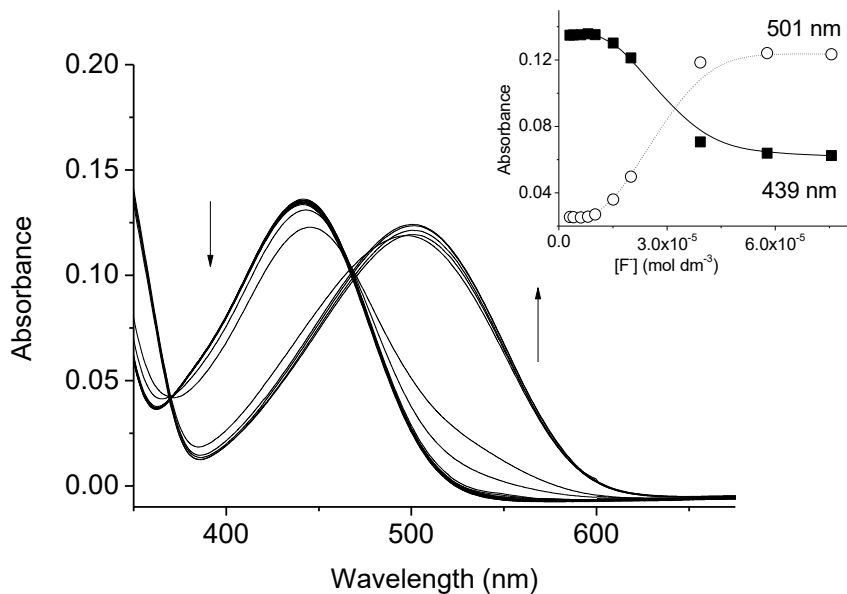


Figure SI-2.3.3. UV-Vis titration profiles of receptor **2d** ($1.0 \times 10^{-5} \text{ mol dm}^{-3}$ in acetonitrile) obtained upon the addition of F^- anion.

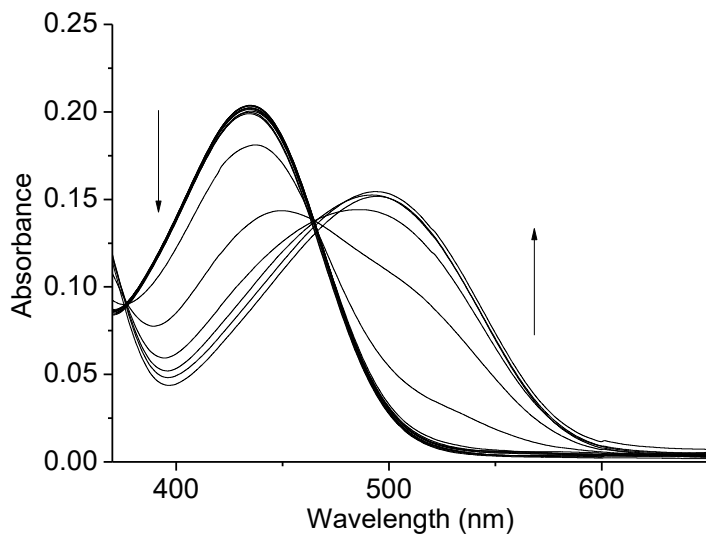


Figure SI-3.2.4. UV-Vis titration profiles of receptor **2b** ($1.0 \times 10^{-5} \text{ mol dm}^{-3}$ in acetonitrile) obtained upon the addition of OH^- anion.

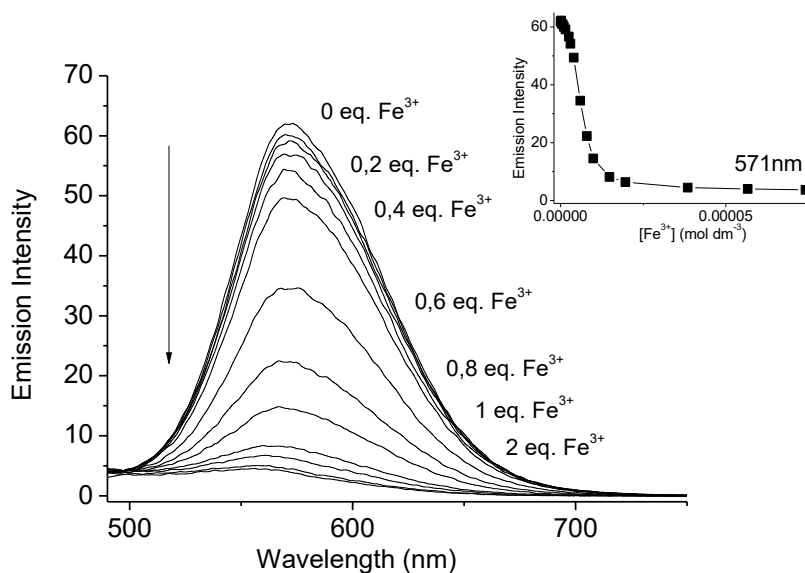


Figure SI-3.2.5. Emission spectra of receptor **2b** ($1.0 \times 10^{-5} \text{ mol dm}^{-3}$) in acetonitrile upon addition of increasing quantities of Fe^{3+} cation. The inset shows the changes in the emission intensity at 571 nm vs Fe^{3+} concentration.

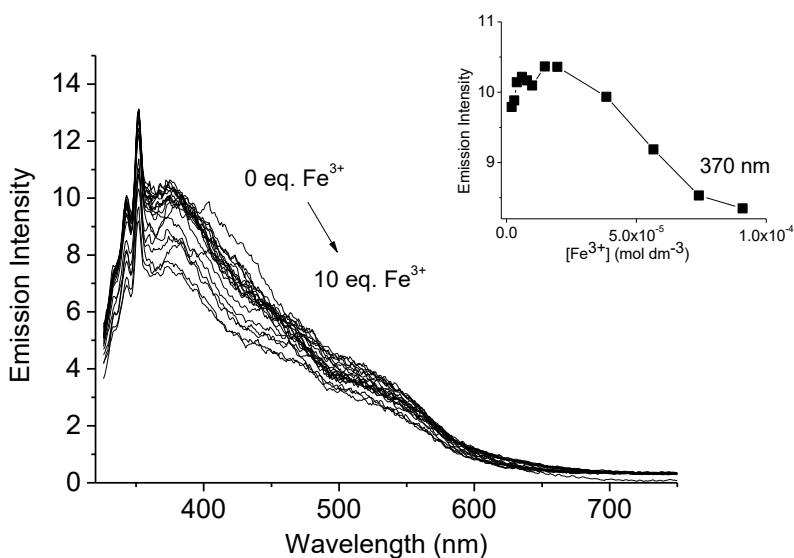


Figure SI-3.2.6. Emission spectra of receptor **2c** ($1.0 \times 10^{-5} \text{ mol dm}^{-3}$) in acetonitrile upon addition of increasing quantities of Fe^{3+} cation. The inset shows the changes in the emission intensity at 370 nm vs Fe^{3+} concentration.

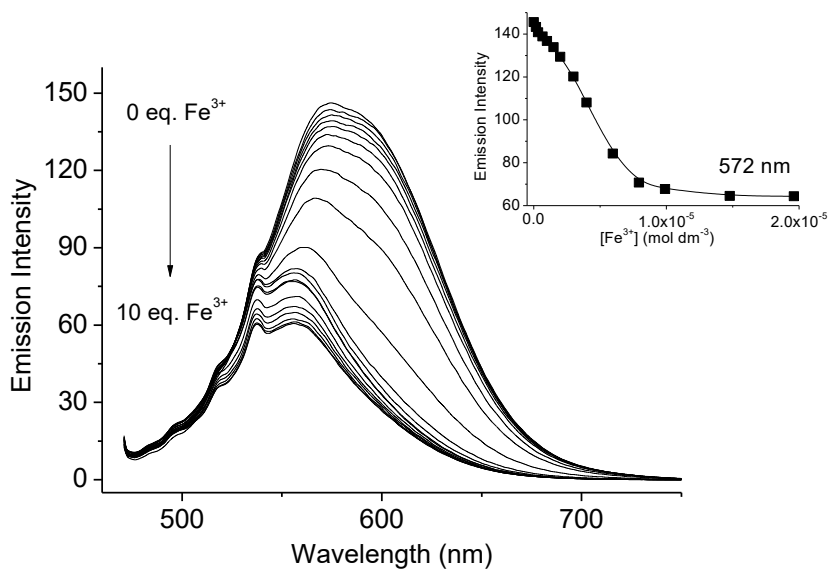
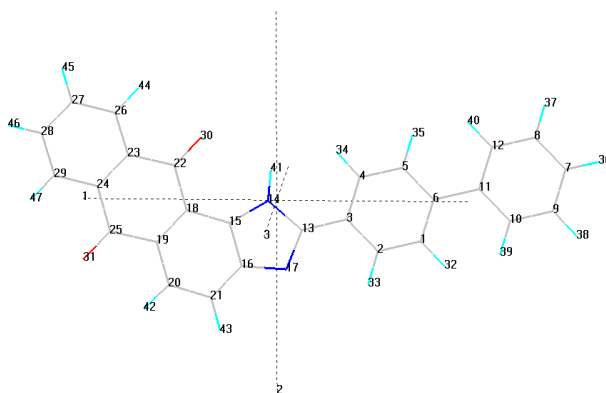
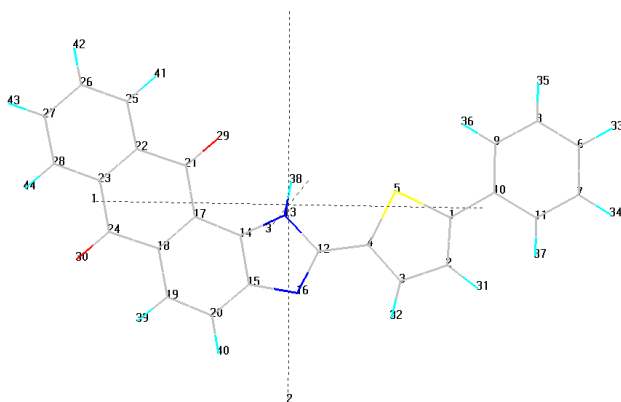


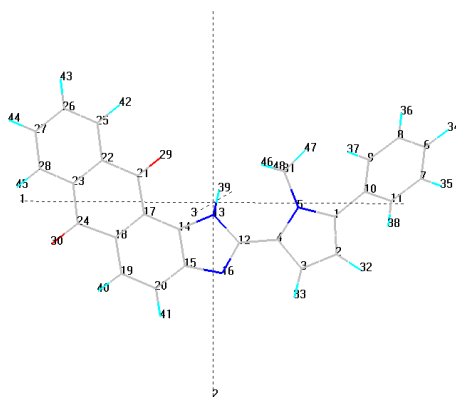
Figure SI-3.2.7. Emission spectra of receptor **2d** ($1.0 \times 10^{-5} \text{ mol dm}^{-3}$) in acetonitrile upon addition of increasing quantities of Fe^{3+} cation. The inset shows the changes in the emission intensity at 572 nm vs Fe^{3+} concentration.

Cartesian coordinates of the optimized geometries for the ground state S_0 of **2a**

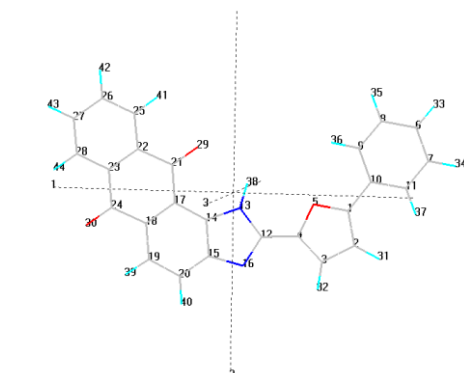
HETATM	1	C	1	7.251	0.979	0.000	HETATM	25	C	25	-2.254	-1.270	0.000
HETATM	2	C	2	6.031	0.317	0.000	HETATM	26	C	26	-3.051	2.440	0.000
HETATM	3	C	3	4.837	1.046	0.000	HETATM	27	C	27	-4.442	2.415	0.000
HETATM	4	C	4	4.890	2.445	0.000	HETATM	28	C	28	-5.113	1.200	0.000
HETATM	5	C	5	6.113	3.098	0.000	HETATM	29	C	29	-4.395	0.008	0.000
HETATM	6	C	6	7.312	2.376	0.000	HETATM	30	O	30	-0.240	2.369	0.000
HETATM	7	C	7	11.071	4.399	0.000	HETATM	31	O	31	-2.850	-2.334	0.000
HETATM	8	C	8	9.887	5.128	0.000	HETATM	32	H	32	8.190	0.402	0.000
HETATM	9	C	9	11.027	3.008	0.000	HETATM	33	H	33	6.008	-0.780	0.000
HETATM	10	C	10	9.804	2.349	0.000	HETATM	34	H	34	3.973	3.046	0.000
HETATM	11	C	11	8.606	3.073	0.000	HETATM	35	H	35	6.151	4.198	0.000
HETATM	12	C	12	8.663	4.471	0.000	HETATM	36	H	36	12.036	4.917	0.000
HETATM	13	C	13	3.559	0.342	0.000	HETATM	37	H	37	9.917	6.222	0.000
HETATM	14	N	14	2.295	0.970	0.000	HETATM	38	H	38	11.957	2.431	0.000
HETATM	15	C	15	1.306	-0.032	0.000	HETATM	39	H	39	9.767	1.249	0.000
HETATM	16	C	16	2.015	-1.265	0.000	HETATM	40	H	40	7.725	5.047	0.000
HETATM	17	N	17	3.396	-0.998	0.000	HETATM	41	H	41	2.138	1.948	0.000
HETATM	18	C	18	-0.100	0.012	0.000	HETATM	42	H	42	-0.616	-3.377	0.000
HETATM	19	C	19	-0.764	-1.215	0.000	HETATM	43	H	43	1.871	-3.436	0.000
HETATM	20	C	20	-0.051	-2.435	0.000	HETATM	44	H	44	-2.525	3.404	0.000
HETATM	21	C	21	1.330	-2.484	0.000	HETATM	45	H	45	-5.004	3.356	0.000
HETATM	22	C	22	-0.835	1.301	0.000	HETATM	46	H	46	-6.209	1.176	0.000
HETATM	23	C	23	-2.322	1.249	0.000	HETATM	47	H	47	-4.934	-0.949	0.000
HETATM	24	C	24	-2.999	0.022	0.000							

Cartesian coordinates of the optimized geometries for the ground state S_0 of **2b**

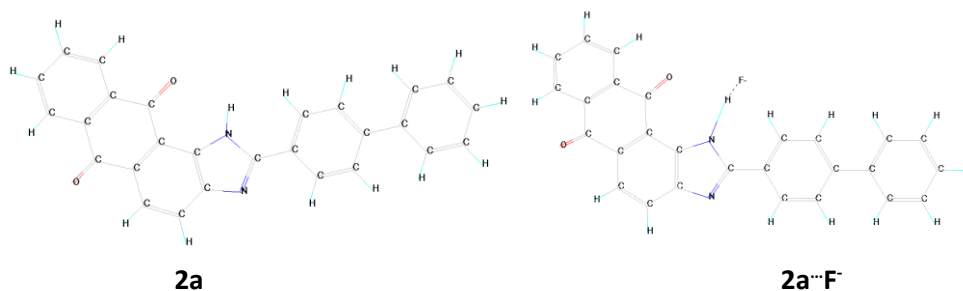
HETATM	1	C	1	-0.064	5.017	-0.000	HETATM	23	C	23	5.988	-3.068	-0.000
HETATM	2	C	2	-1.184	4.219	-0.000	HETATM	24	C	24	4.602	-3.616	-0.000
HETATM	3	C	3	-0.883	2.824	-0.000	HETATM	25	C	25	7.531	-1.205	-0.000
HETATM	4	C	4	0.471	2.580	-0.000	HETATM	26	C	26	8.605	-2.089	-0.000
HETATM	5	S	5	1.396	4.062	-0.000	HETATM	27	C	27	8.377	-3.458	-0.000
HETATM	6	C	6	-0.216	9.260	-0.000	HETATM	28	C	28	7.073	-3.946	-0.000
HETATM	7	C	7	-1.390	8.514	-0.000	HETATM	29	O	29	5.285	0.486	-0.000
HETATM	8	C	8	1.017	8.614	-0.000	HETATM	30	O	30	4.407	-4.821	-0.000
HETATM	9	C	9	1.080	7.226	-0.000	HETATM	31	H	31	-2.202	4.626	-0.000
HETATM	10	C	10	-0.097	6.471	-0.000	HETATM	32	H	32	-1.652	2.048	-0.000
HETATM	11	C	11	-1.334	7.127	-0.000	HETATM	33	H	33	-0.261	10.354	-0.000
HETATM	12	C	12	1.046	1.254	-0.000	HETATM	34	H	34	-2.362	9.020	-0.000
HETATM	13	N	13	2.429	0.966	-0.000	HETATM	35	H	35	1.941	9.201	-0.000
HETATM	14	C	14	2.581	-0.434	-0.000	HETATM	36	H	36	2.054	6.720	-0.000
HETATM	15	C	15	1.260	-0.962	-0.000	HETATM	37	H	37	-2.255	6.524	-0.000
HETATM	16	N	16	0.341	0.103	-0.000	HETATM	38	H	38	3.161	1.634	-0.000
HETATM	17	C	17	3.710	-1.273	-0.000	HETATM	39	H	39	2.010	-4.250	-0.000
HETATM	18	C	18	3.468	-2.647	-0.000	HETATM	40	H	40	0.024	-2.753	-0.000
HETATM	19	C	19	2.152	-3.161	-0.000	HETATM	41	H	41	7.718	-0.123	-0.000
HETATM	20	C	20	1.039	-2.343	-0.000	HETATM	42	H	42	9.630	-1.701	-0.000
HETATM	21	C	21	5.087	-0.721	-0.000	HETATM	43	H	43	9.220	-4.158	-0.000
HETATM	22	C	22	6.220	-1.685	-0.000	HETATM	44	H	44	6.900	-5.030	-0.000

Cartesian coordinates of the optimized geometries for the ground state S_0 of **2c**

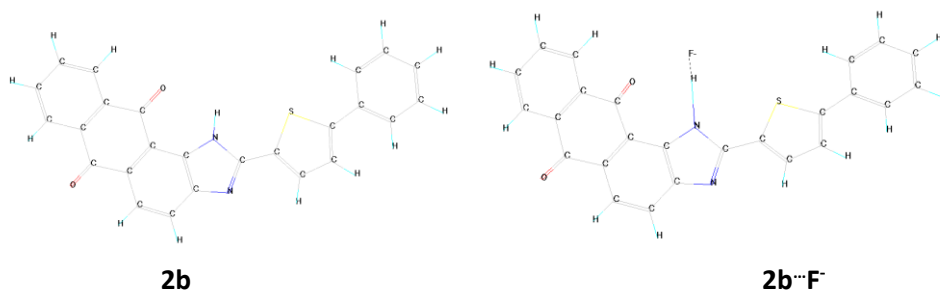
HETATM	1	C	1	-0.771	4.512	0.020	HETATM	25	C	25	7.858	0.671	-0.398
HETATM	2	C	2	-1.822	3.589	-0.035	HETATM	26	C	26	9.126	0.141	-0.175
HETATM	3	C	3	-1.280	2.286	0.013	HETATM	27	C	27	9.288	-1.228	-0.007
HETATM	4	C	4	0.111	2.395	0.090	HETATM	28	C	28	8.183	-2.074	-0.064
HETATM	5	N	5	0.426	3.776	0.095	HETATM	29	O	29	5.229	1.530	-1.111
HETATM	6	C	6	-1.321	8.726	-0.140	HETATM	30	O	30	5.853	-3.647	-0.586
HETATM	7	C	7	-2.119	7.874	-0.897	HETATM	31	C	31	1.771	4.322	0.281
HETATM	8	C	8	-0.318	8.199	0.665	HETATM	32	H	32	-2.880	3.835	-0.100
HETATM	9	C	9	-0.113	6.825	0.718	HETATM	33	H	33	-1.844	1.355	-0.008
HETATM	10	C	10	-0.913	5.961	-0.034	HETATM	34	H	34	-1.482	9.809	-0.180
HETATM	11	C	11	-1.920	6.500	-0.846	HETATM	35	H	35	-2.908	8.286	-1.535
HETATM	12	C	12	1.040	1.291	0.127	HETATM	36	H	36	0.312	8.866	1.262
HETATM	13	N	13	2.420	1.361	-0.184	HETATM	37	H	37	0.694	6.421	1.345
HETATM	14	C	14	2.952	0.059	-0.092	HETATM	38	H	38	-2.555	5.832	-1.440
HETATM	15	C	15	1.867	-0.771	0.305	HETATM	39	H	39	2.889	2.168	-0.528
HETATM	16	N	16	0.708	0.021	0.434	HETATM	40	H	40	3.491	-3.730	0.402
HETATM	17	C	17	4.241	-0.458	-0.290	HETATM	41	H	41	1.218	-2.786	0.804
HETATM	18	C	18	4.396	-1.834	-0.109	HETATM	42	H	42	7.734	1.752	-0.538
HETATM	19	C	19	3.317	-2.654	0.278	HETATM	43	H	43	9.995	0.807	-0.135
HETATM	20	C	20	2.050	-2.143	0.498	HETATM	44	H	44	10.285	-1.646	0.167
HETATM	21	C	21	5.388	0.403	-0.666	HETATM	45	H	45	8.315	-3.156	0.058
HETATM	22	C	22	6.745	-0.168	-0.447	HETATM	46	H	46	2.456	3.962	-0.505
HETATM	23	C	23	6.909	-1.550	-0.282	HETATM	47	H	47	1.751	5.424	0.252
HETATM	24	C	24	5.729	-2.459	-0.347	HETATM	48	H	48	2.185	4.025	1.256

Cartesian coordinates of the optimized geometries for the ground state S_0 of **2d**

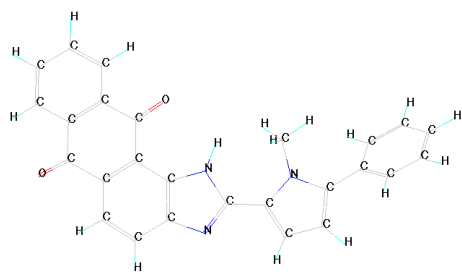
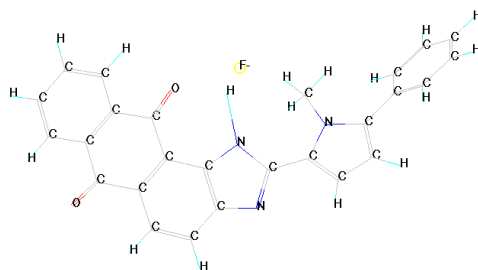
HETATM	1	C	1	-0.984	3.931	-0.000	HETATM	23	C	23	6.623	-1.889	-0.000
HETATM	2	C	2	-2.139	3.172	-0.000	HETATM	24	C	24	5.470	-2.834	-0.000
HETATM	3	C	3	-1.733	1.796	-0.000	HETATM	25	C	25	7.525	0.355	-0.000
HETATM	4	C	4	-0.354	1.799	-0.000	HETATM	26	C	26	8.818	-0.159	-0.000
HETATM	5	O	5	0.129	3.104	-0.000	HETATM	27	C	27	9.017	-1.534	-0.000
HETATM	6	C	6	-0.450	8.144	-0.000	HETATM	28	C	28	7.924	-2.395	-0.000
HETATM	7	C	7	-1.728	7.594	-0.000	HETATM	29	O	29	4.871	1.282	-0.000
HETATM	8	C	8	0.663	7.310	-0.000	HETATM	30	O	30	5.651	-4.040	-0.000
HETATM	9	C	9	0.506	5.929	-0.000	HETATM	31	H	31	-3.166	3.529	-0.000
HETATM	10	C	10	-0.777	5.370	-0.000	HETATM	32	H	32	-2.391	0.929	-0.000
HETATM	11	C	11	-1.894	6.215	-0.000	HETATM	33	H	33	-0.322	9.232	-0.000
HETATM	12	C	12	0.603	0.719	-0.000	HETATM	34	H	34	-2.606	8.248	-0.000
HETATM	13	N	13	2.005	0.870	-0.000	HETATM	35	H	35	1.669	7.742	-0.000
HETATM	14	C	14	2.575	-0.418	-0.000	HETATM	36	H	36	1.395	5.289	-0.000
HETATM	15	C	15	1.477	-1.324	-0.000	HETATM	37	H	37	-2.904	5.787	-0.000
HETATM	16	N	16	0.277	-0.591	-0.000	HETATM	38	H	38	2.500	1.727	-0.000
HETATM	17	C	17	3.907	-0.874	-0.000	HETATM	39	H	39	3.195	-4.228	-0.000
HETATM	18	C	18	4.095	-2.256	-0.000	HETATM	40	H	40	0.846	-3.407	-0.000
HETATM	19	C	19	2.998	-3.147	-0.000	HETATM	41	H	41	7.374	1.442	-0.000
HETATM	20	C	20	1.689	-2.707	-0.000	HETATM	42	H	42	9.676	0.522	-0.000
HETATM	21	C	21	5.050	0.072	-0.000	HETATM	43	H	43	10.033	-1.943	-0.000
HETATM	22	C	22	6.422	-0.502	-0.000	HETATM	44	H	44	8.090	-3.480	-0.000

Energies for the interaction between probes **2a-d** and fluoride anion

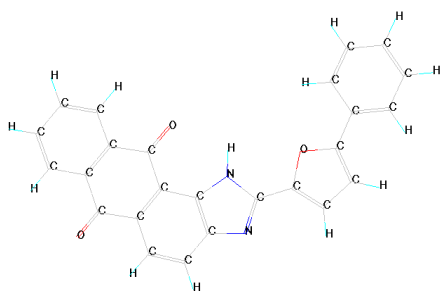
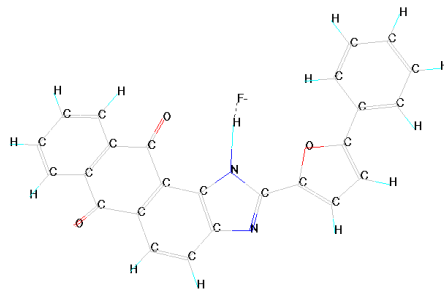
		Total Energy (kcal/mol)	Binding Energy (kcal/mol)	Heat of Formation (kcal/mol)	Electronic Energy (kcal/mol)	Nuclear Energy (kcal/mol)
LH	2a	-100430.6884	-5735.53467	57.2453303	-812310.4386	711879.7502
LH...F ⁻	2a...F⁻	-110657.8384	-5873.105219	-61.43521949	-888680.9799	778023.1415
Δ	Δ	-10,227.1500	-137.5705	-118.6805	-76,370.5413	66,143.3913



		Total Energy (kcal/mol)	Binding Energy (kcal/mol)	Heat of Formation (kcal/mol)	Electronic Energy (kcal/mol)	Nuclear Energy (kcal/mol)
LH	2b	-98536.2805	-5343.5971	69.5989	-777663.5916	679127.3110
LH...F ⁻	2b...F⁻	-108761.9407	-5479.6778	-47.5918	-852399.9225	743637.9817
Δ	Δ	-10225.6602	-136.0806	-117.1906	-74736.3309	64510.6707

**2c****2c^{••}F[•]**

		Total Energy (kcal/mol)	Binding Energy (kcal/mol)	Heat of Formation (kcal/mol)	Electronic Energy (kcal/mol)	Nuclear Energy (kcal/mol)
LH	2c	-101792.3155	-5726.0240	60.9680	-850809.4459	749017.1304
LH ^{••} F [•]	2c^{••}F[•]	-112019.0416	-5863.1705	-57.2885	-931273.6158	819254.5742
Δ	Δ	-10226.7261	-137.1465	-118.2565	-80464.1699	70237.4438

**2d****2d^{••}F[•]**

		Total Energy (kcal/mol)	Binding Energy (kcal/mol)	Heat of Formation (kcal/mol)	Electronic Energy (kcal/mol)	Nuclear Energy (kcal/mol)
LH	2d	-101008.8694	-5374.3028	32.0522	-797433.7592	696424.8898
LH ^{••} F [•]	2d^{••}F[•]	-111235.6714	-5511.5253	-86.2803	-876857.4458	765621.7744
Δ	Δ	-10226.8020	-137.2225	-118.3325	-79423.6866	69196.8846

***2.4. Synthesis and evaluation of the
chromo-fluorogenic recognition ability of
imidazoquinoline derivatives towards ions***

Synthesis and evaluation of the chromo-fluorogenic recognition ability of imidazoquinoline derivatives toward ions

*Cristina Marín-Hernández,^{a,b} Luis E. Santos-Figueroa,^{a,b}
Sameh El Sayed,^{a,b} Teresa Pardo,^{a,b} M. Manuela M. Raposo,^c
Rosa M. F. Batista,^c Susana P. G. Costa,^c Félix Sancenón^{a,b}
and Ramón Martínez-Máñez*^{a,b}*

^a *Centro de Reconocimiento Molecular y Desarrollo Tecnológico (IDM), Unidad Mixta Universidad de Valencia-Universidad Politécnica de Valencia. Camino de Vera s/n, 46022 Valencia, Spain.*

^b *CIBER de Bioingeniería, Biomateriales y Nanomedicina (CIBER-BBN).*

^c *Centro de Química, Universidade do Minho, Campus de Gualtar, 4710-057 Braga, Portugal.*

Published online: November, 2015

(Reprinted with permission from

Dyes and Pigments, 2015, 122, 50–58

Copyright © 2015 Published by Elsevier Ltd.)

2.4.1. Abstract

Four imidazoquinolines functionalized with different carbocycles and heterocycles have been synthesized and characterized. Acetonitrile solutions of the four receptors presented absorption bands in the 330-370 nm range. The four probes were also emissive with fluorescence bands in the 390-460 nm interval. In a first step, the chromo-fluorogenic behaviour of the four probes was evaluated in the presence of selected anions. Addition of F^- induced the appearance of a new red-shifted absorption band together with a moderate quenching of the fluorescence in all four receptors. In a second step, the UV-visible and emission behaviour of the four receptors in the presence of cations was tested. Addition of Hg^{2+} , Cu^{2+} , Co^{2+} , Fe^{3+} , Fe^{2+} , Zn^{2+} , Pb^{2+} , Cd^{2+} , Cr^{3+} and Al^{3+} induced a similar optical change in all four receptors (appearance of a broad red-shifted absorption band together with a remarkable quenching of the emission band).

2.4.2. Introduction

From the early years of supramolecular chemistry foundations, two concepts that have been extensively developed are the preparation of molecular receptors and, more recently, the design of chemical sensors.¹ Molecular receptors are chemical species designed to achieve a high degree of complementarity with a selected guest. When synthetic receptors are coupled with certain signaling units, that could change one or more physical properties (e.g. color, fluorescence, redox potential) upon receptor-guest interaction, a molecular sensor is obtained.² In this field especially appealing is the use of optical outputs such as changes in color and/or fluorescence that allow the use low-cost and widely available instrumentation.³ Moreover, in the case of chromogenic chemosensors, a straightforward semiquantitative and *in situ* “naked-eye” (direct visual observation) detection is possible⁴ and chromo-fluorogenic chemosensors displaying a displacement of the absorption or emission bands are interesting for the development of ratiometric procedures.⁵

Three main paradigms have been used in the development of chromo-fluorogenic chemosensors namely (i) the binding site-signaling subunit approach,

(ii) the displacement approach and (iii) the chemodosimeter approach.⁶ In the first paradigm, the binding site, designed in such a way that possesses a high degree of complementarity with selected guests, is covalently linked with a signaling subunit that is able to change color of absorption/emission upon guest coordination with the binding site.⁷ The displacement approach also uses a binding site and a signaling subunit which are not covalently linked yet forming a coordination complex. In the presence of the target guest the signaling subunit is displaced and an optical signal is generated.⁸ Finally, the chemodosimeter approach makes use of specific chemical reactions induced by the guest on the designed probe that are coupled to color modulations.⁹ Based on these three paradigms cited above a number of chromo-fluorogenic sensors for anions, cations and neutral molecules have been described recently.¹⁰ Perhaps, the most widely used approach to design probes is the binding site-signaling subunit paradigm.¹¹ However, the covalent linking of binding sites with signaling subunits require in most cases great synthetic efforts in order to achieve certain selectivity with the guest and to impart the desired functionality, regarding color and/or emission changes upon coordination. In order to minimize the synthetic requirements, recently, the preparation of simple chemical species that integrated binding subunits into the structure of certain dyes or fluorophores has deserved great attention.¹² Moreover, the possibility of using the same probe to sense both anions and cations is an area of importance within the chemical sensing field.¹³

From another point of view, imidazole derivatives have been demonstrated to be good neutral binding groups for coordinating anions.¹⁴ Besides, the coordination ability of the imidazole group depends on the acidity of the NH proton that can be modulated by the presence in the structure of easily delocalizable heteroaromatic rings, such as thiophene, pyrrole and furan.^{12a,15} Moreover, the presence in imidazole derivatives of two nitrogen atoms, one of them with a free electron pair, favors the coordination of metal cations with this five-membered heterocycle.¹⁶ Also, some quinoline derivatives have been reported to be suitable systems for the colorimetric sensing of certain anions and for the recognition of metal cations.¹⁷ Moreover quinolines have been increasingly

studied by their bioactive properties and have been used as antimalarial,¹⁸ antiviral,¹⁹ anticonvulsant²⁰ and anticancer agents.²¹

Taking into account the above mentioned facts and our interest in the development of optical probes,²² we report herein the synthesis, characterization and binding studies toward anions and cations of a family of probes containing imidazoquinoline moieties as both binding and signaling subunit. The probes contained electron donor rings of different strength (i.e. *N*-methylpyrrole, furan, thiophene and benzene) in the structures in order to modulate their response as chemosensors. The interaction of the four probes with anions and cations was studied by means of UV-visible, fluorescence and ¹H NMR measurements.

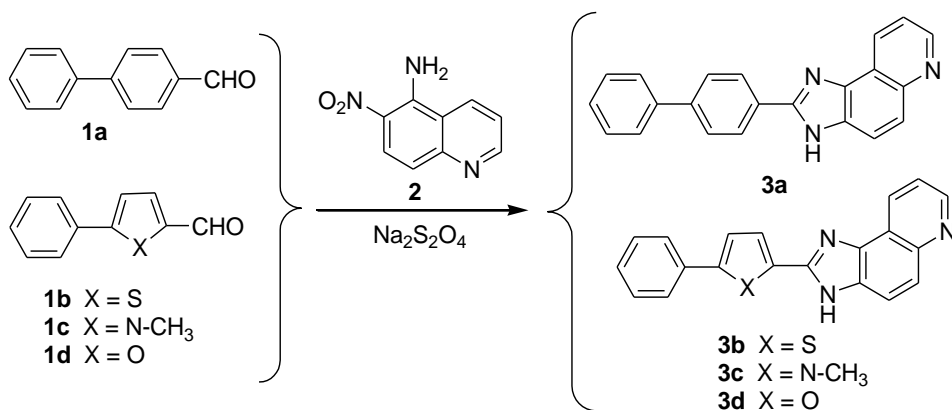
2.4.3. Results and discussion

Synthesis and characterization

The new compounds **3a-d** with biphenyl, arylthiophene, arylpyrrole and arylfuran π -conjugated bridges were synthesized in good to excellent yields, 52-87%. The synthesis of the formyl precursor **1c** was recently reported by us through a Suzuki coupling followed by a Vilsmeier reaction.^{12a} Imidazoquinolines **3a-d** were obtained through a one step reaction involving Na₂S₂O₄ reduction of 5-amino-6-nitroquinoline **2** in the presence of commercially available biphenyl, arylthiophene, and arylfuran aldehydes **1a-b**, **1d**, and aldehyde **1c** in DMSO at 80 °C (Scheme 1).²³ The crude products were purified by column chromatography on silica with chloroform or through recrystallization from dichloromethane to give the pure compounds, which were completely characterized through the use of common spectroscopic and analytical methods (see Scheme 2.4.1).

The most characteristic signals in the ¹H NMR spectrum of this family of imidazoquinoline derivatives were those corresponding to N-H proton in the imidazole moiety, which were found as singlets in the 12.13-13.55 ppm range. A certain correlation could be observed between the donor properties of the π -conjugated bridges attached to position 2 of the imidazole nucleus and the chemical shift of the nitrogen proton of the imidazole ring in **3a-3d** (Table 2.4.1).

In this context, compound **3c** bearing a more electron rich heterocyclic π -bridge exhibited the lowest chemical shift for the nitrogen proton of the imidazole ring.



Scheme 2.4.1. Synthesis of imidazoquinoline probes **3a-d**.

Table 2.4.1. Yields and ¹H NMR data of imidazoquinoline probes **3a-d**.

Formyl precursor	Compound	Yield (%)	$\delta_{\text{H}} \text{NH}$ (ppm)
1a	3a	64	13.53 ^a
1b	3b	65	13.55 ^b
1c	3c	52	12.13 ^a
1d	3d	87	13.52 ^a

^a 400 MHz, DMSO-*d*₆. ^b 300 MHz, DMSO-*d*₆.

Spectroscopic characterization

The spectroscopic characterization of acetonitrile solutions of the four probes was carried out. The four probes showed intense absorption bands ($\log \epsilon \approx 4.2$) in the 260-370 nm region (see Table 2.4.2). The position of the red shifted absorption bands were clearly dependent on the electron donor strength of the (hetero)aromatic group which was used as π -bridge between the imidazoquinoline and the terminal phenyl ring. When the π -bridge was a

benzene ring (the least electron donor) as in **3a**, the absorption band was centred at 338 nm. On changing the π -bridge to methylpyrrole (**3c**) the absorption maximum suffered a small bathochromic shift to 341 nm whereas if the π -bridge was a furan (**3d**) or a thiophene (**3b**), the red shift was larger, to 352 and 361 nm respectively. Moreover, upon excitation at the corresponding maximum wavelength, the four probes showed broad unstructured emission bands in the 390-458 nm range (see Table 2.4.2). Also, quantum yields of the four probes were measured (using quinine sulphate in 0.5 mol dm⁻³ in H₂SO₄). The values obtained ranged from 0.12 to 0.36 and were shown in Table 2.4.2.

In order to assess the nature of the main absorption band of each of the four probes the HOMO and LUMO differences in energy for **3a-d** by quantum chemical calculations at the semiempirical level employing the PM3 model and with RMS gradient of 0.001 were determined. For the four probes, the HOMO and LUMO orbitals were distributed throughout the molecule. As a representative example, Figure 2.4.1 shows the HOMO and LUMO orbitals for probe **3a**. As can be seen in the figure the HOMO and LUMO orbitals of **3a** are symmetric and delocalised over the entire π -system clearly resembling those of cyanine dyes.

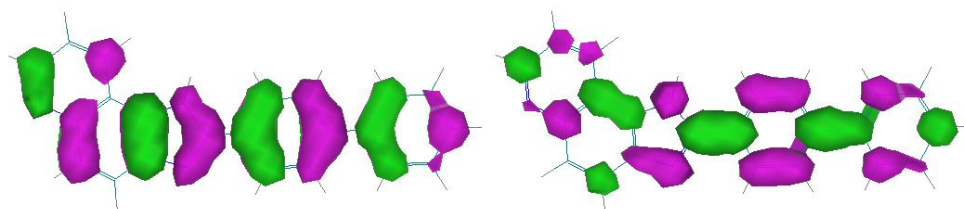


Figure 2.4.1. HOMO (left) and LUMO (right) orbitals for probe **3a**.

Spectroscopic behavior of **3a-d** in presence of anions

The chromogenic behaviour of the four probes in the presence of selected anions was tested. For this purpose, acetonitrile solutions of **3a-d** (1.0 x 10⁻⁴ mol dm⁻³) were prepared and the changes in the UV-visible profiles tested upon addition of 10 equivalents of anions with different sizes, shapes and

charges (*i.e.* F^- , Cl^- , Br^- , I^- , OCN^- , BzO^- , ClO_4^- , AcO^- , HSO_4^- , $H_2PO_4^-$ and CN^-) at 25°C. The four probes showed a very similar chromogenic response in the presence of anions. In particular only the addition of F^- induced a remarkable colour modulation from colourless to pale yellow that was visible to the naked eye. Other anions tested were unable to induce any such remarkable colour change.

Once assessed the response of probes **3a-d** toward anions, UV-visible changes in the presence of F^- were studied more in detail. The response observed for the four receptors was quite similar and as an example Figure 2.4.2 shows the UV-visible titration profiles of probe **3a** with F^- . Acetonitrile solutions of probe **3a** displayed two intense absorption bands at 297 and 338 nm that, upon addition of increasing quantities of F^- anion, suffered a decrease in intensity concomitant with small bathochromic shifts. Besides, a new broad absorption centred at 377 nm was developed. UV-visible titration experiments carried out with probes **3b**, **3c** and **3d** showed the same behaviour as that observed for **3a**. Namely, only the addition of F^- induced a remarkable reduction of the two main absorption bands of the probes with a clear simultaneous growth of a red shifted absorption band.

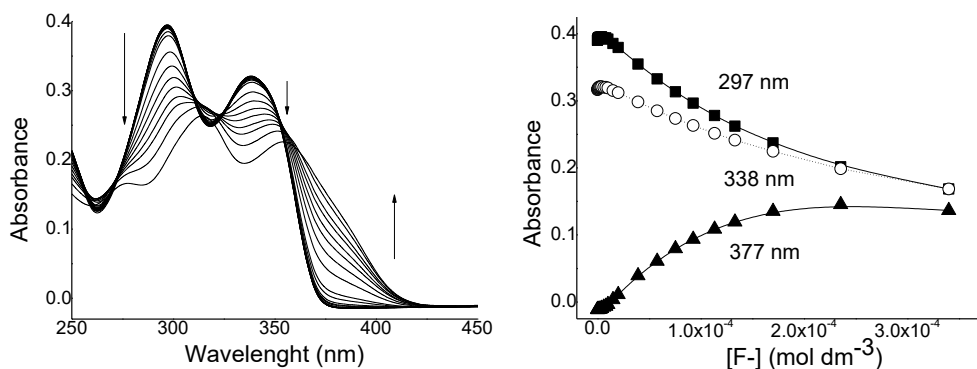


Figure 2.4.2. UV-vis titration profile of receptor **3a** (1.0×10^{-5} mol dm^{-3} in acetonitrile) obtained upon the addition of increasing quantities of F^- (left) and the changes in absorbance at 297, 338 and 377 nm (right).

The fact that colour modulations in the four probes were induced only by the addition of the more basic anion, i.e. F^- , pointed to a proton transfer process as the mechanism for the chromogenic response observed.²⁴ Taking this into account, addition of F^- would induce the deprotonation of the N-H of the imidazoquinoline moiety, which is common to all four probes. The mechanism of the chromogenic response was assessed with additional titration experiments carried out with probes **3a-d** and tetrabutylammonium hydroxide that showed an identical behaviour to that found in the presence of F^- (data not shown). One remarkable feature of probes **3a-d** is their lack of response upon addition of the basic and nucleophilic CN^- . However this lack of response has also been described in other similar probes.²⁵

Furthermore, the limits of detection (LOD) of probes **3a-d** for F^- were determined from the corresponding absorbance titration profiles (see experimental section). The values obtained were quite similar and in all cases near $5 \mu M$. The chromogenic behavior of the four probes toward F^- was rather selective. In particular it was found that F^- gave a very similar response alone or in a complex mixture containing the selected anions Cl^- , Br^- , I^- , OCN^- , BzO^- , ClO_4^- , HSO_4^- and CN^- .

Once assessed the UV-visible behaviour of probes **3a-d** in the presence of selected anions, fluorogenic studies with F^- were performed. F^- was selected because it was the only anion able to induce chromogenic changes in the four probes tested. Fluorescence measurements of acetonitrile solutions of the four probes were carried out in the presence of increasing quantities of F^- . Excitation wavelengths were selected at the corresponding isosbestic points observed in the course of the corresponding UV-visible titrations.

The emission changes observed for the four probes were quite similar and, as an example, Figure 2.4.3 shows the set of spectra obtained for **3b** upon addition of increasing quantities of F^- . Upon excitation at the isosbestic point observed in the UV-vis titration, probe **3b** showed a broad structured emission band centred at 425 nm. As it can be seen, the intensity of the emission band centred at 425 nm decreased gradually as the amount of F^- increased. Also, together with this quenching of the emission, a progressive red shift (from 425

to 467 nm) of the fluorescence was observed. As a general trend, probes **3b-d** also showed a moderate bathochromic shift and a simultaneous partial quenching of their original emission band upon the addition of increasing amounts of F^- . However, a more detailed examination of the titration experiments showed that to induce the same behaviour larger amounts of fluoride were required for receptors **3b**, **3c** and **3d** than for receptor **3a**. Emission data of the four probes alone and in the presence of F^- are shown in Table 2.4.2.

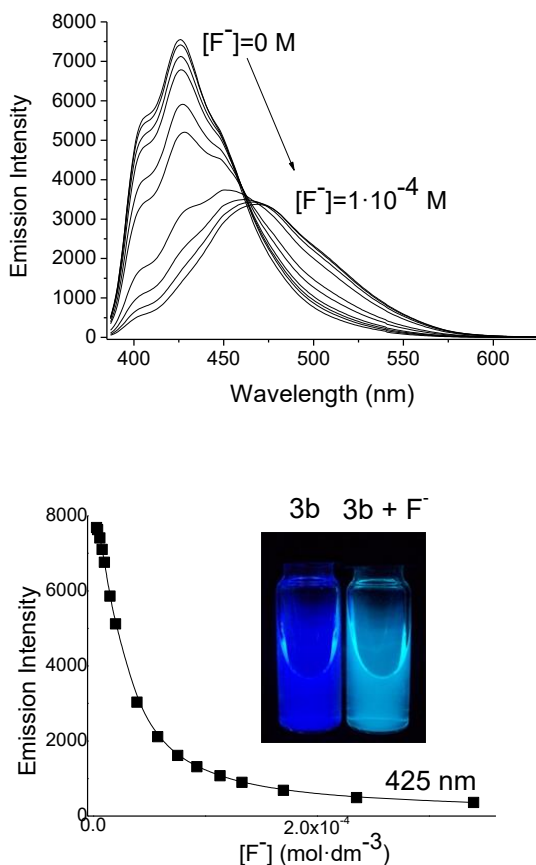


Figure 2.4.3. Emission spectra of probe **3b** (1.0×10^{-5} mol dm^{-3} in acetonitrile) at 425 nm upon the addition of increasing quantities of F^- anion (above) and the changes in emission intensity of the band centred at 425 nm toward the concentration of F^- in the solution (below). In the inset it can be seen the changes observed with ultraviolet radiation for this probe (1.0×10^{-4} mol dm^{-3} in acetonitrile) upon addition of 20 eq. of F^- .

Table 2.4.2. Spectroscopic data for the interaction of probes **3a-d** with fluoride anion.

	Absorption data				Fluorescence data					
	λ_{ab} LH (nm)	Log ϵ	λ_{ab} L ⁻ (nm) ^a	$\Delta\lambda_{ab}$ (nm)	λ_{ex} LH (nm)	λ_{em} LH (nm)	λ_{em} L ⁻ (nm) ^a	$\Delta\lambda_{em}$ (nm)	Stokes shift (cm ⁻¹)	Quantum Yields
3a	262	4.09	262 ↑	0						0.33
	297	4.59	315 ↑	18						
	338	4.51	354 ↓	16	367	390	390 ↓	0	3945	
	377	2.00	377 ↑	0						
3b	274	4.11	274 ↑	0						0.36
	310	4.37	325 ↑	15						
	361	4.65	382 ↓	21	377	425	467 ↓	42	4171	
	427	3.32	427 ↑	0						
3c	269	4.03	269 ↑	0						0.12
	301	4.46	302 ↑	1						
	341	4.41	344 ↓	3	371	458	467 ↓	9	7494	
	425	2.54	425 ↑	0						
3d	274	3.98	274 ↑	0						0.27
	306	4.37	307 ↑	1						
	352	4.51	367 ↓	15	368	405	405 ↓	0	3718	
	412	2.59	412 ↑	0						

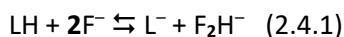
↑ Increasing absorption band upon addition of F⁻.↓ Decreasing absorption band upon addition of F⁻.

The quenching of the initial emission together with the appearance of new red-shifted band was attributed the F⁻-induced deprotonation in the four probes. This deprotonation process induced the formation of an imidazolate anion with a negative charge, as a consequence of which an increase in the intensity of the electrical dipole was produced.²⁶ This increase in the electrical dipole was the responsible of the observed changes in the UV-visible and emission bands.

Taking into account the selective chromo-fluorogenic changes observed for **3a-d** in the presence of F⁻ the response of the four probes in aqueous environments was tested. Unfortunately, the chromo-fluorogenic changes observed in the presence of F⁻, when acetonitrile was used as solvent, disappeared upon addition of small quantities of water (as low as 2%). This lack of response was ascribed to the reduced basicity of F⁻ in aqueous environments due to its favourable solvation by water molecules.

Determination of stability constants and quantum mechanical studies with anions

As cited above, F⁻ was able to deprotonate probes **3a-d**. Equation 2.4.1 represents this proton transfer equilibrium in which LH is the probe.



In order to complete the characterization of the interaction of **3a-d** with F⁻, the deprotonation process was studied *via* the evaluation of the corresponding stability constants, which were determined, using the HypSpec software, from UV-Vis spectroscopic titrations. The studies were performed using the UV-Vis isotherms of the red shifted absorption bands (at 377, 427, 425 and 412 nm for **3a**, **3b**, **3c** and **3d**, respectively) obtained upon addition of F⁻ because this was the only anion which induced remarkable changes (*vide ante*). The results are shown in Table 2.4.3.

Table 2.4.3 shows that the logarithms of the stability constants for the deprotonation process were rather similar for **3a**, **3b** and **3d** (log K from 4.0 to 3.68), whereas for **3c** log K was lower (log K = 2.71). The values of the stability constants for the deprotonation reactions can be correlated with the electron donor ability of the π -bridge present in the structure of the probes. In this respect, the most acidic probe was **3a** that contained, as π -bridge, a phenyl group which was the least electron donor ring. On the other hand, the less acidic probe was **3c** which contained the most electron donor *N*-methylpyrrole ring as π -bridge. In summary, the acidity order of the four probes **3a** > **3b** > **3d** > **3c** matched well with the electron donor character of the π -bridge present in its chemical structure (benzene < thiophene < furan < *N*-methylpyrrole). Besides, the logarithms of the stability constants for the proton transfer reactions for probes **3a-d** are similar to those reported for closely related compounds.²⁷

Table 2.4.3. Logarithms of the stability constants measured for the interaction of probes **3a-d** with F⁻.

Receptor	3a	3b	3c	3d
log K	4.00 ± 0.11	3.82 ± 0.07	2.71 ± 0.26	3.68 ± 0.08

It has been reported that the hydrogen bond-donating or accepting ability of a molecule in a particular group can be assessed by gas-phase deprotonation energy studies determined by quantum chemical calculations by subtracting the energy of the probe alone and that of the deprotonated form.²⁸ Calculations for probes **3a-d** (assuming that the N-H moiety of the four receptors was deprotonated) were carried out using a PM3 semi-empirical model and the results are shown in Table 2.4.4.

Data in Table 2.4.4 indicated that the most acidic probe was **3a** (the more the negative the value of the difference, the stronger the hydrogen-bond donor character), whereas **3c** was the less acidic. These results correlated well

with the measured stability constants for the proton transfer reactions (see Table 2.4.3). However, the stabilization energy indicated that probe **3d** was more acidic than **3b**, contradicting the stability constants determined from UV-titrations. This inconsistency may be related to the fact that stabilization energy for the deprotonation was calculated in the vacuum without the influence of the solvent molecules.

Table 2.4.4. Stabilization energy of the deprotonation for probes **3a-d**.

Receptor	$E_{(LH)}$ (kcal/mol)	$E_{(L^-)}$ (kcal/mol)	$E_{(LH)} - E_{(L^-)}$ (kcal/mol)
3a	-4762.4	-4754.6	-7.8
3b	-4370.9	-4364.3	-6.6
3c	-4752.5	-4746.2	-6.3
3d	-4401.6	-4393.9	-7.6

Spectroscopic behaviour of **3a-d** with cations

Probes **3a-d** contain in their structures three nitrogen atoms that could be able to coordinate with transition metal cations. For this reason, the interaction of **3a-d** (1.0×10^{-4} mol dm⁻³) with selected cations (Hg²⁺, Cu²⁺, Co²⁺, Mg²⁺, Fe³⁺, Ba²⁺, Fe²⁺, Ni²⁺, Ca²⁺, Zn²⁺, Pb²⁺, Cd²⁺, Cr³⁺, Al³⁺, K⁺ and Li⁺) in acetonitrile was studied. Unfortunately, the observed response was unselective and it was found that the addition of Hg²⁺, Cu²⁺, Co²⁺, Fe³⁺, Fe²⁺, Zn²⁺, Pb²⁺, Cd²⁺, Cr³⁺ and Al³⁺ induced similar colour changes (from colourless to pale yellow) in all four probes. Exploring this initial behaviour, we selected Al³⁺ as a model cation for further studies. Moreover it was confirmed that the UV-visible and fluorescence (*vide infra*) response in the presence of Al³⁺ cation was nearly identical for the four probes and, for this reason, only changes observed for **3b** as model ligand will be detailed.

Acetonitrile solutions of probe **3b** showed absorption bands located in the

UV centred at 274, 310 and 361 nm (see Figure 2.4.4). Addition of increasing amounts of Al^{3+} induced moderate changes in the absorption located in the UV whereas the most remarkable feature was the appearance of a new band at 427 nm which was responsible for the yellow colour developed upon addition of this cation. Figure 2.4.4 also displays the changes in the absorbance at 267, 323, 353 and 427 nm observed upon addition of increasing quantities of Al^{3+} . Moreover from Job's plot based in UV-visible measurements it was found that probes **3a-d** formed 1:1 complexes with Al^{3+} .

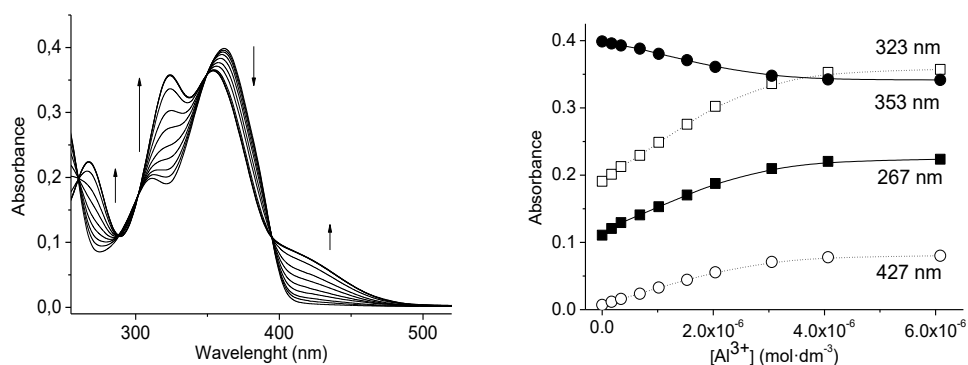


Figure 2.4.4. UV-vis titration of probe **3a** (1.0×10^{-5} mol dm⁻³ in acetonitrile) obtained upon the addition of Al^{3+} (left) and the changes in absorbance at 297, 338 and 377 nm (right).

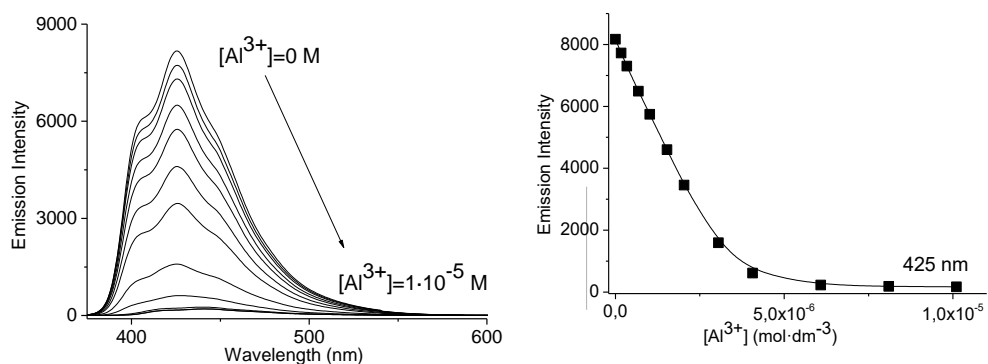


Figure 2.4.5. Emission spectra of probe **3b** (1.0×10^{-5} mol dm⁻³ in acetonitrile) upon the addition of increasing quantities of Al^{3+} (left) and the emission changes at 425nm vs. the concentration of Al^{3+} in the solution (right).

The emission behaviour of the four probes in the presence of cations was also studied. The four probes presented the same response upon addition of certain cations (i.e. Hg^{2+} , Cu^{2+} , Co^{2+} , Fe^{3+} , Fe^{2+} , Zn^{2+} , Pb^{2+} , Cd^{2+} , Cr^{3+} and Al^{3+}) namely a marked emission quenching. As an example, Figure 2.4.5 shows the titration profile obtained for probe **3b** and Al^{3+} . Probe **3b** shows in acetonitrile a broad structured emission band at 425 nm upon excitation at the isosbestic point observed in the UV-vis titration. Addition of increasing quantities of Al^{3+} induced a progressive quenching of the emission band. The Stern-Volmer plot of relative fluorescence intensity (I_0/I) of **3b** versus Al^{3+} concentration (see Figure 2.4.6) presented an upward curvature indicating a combination of static (formation of 1:1 stoichiometry complex between the probe and cation) and dynamic quenching.

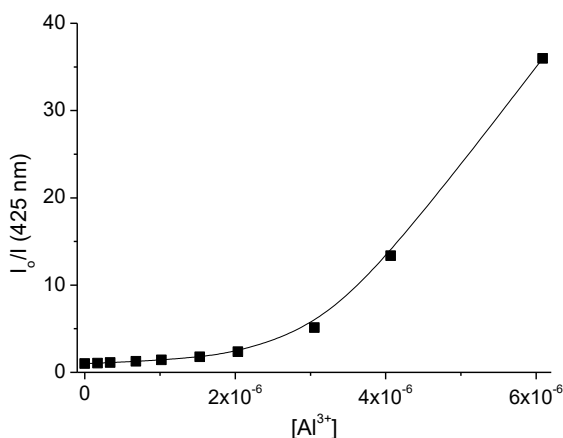


Figure 2.4.6. Stern-Volmer plot for the emission quenching of probe **3b** (1.0×10^{-5} mol dm⁻³ in acetonitrile) by Al^{3+} cation.

From the absorbance titration profiles, obtained for the four probes upon addition of increasing quantities of Al^{3+} , the limits of detection were estimated (see experimental section). The values obtained are shown in Table 2.4.5. As it can be seen, the values measured were quite similar for probes **3a-d** and ranged from 0.33 to 0.81 μM . Besides, the changes in the UV-visible and emission spectra of the four probes in the presence of Al^{3+} were summarized in Table 2.4.6.

Table 2.4.5. Limits of detection for **3a-d** probes to Al^{3+} (μM).

Receptor	Al^{3+}
3a	0.363
3b	0.333
3c	0.808
3d	0.496

Table 2.4.6. Spectroscopic data of the main bands for probes **3a-d** in the presence of Al^{3+} .

Receptor	Abs. Wavelength (nm)		Em. Wavelength (nm) ^a	
	LH	LH· Al^{3+}	LH	LH· Al^{3+}
3a	262	262 ↑		
	297	303 ↑		
	338	338 ↓	390	394 ↓
	400	400 ↑		
3b	274	274 ↑		
	310	323 ↑		
	361	353 ↓	425	425 ↓
	427	427 ↑		
3c	269	269 ↑		
	301	317 ↑		
	371	371 ↓	462	464 ↓
	425	425 ↑		
3d	274	274 ↑		
	306	319 ↑		
	352	348 ↓	406	406 ↓
	412	412 ↑		

^a Measured upon excitation at isosbestic-point in the UV-vis titration.

↑ Increasing absorption band upon addition of Al^{3+} .

↓ Decreasing absorption band upon addition of Al^{3+} .

¹H-NMR spectroscopic studies in the presence of cations

In order to study, in more depth, the coordination mode of probes **3a-d** with cations ¹H-NMR titration experiments were performed. For this purpose we selected receptor **3a** and changes in ¹H-NMR spectra (in CD₃CN) upon addition of increasing quantities of Al³⁺ were studied. The ¹H-NMR spectra of probe **3a** in CD₃CN showed (see Figure 2.4.7 for proton assignment) the protons of the quinoline heterocycle centred at 8.87 (dd, Ha), 7.89 (dd, Hb overlapped with He), 7.60 (dd, Hc), 7.98 (br d, Hd) and 7.92 (d, He overlapped with Hb) ppm. The protons of the 1,4-disubstituted benzene ring (linked with the quinoline and the monosubstituted benzene ring) appeared as doublets at 8.26 (Hf) and 7.87 (Hg) ppm. Finally, the protons of the monosubstituted benzene ring appeared at 7.76 (dd, Hh), 7.53 (t, Hi) and 7.43 (t, Hj) ppm. As general trend (see Figure 2.4.7), addition of Al³⁺ induced marked downfield shifts of the signals corresponding to the quinoline and 1,4-disubstituted benzene rings, whereas the protons of the monosubstituted benzene remained unaltered. Besides, the shifts of the proton resonances stopped upon addition of 1 eq. of Al³⁺ cation suggesting the formation of 1:1 (probe-cation) complexes.

In more detail, the most remarkable shifts observed upon addition of 1 eq. of Al³⁺ cation, were those of protons Hf (from 8.26 to 9.62 ppm), Hc (from 7.60 to 8.25 ppm) and Ha (from 8.87 to 9.08 ppm). Hc and Ha protons are located in the quinoline heterocycle whereas Hf is located in the 1,4-disubstituted benzene ring. These facts suggested a preferential coordination of Al³⁺ with the nitrogen of the imidazole heterocycle.

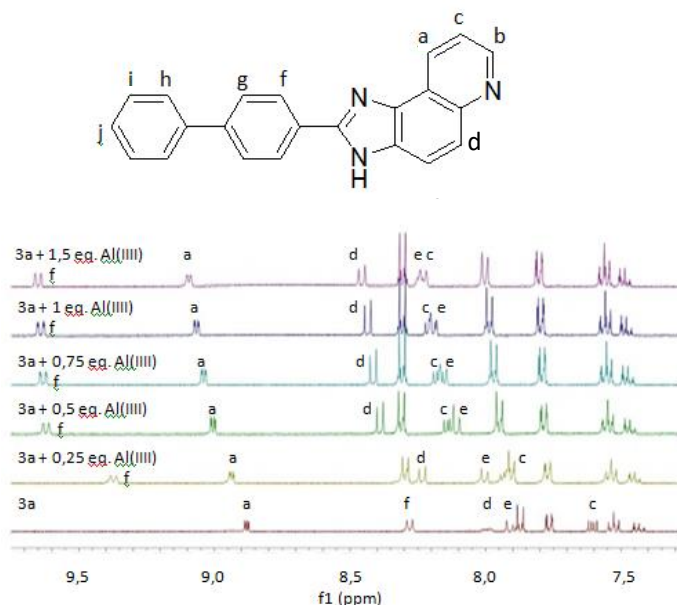


Figure 2.4.7. $^1\text{H-NMR}$ spectra of probe **3a** in CD_3CN alone and in the presence of increasing quantities of Al^{3+} .

2.4.4. Conclusions

We have reported herein the synthesis, characterization and UV-visible and emission behaviour toward cations and anions of a novel series of imidazoquinoline probes (**3a-d**). Among all of the anions tested, only F^- was able to induce the appearance of a red-shifted emission band which was reflected in a colour change from colourless to yellow. Also, F^- induced a moderate emission quenching together with a progressive red shift for **3a-d**. These changes were ascribed to a deprotonation process of the N-H moiety presented in the structure of the four probes. The low acidity of **3a-d** precluded the observation of any changes upon addition of other basic anions such as AcO^- , BzO^- , HSO_4^- and H_2PO_4^- . The interaction of the four probes with transition metal cations was also studied by UV-visible and fluorescence measurements. The response of the four probes toward cations was unselective and the addition of Hg^{2+} , Cu^{2+} , Co^{2+} , Fe^{3+} , Fe^{2+} , Zn^{2+} , Pb^{2+} , Cd^{2+} , Cr^{3+} and Al^{3+} induced optical changes. Coordination of the four

probes with these cations induced the appearance of red shifted absorptions and a marked quenching of the emission band. $^1\text{H-NMR}$ measurements carried out with probe **3a** and Al^{3+} suggested the formation of 1:1 stoichiometry complexes and a coordination at the imidazole moiety.

2.4.5. Experimental section

Materials and methods:

General. Melting points were measured on a Stuart SMP3 melting point apparatus. TLC analyses were carried out on 0.25 mm thick precoated silica plates (Merck Fertigplatten Kieselgel 60F₂₅₄) and spots were visualised under UV light. Chromatography on silica gel was carried out on Merck Kieselgel (230-240 mesh). NMR spectra were obtained on a Varian Unity Plus Spectrometer at an operating frequency of 300 MHz for ^1H and 75.4 MHz for ^{13}C or a Bruker Avance III 400 at an operating frequency of 400 MHz for ^1H and 100.6 MHz for ^{13}C using the solvent peak as internal reference at 25 °C. All chemical shifts are given in ppm using δ_{H} $\text{Me}_4\text{Si} = 0$ ppm as reference and J values are given in Hz. Fluorescence spectra were carried out with Jasco FP-8500 Spectrofluorometer and absorbance spectra were obtained with Jasco V-650 Spectrophotometer. Limits of detection for fluoride (at 377, 427, 425 and 412 nm for **3a**, **3b**, **3c** and **3d** respectively) and Al^{3+} (at 303, 323, 317 and 319 nm for **3a**, **3b**, **3c** and **3d** respectively) were calculated from UV-visible titration profiles. From the profiles the limit of detection concurs with the inflection point of the two slopes observed for the concentration ranges studied. Mass spectrometry analyses were performed at the Servei d'Espectrometria de Masses of the Universitat de València, Spain, on a Quadrupole time of flight (QqTOF) 5600 system (Applied Biosystems-MDS Sciex) spectrometer for high resolution mass spectra.

General procedure for the synthesis of imidazoquinolines **3a-d**

A solution of 5-amino-6-nitroquinoline **2** (1.05 equiv.) and formyl precursors **1a-d** (1 equiv.) in DMSO-EtOH (1:2, v/v) (5 mL) was treated with $\text{Na}_2\text{S}_2\text{O}_4$ (3 equiv), dissolved in a small volume of water, and heated at 80 °C with stirring for 15 h.

The mixture was then cooled to room temperature and neutralized with NH_4OH 5 M. The mixture was extracted with ethyl acetate and the organic phase was dried with magnesium sulphate and evaporated at reduced pressure to dryness. The pure product was obtained through recrystallization from dichloromethane or purified by column chromatography on silica with chloroform.

2-([1',1''-Biphenyl]-4'-yl)-3H-imidazo[4,5-f]quinoline (3a). Light yellow solid (45 mg, 64 %). Mp = 269–271 °C. ^1H NMR (400 MHz, $\text{DMSO}-d_6$): δ = 7.39–7.43 (m, 1H, H-4''), 7.48–7.53 (m, 2H, H-3'' and H-5''), 7.63–7.66 (m, 1H, H-5), 7.77–7.79 (m, 2H, H-2'' and H-6''), 7.84 (d, 1H, J = 8.8 Hz, H-9), 7.89–7.92 (dd, 2H, J = 8.8 and 2.0 Hz, H-2' and H-6'), 8.00 (d, 1H, J = 8.8 Hz, H-8), 8.34 (dd, 2H, J = 8.4 and 1.6 Hz, H-3' and H-5'), 8.87–8.92 (m, 2H, H-4 and H-6), 13.53 (broad s, 1H, NH) ppm. ^{13}C NMR (100.6 MHz, $\text{DMSO}-d_6$) δ = 121.1, 124.0, 126.7, 126.8, 127.2, 127.9, 129.0, 129.7, 139.2, 141.1, 145.3, 148.0, 150.4 ppm. HRMS: (FAB) m/z (%) for $\text{C}_{22}\text{H}_{15}\text{N}_3$; calcd 321.1266; found 322.1339 $[\text{M}+\text{H}]^+$.

2-(5'-Phenylthiophen-2'-yl)-3H-imidazo[4,5-f]quinoline (3b). Orange solid (50 mg, 65 %). Mp = 266–268 °C. ^1H NMR (300 MHz, $\text{DMSO}-d_6$): δ = 7.36 (t, 1H, J = 7.2 Hz, H-4''), 7.44–7.49 (m, 2H, H-3'' and H-5''), 7.62–7.66 (m, 2H, H-5 and H-4'), 7.76 (d, 2H, J = 7.2 Hz, H-2'' and H-6''), 7.82–7.87 (m, 2H, H-9 and H-3'), 7.98 (d, 1H, J = 9.0 Hz, H-8), 8.82–8.88 (m, 2H, H-4 and H-6), 13.55 (broad s, 1H, NH) ppm. ^{13}C NMR (75.4 MHz, $\text{DMSO}-d_6$) δ = 121.2, 123.9, 124.8, 125.5, 127.5, 128.3, 129.3, 130.0, 132.5, 133.1, 145.1, 145.2, 146.2, 148.0 ppm. HRMS: (FAB) m/z (%) for $\text{C}_{20}\text{H}_{13}\text{N}_3\text{S}$; calcd 327.0830; found 328.0825 $[\text{M}+\text{H}]^+$.

2-(1'-Methyl-5'-phenyl-1H-pyrrol-2'-yl)-3H-imidazo[4,5-f]quinoline (3c). Dark orange solid (28 mg, 52 %). Mp = 201–203 °C. ^1H NMR (400 MHz, $\text{DMSO}-d_6$): δ = 4.15 (s, 3H, CH_3), 6.36 (d, 1H, J = 4.0 Hz, H-4'), 7.01 (d, 1H, J = 3.2 Hz, H-3'), 7.37–7.41 (m, 1H, H-4''), 7.46–7.51 (m, 2H, H-3'' and H-5''), 7.53–7.56 (m, 2H, H-2'' and H-6''), 7.59–7.62 (m, 1H, H-5), 7.80 (d, 1H, J = 8.8 Hz, H-9), 7.95 (broad d, 1H, J = 7.2 Hz, H-8), 8.83–8.85 (m, 2H, H-4 and H-6), 13.05 (broad s, 1H, NH) ppm. ^{13}C NMR (100.6 MHz, $\text{DMSO}-d_6$) δ = 34.8, 109.2, 111.2, 121.0, 123.4, 124.8, 127.5, 128.6, 128.7, 129.6, 132.3, 138.2, 145.2, 146.0, 147.9 ppm. HRMS: (FAB) m/z (%) for $\text{C}_{21}\text{H}_{16}\text{N}_4$; calcd 324.1375; found 325.1448 $[\text{M}+\text{H}]^+$.

2-(5'-Phenylfuran-2'-yl)-3H-imidazo[4,5-f]quinoline (3d). Dark yellow solid (62 mg, 87 %). Mp = 264–266 °C. ^1H NMR (400 MHz, DMSO- d_6): δ = 7.22 (d, 1H, J = 3.6 Hz, H-4'), 7.33–7.39 (m, 2H, H-4'' and H-3'), 7.49–7.53 (m, 2H, H-3'' and H-5''), 7.60–7.64 (m, 1H, H-5), 7.85–7.87 (m, 1H, H-9), 7.93–7.98 (m, 3H, H-2'' and H-6'', H-8), 8.86–8.87 (m, 2H, H-4 and H-6), 13.52 (broad s, 1H, NH) ppm. ^{13}C NMR (100.6 MHz, DMSO- d_6) δ = 108.3, 112.3, 115.5, 121.3, 123.9, 124.5, 128.2, 129.0, 129.6, 130.5, 138.4, 142.8, 144.9, 145.6, 148.2, 154.1 ppm. HRMS: (FAB) m/z (%) for $\text{C}_{20}\text{H}_{13}\text{N}_3\text{O}$; calcd 311.1059; found 312.1131 $[\text{M}+\text{H}]^+$.

Physical measurements:

Stock solutions of the anions (F^- , Cl^- , Br^- , I^- , OCN^- , BzO^- , ClO_4^- , AcO^- , HSO_4^- , H_2PO_4^- and CN^- as tetrabutylammonium salts) and cations (Hg^{2+} , Cu^{2+} , Co^{2+} , Mg^{2+} , Fe^{3+} , Ba^{2+} , Fe^{2+} , Ni^{2+} , Ca^{2+} , Zn^{2+} , Pb^{2+} , Cd^{2+} , Cr^{3+} , Al^{3+} , K^+ and Li^+ as perchlorate salts) were prepared at 1×10^{-3} mol dm^{-3} in acetonitrile. The concentrations of ligands used in spectroscopy measurements were ca. 1×10^{-4} and 1×10^{-5} mol dm^{-3} . We took care that the maximum addition of anion solutions did not exceed 10% of the volume of the receptor to avoid significant changes in the total solution concentration. In the experiments that required the addition of excess of ions (30 equiv.), corrections of the volume and concentration were made. The UV-Vis and Fluorimetric titrations were carried out at room temperature (25 °C).

Theoretical studies:

Quantum chemical calculations at the semi-empirical level (PM3, within restricted Hartree–Fock level) were carried out in vacuum with the aid of Hyperchem V6.03. The Polar–Ribiere algorithm was used for optimization. The convergence limit and the RMS gradient were set to 0.01 kcal mol^{-1} . Stability constants were estimated with the HypSpec Software V1.1.18 using the data of the titration of receptors with selected anions.

2.4.6. Acknowledgements

We thank the Spanish Government (project MAT2012-38429-C04) and the Generalitat Valenciana (project PROMETEO/2009/016) for support. C. Marín-Hernández thanks the Spanish Ministry of Economy and Competitiveness for her grant. Thanks are also given to the Fundación Carolina and UPNFM-Honduras for a doctoral grant to L. E. Santos-Figueroa and to Generalitat Valenciana for Santiago Grisolia fellow to Sameh El Sayed. Thanks are also due to the Fundação para a Ciência e Tecnologia (Portugal) and FEDER-COMPETE for financial support through the Centro de Química - Universidade do Minho, Project PEst-C/QUI/ UI0686/2013 (FCOMP-01-0124-FEDER-037302) and a Post-doctoral grant to R.M.F. Batista (SFRH/BPD/79333/2011). The NMR spectrometer Bruker Avance III 400 is part of the National NMR Network and was purchased within the framework of the National Program for Scientific Re-equipment, with funds from FCT. We are also grateful to the Instituto da Educação of Universidade do Minho for providing the laboratory infrastructure necessary for the development of this work.

2.4.7. Notes and references

- 1 (a) Schmidtchen FP. Artificial host molecules for the sensing of anions. *Top Curr Chem* 2005;255;1-29. (b) Gale PA. Structural and Molecular Recognition Studies with Acyclic Anion Receptors. *Acc Chem Res* 2006;39;465-475. (c) Kaur K, Saini R, Kumar A, Luxami V, Kaur N, Singh P, Kumar S. Chemodosimeters: An approach for detection and estimation of biologically a medically relevant metal ion, anions and thiols. *Coord Chem Rev* 2012;256;1992-2028. (d) Ikeda A, Shinkai S. Novel Cavity Design Using Calix[n]arene Skeletons: Toward Molecular Recognition and Metal Binding. *Chem Rev* 1997;97;1713-1734.
- 2 (a) Rurack K. Flipping the light switch 'ON' - the design of sensor molecules that show cation-induced fluorescence enhancement with heavy and transition metal ions. *Spectrochim Acta, Part A* 2001;57A;2161-2195; (b) Lloris JM, Martínez-Máñez R, Padilla-Tosta ME, Pardo T, Soto J, Beer PD, Cadman J, Smith DK. Cyclic and open-chain aza-oxa ferrocene-functionalised derivatives as receptors for the selective electrochemical sensing of toxic heavy metal ions in aqueous environments. *J Chem Soc, Dalton Trans* 1999;14;2359-2369.

- 3 (a) Fabbrizzi L, Poggi A. Sensors and switches from supramolecular chemistry. *Chem Soc Rev* 1995;197-202. (b) Valeur B, Leray I. Design principals of fluorescent molecular sensors for cations recognition. *Coord Chem Rev* 2000;205;3-40.
- 4 Miyaji H, Sessler JL. Off the shelf colorimetric anion sensors. *Angew Chem Int Ed* 2001;40;154-157.
- 5 (a) Yuan L, Lin W, Zheng K, Zhu S. FRET- based small-molecule fluorescent probes: rational design and bioimaging applications. *Acc Chem Res* 2013;46;1462-1473; (b) Doussineau T, Schulz A, Lapresta-Fernandez A, Moro A, Körsten S, Trupp S, Mohr GJ. On the design of fluorescent ratiometric nanosensors. *Chem Eur J* 2010;16;10290-10299; (c) Wang S, Li N, Pan W, Tang B. Advances in functional fluorescent and luminiscent probes for imaging intracellular small-molecule reactive species. *Trends Anal Chem* 2012;39;3-37.
- 6 Martínez-Máñez R, Sancenón F. Fluorogenic and chromogenic chemosensors and reagents for anions. *Chem Rev* 2003;103;4419-4476.
- 7 Bissell RA, de Silva AP, Gunaratne HQN, Lynch PLM, Maguire GEM, Sandanayake KRAS. Molecular fluorescent signalling with 'fluor-spacer-receptor' systems: approaches to sensing and switching devices via supramolecular photophysics. *Chem Soc Rev* 1992;21;187-195.
- 8 Wiskur SL, Aït-Haddou H, Lavigne JJ, Anslyn EV. Teaching old indicators new tricks. *Acc Chem Res* 2001;34;963-972.
- 9 (a) Chae MY, Czarnik AW. Fluorometric chemodosimetry. Mercury (II) and silver (I) indication in water via enhanced fluorescence signaling. *J Am Chem Soc* 1992;114;9704-9705. (b) Dujols V, Ford F, Czarnik AW. A long-wavelength fluorescent chemodosimeter selective for Cu(II) ion in water. *J Am Chem Soc* 1997;119;7386-7387.
- 10 (a) Santos-Figueroa LE, Moragues ME, Climent E, Agostini A, Martínez-Máñez R, Sancenón F. Chromogenic and fluorogenic chemosensors and reagents for anions. A comprehensive review of the years 2010-2011. *Chem Soc Rev* 2013;42;3489-3613. (b) Moragues ME, Martínez-Máñez R, Sancenón F. Chromogenic and fluorogenic chemosensors and reagents for anions. A comprehensive review of the year 2009. *Chem Soc Rev* 2011;40;2593-2643. (c) Salinas Y, Martínez-Máñez R, Marcos MD, Sancenón F, Costero AM, Parra M, Gil S. Optical chemosensors and reagents to detect explosives. *Chem Soc Rev* 2012;41;1261-1296. (d) Kim SK, Lee DH, Hong JI, Yoon J. Chemosensors for pyrophosphate. *Acc Chem Res* 2009;42;23-31. (e) Chen X, Zhou Y, Peng X, Yoon. Fluorescent and colorimetric probes for

- detection of thiols. *J. Chem Soc Rev* 2010;39;2120-2135. (f) de Silva AP, Gunaratne HQN, Gunnlaugsson T, Huxley AJM, McCoy CP, Rademacher JT, Rice TE, Signaling recognition events with fluorescent sensors and switches. *Chem Rev* 1997;97;1515-1566.
- 11 Formica M, Fusi V, Giorgi L, Micheloni M. New fluorescent chemosensors for metal ions in solution. *Coord Chem Rev* 2012;256;170-192.
- 12 (a) Marín-Hernández C, Santos-Figueroa LE, Moragues ME, Raposo MMM, Batista RMF, Costa SPG, Pardo T, Martínez-Máñez R, Sancenón F. Imidazoanthraquinone derivatives for chromofluorogenic sensing of basic anions and trivalent metal cations. *J Org Chem* 2014;79;10752-10761. (b) Kar C, Samanta S, Mukherjee S, Datta BK, Ramesh A, Das G. A simple and efficient fluorophoric probe for dual sensing of Fe^{3+} and F^- : application to bioimaging in native cellular iron pools and live cells. *New J Chem* 2014;38;2660-2669. (c) Rosen CB, Hansen DJ, Gothelf KV. Efficient colorimetric and fluorescent detection of fluoride in DMSO-water mixtures with arylalldoximes. *Org Biomol Chem* 2013;11;7916-7922.
- 13 See for example: (a) González MC, Otón F, Espinosa A, Tárraga A, Molina P. A densely decorated disubstituted ferrocene as an iron-pair recognition receptor. *Chem Commun* 2013;49;9633-9635. (b) Piatek P. A selective chromogenic chemosensor for carboxylate salt recognition. *Chem Commun* 2011;47;4745-4747. (c) Ni XL, Zeng X, Redshaw C, Yamato T. Ratiometric fluorescent receptors for both Zn^{2+} and H_2PO_4^- ions based on a pyrenyl-linked triazole-modified Homooxalix[3]arene: a potential molecular traffic signal with an R-S latch logic circuit. *J Org Chem* 2011;76;5696-5702. (d) Shahid M, Srivastava P, Misra A. An efficient naphthalimide based fluorescent dyad (ANPI) for F^- and Hg^{2+} mimicking OR, XNOR and INHIBIT logic functions. *New J Chem* 2011;35;1690-1700. (e) Sahin O, Akceylan E. A phenantrene-based calix[4]arene as a fluorescent sensor for Cu^{2+} and F^- . *Tetrahedron* 2014;70;6944-6950. (f) Ding L, Wu M, Li Y, Chen Y, Su J. New fluoro- and chromogenic chemosensor for the dual –channel detection of Hg^{2+} and F^- . *Tetrahedron Lett* 2014;55;4711-4715.
- 14 (a) Muniz FM, Alcazar V, Sanz F, Simon L, de Arriba ALF, Raposo C, Moran JR. A xanthene-benzimidazole receptor with multiple h-bond donors for carboxylic acids. *Eur J Org Chem* 2010;6179-6185; (b) Molina P, Tarraga A, Oton F. Imidazole derivatives: a comprehensive survey of their recognitivon properties. *Org Biomol Chem* 2012;10;1711-1724; (c) Boiocchi M, Del Boca L, Gómez DE, Fabbri L, Licchelli M, Monzani E. Nature of urea-fluoride interaction: incipient and definitive proton transfer.

- J Am Chem Soc 2004;126;16507-16514; (d) Gómez DE, Fabbrizzi L, Licchelli M, Monzani E. Urea vs thiourea in anion recognition. *Org Biomol Chem* 2005;3;1495-1500; (e) Amendola V, Boiocchi M, Fabbrizzi L, Palchetti A. Anion receptor containing –NH binding sites: hydrogen-bond formation or neat proton transfer. *Chem Eur J* 2005;11;120-127; (f) Boiocchi M, Del Boca L, Gómez DE, Fabbrizzi L, Licchelli M, Monzani E. Anion-induced urea deprotonation. *Chem Eur J* 2006;11;3097-3104; (g) Gómez DE, Fabbrizzi L, Licchelli M. Why, on interaction of urea-based receptors with fluoride, beautiful color develop. *J Org Chem* 2005;70;5717-5720.
- 15 (a) Noszal B, Rabenstein DL. Nitrogen protonation microequilibria and C(2)-deprotonation microkinetics of histidine, histamine and related compounds. *J Phys Chem* 1991;95;4761-4765. (b) Batista RMF, Costa SPG, Raposo MMM. Selective colorimetric and fluorimetric detection of cyanide in aqueous solution using novel heterocyclic imidazo-anthraquinones. *Sensors Act B Chem* 2014;191;791-799;
- 16 (a) Raposo MMM, García-Acosta B, Ábalos T, Calero P, Martínez-Máñez R, Ros-Lis JV, Soto J. Synthesis and study of the use of heterocyclic thiosemicarbazones as signaling scaffolding for the recognition of anions. *J Org Chem* 2010;75;2922-2933; (b) Santos-Figueroa LE, Moragues ME, Raposo MMM, Batista RMF, Costa SPG, Ferreira RCM, Sancenón F, Martínez-Máñez R, Ros-Lis JV, Soto J. Synthesis and evaluation of thiosemicarbazones functionalized with furyl moieties as new chemosensors for anion recognition. *Org Biomol Chem* 2012;10;7418-7428.
- 17 (a) Patra S, Gunupuru R, Lo R, Suresh E, Ganguly B, Paul P. Cation-induced fluorescence excimer emission in calix [4] arene-chemosensors bearing quinoline as a fluorogenic unit: experimental, molecular modeling and crystallographic studies. *New J Chem* 2012;36; 988-1002; (b) Jiang Z, Lv H, Zhu J, Zhao B. New fluorescent chemosensor based on quinoline and coumarine for Cu²⁺. *Synthetic Met* 2012; 162;2112-2116.
- 18 Backman GB, Bennet GE, Barker RS. Synthesis of substituted quinolyamines. Derivatives of 4-amino-7-chloroquinoline. *J Org Chem* 1950;15;1278-1284.
- 19 (a) Karashima T, Komatsu T, Niimura M, Kawada C, Kamada M, Inoue K, Udaka K, Kuroda N, Shuin T. Novel combination therapy with imiquimod and sorafenib for renal cell carcinoma. *Int J Urol* 2014;21;;702-706.
- 20 Jain PC, Kapoor V, Anand N, Patnaik GK, Ahmad A, Vorah MC. Chemical and pharmacological investigations of some omega.-substituted alkylamino-3-aminopyridines. *J Med Chem* 1968;11;87-92.

- 21 Kayarmar R, Nagaraja GK, Bhat M, Naik P, Rajesh KP, Shetty S, Arulmoli T. Synthesis of azabicyclo [4.2.0] octa-1,3,5-trien-8-one analogues of 1H-imidazo[4,5-c]quinoline and evaluation of their antimicrobial and anticancer activities. *Med Chem Res* 2014;23;2964-2975.
- 22 See for example: (a) Agostini A, Campos I, Milani M, Elsayed S, Pascual LI, Martínez-Máñez R, Licchelli M, Sancenón F. A surfactant-assisted probe for the chromo-fluorogenic selective recognition of GSH in water. *Org Biomol Chem* 2014;12;1871-1874; (b) Climent E, Mondragón L, Martínez-Máñez R, Sancenón F, Marcos MD, Murguía JR, Amorós P, Rurack K, Pérez-Payá E. Selective, highly sensitive, and rapid detection of genomic DNA by using gated materials: mycoplasma detection. *Angew Chem Int Ed* 2013;52;8939-8942; (c) Santos-Figueroa LE, Giménez C, Agostini A, Aznar E, Marcos MD, Sancenón F, Martínez-Máñez R, Amorós P. Selective and sensitive chromofluorogenic detection of the sulfite anion in water using hydrophobic hybrid organic-inorganic silica nanoparticles. *Angew Chem Int Ed* 2013;52;13712-13716; (d) Climent E, Gröninger D, Hecht M, Walter MA, Martínez-Máñez R, Weller MG, Sancenón F, Amorós P, Rurack K. Selective, sensitive and rapid analysis with lateral-flow assays based on antibody-gated dye-delivery systems: the example of triacetone triperoxide. *Chem Eur J* 2013;19;4117-4122; (e) Moragues ME, Esteban J, Ros-Lis JV, Martínez-Máñez R, Marcos MD, Martínez M, Soto J, Sancenón F. Sensitive and selective chromogenic sensing of carbon monoxide via reversible axial CO coordination in binuclear rhodium complexes. *J Am Chem Soc* 2011;133;15762-15772; (f) Climent E, Marcos MD, Martínez-Máñez R, Sancenón F, Soto J, Rurack K, Amorós P. The determination of methylmercury in real samples using organically capped mesoporous inorganic materials capable of signal amplification. *Angew Chem Int Ed* 2009;48;8519-8522; (g) Batista RMF, Costa SPG, Silva RMP, Lima NEM, Raposo MMM. Synthesis and evaluation of arylfuryl-bis(indolyl)methanes as selective chromogenic and fluorogenic ratiometric receptor for mercury ion in aqueous solution. *Dyes Pigm* 2014;102;293-300; (h) Batista RMF, Oliveira E, Costa SPG, Lodeiro C, Raposo MMM. (Oligo)thienyl-imidazo-crown ether derivatives synthesis, photophysical studies and evaluation of their chemosensors properties. *Talanta* 2011;85; 2470-2478.
- 23 Yang D, Fokas D, Li J, Yu L, Baldino CM. A versatile method for the synthesis of benzimidazoles from o-nitroanilines and aldehydes in one step via a reductive cyclization. *Synthesis* 2005;47-56.

- 24 See for example: (a) Amendola V, Esteban-Gómez D, Fabbrizzi L, Licchelli M. What anions do to N-H-containing receptors. *Acc Chem Res* 2006;39;343-353. (b) Chen J, Liu C, Zhang J, Ding W, Zhou M, Wu F. A novel chemodosimeter for fluoride ions based on deprotonation of the C-H group followed by an autoxidative decyanation process. *Chem Commun* 2013;49;10814-10816. (c) He X, Herranz F, Cheng ECC, Vilar R, Yam VWW. Design, synthesis, photophysics, and anion-binding studies of bis(dicyclohexylphosphino)methane-containing dinuclear gold (I) thiolate complexes with urea receptors. *Chem Eur J* 2010;16;9123-9131. (d) Carasel IA, Yamnitz CR, Winters RK, Gokel GW. Halide ions complex and deprotonate dipicolinamides and isophthalamides: assessment by mass spectrometry and UV-visible spectroscopy. *J Org Chem* 2010;75;8112-8116. (e) Rostami A, Colin A, Li XY, Chudzinski MG, Lough AJ, Taylor MS. N,N'-diarylsquaramides: general, high-yielding synthesis and applications in colorimetric anion sensing. *J Org Chem* 2010;75;3983-3992. (f) Amendola V, Bergamaschi G, Boiocchi M, Fabbrizzi L, Milani M. Tghe squaramide versus urea contest for anion recognition. *Chem Eur J* 2010;16;4368-4380.
- 25 Batista RMF, Oliveira E, Costa SPG, Lodeiro C, Raposo MMM. Synthesis and ion sensing properties of new colorimetric and fluorimetric chemosensors based on bithienyl-imidazo-anthraquinone chromophores. *Org Lett* 2007;9;3201-3204.
- 26 See for example: (a) Maity D, Chakraborty A, Gunupuru R, Paul P. Calix[4]arene based molecular sensors with pyrene as fluorogenic unit: effect of solvent in ion selectivity and colorimetric detections of fluoride. *Inorg Chim Acta* 2011;372;126-135. (b) Ghosh K, Kar D, Chowdhury PR. Benzimidazolium-based simple host for fluorimetric sensing of H_2PO_4^- , F^- , PO_4^{3-} and AMP under different conditions. *Tetrahedron Lett* 2011;52;5098-5103. (c) Park JJ, Kim YH, Kim C, Kang J. Naked eye detection of fluoride and pyrophosphate with an anion receptor utilizing anthracene and nitrophenyl group as signaling group. *Tetrahedron Lett* 2011;52;2759-2763. (d) Liu R, Gao Y, Zhang Q, Yang X, Lu X, Ke Z, Zhou W, Qu J. A fluorescent probe based on hydroxynaphthalene 2-cyanoacrylate: fluoride ion detection and its bio-imaging in live cells. *New J Chem* 2014;38;2941-2945.
- 27 (a) Kumari N, Jha S, Bhattacharya S. Colorimetric probes based on anthraimidazolediones for selective sensing of fluoride and cyanide ion via intramolecular charge transfer. *J Org Chem* 2011;76;8215-8222
- 28 (a) Diaz DD, Finn MG, Mishima M. Substituent effect on the gas-phase basicity of formamidinium ureas. *Eur J Org Chem* 2006;235-240. (b) Schmidt am Busch M, Knapp

EW. Accurate pKa determination for a heterogeneous group of organic molecules. *Chem Phys Chem* 2004;5;1513-1522. (c) da Silva EF. Comparison of quantum mechanical and experimental gas-phase basicities of amines and alcohols. *J Phys Chem A* 2005;109;1603-1607. (d) Remko M, Lyne PD, Richards WG. Molecular structure, gas-phase acidity and basicity of N-hydroxyurea. *Phys Chem Chem Phys* 1999;1;5353-5357. (e) Ros-Lis JV, Martínez-Máñez R, Sancenón F, Soto J, Rurack K, Weisshoff H. Signalling mechanisms in anion-responsive push-pull chromophores: the hydrogen-bonding deprotonation and anion-exchange chemistry of functionalized azo dyes. *Eur J Org Chem* 2007;15;2449-2458.

2.5. Conclusions

The optical detection of anions and cations is a crucial issue due to the important roles that this ionic species played in environmental and biological processes. In this chapter we prepared two families of chemosensors, based on imidazoanthraquinone and imidazoquinoline heterocycles, and studied their optical behavior in the presence of selected anionic and cationic species. Bearing this in mind, following conclusions can be drawn from this chapter:

- A family of four imidazoanthraquinone probes was synthesized and their coordination behaviour toward anions and cations tested. The four probes presented absorption bands in the 400-470 nm interval and are moderately emissive (in the 530-580 nm interval). Of all the anions tested, only fluoride induced a marked red-shift of the absorption bands due to a deprotonation process of the imidazole ring. Besides, fluoride induced an initial moderate quenching (upon addition of small anion quantities) together with the appearance of a new red-shifted emission at higher anion concentrations. On the other hand, of all the cations tested, only Fe^{3+} , Al^{3+} and Cr^{3+} induced a marked blue-shift of the visible band of the four probes and a marked emission quenching. The optical changes observed in the presence of trivalent cations are due to a preferential coordination with the nitrogen atoms of the anthraquinone and imidazole rings.
- Four imidazoquinoline probes are prepared and their coordination behaviour toward anions and cations tested. Acetonitrile solutions of the four probes presented intense absorption (in the 330-370 nm interval) and emission (in the 390-460 nm range) bands. Of all the anions tested, only fluoride induced the appearance of a red-shifted absorption band with a moderate quenching of the emission for the four receptors. These changes were ascribed to a fluoride-induced deprotonation of the imidazole ring in the four probes. The response with cations was unselective and the addition of Hg^{2+} , Cu^{2+} , Co^{2+} , Fe^{3+} , Fe^{2+} , Zn^{2+} , Pb^{2+} , Cd^{2+} , Cr^{3+} and Al^{3+} induced the appearance of red-shifted absorptions and marked emission quenching for the four probes.

3. CO Sensors

3.1. Introduction

3.1.1. Carbon monoxide

Properties

Carbon monoxide (CO) consists of one carbon and one oxygen atoms linked through a triple bond. Its length is 112.8 pm and its dissociation energy, 1072 kJ/mol, which makes it the strongest chemical bond known.¹ Its molar mass is 28.01 g/mol, which makes it slightly lighter than air. Finally, CO has a boiling point of $-191.5\text{ }^{\circ}\text{C}$ and a melting point of $-205.02\text{ }^{\circ}\text{C}$, it is a gas at normal conditions.

Reactivity

Carbon monoxide takes part in the synthesis of multiple organic compounds. For instance, aldehydes are produced by the hydroformylation of alkenes with CO and H₂. CO can be reduced to methanol by hydrogenation process. Moreover, CO and methanol can give acetic acid when in the presence of a rhodium catalyst and hydroiodic acid. Also, phosgene (COCl₂) is produced by passing purified CO and chlorine gas through a bed of porous activated carbon, which serves as a catalyst. From an inorganic point of view, carbon monoxide is involved in the industrial preparation of methane (natural gas), and it is also used as industrial reductor in the extraction of metals, from the corresponding metal oxide ores.

Toxicity

This highly toxic gas is colorless, odorless and tasteless. That is the reason why it is known as “the silent killer”. When inhaled, CO is readily absorbed from the lungs into the bloodstream, where it combines with hemoglobin (Hb) and usurps the space that normally carries oxygen, resulting in carboxyhemoglobin (COHb). CO binds 200 times more effectively to Hb than oxygen. The presence of COHb in the blood decreases the oxygen carrying capacity, reducing the availability of oxygen to body tissues and resulting in tissue hypoxia. A reduction in oxygen delivery because of the elevated COHb level, exacerbated by impaired perfusion resulting from hypoxic cardiac dysfunction, potentially will impair cellular

¹ T. L. Cottrell, *The Strengths of Chemical Bonds*, 2nd ed., Butterworths Scientific Publications, London, 1958.

oxidative metabolism. COHb levels greater than 20 % are typically associated with symptoms of clinical toxicity. Elevated or chronic exposures may lead to neurotoxicity, cognitive and visual impairment, and unconsciousness, with death occurring in the range of 50 to 80 % COHb.²

The health risks associated with CO vary depending on its concentration and duration of exposure. The risks associated with the relatively low ambient concentrations found in the environment and in contaminated work places have been extensively studied and reviewed.³ 0.2 ppm (parts per million) is the natural CO levels in air and the maximum recommended indoor CO level rises to 9 ppm. Above this quantity and up to 24 ppm, it can produce possible health effects with long-term exposure. Just a bit more, 25 ppm is the maximum exposure for 8-hour-work-day, and 50 ppm corresponds to the maximum permissible exposure in workplace. CO concentrations above 100 ppm can induce slight headache after 1-2 hours, whereas this symptom can be intensified and accompanied with nausea at 400 ppm of CO. If CO levels are about 800 ppm, it can cause unconsciousness after 1 hour, and death within 2-3 hours.

Indoor levels⁴ of CO range from 0.5 to 5 ppm but may reach much higher values (e.g. 100 ppm) with inefficient heating or ventilation, or in the presence of environmental tobacco smoke. In urban areas, ambient levels⁵ are typically 20 to 40 ppm, but may peak at much higher levels in heavily congested areas or alongside highways.

Carbon monoxide poisoning is the most common type of fatal air poisoning in many countries. The Centers for Disease Control and Prevention estimate that several thousand people go to hospital emergency rooms every year to be treated

² D. Gorman, A. Drewry, Y. L. Huang, C. Sames, *Toxicology*, **2003**, *187*, 25-38.

³ a) D. G. Penney, *Carbon Monoxide*, CRC Press, Boca Raton, FL, **1996**; b) R. Bascom, P. A. Bromberg, D. L. Costa, R. Devlin, D. W. Dockery, M. W. Frampton, W. Lambert, J. M. Samet, F. E. Speizer, M. Utell, *Am. J. Respir. Crit. Care Med.* **1996**, *153*, 477-498; c) US Environmental Protection Agency, *Air Quality Criteria for Carbon Monoxide*, EPA/600/P-99/001. *National Center for Environmental Assessment*, Research Triangle Park, NC, **1999**.

⁴ D. Penney, V. Benignus, S. Kephelopoulos, D. Kotzias, M. Kleinman, A. Verrier, *WHO Guidelines for Indoor Air Quality: Selected Pollutants*, Copenhagen, **2010**, 55.

⁵ J. Raub, *WHO Environmental Health Criteria: Carbon Monoxide*, Geneva, **1999**, 70.

for carbon monoxide poisoning.⁶ Because of the risk of occult poisoning, some communities now require the installation of CO detectors in residences, along with smoke detectors and fire alarms.

Occurrence

Carbon monoxide occurs in various natural and artificial environments. It is present in small amounts in the atmosphere, mainly as a product of volcanic activity but also from natural and man-made fires (such as forest and bushfires, burning of crop residues, and sugarcane fire-cleaning).⁷

This gas is a temporary atmospheric pollutant in some urban areas, mainly from the exhaust of internal combustion engines (including vehicles, portable and back-up generators, etc.), but also from incomplete combustion of various other fuels (including wood, coal, oil, paraffin, propane, natural gas, and trash).⁸

In closed environments, the concentration of carbon monoxide can easily rise to lethal levels due to malfunctioning fuel-burning appliances such as furnaces, ranges, water heaters, and gas and kerosene room heaters; engine-powered equipment such as portable generators; fireplaces; and charcoal that is burned in homes and other enclosed areas. Still others die from carbon monoxide produced by non-consumer products, such as cars left running in attached garages.⁹

Despite not being the anhydride of any acid, CO can be produced in the laboratory by the dehydration of formic acid, for example with sulfuric acid.

⁶ Centers for Disease Control and Prevention, National Environmental Public Health Tracking Network, Carbon Monoxide Poisoning, accessed **2009**.

⁷ A. Sigel and R. K. O. Sigel, Roland, *Metal-Carbon Bonds in Enzymes and Cofactors*, Royal Society of Chemistry, **2009**.

⁸ M. Pommier, C. A. McLinden and M. Deeter, *Geophysical Research Letters*, **2013**, *40*, 3766.

⁹ U.S Consumer Product Safety Commission, *Carbon Monoxide Questions and Answers*, **2009**.

CO use in medical therapies

The interest in this gas has intensified in part due to the discovery of the therapeutic and cell-signalling role that this small molecule plays in biological systems.

CO can confer modulatory effects on the regulation of several fundamental biological processes¹⁰ including vascular tone,¹¹ inflammation,¹² neurotransmission,¹³ cell proliferation,¹⁴ programmed cell death,¹⁵ mitochondrial biogenesis¹⁶ and autophagy.¹⁷

The initial evidence supporting a beneficial action of CO originated from studies on lung injury in animals¹⁸ and was reproduced later in almost all tissues examined, including heart, liver, kidney, intestine and reticulo-endothelial system.¹⁹

Despite the interesting biological activities discovered, the development of methods for delivering CO is in its infancy. Since CO is toxic at high concentrations, the precise control of the location, timing, and dosages of CO is the critical factor for appropriate therapeutic responses. In addition, the fact that CO is a gaseous molecule makes its controlled delivery more challenging. At the present, three different approaches have been proposed for examining the therapeutic potential of CO: (1) direct administration of CO gas; (2) use of prodrugs (i. e. methylene

¹⁰ a) R. Motterlini, B. E. Mann, T. R. Johnson, J. E. Clark, R. Foresti, C. J. Green, *Curr. Pharm. Des.*, **2003**, *9*, 2525-2539; b) T. R. Johnson, B. E. Mann, J. E. Clark, R. Foresti, C. J. Green, R. Motterlini, *Angew. Chem. Int. Ed.*, **2003**, *42*, 3722-3729.

¹¹ W. Durante, F. K. Johnson, R. A. Johnson, *J. Cell. Mol. Med.*, **2006**, *10*, 672-686.

¹² L. E. Otterbein, F. H. Bach, J. Alam, *Nat. Med.*, **2000**, *6*, 422-428.

¹³ A. Verma, D. J. Hirsch, C. E. Glatt, G. V. Ronnett, S. H. Snyder, *Science*, **1993**, *259*, 381-384.

¹⁴ T. Morita, S. A. Mitsialis, H. Koike, Y. Liu, S. Kourembanas, *J. Biol. Chem.*, **1997**, *272*, 32804-32809.

¹⁵ S. Brouard, L. E. Otterbein, J. Anrather, *J. Exp. Med.*, **2000**, *192*, 1015-1026.

¹⁶ H. B. Suliman, M. S. Carraway, L. G. Tatro, C. A. Piantadosi, *J. Cell. Sci.*, **2007**, *120*, 299-308.

¹⁷ S. J. Lee, S. W. Ryter, J. F. Xu, *Am. J. Respir. Cell. Mol. Biol.*, **2011**, *45*, 867-873.

¹⁸ L. E. Otterbein, L. L. Mantell, A. M. K. Choi, *Am. J. Physiol.*, **1999**, *276*, L688-L694.

¹⁹ a) H. P. Kim, S. W. Ryter, A. M. Choi, *Annu. Rev. Pharmacol. Toxicol.*, **2006**, *46*, 411-449; b) S. W. Ryter, J. Alam, A. M. Choi, *Physiol. Rev.*, **2006**, *86*, 583-650.

chloride) that are catabolized by hepatic enzymes to generate CO;²⁰ and (3) transport and delivery of CO by means of specific CO carriers.

The simplest administration method is the inhalation of CO at a known and low concentration, which has shown therapeutic benefits in preclinical animal models of acute lung injury, ischemia/reperfusion injury, sepsis, vascular injury, organ transplantation and others.

As an alternative approach to the administration of CO gas by inhalation, chemical CO-donor compounds termed carbon monoxide releasing molecules (CORMs) have been recently developed. CO liberated from CORMs present some advantages: it can be precisely controlled and delivered, CORMs release CO in a very specific way, and moreover, they deliver it with less COHb formation than inhalation. There are several prototypical CORMs including Mn₂CO₁₀ (CORM-1)²¹ and ruthenium compounds [Ru(CO)₃Cl₂]₂ (CORM-2)²² and Ru(CO)₃Cl(glycinate) (CORM-3). Derived from these CORMs are PhotoCORMs²³ that are able to release CO in a controlled manner via photoactivation.

3.1.2. Carbon monoxide detection

The majority of sensors used for the detection of CO in air are based on electrochemical cells and on semiconducting metal oxides (typically tin dioxide).²⁴ However, significant progress has been made recently towards the development of new, inexpensive CO sensors using different technologies. In this context,

²⁰ C. Chauveau, D. Bouchet, J. C. Roussel, P. Mathieu, C. Braudeau, K. Renaudin, L. Tesson, J. P. Souillou, S. Iyer, R. Buelow, I. Aegon, *Am. J. Transplant.*, **2002**, *2*, 581-592.

²¹ a) R. Motterlini, J. E. Clark, R. Foresti, P. Sarathchandra, B. E. Mann, C. J. Green, *Circ. Res.*, **2002**, *90*, E17-E24; b) E. Fiumana, H. Parfenova, J. H. Jagger, C. W. Leffler, *Am. J. Physiol. Heart Circ. Physiol.*, **2003**, *284*, H1073-H1079; c) B. Arregui, B. Lopez, M. G. Salom, F. Valero, C. Navarro, F. J. Fenoy, *Kidney Int.*, **2004**, *65*, 564-574.

²² a) J. Megias, J. Busserolles, M. J. Alcaraz, *Br. J. Pharmacol.*, **2007**, *150*, 977-986; b) B. W. Sun, Z. Y. Chen, X. Chen, C. Liu, *J. Burn. Care Res.*, **2007**, *28*, 173-181; c) M. Allanson, V. E. Reeve, *Cancer Immunol. Immunother.*, **2007**, *56*, 1807-1815; d) K. Srisook, S. S. Han, H. S. Choi, M. H. Li, H. Ueda, C. Kim, Y. N. Cha, *Biochem. Pharmacol.*, **2006**, *71*, 307-318.

²³ a) R. Motterlini and L. E. Otterbein, *Nature Rev.*, **2010**, *9*, 728-743; b) C. Szabo, *Nature Rev. Drug. Discovery*, **2016**, *15*, 185-203.

²⁴ B. Wang, Y. Zhao, D. Yu, L. M. Hu, J. S. Cao, F. L. Gao, Y. Liu and L. J. Wang, *Chin. Sci. Bull.* **2010**, *55*, 228-232; b) H. Ge and J. Liu, *Sens. Actuators B*, **2006**, *117*, 408-414.

colorimetric and fluorimetric probes for carbon monoxide, that exhibit striking optical changes visible to the 'naked eye' at low concentrations of the analyte, are seen as a powerful alternative to the established systems.

Since the discovery of the benign role of carbon monoxide, a whole new research field, focused on the real-time detection of CO in living cells and tissues, has emerged. This coincides with the interest in the therapeutic potential of CO-releasing molecules. The growth of these fields has led to attempts to develop luminescent chemosensors capable of quantifying the production of endogenous CO or the generation of CO by CORMs in cells.²⁵ However, despite this attention, only a few systems capable of the fluorogenic detection of CO in cells and tissues have been reported.

Most of the probes developed for the optical sensing of CO, both for detection in air or in cells, are based on metal complexes, as they possess many promising attributes suited to the design of chromo- or fluorogenic probes²⁶ The possibility of tuning the steric and/or electronic properties of metal complexes enables a subtle control to be exerted over the selectivity and reactivity of the metal towards CO.²⁷ In terms of CO-detection, the sensing mechanism is intrinsically related to the reactivity of the metal centre towards carbon monoxide and in most cases the detection is often unsurprisingly related to the direct coordination of CO to the metal. The binding of CO to the metal centre can occur at a vacant coordination site or through the displacement of a labile ligand (*vide infra*).

When using metal complexes the optical response can be triggered in two different ways. It can arise from (a) the OFF-ON switching of the optical response from the metal complex, which acts as both receptor and signalling unit, or (b) via the revival of the optical signal of a displaced ligand, which was previously quenched by its close proximity to the metal centre.²⁷ Alternatively, transition-metal catalysed carbonylation, hydrocarboxylation and azidocarbonylation reactions in the presence of CO have also proved to be useful in generating highly

²⁵ S. H. Heinemann, T. Hoshi, M. Westerhausen and A. Schiller, *Chem. Commun.*, **2014**, 50, 3644-3660.

²⁶ K. K.-W. Lo and S. P.-Y. Li, *RSC Adv.*, **2014**, 4, 10560-10585.

²⁷ C. W. Rogers and M. O. Wolf, *Coord. Chem. Rev.*, **2002**, 233-234, 341-350.

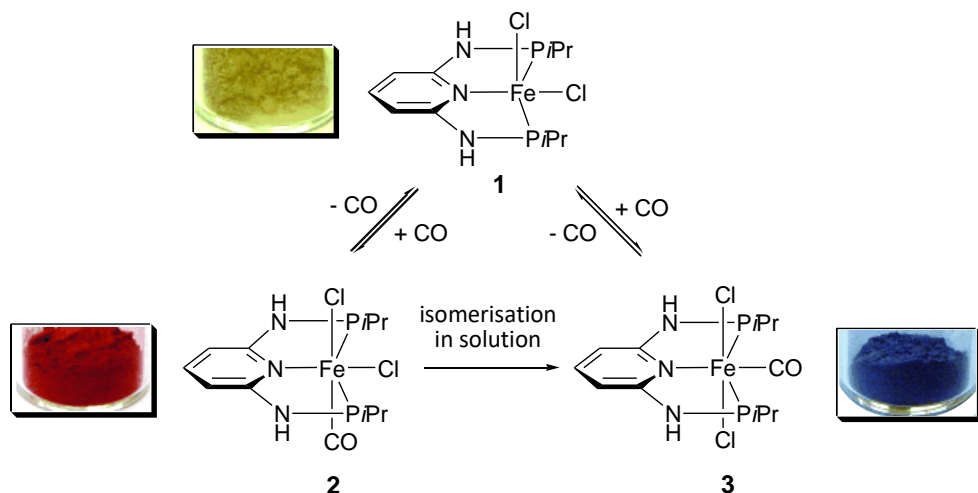
fluorescent derivatives from poorly emissive organic precursors. Ideally, such reactions should be immediate and need to take place under mild temperatures and at atmospheric pressure.

Chromogenic CO sensors

All examples in this section are based on the use of transition metal complexes that show a clear colour change in the presence of CO in air or when air containing CO is bubbled through solutions of the complexes. For all complexes detailed below the coordination of CO to the electron-rich metal centre induces a variation of the electron density and/or change of the spin-state of the metal, thus modifying the coordination environment, which ultimately results in a clear colour change.

An early example from 2008, presented by Kirchner and co-workers, is based on the use of the coordinatively-unsaturated iron pincer complex **1** [FeCl₂(PNP-*i*Pr)], (PNP-*i*Pr = *N,N'*-bis(diisopropylphosphino)-2,6-diaminopyridine), which binds CO in a stereospecific and reversible manner.²⁸ Complex **1** was found to react selectively with CO in both solution and the solid state, affording the *cis* or *trans* isomers **2** and **3**. In the presence of CO, the light yellow complex **1** converts to the deep red complex **2**, while retaining its crystallinity. Moreover, in the absence of CO, the heating of complex **2** under vacuum results in the complete regeneration of **1** and the recovery of the initial yellow colour. This remarkable solid-state reaction is fully reversible with no decomposition reported. Alternatively, the deep blue *trans* complex **3** can be obtained by bubbling CO through an acetone solution of **1** for 2 minutes or by a *cis-trans* isomerisation reaction of complex **2** in DMSO (Scheme 3.1.1). Although these complexes show outstanding optical properties in the presence of CO, they are not suitable probes for CO detection in terms of air-stability and ease of handling.

²⁸ D. Benito-Garagorri, M. Puchberger, K. Mereiter and K. Kirchner, *Angew. Chem. Int. Ed.*, **2008**, *47*, 9142-9145.



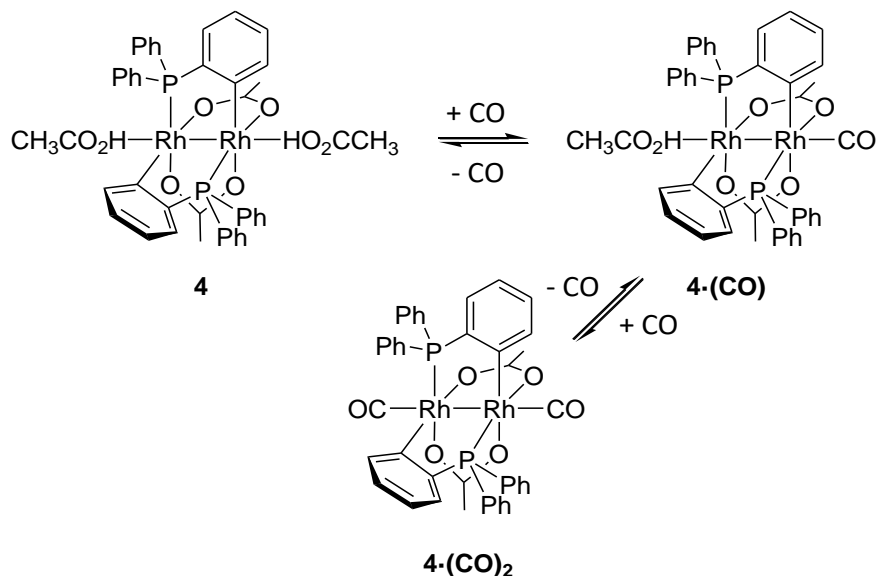
Scheme 3.1.1. Reaction of the iron complex **1** with CO, showing the associated colour changes. Adapted and reprinted with permission from ref. 28. Copyright 2008 Wiley-VCH.

An ideal chromogenic system, not only selective and sensitive, but also air- and photo- stable, was reported in 2010 by Martínez-Mañez and co-workers. It is based on a binuclear rhodium complex that shows colour change in the presence of increasing concentrations of CO.²⁹

Complex **4** enables the detection of CO as its colour varies from violet to orange-yellow when air samples containing CO are bubbled through chloroform solutions of the complex. Colour modulations are due the displacement of the carboxylic acid ligands in the axial positions and the subsequent coordination of up to two molecules of CO (compounds **4·CO** and **4·(CO)₂** in Scheme 3.1.2). The system is reversible and, when carbon monoxide is removed from the atmosphere, the initial violet colour is recovered without significant degradation of the compound. The operational advantage of this system rests on the intrinsic reactivity of this probe in the solid state. Once probe **4** is immobilised on silica gel, the reaction with CO in air takes place in just a few minutes, resulting in a change in colour visible to the naked eye at subtoxic concentrations of CO (50 ppm). Moreover, using diffuse reflectance methods, the limit of detection is calculated

²⁹ J. Esteban, J. V. Ros-Lis, R. Martínez-Mañez, M. D. Marcos, M. E. Moragues, J. Soto and F. Sancenón, *Angew. Chem., Int. Ed.*, **2010**, *49*, 4934-4937.

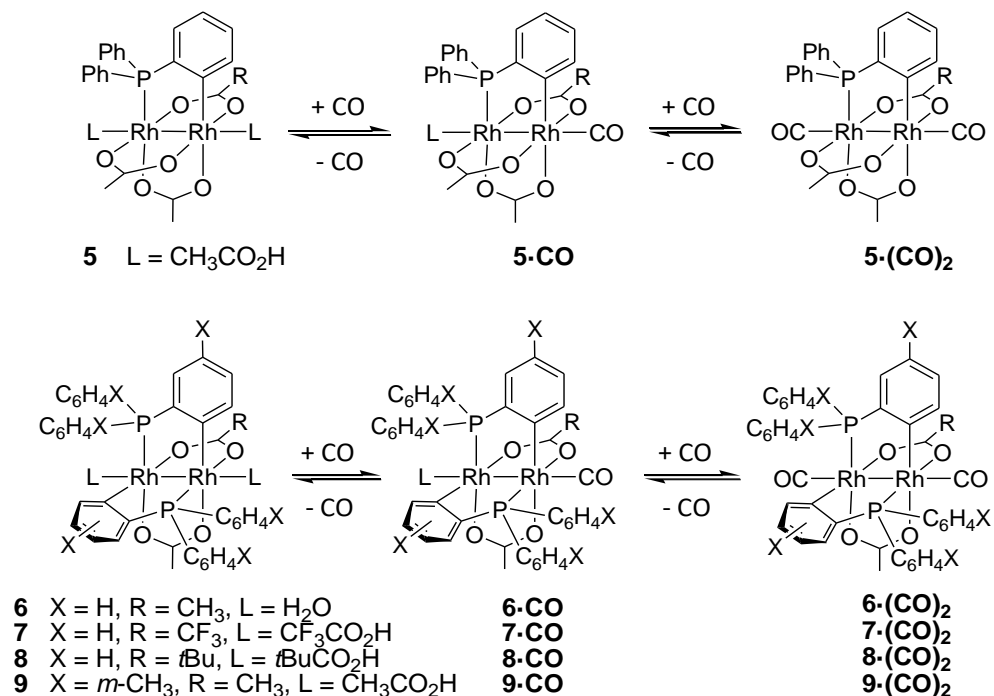
to be as low as 0.5 ppm. The probe shows high selectivity towards carbon monoxide over other common gases (CO_2 , N_2 , O_2 , Ar, SO_2 , NO, NO_2 and water vapour) and volatile organic compounds (acetone, chloroform, ethanol, formaldehyde, hexane, toluene and xylene). This aspect allows molecular sensors to avoid the drawbacks of many commercial devices based on semiconducting metal oxides, which have to be sited carefully to avoid exposure to high levels of steam or particulates. False alarms can also be caused by solvents from cleaning or cosmetic products (e.g., hairspray), so screening for potential interferents is particularly important if the probe is to be used in domestic or workplace settings for CO detection in air.



Scheme 3.1.2. Binuclear rhodium complex **4** and the formation of the corresponding complexes upon coordination of one (**4·CO**) or two (**4·(CO)₂**) molecules of CO in axial positions.

Following this, in 2011, same researchers reported a family of binuclear rhodium complexes of general formula $[\text{Rh}_2\{(\text{XC}_6\text{H}_3)\text{P}(\text{C}_6\text{H}_4\text{X})_2\}_n(\text{O}_2\text{CR})_{4-n}] \cdot \text{L}$, bearing

one ($n = 1$) (**5**) or two ($n = 2$) (**6** to **9**) differently meta-substituted ($X = \text{H}, \text{CH}_3$) cyclometallated phosphines.



Scheme 3.1.3. Binuclear rhodium complexes **5-9** and the corresponding products obtained upon coordination of one and two molecules of CO in the axial positions.

Further tuning proved possible using various different equatorial ligands ($R = \text{CH}_3, \text{CF}_3$, or $t\text{Bu}$) and axial groups ($L = \text{CH}_3\text{CO}_2\text{H}, \text{CF}_3\text{CO}_2\text{H}, t\text{BuCO}_2\text{H}$, or H_2O).³⁰

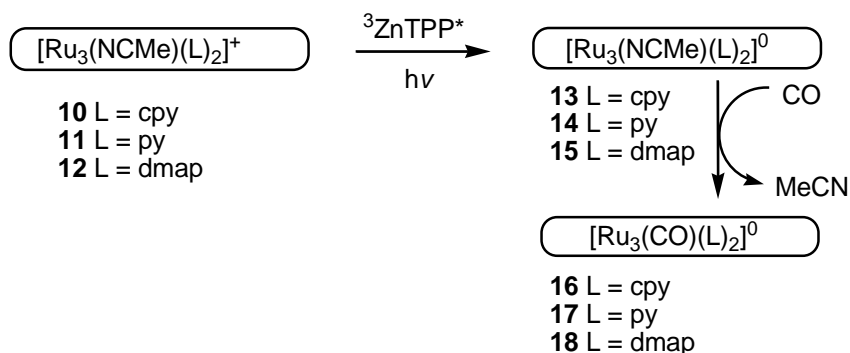
In a similar manner to complex **4**, this family of dirhodium complexes shows remarkable selectivity and sensitivity towards CO in air, with ‘naked eye’ detection limits as low as 0.2 ppm when immobilised on solid supports (silica gel and cellulose strips). As in the case of **4**, colour changes were observed due to the coordination of one (**5·CO** to **9·CO**) or two (**5·(CO)₂** to **9·(CO)₂**) carbonyl ligands

³⁰ M. E. Moragues, J. Esteban, J. V. Ros-Lis, R. Martínez-Mañez, M. D. Marcos, M. Martínez, J. Soto and F. Sancenón, *J. Am. Chem. Soc.*, **2011**, *133*, 15762-15772.

(depending on the structure of the complex) at the axial sites (Scheme 3.1.3). The studies based on these rhodium complexes clearly show that, by combining the electron-withdrawing/donating properties of the equatorial and axial ligands, it is possible to tune the level of electron density on the rhodium centre, and thus modulate the $d-\pi^*$ back-donation. It was then possible to go on to demonstrate that these properties are connected to the kinetic rate of CO release of **5**·(CO)₂ and **9**·(CO)₂, as stronger back-donation corresponds to a weaker ability to release the two carbonyl groups and to recover the initial colour.

Another example of chromogenic CO detection involves the use of the oxo-acetato-bridged triruthenium complex $[\text{Ru}_3(\text{NCMe})(\text{cpy})_2]^+$ (cpy = 4-cyanopyridine) (**10**). This complex exhibits a cyan colour in acetonitrile solutions due to the presence of the main broad absorption band centred at 705 nm.³¹ The presence of zinc tetraphenylporphyrin (ZnTPP) under irradiation induces the formation of $[\text{Ru}_3(\text{NCMe})(\text{cpy})_2]^0$ (**13**) (Scheme 3.1.4). This new compound shows an orange colour with bands at 480 and 943 nm. When orange acetonitrile solutions of complex **13** are saturated with CO, a colour change to blue is observed due to the formation of $[\text{Ru}_3(\text{CO})(\text{cpy})_2]^0$ (**16**). The same results are obtained for complexes $[\text{Ru}_3(\text{NCMe})(\text{py})_2]^+$ (**11**) and $[\text{Ru}_3(\text{NCMe})(\text{dmap})_2]^+$ (**12**) (py = pyridine; dmap = 4-dimethylaminopyridine) which were transformed into **14** and **15** in the presence of ZnTPP under irradiation and gave the corresponding complexes **17** and **18** in the presence of CO. Despite the remarkable colour changes observed upon CO addition, the authors did not report any data on detection limits or the response towards CO in the presence of other possible interfering species.

³¹ M. Itou, Y. Araki, O. Ito and H. Kido, *Inorg. Chem.*, **2006**, *45*, 6114-6116.



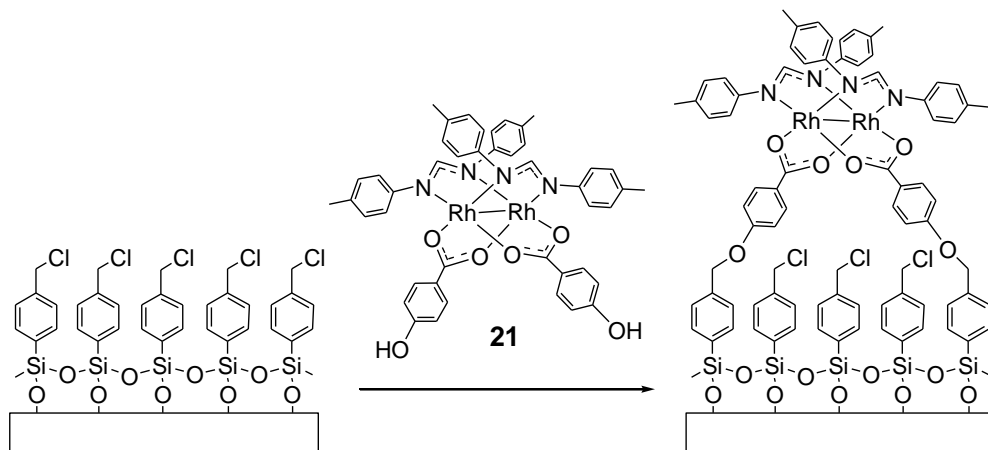
Scheme 3.1.4. The reaction of trinuclear ruthenium complexes **10-12** with CO.

Some of the binuclear rhodium probes described above show a remarkable colour change with CO in air when adsorbed on silica. This reflects the increasing use of inorganic supports for molecular probes, following the widespread development of ‘smart materials’ with organised active surfaces in a number of research fields.³² From a sensing perspective, the organisation, fine control and distribution of the probes on a host support/matrix can maximise the detection response and enable the incorporation of sensing molecules into optoelectronic devices. Moreover, the attachment of a molecular probe to a physical support can improve the stability of the chemosensor itself and facilitate handling without losing the specificity of the probe. Dunbar *et al.*³³ adopted this approach to investigate the synthesis and CO binding properties of zirconia and titania glasses impregnated with the rhodium(I) complex $[\text{Rh}(\text{CO})(\text{TMPP})_2][\text{BF}_4]$ (**19**, TMPP = tris(2,4,6-trimethoxyphenyl)phosphine). This unusually air-stable rhodium(I) complex undergoes a reversible reaction with carbon monoxide to form the dicarbonyl species **20** (Scheme 3.1.5).

³² a) L. Basabe-Desmonts, D. N. Reinhoudt and M. Crego-Calama, *Chem. Soc. Rev.*, **2007**, 36, 993-1017; b) A. B. Descalzo, R. Martínez-Máñez, F. Sancenón, K. Hoffmann and K. Rurack, *Angew. Chem. Int. Ed.*, **2006**, 45, 5924-5948.

³³ a) K. R. Dunbar, S. C. Haefner and P. N. Swepston, *J. Chem. Soc. Chem. Commun.*, **1991**, 460-462. b) S. C. Haefner, K. R. Dunbar and C. Bender, *J. Am. Chem. Soc.*, **1991**, 113, 9540-9553.

p-chlorobenzyl moiety, presented by van der Boom and co-workers (Scheme 3.1.6).³⁴



Scheme 3.1.6. Schematic representation of the bimetallic rhodium complex **21** and its attachment to a siloxane-based monolayer.

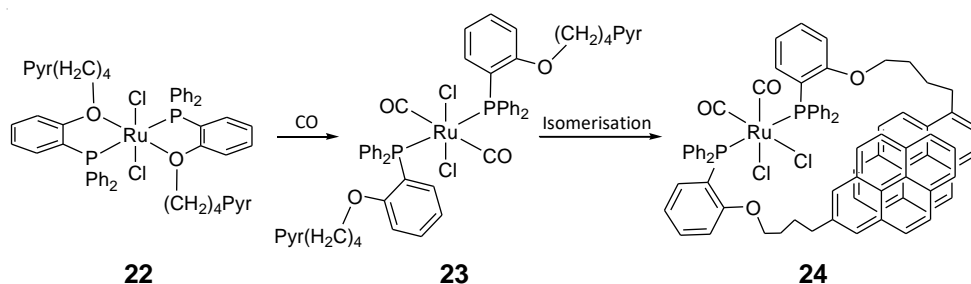
The surface formed can be used for selective and sensitive CO monitoring by UV-visible measurements. Glass monolayers of complex **21** (recorded in the transmission mode) show a broad absorption band (ranging from 280 to 750 nm) with a maximum centred at ca. 290 nm. Exposure of the monolayers to air containing 5 ppm of CO induces an increase in the absorption intensity of the entire spectrum. This behaviour is ascribed to an enhancement of the ligand-to-metal charge transfer (LMCT) promoted by CO coordination to the metal centres. Moreover, a low-intensity absorption at 560 nm also appears, which is indicative of the formation of Rh-CO bonds. The response of the monolayer is relatively selective because only CO, among all the other gases tested (Ar, N₂, N₂O, O₂, NO_x, H₂, CO₂, CH₄, ethylene and propylene), is able to induce the appearance of the 560 nm band. Importantly, air and water-saturated air fail to induce changes within

³⁴ A. Gulino, T. Gupta, M. Altman, S. Lo Schiavo, P. G. Mineo, I. L. Fragalà, G. Evmenenko, P. Dutta and M. E. van der Boom, *Chem. Commun.*, **2008**, 2900-2902.

the UV-visible region. The authors did not report a limit of detection but indicate that monolayers are able to respond to CO concentrations of 0.3 ppm in air. The regeneration of the sensor can be achieved by heating or by purging the monolayers with air, argon or nitrogen.

Fluorogenic CO sensors

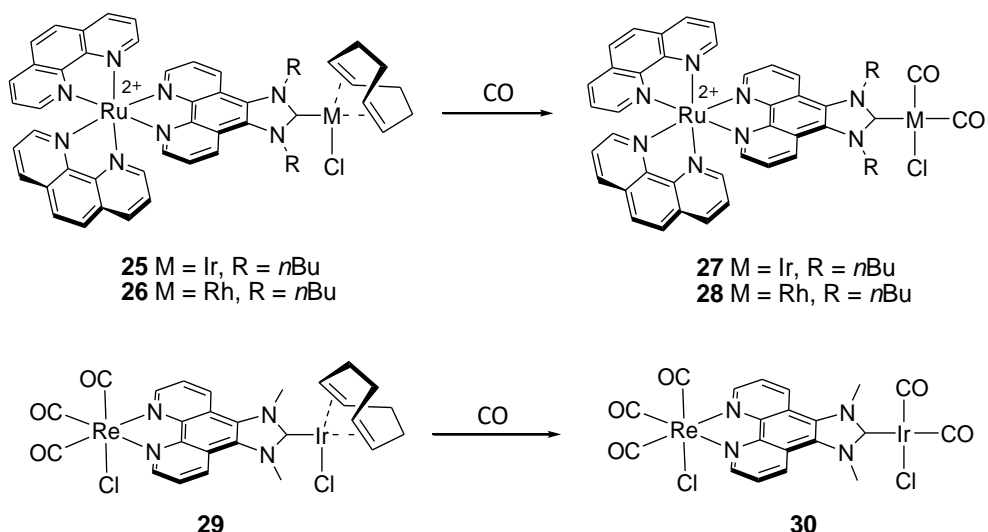
The first fluorogenic CO probe was reported in 2002 by Wolf and co-workers.³⁵ The authors reported that the ruthenium(II) complex **22**, bearing a hemilabile phosphine pyrene ether, reacts rapidly at room temperature with carbon monoxide to produce a remarkable monomer-to-excimer emission. In this reaction, a *trans*-dicarbonyl complex **23** is formed initially, but then undergoes isomerization to form the *cis*-dicarbonyl complex **24**. The change from blue (pyrene) to blue-green (excimer) emission is due to the formation of the more thermodynamically stable isomer **24** via the partial dissociation of the hemilabile ligand (Scheme 3.1.7). The strong excimer emission is observed in both concentrated (10^{-2} M) and dilute (10^{-6} M) solutions and is due to the favoured inter- and intramolecular π -stacking of the pyrene units. Air samples containing 0.05% (ca. 850 ppm) of CO can be analysed by measuring the emission variations in a 10^{-6} M dichloromethane solution of **22**.



Scheme 3.1.7. Reactivity of the ruthenium complex **22** with CO.

³⁵ a) C. W. Rogers and M O. Wolf, *Angew. Chem. Int. Ed.*, **2002**, *41*, 1898-1900; b) K. M. Matkovich, L. M. Thorne, M. O. Wolf, T. C. S. Pace, C. Bohne and B. O. Patrick, *Inorg. Chem.*, **2006**, *45*, 4610-4618.

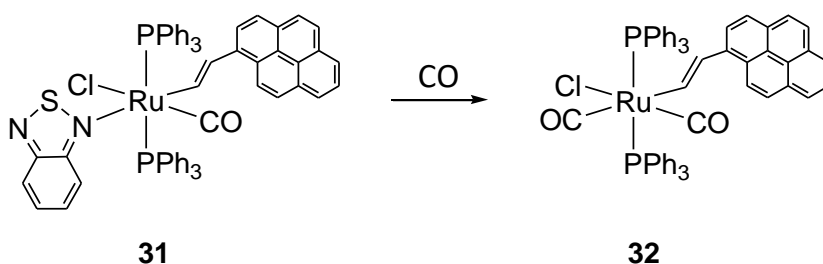
Chung and co-workers have also exploited the reactivity of transition metals (rhodium and iridium) towards CO by developing two families of bimetallic complexes, all bearing a bifunctional 1,10-phenanthroline *N*-heterocyclic carbene ligand (compounds **25**, **26** and **29**).³⁶ These metal complexes exhibit high molar extinction coefficients, moderately long-lived lifetimes and strong metal-to-ligand charge transfer (MLCT) emission. The photophysical properties are dependent on the different metals. Solutions of the bimetallic complexes **25**, **26** and **29** in solvents such as acetonitrile, DMF and DMSO are quantitatively converted into the respective dicarbonyl complexes **27**, **28** and **30** when carbon monoxide is present (Scheme 3.1.8). Generally, the resulting dicarbonyl complexes show higher emission intensities and quantum yields than the metal-COD precursors (COD = 1,5-cyclooctadiene). In the case of **25**, the conversion rate to **27** was found to be quite slow and proportional to the concentration of Ru CO added. In the same manner, complex **29** reacts only slowly with high concentrations (1000 ppm) of carbon monoxide to afford the final product **30**. In all cases, the reaction with CO is reported to be completely irreversible.



Scheme 3.1.8. Reactivity of the bimetallic complexes **25**, **26** and **29** with CO.

³⁶ a) H.-J. Park and Y. K. Chung, *Inorg. Chim. Acta*, **2012**, *391*, 105-113; b) H.-J. Park, K. Kim and Y. K. Chung, *Inorg. Chim. Acta*, **2014**, *410*, 214-220.

Very recently, Wilton-Ely, Mat3nez-Ma3nez and co-workers have produced a ruthenium(II) pyrenylvinyl complex **31**, which shows an exceptional chromo-fluorogenic response towards CO in both solution and in solid state (Scheme 3.1.9). Using **31**, CO can be detected at extremely low levels (5 ppb) thanks to the striking colour change from orange to bright yellow in the presence of carbon monoxide.³⁷ An even lower detection limit (1 ppb) is achieved via the fluorescence response generated by the system. At the centre of the sensing mechanism are two mutually *trans* ligands attached to the metal centre. One is the pyrenylvinyl group, responsible for the fluorescence response, and the other is the labile N-donor ligand 2,1,3-benzothiadiazole (BTD). In the presence of CO, the initial complex is converted to the corresponding pyrenylvinyl dicarbonyl compound via displacement of the BTD ligand. The change in the coordination environment produces not only the chromogenic effect (even at subtoxic concentrations) but also the concomitant revival of the emission of the pyrenyl group, which was previously quenched by the interaction with the BTD ligand.



Scheme 3.1.9. Reaction of the complex **31** with CO.

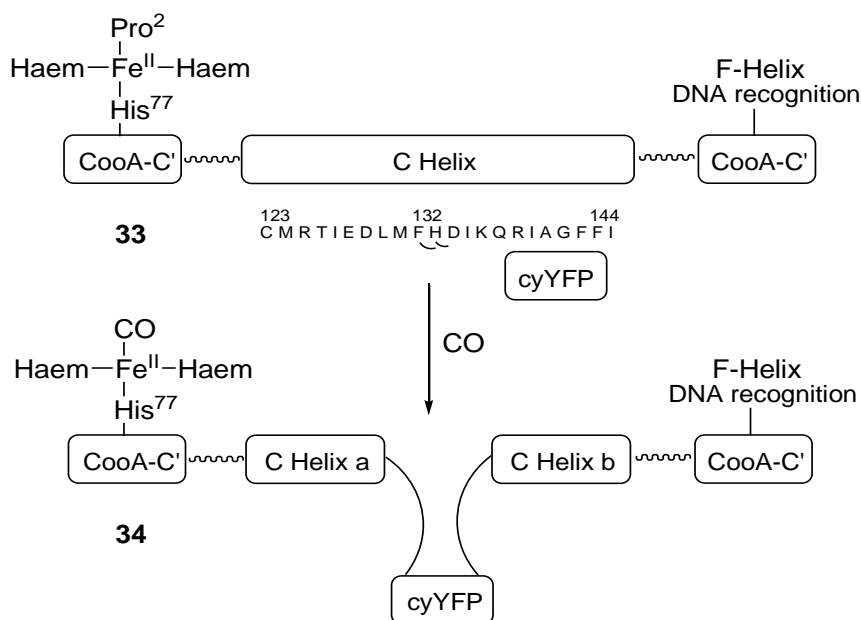
This represents a subtly different mechanism to the heavy atom effect usually used to suppress the fluorescence in the 'off' complex, as the metal-fluorophore connectivity remains unchanged during sensing. In terms of selectivity, no

³⁷ M. E. Moragues, A. Toscani, F. Sancen3n, R. Mart3nez-Ma3nez, A. J. P. White and J. D. E. T. Wilton-Ely, *J. Am. Chem. Soc.*, **2014**, *136*, 11930-11933.

response is observed with other common gases, steam or volatile organic compounds.

In order to unravel the biochemistry of CO within biological systems, researchers have been investigating fluorescence imaging and sensing as potential techniques to detect and monitor the presence of carbon monoxide in living cells.

He and co-workers³⁸ were the first to describe a genetically encoded fluorescent protein (**33**) capable of the selective imaging of CO in living cells.



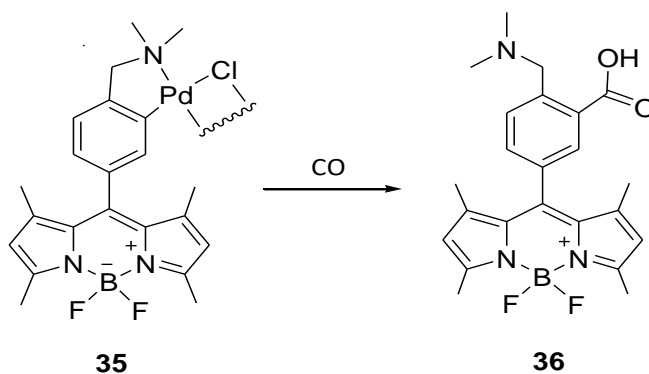
Scheme 3.1.10. Changes in the long C helix of CoxA after CO binding (probe **33**).

Despite the complexity of the probe, the sensing mechanism is relatively simple and is based on the affinity of CO towards the iron(II) centre of the haem cofactor situated in the binding domain (Scheme 3.1.10). While the quaternary structure of this type of protein normally consists of only two major domains (the haem effector-binding domain and a DNA-binding domain), in this genetically

³⁸ J. Wang, J. Karpus, B. S. Zhao, Z. Luo, P. R. Chen and C. He, *Angew. Chem. Int. Ed.*, **2012**, *51*, 9652-9656.

encoded system a new domain (yellow fluorescent protein) is introduced in the sequence to induce the fluorogenic response in the presence of carbon monoxide. Upon reaction of the haem-iron(II) unit with CO to form **34**, the encoded protein undergoes a conformational change that exposes the yellow fluorescent protein, resulting in a 2-fold fluorescence enhancement at 528 nm. The probe response is selective over other known gasotransmitters such as NO and H₂S.

Shortly after this contribution, Chang and co-workers³⁹ reported a palladium-BODIPY complex (**35**) with a CO-sensing mechanism based on a selective, palladium-mediated carbonylation conducted under mild conditions to release the modified BODIPY ligand **36** (Scheme 3.1.11).



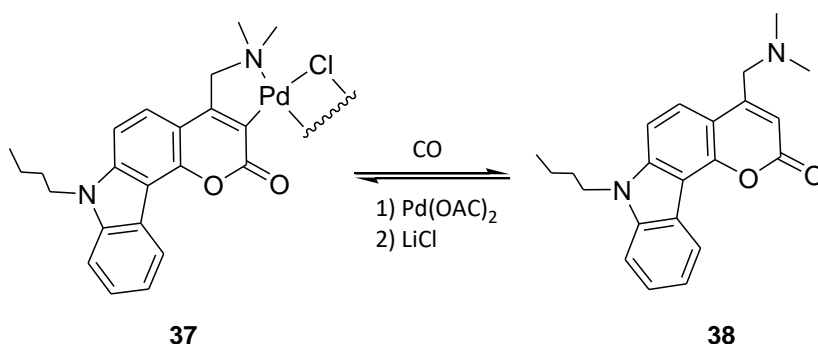
Scheme 3.1.11 Reactivity of the palladium complex **35** with CO.

The removal of the partial quenching provided by the palladium centre in **35**, via the heavy-atom effect, leads to the revival of the fluorescence of the BODIPY unit. The fluorescence properties and reactivity towards CO of **35** were monitored in aqueous solution buffered to physiological pH. The addition of 50 μ M of [RuCl(glycinate)(CO)₂] (an easily handled CO source, CORM-3) resulted in a 10-fold increase in fluorescence within 60 minutes of reaction. The experiment, run in a Dulbecco's phosphate-buffered saline (DPBS) showed a detection limit as low as 1 μ M (\approx 28 ppb CO). Overall, the probe also exhibits a good selectivity for CO over other small molecules such as H₂S, glutathione, NO, O₂, CN⁻, imidazole and other

³⁹ B. W. Michel, A. R. Lippert and C. J. Chang, *J. Am. Chem. Soc.* **2012**, *134*, 15668-15671.

species. When HEK293T cells were incubated with CORM-3 and treated with **35**, a significant, dose-dependent increase in the intracellular fluorescence was observed. In addition, the palladium-based probe **35** was found to be non-toxic to the cells tested.

Finally, inspired by the pioneering work of Chang, a cyclometallated palladium complex bearing a carbazole-coumarin-fused unit (**37**) has recently been reported for imaging carbon monoxide in living tissues (Scheme 3.1.12).⁴⁰



Scheme 3.1.12 Synthesis of the palladium complex **37** and its reaction with CO.

The metal-free carbazole-coumarin derivative (**38**) shows two-photon fluorescence due to the presence of a carbazole electron-donor group as well as a carbonyl electron-acceptor group, which together create a highly conjugated push-pull structure. The functionalisation of the coumarin derivative at the 4'-position allows the facile (re)generation of the cyclometallated palladium probe **37** from **38**. Due to the heavy atom effect of the palladium, a solution of **37** in PBS buffer and DMSO (9:1 v/v) at pH 7.4 and 37 °C displays a very weak one-photon fluorescence ($\Phi = 0.07$) and a negligible two-photon emission. However, after the addition of $[\text{Ru}_2\text{Cl}_4(\text{CO})_6]$ (CORM-2), a remarkable emission due to **38** is observed. The probe shows high sensitivity towards CO with a detection limit of 0.653 μM . Unlike the Pd-BODIPY probe (**35**) reported by Chang, **37** undergoes a protonolysis

⁴⁰ K. Zheng, W. Lin, L. Tan, H. Chen and H. Cui, *Chem. Sci.*, **2014**, 5, 3439-3448.

reaction in the presence of CO leading to the formation of **38**. This is strongly fluorescent, affording a one-photon fluorescence spectrum at 477 nm ($\Phi = 0.51$) and a high two-photon cross section ($\sigma = 50.1 \text{ GM}$) at 740 nm. Further studies at different pH values indicated that the probe is sufficiently stable with a maximum fluorescence response in the pH range of 7.0-9.0. The authors demonstrated that other biologically relevant analytes such as anions, reactive oxygen species (ROS), reducing agents, NO and H₂S induced no emission changes indicating that the probe is highly selective towards CO. Moreover, the incubation of the probe in the absence or presence of CORM-2 with HeLa, MCF-7 and MKN-28 cells was carried out and resulted in a strong one-photon fluorescence response. Additionally, probe **37** was also found to be capable of detecting CO in living tissue slices of liver incubated with CORM-2 when subjected to two-photon fluorescence microscopic analysis.

3.2. Objectives

Taking into account the growing current interest in the synthesis and evaluation of new metal complexes for the sensitive and selective carbon monoxide detection our objectives are the preparation of a set of ruthenium(II) and osmium(II) complexes for the optical sensing of this poisonous gas. Particularly our aims are:

- To prepare a set of vinyl ruthenium(II) and osmium(II) complexes bearing 2,1,3-benzothiadiazole and 5-(3-thienyl)-2,1,3-benzothiadiazole for the chromo-fluorogenic sensing of CO.
- To prepare a set of vinyl ruthenium(II) and osmium(II) complexes bearing 5-(3-thienyl)-2,1,3-benzothiadiazole and poly(ethylene)glycol chains for the fluorogenic detection of CO in water.
- To prepare poly(ethylene)glycol derivatized gold nanoparticles bearing vinyl ruthenium(II) and osmium(II) complexes bearing 5-(3-thienyl)-2,1,3-benzothiadiazole for the fluorogenic detection of CO in water.
- To characterize the new prepared probes by standard methods (NMR, HRMS, IR, UV/Vis, emission spectroscopy and X-ray diffraction).
- To test chromogenic and fluorogenic responses of the prepared complexes in the presence of CO both in solution and in air.
- To test the fluorogenic response of the water soluble complexes for the fluorogenic detection of CO in living cells.

3.3. Ruthenium (II) and osmium (II) alkenyl complexes as highly sensitive and selective chromogenic and fluorogenic probes for the sensing of carbon monoxide in air

**Ruthenium (II) and osmium (II) alkenyl complexes
as highly sensitive and selective chromogenic
and fluorogenic probes for the sensing of carbon
monoxide in air**

Anita Toscani,^{d,+} Cristina Marín-Hernández,^{a,b,c,+} María E.
Moragues,^{a,b,c} Félix Sancenón,^{a,b,c} Paul Dingwall,^d Neil J.
Brown,^d Ramón Martínez-Máñez,^{a,b,c,*} Andrew J. P. White^d
and James D. E. T. Wilton-Ely^{d,*}

^a Centro de Reconocimiento Molecular y Desarrollo Tecnológico (IDM), Unidad Mixta Universidad de Valencia-Universidad Politécnica de Valencia. Spain.

^b Departamento de Química, Universidad Politécnica de Valencia, Camino de Vera s/n, E-46022 Valencia, Spain.

^c CIBER de Bioingeniería, Biomateriales y Nanomedicina (CIBER-BBN).

^d Department of Chemistry, Imperial College London, SW7 2AZ, London, UK.

⁺ Both authors contributed equally to the present work.

Published online: August 13, 2015

(Reprinted with permission from:

Chem. Eur. J. 2015, 21, 14529–14538

Copyright © 1999–2016 John Wiley & Sons)

3.3.1. Abstract

The detection of carbon monoxide in both solution and air has been achieved using simple, inexpensive systems based on the vinyl complexes $[M(CH=CHR)Cl(CO)(BTD)(PPh_3)_2]$ ($R = \text{aryl}$, $BTD = 2,1,3\text{-benzothiadiazole}$). Depending on the nature of the vinyl group, chromogenic and fluorogenic responses signalled the presence of this odourless, tasteless, invisible and toxic gas. Chloroform solutions of the complexes underwent rapid change between easily differentiated colours when exposed to air samples containing CO. More significantly, adsorbing the complexes on silica produced colorimetric probes for the 'naked eye' detection of CO in the gas phase. Structural data for key species before and after addition of carbon monoxide were obtained by single X-ray diffraction techniques. In all cases the ruthenium and osmium vinyl complexes studied showed a highly selective response to CO with exceptionally low detection limits. Naked eye detection of CO at concentrations as low as 5 ppb in air was achieved with the onset of toxic levels (100 ppm) resulting in a remarkably clear colour change. Moreover, complexes bearing pyrene, naphthalene and phenanthrene moieties were fluorescent and greater sensibilities were achieved (through turn-on emission fluorescence) in the presence of carbon monoxide, both in solution and in air. This behaviour was explored computationally using TDDFT experiments. Additionally, the systems were shown to be selective for CO over all other gases tested, including water vapour and common organic solvents. Supporting the metal complexes on cellulose strips for use in an existing optoelectronic device may provide numerical readings for CO concentration and an alarm.

3.3.2. Introduction

The selective detection of gases which are toxic at low concentrations is one of the most promising applications of optical sensors. Among such gases, carbon monoxide stands out due to its high toxicity and its common presence in both domestic and work settings as well as other environments frequented by the general public. Traditionally, electrochemical cells, solid-state sensors and thermocouples have been used to accomplish routine CO detection.

Electrochemical sensors based on metal-oxide semiconductors generally possess reasonably good resolution and measuring ranges. However, these are very sensitive to temperature and pressure.¹ In relation to solid-state CO sensors, based on ZnO and SnO₂, these require such high working temperatures that their use is restricted to specific laboratory applications.² Moreover optical sensors which have been reported use either spectrally narrowband lasers³ or non-dispersive infrared (NDIR)⁴ systems. Although currently the most accurate method to measure CO concentrations in urban air, NDIR systems are sensitive to relatively low concentrations of other common gases (interferents), such as CO₂, NO_x, hydrocarbons or water vapour. Current commercial CO detectors have to be sited carefully in environments where water vapour (steam) or particulates (smoke) are generated, such as kitchens and bathrooms, in order to avoid false alarms. These can also be triggered by the presence of solvents (from cleaning products, hairspray) or fuels (e.g., in mechanical or automotive workshops). Therefore, there is an increasing interest in the development of chemical sensor systems capable of selectively detecting the presence of carbon monoxide in air at low concentrations. In this context, colorimetric methods are especially undemanding, offering several advantages over other analytical procedures, such as real-time monitoring and the use of very simple and inexpensive instrumentation. Additionally, certain colorimetric changes, even at low concentration of analytes, can be observed by the naked eye, making chromogenic approaches unbeatable for certain applications. In the context of these factors, several chromogenic probes for CO detection have been reported recently. One of the first examples, by Ito and co-workers, uses acetonitrile solutions of an oxo-acetato-bridged triruthenium cluster. In this system, a photosensitizing electron donor (zinc tetraphenylporphyrin) controls the redox state of the metal centre, allowing the exchange of weakly coordinating solvent molecules by CO, resulting in colour changes.⁵ Another example involves the selective optical monitoring of CO by covalently immobilized bimetallic rhodium complexes on glass substrates. Despite the poorly resolved changes in colour, a detection limit as low as 2.5 ppm of CO can be determined by UV-Vis measurements on this monolayer-based sensor.⁶ Kirchner and co-workers

prepared a penta-coordinate iron diisopropylphosphino diaminopyridine pincer complex that gives rise to a clear colour change (from yellow to red) in the solid state upon exposure to CO, but only with high concentrations of the gas (1 atm). However, the generation of the resultant hexa-coordinate derivative is stereospecific and the CO binding is fully reversible.⁷ Redox polymers functionalized with porphyrins have also been used for the recognition of CO. Polypyrrole can be functionalized with tetraphenylporphyrin iron(III) chloride units and the polymer formed is able to detect CO in water/methanol solutions with a detection limit as low as 100 ppm.⁸ Very recently, sensitive and selective CO detection in air was accomplished by some of us via the use of binuclear rhodium complexes. Silica probes of these rhodium(II) complexes allowed the 'naked eye' detection of CO concentrations of around 50 ppm, resulting from a colour change on axial coordination of the CO to the metal complexes.⁹ Finally, a P-S-N iron(II) complex was reported recently which achieves the chromogenic sensing of CO (albeit only in solution). Purple acetonitrile solutions of the complex become orange on exposure to high concentrations of CO (passing a 1 atm stream of CO through the solution for 5 mins). The colour change observed is ascribed to the reversible binding of CO to form the corresponding octahedral iron monocarbonyl complex.¹⁰

In spite of the significant progress made during the past decade, developing a readily applicable and highly sensitive molecular visual detection system for CO in air remains a challenge. The design of such systems requires not only selectivity and sensitivity towards a given analyte but, in the case of highly poisonous gases such as CO, the detection process must be both rapid and reliable (stable). While the systems described above display novel and ingenious approaches to CO sensing, some of them have drawbacks such as detecting CO only in solution, requiring expensive, non-portable instrumentation or showing limits of detection unsuitable for the early warning of the presence of sub-acute levels of CO in air. In addition, the relative cost, synthetic difficulty and stability of these systems are also potential issues. Lastly, in order to compete with current electronic systems, a molecular probe must be readily integrated into a device which can display a reading and sound an alarm.

In order to understand the extent of the issues surrounding human exposure to carbon monoxide, it is helpful to describe its occurrence. Carbon monoxide is produced as a result of the incomplete burning of carbon-based fuels (i.e., propane, gasoline, kerosene, wood, coal, charcoal etc.) in inadequately vented heaters and furnaces. Carbon monoxide levels can vary widely within an enclosed or semi-enclosed area such as a domestic room, office, garage or workshop; and can also fluctuate enormously over a short period of time as conditions change. For this reason, the level of CO concentration in air is often measured using the Time-Weighted Average (TWA). This determines an average exposure to CO over time (usually expressed in parts per million, ppm). Carbon monoxide poisoning symptoms vary widely between individuals. A person exposed to relatively low carbon monoxide levels over a longer period can display only mild symptoms while actually becoming seriously poisoned. Normal fresh air contains 0-0.2 ppm carbon monoxide. The American Society of Heating Refrigeration and Air Conditioning Engineers (ASHRAE) lists a maximum allowable short term limit of 9 ppm CO. The Environmental Protection Agency (EPA)¹¹ has set two national health protection standards for CO: a 1-hour TWA of 35 ppm, and an 8-hour TWA of 9 ppm. These standards make it clear that any carbon monoxide reading over 9 ppm should be investigated and acted upon. The UK Department of Health reported in 2013 that 50 people die each year from carbon monoxide poisoning in the UK.¹² Many factors play a role in the severity of symptoms while in the body. Some health effects due to prolonged exposure to various concentrations of CO are summarized in Table 3.3.1. From mild to extreme CO exposure; passing through medium exposure, symptoms evolve as stated to result in headache, nausea, dizziness, fatigue, collapse, loss of consciousness and danger of death. Significantly, the less severe of these symptoms can often be mistaken for other ailments, such as mild food poisoning or dehydration, leading to prolonged exposure.

Table 1. Health effects^a of CO upon exposure to levels^b of CO considered dangerous.

Level of CO exposure (ppm)	Time exposed (hours)						
	1	2	4	8	12	16	24
35							
50							
75							
100							
200							
400							

^a The images typify the following symptoms in order of harshness: headache, nausea, dizziness, fatigue, collapse and loss of consciousness.

^b US Environmental Protection Agency (EPA) standards.

Taking into account the facts mentioned above and following our interest in the design of novel chromo-fluorogenic systems,¹³ we present here the application of ruthenium(II) and osmium(II) vinyl complexes as sensitive, selective, colorimetric and fluorimetric probes for the sensing of CO using their well-known ability to react with small molecules, such as carbon monoxide.¹⁴ We have recently reported preliminary data on the development of a chromo-fluorogenic probe based on the ruthenium(II) pyrenylvinyl complex **1** of formula $[\text{Ru}(\text{CH}=\text{CHPyr-1})\text{Cl}(\text{CO})(\text{BTD})(\text{PPh}_3)_2]$.¹⁵ Based on the initial sensing results obtained for this ruthenium complex in terms of selectivity and sensitivity, we report herein an extended study using a set of synthetically accessible and relatively inexpensive ruthenium(II) and osmium(II) vinyl complexes of general formula $[\text{M}(\text{CH}=\text{CHR})\text{Cl}(\text{CO})(\text{BTD})(\text{PPh}_3)_2]$ containing the 2,1,3-benzothiadiazole

(BTD) chromophore and various different vinyl ligands. For these compounds the colour modulations observed in the presence of carbon monoxide, induced by the displacement of the BTD ligand upon coordination of the CO group, have been studied spectroscopically and computationally. Also the changes in the emission of the complexes bearing pyrene, naphthalene and phenanthrene fluorophores induced by CO in solution and in air was studied.

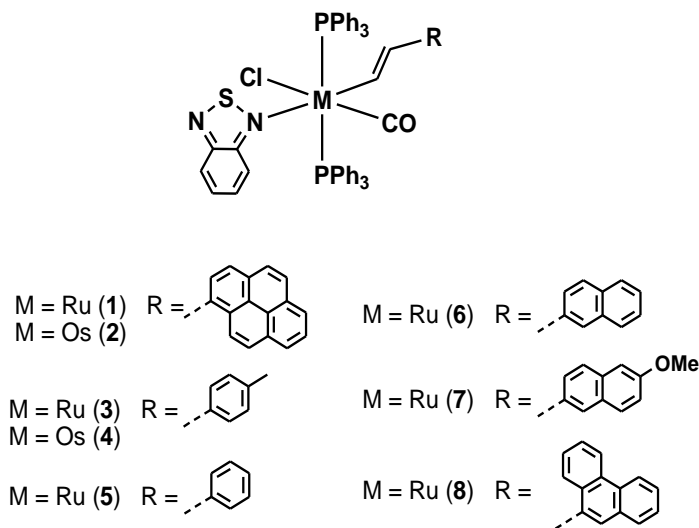
3.3.3. Results and discussion

Design of the probe complexes

The design of the chromo-fluorogenic probes involves the use of brightly coloured σ -vinyl 18-electron complexes and their well-documented ability to react with neutral, two-electron donors, such as carbon monoxide. The vinyl ligand is an important member of the σ -organyl ligand family, and is believed to be present as an intermediate in many catalytic reactions. Well-established synthetic routes such as hydrometallation and the reaction of coordinated alkynes with electrophiles or nucleophiles are known to yield vinyl complexes of many metals, often those belonging to group 8.¹⁶ Since the discovery of hydrometallation of alkynes by the compounds $[\text{RuHCl}(\text{CO})(\text{PPr}^i_3)_2]$ and $[\text{RuHCl}(\text{CO})(\text{PPh}_3)_3]$, the resulting vinyl complexes have been studied extensively by many researchers (see examples by Werner,¹⁷ Esteruelas,¹⁸ Santos,¹⁹ Caulton,²⁰ Winter²¹ and Hill²²), as well as by some of us,²³ covering functional-group transformation, ligand exchange and theoretical calculations.

The effect of nitrogen donor ligands on the reactivity of ruthenium hydrides²⁴ and vinyl ruthenium complexes^{21c} has been examined in detail. Yet, the most convenient triphenylphosphine-stabilised vinyl complexes to be used as starting materials are those of the form $[\text{M}(\text{CR}=\text{CHR})\text{Cl}(\text{CO})(\text{PPh}_3)_2]$ (M = Ru only)²⁵ or $[\text{M}(\text{CR}=\text{CHR})\text{Cl}(\text{CO})(\text{BTD})(\text{PPh}_3)_2]$ (M = Ru, Os). The BTD heterocycle confers both high crystallinity and enhanced visible properties to the materials and competes successfully with any excess triphenylphosphine present to avoid contamination by tris(phosphine) byproducts. Moreover, the lability of the BTD ligand in these complexes is remarkably well balanced, being displaced by better donors but

resisting exchange with potentially coordinating solvents such as alcohols, tetrahydrofuran or even high concentrations of acetonitrile. As a result, a rich and varied chemistry has been developed from vinyl complexes bearing this heterocycle.^{22c}



Scheme 3.3.1. Structures of the ruthenium and osmium vinyl complexes (**1-8**) used in this work.

With these design concepts in mind, and based on the possible modulation of the sensing features via changes in the metal centre and the donor-acceptor properties of the vinyl ligands, a set of ruthenium and osmium vinyl complexes was prepared (structures **1-8** in Scheme 3.3.1) of general formula $[M(\text{CH}=\text{CHR})\text{Cl}(\text{CO})(\text{BTD})(\text{PPh}_3)_2]$; containing two different metals as central atoms (Ru or Os) and six different vinyl ligands (R = Pyr-1, Ph-9, Nap-2, Nap-2-OMe-6, C₆H₄Me-4 or C₆H₅) *trans* to the 2,1,3-benzothiadiazole (BTD) chromophore. Two triphenylphosphine ligands, a chloride and a carbonyl unit complete the coordination sphere of the 18-electron octahedral complexes. The synthesis and chromo-fluorogenic features of complex $[\text{Ru}(\text{CH}=\text{CHPyr-1})\text{Cl}(\text{CO})(\text{BTD})(\text{PPh}_3)_2]$ (**1**) have been recently reported by us in a preliminary communication.¹⁵

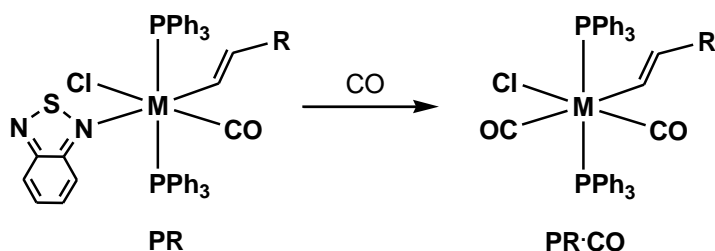
Reactivity with carbon monoxide in solution

Once the set of ruthenium and osmium derivatives had been prepared, UV-Vis spectrophotometric studies were performed for the coordination of CO to compounds **1-8**. Chloroform solutions of the ruthenium complexes **1**, **3**, **5-8** displayed an orange colour that changes to yellow when CO-containing air samples were bubbled through their solutions (see Table 3.3.2). In contrast, the osmium complexes **2** and **4** displayed a CO-induced colour change from purple to light yellow (see Table 3.3.2). The observed colour modulations are consistent with the formation of the corresponding dicarbonyl complexes, through displacement of the BTD ligand (Scheme 3.3.2).

Table 3.3.2. UV-Vis and diffuse reflectance spectral data at room temperature for complexes **1-8** in chloroform solutions and supported on silica.

Compound	CHCl ₃ solution		Solid λ_{\max} (nm)
	Absence of CO λ_{\max} (nm)	Presence of CO λ_{\max} (nm)	
1	500; 402; (361; 345) ^a	(361; 345) ^{a,b}	499
2	547; (418; 402) ^a	(395; 377) ^a	547
3	487; 400	-	513
4	540	-	558
5	483; 400	-	500
6	487; (311; 297; 277; 255) ^c	(309; 297; 271; 255) ^c	478
7	492; (299; 287; 279; 251) ^c	(299; 287; 279; 251) ^c	489
8	478; (301; 255) ^d	(306; 260) ^d	477

^a Pyrene signals. ^b Enhanced signals. ^c Naphthalene signals. ^d Phenanthrene signals



Scheme 3.3.2. Reactivity of the complexes acting as probes, simplified as **PR**, with carbon monoxide to give the corresponding dicarbonyl products, simplified as **PR·CO**.

Characterization of the dicarbonyl complexes

Crystal structures of numerous transition metal complexes containing phosphines and vinyl ligands have been reported.¹⁶ The molecular structures of complexes **1** to **8** are very similar with all containing one metal centre bonded to two triphenylphosphine ligands, one chloride, a CO molecule and a BTD heterocycle *trans* to the vinyl ligand. This results in a pseudo-octahedral arrangement around the metal centres. A significant structural feature of these complexes is the coplanar orientation of the vinyl and carbonyl ligands. Participation of the empty π^* orbitals of the vinyl ligands in back-bonding interactions will result in a strengthened metal-carbon bond. When a vinyl complex contains other π -acceptor ligands (e.g., the CO molecule), competition for back-donation, and therefore the relative orientation of the vinyl ligand, will have an impact on the stability of the complex.²⁶ Favourable back-donation is found for vinyl and carbonyl ligands due to their *trans* arrangement.

In order to understand the ability of carbon monoxide to bind to these divalent metal vinyl complexes, it is helpful to draw a comparison between related structures reported previously and those of the corresponding BTD and CO-substituted complexes. Suitable crystals for single X-ray diffraction were obtained (Figure 3.3.1) by vapour diffusion of diethyl ether onto (in the case of **5·CO**, CO-infused) dichloromethane solutions of the complexes. The crystal structures of BTD complexes with three different vinyl ligands have been obtained (**1** reported in a recent communication¹⁵ and **4** and **6** reported here) as well as two dicarbonyl

examples, formed after addition of carbon monoxide (**1-CO** and **5-CO** reported in previous and present work, respectively).

The molecular structure of compound **4** (Figure 3.3.1a) consists of an osmium centre with two triphenylphosphine ligands, while the labile BTD unit is situated *trans* to the tolylvinyl ligand. A chloride and a CO molecule complete the coordination sphere. Relevant crystallographic data for all structures are collected in the Supporting Information.

The structures reported here, together with the one recently reported for complex **1**,¹⁵ allow the comparison of the series of analogous $[M(\text{CH}=\text{CHR})\text{Cl}(\text{CO})(\text{BTD})(\text{PPh}_3)_2]$ compounds differing only in the metal ($M = \text{Ru}$ or Os) and in the vinyl substituents ($R = \text{Pyr-1}$, Nap-2 or $\text{C}_6\text{H}_4\text{Me-4}$). Table 3.3.3 collects the main metal-ligand structural data.

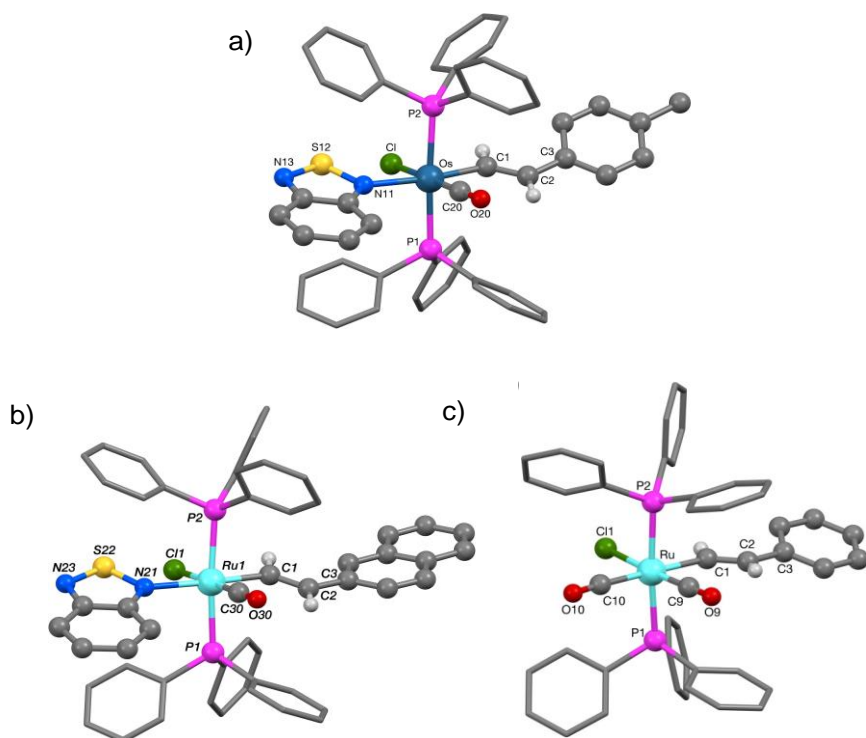


Figure 3.3.1. Crystal structures of a) $[\text{Os}(\text{CH}=\text{CHC}_6\text{H}_4\text{Me-4})\text{Cl}(\text{CO})(\text{BTD})(\text{PPh}_3)_2]$ (**4**) b) $[\text{Ru}(\text{CH}=\text{CHNap-2})\text{Cl}(\text{CO})(\text{BTD})(\text{PPh}_3)_2]$ (**6**) and c) $[\text{Ru}(\text{CH}=\text{CHC}_6\text{H}_5)\text{Cl}(\text{CO})_2(\text{PPh}_3)_2]$ (**5-CO**).

Table 3.3.3. Relevant bond distances (Å) for the divalent vinyl complexes used in this work.

	1 ^[15]	1·CO ^[15]	4	6	5·CO
$d_{M-C_{CO}}$	1.824(3)	1.857(2)	1.831(2)	1.827(3)	1.858(6)
d_{M-Cl}	2.4663(7)	2.4472(5)	2.4591(6)	2.4673(8)	2.4688(14)
$d_{M-C_{vinyl}}$	2.048(3)	2.104(2)	2.068(2)	2.061(3)	2.115(5)
d_{M-N}	2.238(3)	-	2.2073(19)	2.248(3)	-
$d_{M-C_{CO2}}$	-	1.957(2)	-	-	1.971(6)
d_{M-P1}	2.4064(7)	2.4126(5)	2.3878(6)	2.3920(9)	2.4061(14)
d_{M-P2}	2.4099(6)	2.4060(5)	2.4158(6)	2.4114(9)	2.4037(14)

In structures **4**, **6** and **5·CO** (Figure 3.3.1), an approximate octahedral arrangement is adopted. Somewhat surprisingly given their use over a number of decades, the structures of **1**, **4** and **6** are the first examples of structurally characterised vinyl complexes bearing the BTD ligand. The *trans* relationship adopted by **4** and **6** (and also **1**) is in contrast to the mutually *cis* disposition of the BTD ligand and the hydride ligand in the complex $[RuHCl(CO)(BTD)(PPh_3)_2]$,²⁷ which is a precursor to the compounds $[Ru(CH=CHR)Cl(CO)(BTD)(PPh_3)_2]$. This indicates that substantial reorganisation occurs on hydrometallation of the alkyne by the hydride precursor. Also, noteworthy is the fact that the M-C_{CO} bond distances for the two carbonyl ligands in the dicarbonyl complex (**5·CO**) differ substantially. This can be taken as evidence of the substantial *trans* influence exerted by the vinyl group, resulting in an elongation of the M-C_{CO} bond *trans* to the vinyl ligand. This effect is also observed in the pyrenylvinyl complex **1·CO**. Comparing the structure of the BTD complex **1** with that of the dicarbonyl **1·CO**, a greater M-C_{vinyl} distance is observed also for the vinyl ligand in the dicarbonyl structure. In the absence of significantly greater steric congestion, this must also be taken as evidence of the greater *trans* influence of the CO ligand compared to

that of the BTD ligand. It would be expected that the Os-N distance (2.2073(19) Å) in **4** would be similar if not slightly longer than the Ru-N bond length in the analogous ruthenium complex (**1**). However, it is in fact substantially shorter ($d_{\text{Ru-N}}$ in **1** is 2.238(3) Å). This could be due to a release of steric congestion on replacing the pyrenylvinyl in **1** with the less bulky tolylvinyl in **4**. Otherwise, the structures are as expected and the bond data are in agreement with those reported previously for comparable compounds with monodentate N-donors such as $[\text{Ru}(\text{CH}=\text{CHBu}^t)\text{Cl}(\text{CO})(\text{Me}_2\text{Hpz})(\text{PPh}_3)_2]$ (Me_2Hpz = 3,5-dimethylpyrazole).²⁸ Further details and bond data can be found in the Supplementary Information.

Carbon monoxide sensing behaviour in air

Despite the encouraging spectrophotometric response of the ruthenium and osmium vinyl complexes **1-8** in chloroform solution, the detection of CO in the gas phase was of paramount importance in the design of a probe to be used in air. In order to address this aim, the eight complexes were adsorbed on an inorganic matrix (thus hugely increasing the surface area exposed to the gas) and their chromogenic response toward CO in air studied. Adsorption of probes **1-8** on silica was achieved by dissolution of each complex in a minimum amount of chloroform followed by the addition of conventional lab silica at a weight ratio of 250 times. This resulted in orange (when **1**, **3**, **5**, **6**, **7** and **8** are used) and purple solids (using **2** and **4**) after solvent removal on a rotary evaporator. The resulting solids were left to stand at least 1 h before use, so that a stable initial colour was achieved. Diffuse reflectance maxima for the complexes adsorbed on silica are included in Table 3.3.2. This illustrates that the sensory materials show intense absorption bands in the 470-560 nm range.

The coloured silica probes containing the ruthenium and osmium vinyl complexes (Figure S4 in Supporting Information) underwent significant colour changes within 2-4 seconds when exposed to air containing different concentrations of carbon monoxide inducing a progressive reduction in the absorbance of the visible bands in the 470-560 nm range (Figure S5). As an example, Figure 3.3.2 and Figure 3.3.3 show the diffuse reflectance spectra of complex **1** and **2** supported on silica and the changes observed upon addition of

100 ppm and 50 ppm of CO, respectively. The behaviour of the remaining complexes (**3**, **4** and **5-8**) on silica is also shown in Figure S5. All these changes are consistent with displacement of the BTD ligand by CO coordination to give the dicarbonyl derivative **PR·CO** (Scheme 3.3.2).

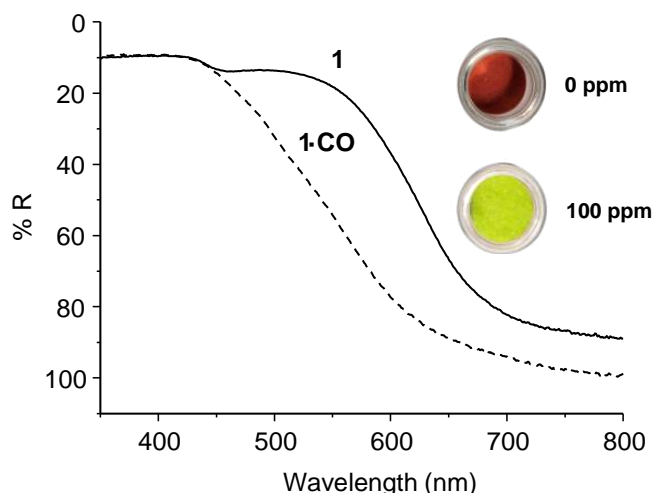


Figure 3.3.2. Diffuse reflectance UV-Vis spectrum of complex **1** supported on silica and the changes observed in the presence of air containing 100 ppm of CO.

Using simple titration profiles of the eight sensor materials with CO, the limits of detection were evaluated and the results are displayed in Table 3.3.4. Together with the values measured using a conventional UV-visible spectrophotometer (see Figure S5 in Supporting Information), Table 3.3.4 shows the estimated detection limit to the naked eye for complexes **1-8** in the presence of CO; i.e. the minimum amount of CO necessary to observe a clear colour change in the materials. As examples of the CO response, the reduction of the intensity of the band centred at 535 nm vs. the log of the concentration of CO in air for **2** adsorbed on silica is shown in Figure 4, whereas pictures of the colour changes observed for **1** on silica gel upon exposure to 0.001, 0.005, 0.05, 50 and 100 ppm CO in air are shown in Figure 3.3.5.

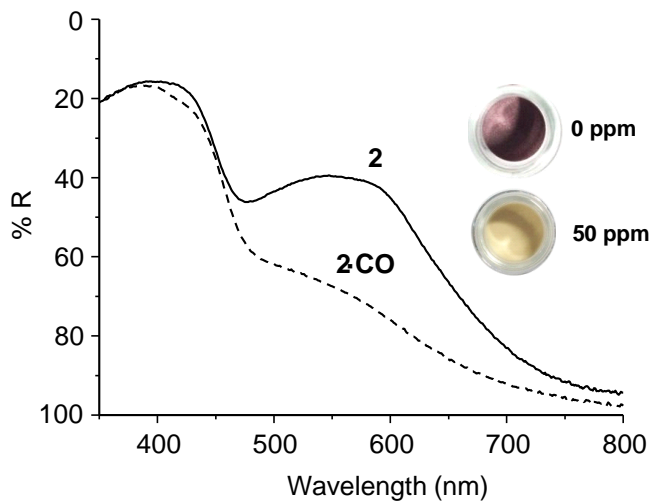


Figure 3.3.3. Diffuse reflectance UV-Vis spectrum of complex **2** on silica with the changes observed in the presence of air containing 50 ppm of CO.

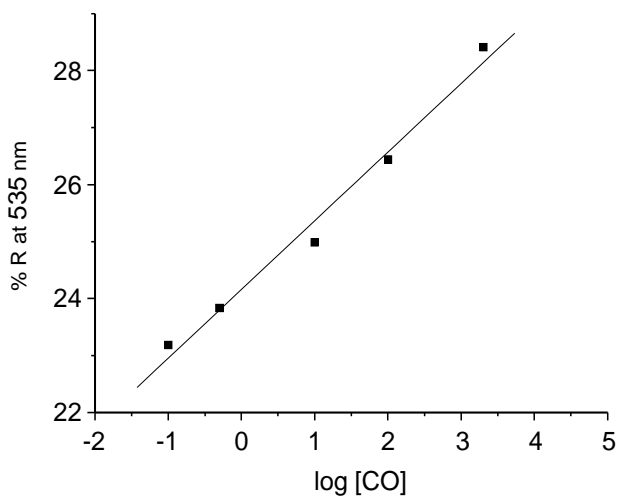


Figure 3.3.4. Reduction of the intensity of the band centred at 535 nm vs. the log of the concentration of CO in air for **2** adsorbed on silica.

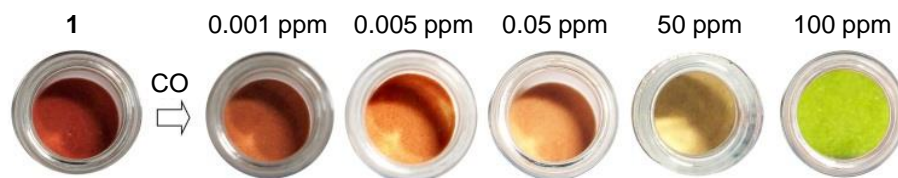


Figure 3.3.5. Colour changes observable to the naked eye for complex **1** on silica gel upon exposure to 0.001, 0.005, 0.05, 50, 100 ppm CO in air.

One of the most remarkable aspects of the behaviour of complexes **1-8** is the clear chromogenic response observed at relatively low concentrations of carbon monoxide. In particular, and remarkably, for silica-supported complexes **2-5**, a chromogenic change to the naked eye was observed at concentrations as low as 0.5 ppm. When complexes **6-8** were used, a chromogenic naked eye response was observed for higher CO concentrations (ca. 5 ppm). However, of all the compounds investigated, complex **1** performs best, due not only to its marked colour modulation observed at concentrations at which CO becomes toxic; but also to its ability to detect extremely low CO concentrations (0.005 ppm). However, the high cost of the 1-ethynylpyrene precursor compared to inexpensive ethynylbenzene would make **5** a more attractive option for sensing carbon monoxide in air in the 10-50 ppm range needed for a domestic alarm. Indeed, the high sensitivity of **1** could even be a drawback in applications where low concentrations of CO are present as part of the background (e.g., in factories).

Moreover, another remarkable feature observed in **1** was that the displacement of the BTD ligand by CO also results in the recovery of the fluorescence emission of the pyrene group. This effect was observed both in solution and in air. For instance methanolic solutions of **1** were poorly fluorescent ($\lambda_{\text{exc}} = 355 \text{ nm}$, $\lambda_{\text{em}} = 458 \text{ nm}$) but addition of CO and formation of **1**·CO resulted in a remarkable 36-fold increase in emission. Moreover, **1** was also found to display a turn-on emission enhancement in the presence of carbon monoxide when the probe was adsorbed on strips of cellulose paper (column silica gel was also tested as support but the emission changes of complex **1** adsorbed were negligible).

Using this support, a remarkable LOD for CO of 0.7 ppb was calculated. In addition to this, a clear optical response to the naked eye was also found for concentrations of ca. 90 ppm using a conventional UV lamp. Detection of carbon monoxide using a fluorescence response has been described in a number of reports, though previous to this work only in solution.²⁹

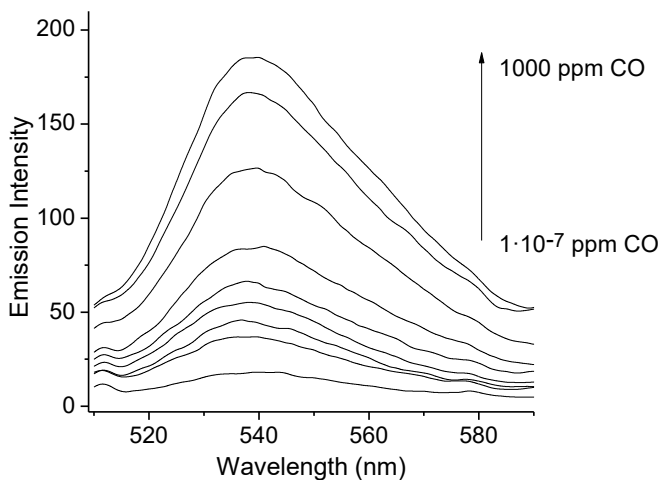


Figure 3.3.6. Turn-on fluorescence response ($\lambda_{\text{ex}} = 492 \text{ nm}$) of a $1 \times 10^{-4} \text{ mol dm}^{-3}$ chloroform solution of **7** upon addition of increasing quantities of CO (0, 1.0×10^{-7} , 1.0×10^{-5} , 1.0×10^{-3} , 0.01, 1, 100, 500 and 1000 ppm).

Encouraged by the remarkable emission enhancement observed for **1** we studied the fluorescence behaviour of complex **7** and **8** upon addition of CO in solution and in gas phase. Chloroform solutions of complex **7** were weakly emissive with an emission band centered at 538 nm ($\lambda_{\text{exc}} = 492 \text{ nm}$). When different concentrations of CO air were bubbled into the chloroform solutions of **7** a remarkable 10.1-fold enhancement of the emission band at 538 nm was observed (see Figure 3.3.6). Nearly the same behaviour, upon addition of increasing quantities of CO, was observed for chloroform solutions of complex **8** with a 19.8-fold enhancement of the emission at 586 nm ($\lambda_{\text{exc}} = 478 \text{ nm}$) (see

Figure S6 in Supporting Information). As for complex **1**, the enhancement in emission intensity observed upon addition of increasing quantities of CO was ascribed to the displacement of the BTB ligand that results in the recovery of the naphthalene and phenanthrene fluorescence. Also, the emission response of silica gel-containing complexes **7** and **8** to CO was tested. After exposing the solids to air containing different CO concentrations a clear emission enhancement at 599 and 586 nm for **7** and **8** respectively was observed. From the corresponding titration profiles LODs of 1.1 and 10 ppb for CO detection using emission data for **7** and **8** were calculated (see Table 3.3.4).

Table 3.3.4. Limits of detection (ppm) for complexes **1-8** in the presence of CO. Limits calculated from UV-visible and emission spectral data, and to the naked eye.

Compound	Detection limits (ppm) of CO		
	Uv-visible	Fluorescence	Naked-Eye
1	0.0006	-	0.005
2	0.19	-	0.5
3	0.1	-	0.5
4	0.015	-	0.5
5	0.084	-	0.5
6	0.65	-	5
7	4.07	0.0011	5
8	0.60	0.01	5

Based on the observation that naked-eye colour changes for probes **2-8** are found at different CO concentrations it is possible to design systems for semi-quantitative *visual* sensing of CO in air. As an example, a sensing array containing

compounds **2-5** and the colour changes observed at concentrations of CO of 0, 0.5, 1, 5, 10 and 50 ppm in air is shown in Figure 3.3.7.

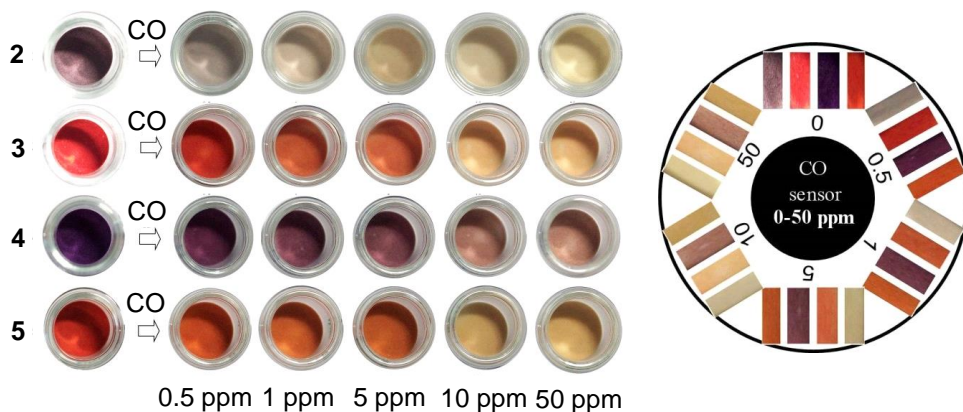


Figure 3.3.7. Sensing array of probes **2-5** for CO detection in air showing naked eye colour changes upon exposure of 0.5, 1, 5, 10, 50 ppm CO.

Selectivity

Once the sensitivity of the eight silica-supported vinyl complexes towards CO had been established, the chromogenic and fluorogenic response in the presence of other gases (CO_2 , N_2 , O_2 , Ar, SO_2 , NO_x and H_2S) and vapours (acetone, chloroform, ethanol, formaldehyde, hexane, toluene and acetonitrile) was studied. In all cases the ruthenium and osmium vinyl complexes displayed a remarkably selective response for carbon monoxide in air. For instance, no reaction was observed in the presence of CO_2 , N_2 , O_2 or Ar at very high concentrations (up to 50000 ppm). Similarly, no colour and emission changes were observed in the presence of volatile organic compounds such as acetone, chloroform, ethanol, formaldehyde, hexane or toluene (up to 30000 ppm in air). However, some colour were observed for all complexes (emission changes only were observed for complex **7** and **8**) in the presence of acetonitrile vapour, although only at concentrations of 600-5000 ppm (levels which are considered toxic to humans). Studies with other potentially coordinating gaseous species,

such as SO₂, NO_x and H₂S were also carried out. No noticeable colour and fluorescence changes were observed with any of the complexes adsorbed on silica in the presence of SO₂ (up to 38000 ppm) or H₂S (up to 200 ppm, well above the level toxic to humans). Exposure to NO_x produced colour changes to orange for all complexes except for **1** (that was already orange) and emission enhancements for **7** and **8**. However, this reactivity was only observed at very high concentrations of nitrogen oxides (around 2200 ppm). The reactivity towards acetonitrile and NO_x, together with relevant concentrations, are summarised in Table 3.3.5.

Table 3.3.5. Summary of the observed behaviour for acetonitrile and NO_x with complexes **1-8**. Responses are shown with the concentration (in ppm) necessary to induce a colour change

Solid	Interferent			
	UV-visible		Fluorescence	
	acetonitrile	NO _x	acetonitrile	NO _x
1	5000	a	b	b
2	2090	2570	-	-
3	2146	2287	-	-
4	3020	2582	-	-
5	1574	2213	-	-
6	2853	870	-	-
7	1460	1449	4168	2290
8	676	812	1584	8709

^a No visible spectroscopic changes

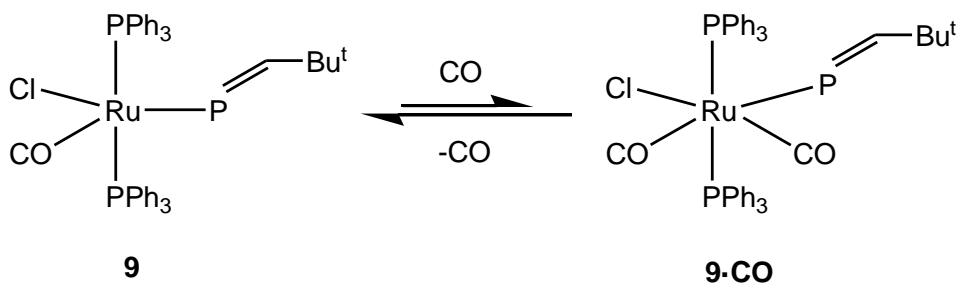
^b Complex **1** adsorbed on silica gel yielded negligible changes.

Reversibility

Coordination of CO with this set of vinyl complexes was found to be essentially irreversible both in solution and in air. Therefore the probes are better defined

(and used) as chemodosimeters and will reflect the cumulative response towards the concentration of CO present in air during a prolonged period of time.

As an attempt to design probes that could be used for the reversible sensing of CO, we focused our attention on the phosphavinyl ruthenium complex $[\text{Ru}(\text{P}=\text{CHBu}^t)\text{Cl}(\text{CO})(\text{PPh}_3)_2]$ (**9**).³⁰ At first glance, complex **9** appears closely related to the conventional vinyl complexes $[\text{Ru}(\text{CH}=\text{CHR})\text{Cl}(\text{CO})(\text{PPh}_3)_2]$. However, in analogy to nitrosyl ligands, the phosphavinyl can act as either a one-electron or a three-electron donor. There is evidence that, in the case of the reaction of **9** with CO, the phosphavinyl ligand demonstrates behaviour similar to that of a 3-electron donor, rendering the coordination sphere of the metal coordinatively-saturated. For example, the analogue $[\text{Ru}(\text{P}=\text{CHBu}^t)\text{Cl}(\text{CO})(\text{BTD})(\text{PPh}_3)_2]$ cannot be prepared as the BTD ligand is ejected after reaction between $[\text{RuHCl}(\text{CO})(\text{BTD})(\text{PPh}_3)_2]$ and $\text{P}\equiv\text{CtBu}$ to form **9** exclusively. In this system it has been shown that coordination of carbon monoxide is reversible (Scheme 3.3.3) and even solid samples of **9**·CO precipitated under an atmosphere of CO lose carbon monoxide over a period of hours to reform **9**.³⁰



Scheme 3.3.3. Reversible reaction of phosphavinyl compound **9** with CO.

In order to explore the possibility of exploiting this in the current study, solutions of **9** in dichloromethane were exposed to a mixture of carbon monoxide in air, resulting in a colour change from yellow-orange to colourless. The colour could be regenerated by purging the solution with air. In the solid state, addition of pure carbon monoxide led to a colour change from orange to pale yellow,

which was reversed on removal of the carbon monoxide atmosphere. However, supporting complex **9** on silica under the same conditions used for the other complexes led to the orange colour being lost and so the exploration of **9** as a probe for the detection of CO in air was not pursued further.

Density functional theory (DFT) study

To further investigate the colour change observed on exposure of the vinyl complexes to carbon monoxide, a computational study was performed using a high level of theory. Three ruthenium vinyl complexes containing either a pyrene (**1**), phenyl (**5**) or naphthyl (**6**) substituent on the vinyl ligand were modelled, both as the BTM precursor (**1**, **5** and **6**) and with CO bound (**1**·CO, **5**·CO and **6**·CO). Calculations were conducted using the B3LYP functional with explicit inclusion of dispersion corrections using the D3 procedure by Grimme, employing the MW28 pseudopotential and basis set for Ru and the TZVP basis set for all other atoms. Solvent effects were included via CPCM. Time-dependent Density Functional Theory (TD-DFT) experiments were conducted at the same level of theory for the first 100 states.

In all three BTM probes **1**, **5** and **6** (before CO is added), the strong colour of the complexes originate from a low intensity π - π^* transition between the aromatic vinyl group and the BTM chromophore (at around 624 nm for **1**, 576 nm for **5** and 585 nm for **6**) and a more intense π - π^* aromatic vinyl transition (at ca. 300-400 nm). Predicted UV-Vis spectra are shown in Figure 3.3.8 and selected MOs can be found in the Supporting Information (Tables S2-S7). Upon coordination of CO the transitions change depending on the nature of the vinyl group, but all compounds lose their distinct coloured transitions > 500 nm. For the electron rich pyrene system, the visible colour of the complex is maintained by a pyrene π - π^* transition at ca. 410 nm. In addition, the UV absorbance at ca. 245 nm increases with coordination of CO. For the comparatively electron poor phenyl group the transition in the visible region is blue-shifted to ca. 240 nm, increasing the UV absorbance of the compound. These results are in good agreement with DFT studies performed by Winter et al^{21c} on related 5-coordinate vinyl model structures and a pyridine adduct.

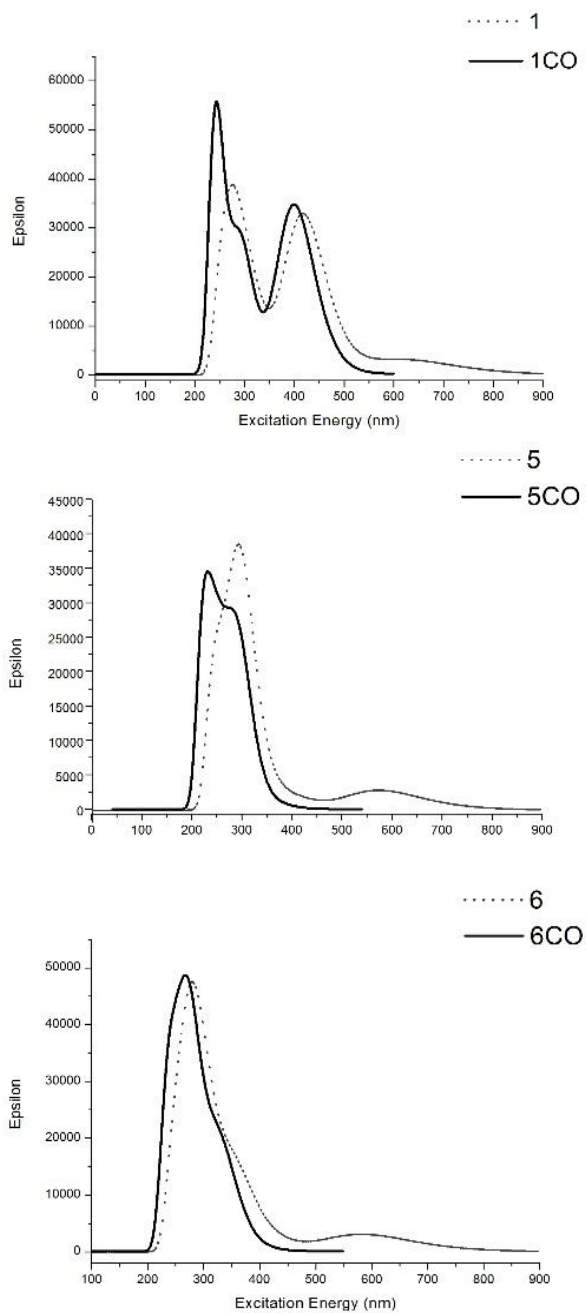


Figure 3.3.8. TD-DFT UV spectra for **1**, **5**, **6** and their carbon monoxide adducts, **1-CO**, **5-CO** and **6-CO**.

3.3.4. Conclusions

Ruthenium(II) and osmium(II) vinyl complexes (**1-8**) of general formula $[M(CH=CHR)Cl(CO)(BTD)(PPh_3)_2]$ containing two different metal centres (Ru or Os) and six different vinyl ligands (R = Pyr-1, Phen-9, Nap-2, Nap-2-OMe-6, C₆H₄Me-4 or C₆H₅) *trans* to a 2,1,3-benzothiadiazole (BTD) chromophore have been investigated as chromo-fluorogenic probes for CO detection. Spectroscopic studies (UV-Vis and fluorescence) were carried out on the complexes, both in solution and immobilized on silica, showing colour changes in the visible region and enhancement in emission intensity due to coordination of CO and displacement of BTD ligand. Remarkable colour modulations from orange to yellow (in the case of ruthenium complexes **1**, **3** and **5-8**) and from purple to yellow (for osmium complexes **2** and **4**) were observed. Further information on these modulations in colour was provided by a TD-DFT computational study. Examples of the probes before (**4** and **6**) and after CO additions (**5-CO**) were also investigated structurally using single crystal X-ray diffraction techniques. In all cases the ruthenium and osmium vinyl complexes studied showed a highly selective response to CO with remarkably low detection limits. Of all VOCs and gases tested as possible interferents, only acetonitrile and NO_x gave indication of colour and emission changes, yet in both cases this was only observed at extremely high (and well above toxic) concentrations unlikely to be encountered in any setting requiring CO sensing. Most notably, the exceptional selectivity for CO over water vapour and all organic solvents tested is of crucial importance in the potential application of this system in domestic or workplace settings where steam, cleaning products or fuel fumes are present (addressing this shortcoming in commercial devices).

While this very high selectivity is vital for a viable CO detector, good sensitivity and a clear indication of the presence of this odourless, tasteless, toxic gas are of great importance. All the complexes tested (**1-8**) displayed very clear and remarkable colour changes, easily visible to the naked eye at very low concentrations of CO. In particular, complex **1** demonstrates distinct changes in colour at CO concentrations as low as 0.005 ppm, even allowing the visual quantification of CO in air. Critically, the chromogenic responses observed cover a

wide spectrum of concentrations, encompassing the toxicity range for humans (Table 3.3.1). This would allow the system described here to be employed in its current form to monitor acute or cumulative exposure to CO in the home or workplace (using a comparison colour chart for various amounts of CO). Cellulose strips impregnated with the complexes¹⁵ would also allow the colour change to be converted to a numerical reading (and hence alarm) using a simple, portable optoelectronic device, such as described by some of us previously.³¹ The attributes described above for complexes **2-6** complement the dual chromo-fluorogenic detection of carbon monoxide by complexes **1, 7** and **8** but using simpler and less expensive reagents. The colour and turn-on emission modulations (**1, 7, 8**) observed are highly selective and due to a displacement of the BTD ligand in the probes by CO to yield the dicarbonyl complexes. Furthermore, the high-yielding and straightforward synthetic procedure used to prepare **1-8** in air, coupled with the commercial availability and relatively low cost of ruthenium and other reagents (especially ethynylbenzene) render the metal complexes both accessible and inexpensive. Complexes **1** and **5** offer subtly contrasting sensitivities, which can suit different applications and environments with diverse amounts of background carbon monoxide presence. Complex **1** costs around €34/g for the materials but less than a cent for the amount on a cellulose strip, while **5** is three times less expensive. The combination of sensitivity, selectivity, simple synthesis and low cost make the system described here a very attractive and efficient chemosensor for the simple chromogenic (and for **1, 7** and **8**, fluorogenic) detection of this colourless, odourless and highly toxic gas.

3.3.5. Acknowledgements

The authors wish to express their gratitude to the Spanish Government (project MAT2012-38429-C04) and Generalitat Valenciana (project PROMETEOII/2014/047) for their support. M.E.M. is grateful to the Spanish Ministerio de Ciencia e Innovación for an FPU grant as well as for the short-stay fellowship, which allowed this profitable collaboration. C.M-H. thanks the Spanish Ministry of Economy and Competitiveness for her grant. The authors thank Johnson Matthey Ltd for a generous loan of ruthenium and osmium salts. A.T.

gratefully acknowledges the support of the Leverhulme Trust (Grant RPG-2012-634) for a studentship. The authors thank Prof. C. K. Williams, Prof. N. J. Long and Dr P. Hunt (Imperial College) for the use of apparatus and assistance.

Keywords

Ruthenium, osmium, carbon monoxide, sensing, gas detection.

3.3.6. References

- 1 a) D. Gutmacher, C. Foelml, W. Vollenweider, U. Hofer, J. Wöllenstein, *Procedia Eng.*, **2011**, 25, 1121-1124; b) C. Kaminski, A. Poll, *Electrochemical or Solid State H₂S Sensors: Which is Right for You?* InTech, USA, 1985.
- 2 a) G. Korotcenkov, V. Brynzari, S. Dmitriev, *Mater. Sci. Eng. B* **1999**, 63, 195-204; b) N. Yamazoe, Y. Kurokawa, T. Seiyama, *Sens. Actuators*, **1983**, 4, 283-289.
- 3 J. Wolfrum, *Proc. Combust. Inst.* **1998**, 27, 1, 1-41.
- 4 K. -H. Cho, S. -W. Lee, J. -H. Lee, K. -S. Choi, *Anal. Sci. Technol.* **2000**, 13, 222-228.
- 5 M. Itou, Y. Araki, O. Ito, H. Kido, *Inorg. Chem.* **2006**, 45, 6114-6116.
- 6 A. Giulino, T. Gupta, M. Altman, S. Lo Schiavo, P. G. Mineo, I. L. Fragalà, G. Evmenenko, P. Dutta, M. E. van der Boom, *Chem. Commun.* **2008**, 2900-2902.
- 7 D. Benito-Garagorri, M. Puchberger, K. Mereiter, K. Kirchner, *Angew. Chem. Int. Ed.* **2008**, 47, 9142-9145.
- 8 S. Paul, F. Amalraj, S. Radhakrishnana, *Synt. Met.* **2009**, 159, 1019-1023.
- 9 a) M. E. Moragues, J. Esteban, J. V. Ros-Lis, R. Martínez-Máñez, M.D. Marcos, M. Martínez, J. Soto, F. Sancenón, *J. Am. Chem. Soc.* **2011**, 133, 15762-15772; b) J. Esteban, J. V. Ros-Lis, R. Martínez-Máñez, M. D. Marcos, M. Moragues, J. Soto, F. Sancenón, *Angew. Chem. Int. Ed.* **2010**, 49, 4934-4937.
- 10 C. W. Tate, A. deMello, A. D. Gee, S. Kealey, R. Vilar, A. J. P. White, N. J. Long, *Dalton Trans.* **2012**, 41, 83-89.
- 11 US Environmental Protection Agency, *Air Quality Criteria for Carbon Monoxide*, EPA/600/P-99/001. *National Center for Environmental Assessment*, Research Triangle Park, NC, 1999.
- 12 <https://www.gov.uk/government/publications/carbon-monoxide-poisoning>.
- 13 See for instance: a) L. E. Santos-Figueroa, C. Giménez, A. Agostini, E. Aznar, M. D. Marcos, F. Sancenón, R. Martínez-Máñez, P. Amorós, *Angew. Chem. Int. Ed.* **2013**, 52, 13712-13716; b) E. Climent, M.D. Marcos, R. Martínez-Máñez, F. Sancenón, J.

- Soto, K. Rurack, P. Amorós, *Angew. Chem. Int. Ed.* **2009**, *48*, 8519-8522; c) E. Climent, A. Bernardos, R. Martínez-Máñez, A. Maquieira, M.D. Marcos, N. Pastor-Navarro, R. Puchades, F. Sancenón, J. Soto, P. Amorós, *J. Am. Chem. Soc.* **2009**, *131*, 14075-14080; d) Comes, E. Aznar, M. Moragues, M.D. Marcos, R. Martínez-Máñez, F. Sancenón, J. Soto, L.A. Villaescusa, L. Gil, P. Amorós, *Chem. Eur. J.* **2009**, *15*, 9024-9033; e) T. Ábalos, S. Royo, R. Martínez-Máñez, F. Sancenón, J. Soto, A.M. Costero, S. Gil, M. Parra, *New. J. Chem.* **2009**, *33*, 1641-1645; f) E. Aznar, C. Coll, M.D. Marcos, R. Martínez-Máñez, F. Sancenón, J. Soto, P. Amorós, J. Cano, E. Ruiz, *Chem. Eur. J.* **2009**, *15*, 6877-6888; g) E. Climent, P. Calero, M.D. Marcos, R. Martínez-Máñez, F. Sancenón, J. Soto, *Chem. Eur. J.* **2009**, *15*, 1816-1820.
- 14 a) H. Loumrhari, J. Ros, M. R. Torres, A. Santos, A. M. Echavarren, *J. Organomet. Chem.* **1991**, *411*, 255-261; b) M. C. J. Harris, A. F. Hill, *Organometallics* **1991**, *10*, 3903-3906.
- 15 M. E. Moragues, A. Toscani, F. Sancenón, R. Martínez-Máñez, A. J. P. White, J. D. E. T. Wilton-Ely, *J. Am. Chem. Soc.* **2014**, *136*, 11930-11933.
- 16 For an overview of alkenyl chemistry of ruthenium(II), see: a) M. K. Whittlesey in *Comprehensive Organometallic Chemistry III*, Eds.: R. H. Crabtree, D. M. P. Mingos, M. I. Bruce, Elsevier: Oxford, U.K., 2006; Vol. 6; b) A. F. Hill in *Comprehensive Organometallic Chemistry II*, Eds.: E. W. Abel, F. G. A. Stone, G. Wilkinson, Pergamon Press: Oxford, U.K., 1995; Vol. 7.
- 17 a) S. Jung, K. Ilg, C. D. Brandt, J. Wolf, H. Werner, *Eur. J. Inorg. Chem.* **2004**, 469-480; b) S. Jung, C. D. Brandt, J. Wolf, H. Werner, *Dalton Trans.* **2004**, 375-383; c) H. Werner, S. Jung, P. Gonzalez-Herrero, K. Ilg, J. Wolf, *Eur. J. Inorg. Chem.* **2001**, 1957-1961; d) S. Jung, K. Ilg, J. Wolf, H. Werner, *Organometallics* **2001**, *20*, 2121-2123; e) H. Werner, W. Stüer, S. Jung, B. Weberndörfer, J. Wolf, *Eur. J. Inorg. Chem.* **2002**, 1076-1080; f) H. Werner, A. Stark, P. Steinert, C. Grunwald, J. Wolf, *Chem. Ber.* **1995**, *128*, 49-62.
- 18 a) M. A. Esteruelas, A. M. López, E. Oñate, *Organometallics* **2007**, *26*, 3260-3263; b) T. Bolano, R. Castarlenas, M. A. Esteruelas, E. Oñate, *J. Am. Chem. Soc.* **2006**, *128*, 3965-3973; c) B. Eguillar, M. A. Esteruelas, M. Oliván, E. Oñate, *Organometallics* **2005**, *24*, 1428-1438; d) R. Castarlenas, M. A. Esteruelas, E. Oñate, *Organometallics* **2001**, *20*, 3283-3292; e) R. Castarlenas, M. A. Esteruelas, E. Oñate, *Organometallics* **2001**, *20*, 2294-2302; f) M. A. Esteruelas, C. García-Yebra, M. Oliván, E. Oñate, M. Tajada, *Organometallics* **2000**, *19*, 5098-5106; g) R. Castarlenas, M. A. Esteruelas, E. Oñate, *Organometallics* **2000**, *19*, 5454-5463; h)

- M. L. Buil, M. A. Esteruelas, C. García-Yebra, E. Gutiérrez-Puebla and M. Oliván, *Organometallics* **2000**, *19*, 2184–2193; i) C. Bohanna, M. L. Buil, M. A. Esteruelas, E. Oñate, C. Valero, *Organometallics* **1999**, *18*, 5176–5179; j) C. Bohanna, B. Callejas, A. Edwards, M. A. Esteruelas, F. J. Lahoz, L. A. Oro, N. Ruiz, C. Valero, *Organometallics* **1998**, *17*, 373–381; k) M. A. Esteruelas, A. V. Gómez, A. M. López, E. Oñate, *Organometallics* **1998**, *17*, 3567–3573; l) M. A. Esteruelas, F. Liu, E. Oñate, E. Sola, B. Zeier, *Organometallics* **1997**, *16*, 2919–2928; m) M. L. Buil, S. Elipe, M. A. Esteruelas, E. Oñate, E. Peinado, N. Ruiz, *Organometallics* **1997**, *16*, 5748–5755; n) M. A. Esteruelas, F. J. Lahoz, E. Oñate, L. A. Oro, E. Sola, *J. Am. Chem. Soc.* **1996**, *118*, 89–99; o) C. Bohanna, M. A. Esteruelas, J. Herrero, A. M. López, L. A. Oro, *J. Organomet. Chem.* **1995**, *498*, 199–206; p) C. Bohanna, M. A. Esteruelas, F. J. Lahoz, E. Oñate, L. A. Oro, E. Sola, *Organometallics* **1995**, *14*, 4825–4831; q) C. Bohanna, M. A. Esteruelas, F. J. Lahoz, E. Oñate, L. A. Oro, *Organometallics* **1995**, *14*, 4685–4696.
- 19 a) B. Gómez-Lor, A. Santos, M. Ruiz, A. M. Echavarren, *Eur. J. Inorg. Chem.* **2001**, 2305–2310; b) A. M. Castaño, A. M. Echavarren, J. López, A. Santos, *J. Organomet. Chem.* **1989**, *379*, 171–175; c) J. Montoya, A. Santos, A. M. Echavarren, J. Ros, *J. Organomet. Chem.* **1990**, *390*, C57–C60; d) J. Montoya, A. Santos, J. López, A. M. Echavarren, J. Ros, A. Romero, *J. Organomet. Chem.* **1992**, *426*, 383–398; e) J. López, A. Romero, A. Santos, A. Vegas, A. M. Echavarren, P. Noheda, *J. Organomet. Chem.* **1989**, *373*, 249–258; f) A. M. Echavarren, J. López, A. Santos, J. Montoya, *J. Organomet. Chem.* **1991**, *414*, 393–400; g) M. R. Torres, A. Vegas, A. Santos, J. Ros, *J. Organomet. Chem.* **1987**, *326*, 413–421; h) M. R. Torres, A. Santos, J. Ros, X. Solans, *Organometallics* **1987**, *6*, 1091–1095.
- 20 a) D. J. Huang, K. B. Renkema, K. G. Caulton, *Polyhedron* **2006**, *25*, 459–468; b) A. V. Marchenko, H. Gérard, O. Eisenstein, K. G. Caulton, *New J. Chem.* **2001**, *25*, 1382–1388; c) A. V. Marchenko, H. Gérard, O. Eisenstein, K. G. Caulton, *New J. Chem.* **2001**, *25*, 1244–1255; d) J. N. Coalter, W. E. Streib, K. G. Caulton, *Inorg. Chem.* **2000**, *39*, 3749–3756; e) A. Pedersen, M. Tilset, K. Folting, K. G. Caulton, *Organometallics* **1995**, *14*, 875–888.
- 21 a) J. Maurer, R. F. Winter, B. Sarkar, J. Fiedler, S. Záliš, *Chem. Commun.* **2004**, 1900–1901; b) J. Maurer, B. Sarkar, W. Kaim, R. F. Winter, S. Záliš, *Chem. Eur. J.* **2007**, *13*, 10257–10272; c) J. Maurer, M. Linseis, B. Sarkar, B. Schwederski, M. Niemeyer, W. Kaim, S. Záliš, C. Anson, M. Zabel, R. F. Winter, *J. Am. Chem. Soc.* **2008**, *130*, 259–268.

- 22 a) A. F. Hill, R. P. Melling, *J. Organomet. Chem.* **1990**, 396, C22–C24; b) A. F. Hill, M. C. J. Harris, R. P. Melling, *Polyhedron* **1992**, 11, 781–787; c) M. C. J. Harris, A. F. Hill, *Organometallics* **1991**, 10, 3903–3906; d) A. F. Hill, A. J. P. White, D. J. Williams, J. D. E. T. Wilton-Ely, *Organometallics* **1998**, 17, 4249–4258; e) J. C. Cannadine, A. F. Hill, A. J. P. White, D. J. Williams, J. D. E. T. Wilton-Ely, *Organometallics* **1996**, 15, 5409–5415; f) A. F. Hill, C. T. Ho and J. D. E. T. Wilton-Ely, *Chem. Commun.* **1997**, 2207–2208; g) A. F. Hill, J. D. E. T. Wilton-Ely, *J. Chem. Soc., Dalton Trans.* **1999**, 3501–3510.
- 23 a) J. D. E. T. Wilton-Ely, M. Wang, D. Benoit, D. A. Tocher, *Eur. J. Inorg. Chem.* **2006**, 3068–3078; b) J. D. E. T. Wilton-Ely, P. J. Pogorzelec, S. J. Honarkhah, D. A. Tocher, *Organometallics* **2005**, 24, 2862–2874; c) J. D. E. T. Wilton-Ely, S. J. Honarkhah, M. Wang, D. A. Tocher, *Dalton Trans.* **2005**, 1930–1939; d) J. D. E. T. Wilton-Ely, M. Wang, S. J. Honarkhah, D. A. Tocher, *Inorg. Chim. Acta* **2005**, 358, 3218–3226.
- 24 A. Santos, J. López, A. Galán, J. J. González, P. Tinoco, A. M. Echavarren, *Organometallics* **1997**, 16, 3482–3488.
- 25 M. R. Torres, A. Vegas, A. Santos, J. Ros, *J. Organomet. Chem.* **1986**, 309, 169–177.
- 26 S.-H. Choi, I. Bytheway, Z. Lin, G. Jia, *Organometallics* **1998**, 17, 3974–3980.
- 27 N. W. Alcock, A. F. Hill, M. S. Roe, *J. Chem. Soc., Dalton Trans.* **1999**, 1737–1740.
- 28 A. Romero, A. Santos, A. Vegas, *Organometallics* **1988**, 7, 1988–1993.
- 29 a) B. W. Michel, A. R. Lippert, C. J. Chang, *J. Am. Chem. Soc.* **2012**, 134, 15668–15671; b) J. Wang, J. Karpus, B. S. Zhao, Z. Luo, P. R. Chen, C. He, *Angew. Chem. Int. Ed.* **2012**, 51, 9652–9656.
- 30 R. B. Bedford, A. F. Hill, C. Jones, A. J. P. White, D. J. Williams, J. D. E. T. Wilton-Ely, *Organometallics* **1998**, 17, 4744–4753.
- 31 M. E. Moragues, R. Montes-Robles, J. V. Ros-Lis, M. Alcañíz, J. Ibañez, T. Pardo, R. Martínez-Mañez, *Sens. Actuators B* **2014**, 191, 257–263.

SUPPORTING INFORMATION

Ruthenium(II) and Osmium(II) Alkenyl Complexes as Highly Sensitive and Selective Chromogenic and Fluorogenic Probes for the Sensing of Carbon Monoxide in air

Anita Toscani, Cristina Marín-Hernández, María E. Moragues, Félix Sancenón, Paul Dingwall, Neil J. Brown, Ramón Martínez-Máñez,* Andrew J. P. White and James D. E. T. Wilton-Ely*

1. Experimental procedures

Reagents

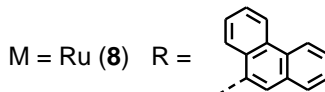
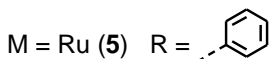
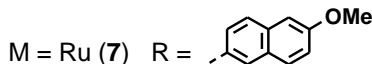
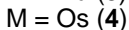
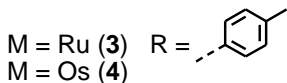
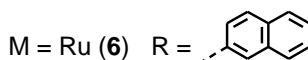
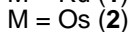
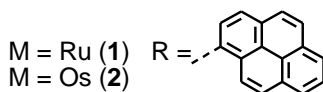
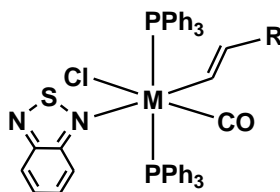
The compounds 1-ethynylpyrene, 4-ethynyltoluene, 4-ethynylbenzene, 9-ethynylphenanthrene, 2-ethynyl-naphthalene, 2-ethynyl-6-methoxynaphthalene and 2,1,3-benzothiadiazole (BTD) were used as purchased. All solvents were of analytical grade. Solvents used for UV-Vis measurements were thoroughly degassed with N₂. Petroleum ether refers to the fraction boiling between 40-60°C. All experiments and manipulations of compounds were conducted in air, unless otherwise specified. Carbon monoxide was provided by commercially available CO cylinders. Mixtures of different concentrations of CO were prepared by mixing CO with CO-free synthetic air. The rest of gases used in this work were generated *in situ*, carbon dioxide (by adding hydrochloric acid to sodium carbonate), nitrogen oxides (by oxidation of copper with nitric acid), sulfur dioxide (by copper oxidation with sulfuric acid) and H₂S (by adding hydrochloric acid to sodium sulphide). The procedures given provide materials of sufficient purity for synthetic and spectroscopic purposes.

Instrumentation

NMR spectroscopy was performed at 25°C using a Bruker AV400 spectrometer, operating at 400.32 MHz for ¹H nuclei and 162.05 MHz for ³¹P nuclei. Spectra were recorded in CDCl₃ unless stated otherwise. Chemical shifts are reported in ppm and coupling constants (*J*) are in Hertz. Infrared data were obtained using a Perkin-Elmer Spectrum 100 FT-IR spectrophotometer. Elemental analysis data were obtained by London Metropolitan University. Solvates were confirmed by integration of the ¹H NMR spectrum. Electrospray (ES) mass analyses were performed at Imperial College London on a Micromass LCT Premier spectrometer. UV-Vis spectra were recorded using a Jasco V-650 spectrophotometer equipped with a diffuse reflectance sphere (model ISV-722) for measurements on solids. In the latter case, measurements were conducted at room temperature over a wavelength range of 350-800 nm with a wavelength step of 1 nm. Carbon monoxide concentrations were measured using an ambient carbon monoxide

analyser (Testo 315-2 model 0632 0317), properly validated with an ISO calibration certificate issued by Instrumentos Testo, Cabrils, Spain. Computational calculations were performed using the B3LYP functional, dispersion corrections were added using the empirical dispersion keyword and Grimme's D3 procedure. MWB28 was used as the pseudo potential and basis set for Ru. Initially, all other atoms were calculated at 6-31G(d) and then refined using the TZVP basis set. Solvent (methanol) was included in all calculations using the CPCM methodology. An ultrafine grid and tight convergence criteria, scf=9, was employed throughout. TD-DFT calculations were carried out on fully optimised structures for the first 100 states using the same functional and basis sets. Molecular orbital diagrams were generated using Gauss view. Full crystallographic data have been deposited in the Cambridge Crystallographic Data Centre for **4**, **6** and **5·CO** with the numbers CCDC 1011581, 1048863 and 1011582, respectively.

Synthesis



General Comments. The complexes $[\text{RuHCl}(\text{CO})(\text{PPh}_3)_3]$,^{S1} $[\text{OsHCl}(\text{CO})(\text{BTD})(\text{PPh}_3)_2]$,^{S2} $[\text{Os}(\text{CH}=\text{CHC}_6\text{H}_4\text{Me-4})\text{Cl}(\text{CO})(\text{BTD})(\text{PPh}_3)_2]$ (**4**),^{S2} $[\text{Os}(\text{CH}=\text{CHC}_6\text{H}_4\text{Me-4})\text{Cl}(\text{CO})_2(\text{PPh}_3)_2]$ (**4·CO**),^{S2} $[\text{Ru}(\text{P}=\text{CH}^t\text{Bu})\text{Cl}(\text{CO})(\text{PPh}_3)_2]$ (**9**),^{S3} $[\text{Ru}(\text{P}=\text{CH}^t\text{Bu})\text{Cl}(\text{CO})_2(\text{PPh}_3)_2]$ (**9·CO**)^{S3} and $[\text{Ru}(\text{CH}=\text{CHC}_6\text{H}_5)\text{Cl}(\text{CO})_2(\text{PPh}_3)_2]$ (**5·CO**)^{S4}

were prepared according to published procedures. Further data are provided for the compounds $[\text{Ru}(\text{CH}=\text{CHPyr-1})\text{Cl}(\text{CO})(\text{BTD})(\text{PPh}_3)_2]$ (**1**),⁵⁵ $[\text{Ru}(\text{CH}=\text{CHPyr-1})\text{Cl}(\text{CO})_2(\text{PPh}_3)_2]$ (**1-CO**).⁵⁵

$[\text{Ru}(\text{CH}=\text{CHPyr-1})\text{Cl}(\text{CO})(\text{BTD})(\text{PPh}_3)_2]$ (1**)**

2,1,3-benzothiadiazole (25 mg, 0.184 mmol) was added to a dichloromethane (10 mL) solution of $[\text{RuHCl}(\text{CO})(\text{PPh}_3)_3]$ (102 mg, 0.107 mmol) and the resulting orange solution was stirred at room temperature for few minutes. 1-ethynylpyrene (37 mg, 0.164 mmol) was then added and the reaction mixture was stirred at room temperature for 1 h, after which methanol (25 mL) was added and the dichloromethane slowly removed under reduced pressure (rotary evaporator). The resulting red-orange crystals were isolated by filtration, washed with ethanol (2 x 10 mL) and dried *in vacuo*. Yield: 106 mg (94%). IR ($\nu_{\text{max}}/\text{cm}^{-1}$): 1928 (CO), 1432, 1232, 1088, 846, 740, 692. NMR δ_{H} (CDCl_3) 7.01 (1H, d, $J_{\text{HH}} = 15.0$ Hz, H β), 7.64 – 7.18 (30H, m, Ph), 7.93 (2H, m, BTD), 7.70 – 7.95 (9H, m, pyrenyl), 8.05 (2H, m, BTD), 9.06 (1H, dt, $J_{\text{HH}} = 15.0$ Hz, J_{HP} unresolved, H α); δ_{P} (CDCl_3) 29.4 (s, PPh_3). MS (ES +ve) m/z 1053 (M^+ , 5%). Elemental analysis: Found: C, 69.4; H, 4.5; N, 2.6. $\text{C}_{61}\text{H}_{45}\text{ClN}_2\text{OP}_2\text{RuS}$ requires C, 69.6; H, 4.3; N, 2.7%.

$[\text{Ru}(\text{CH}=\text{CHPyr-1})\text{Cl}(\text{CO})_2(\text{PPh}_3)_2]$ (1-CO**)**

Compound **2** was prepared by treating a dichloromethane solution (10 mL) of **1** (7.0 mg, 0.007 mmol) with a stream of carbon monoxide for 1 minute. Ethanol (5 mL) was added, forming a yellow precipitate which was filtered, washed with ethanol (10 mL), and dried *in vacuo*. Yield: 6.4 mg (97%). IR ($\nu_{\text{max}}/\text{cm}^{-1}$): 2031 (CO), 1874 (CO) 1481, 1433, 1346, 1160, 1091, 847, 740, 691. NMR δ_{H} (CDCl_3) 7.13 (1H, dt, $J_{\text{HH}} = 15.0$ Hz, J_{HP} unresolved, H β), 7.76 – 7.30 (30H, m, PPh_3), 8.10 – 7.83 (9H, m, pyrenyl), 8.53 (1H, dt, $J_{\text{HH}} = 15.0$ Hz, J_{HP} unresolved, H α); δ_{P} (CDCl_3) 23.7 (s, PPh_3). MS (ES +ve) m/z 945 (M^+ , 10%). Elemental Analysis: Found: C, 70.8; H, 4.4; $\text{C}_{56}\text{H}_{41}\text{ClO}_2\text{P}_2\text{Ru}$ requires C, 71.2; H, 4.4%.

[Os(CH=CHPyr-1)Cl(CO)(BTD)(PPh₃)₂] (2)

A dichloromethane solution (10 mL) of [OsHCl(CO)(BTD)(PPh₃)₂] (70 mg, 0.076 mmol) was treated with 1-ethynylpyrene (19 mg, 0.084 mmol). The resulting dark red solution was stirred for 3 hours at room temperature and then filtered through Celite. Addition of methanol (15 mL) followed by slow reduction of the solvent volume, resulted in a dark red solid, which was washed with cold methanol (10 mL), petroleum ether (10 mL) and dried. Yield: 60 mg (69%). IR ($\nu_{\max}/\text{cm}^{-1}$): 1919 (CO), 1434, 1183, 1117, 745, 719, 691. NMR δ_{H} (CD₂Cl₂) 7.08-7.21 (18H, m, Ph), 7.46 (12H, m, Ph), 7.80 – 7.99 (9H + 1H, m, pyrenyl + H β), 8.15 (2H, d, $J_{\text{HH}} = 7.6$ Hz, BTD), 8.15 (2H, m, BTD), 9.70 (1H, dt, $J_{\text{HH}} = 16.8$ Hz, J_{HP} unresolved, H α); δ_{P} (CD₂Cl₂) -1.2 (s, PPh₃). MS (ES +ve) m/z 1188 (M⁺ + 2Na, 60%). Elemental Analysis: Found: C, 60.3; H, 3.5; N, 2.5. C₆₁H₄₅ClN₂O₂OsP₂S·CH₂Cl₂ requires C, 60.7; H, 3.9; N, 2.3%.

[Os(CH=CHPyr-1)Cl(CO)₂(PPh₃)₂] (2 CO)

Compound **2 CO** was prepared by treating a dichloromethane solution (3 mL) of **2** (25 mg, 0.022 mmol) with a stream of carbon monoxide for 1 minute. Methanol (5 mL) was added and the resulting mustard yellow precipitate was isolated by filtration. The compound was washed with methanol (10 mL) and dried. Yield: 19 mg (84%). IR ($\nu_{\max}/\text{cm}^{-1}$): 2017 (CO), 1954 (CO), 1434, 1092, 847, 740, 692. NMR δ_{H} (CD₂Cl₂) 7.25 (1H, dt, $J_{\text{HH}} = 18.1$ Hz, $J_{\text{HP}} = 2.3$ Hz, H β), 7.33 – 7.43 (18H, m, Ph), 7.58 (1H, d, $J_{\text{HH}} = 8.1$ Hz, pyrenyl), 7.68 – 7.73 (12H, m, Ph), 7.87 (2H, s, pyrenyl), 7.92 – 8.00 (4H, m, pyrenyl), 8.06 (1H, dt, 1H, $J_{\text{HH}} = 18.1$ Hz, $J_{\text{HP}} = 3.0$ Hz, H α), 8.07 – 8.12 (2H, m, pyrenyl); δ_{P} (CD₂Cl₂) -7.3 (s, PPh₃). MS (ES +ve) m/z 1034 (M⁺, 100%). Found: C, 65.0; H, 4.2. C₅₆H₄₁ClO₂OsP₂ requires C, 65.1; H, 4.0 %.

[Ru(CH=CHC₆H₄Me-4)Cl(CO)(BTD)(PPh₃)₂] (3)

4-ethynyltoluene (26 μL , 0.236 mmol) was added to a dichloromethane solution (10 mL) of [RuHCl(CO)(PPh₃)₃] (150 mg, 0.158 mmol) to give a dark red solution. BTD (32 mg, 0.235 mmol) was then added and the solution was stirred for 1 hour at room temperature. EtOH (20 mL) was added and the dichloromethane was slowly removed under vacuum to yield a bright orange

crystalline product. This was filtered and washed with EtOH (2 x 10 mL) and petroleum ether (20 mL) and dried under vacuum. Yield: 131 mg (88 %). IR ($\nu_{\max}/\text{cm}^{-1}$): 1914 (CO), 1482, 1434, 1091, 979, 837, 741, 693. NMR δ_{H} (CD_2Cl_2) 2.29 (3H, s, CH_3), 5.75 (1H, dt, $J_{\text{HH}} = 16.0$ Hz, $J_{\text{HP}} =$ unresolved, H β), 6.77, 6.79 (2 x 2H, AB, $J_{\text{AB}} = 7.9$ Hz, $\text{C}_6\text{H}_4\text{Me}$), 7.12 (12H, t, $J_{\text{HH}} = 7.0$ Hz, Ph), 7.23 (6H, t, $J_{\text{HH}} = 7.0$ Hz, Ph), 7.50 – 7.44 (12H, m, Ph), 7.72 – 7.67 (2H, m, BTD), 7.91 (2H, s br, BTD), 8.63 (1H, dt, $J_{\text{HH}} = 16.0$ Hz, $J_{\text{HP}} = 3.2$ Hz, H α); δ_{P} (CD_2Cl_2) 26.7 (s, PPh_3). MS (ES +ve) m/z 943 (M^+ , 40%). Elemental Analysis: Found: C, 62.1; H, 4.7; N, 2.9. $\text{C}_{52}\text{H}_{43}\text{ClN}_2\text{OP}_2\text{RuS}\cdot\text{CH}_2\text{Cl}_2$ requires C, 62.0; H, 4.4; N, 2.7%.

[Ru(CH=CHC₆H₄Me-4)Cl(CO)₂(PPh₃)₂] (3 CO)

Compound **3 CO** was prepared by treating a dichloromethane solution (3 mL) of **3** (30 mg, 0.032 mmol) with a stream of carbon monoxide for 1 minute. Methanol (5 mL) was added and the resulting precipitate was isolated by filtration. The pale pink compound was washed with methanol (10 mL) and dried. Yield: 25 mg (94 %). IR ($\nu_{\max}/\text{cm}^{-1}$): 2030 (CO), 1968 (CO), 1481, 1434, 1091, 990, 741, 733, 690. NMR δ_{H} (CD_2Cl_2) 2.31 (3H, s, CH_3), 5.85 (1H, dt, $J_{\text{HH}} = 18.0$ Hz, J_{HP} unresolved, H β), 6.80, 7.01 (2 x 2H, AB, $J_{\text{AB}} = 7.9$ Hz, $\text{C}_6\text{H}_4\text{Me}$), 7.37 – 7.47 (18H, m, Ph), 7.52 (1H, dt, $J_{\text{HH}} = 18.0$ Hz, $J_{\text{HP}} = 3.5$ Hz, H α), 7.69-7.74 (12H, m, Ph); δ_{P} (CD_2Cl_2) 23.8 (s, PPh_3). MS (ES +ve) m/z 853 ($\text{M}^+ + \text{H}_2\text{O}$, 9%). Elemental analysis: Found: C, 63.7; H, 4.6. $\text{C}_{47}\text{H}_{39}\text{ClO}_2\text{P}_2\text{Ru}\cdot 0.75\text{CH}_2\text{Cl}_2$ requires C, 63.9; H, 4.5%.

[Ru(CH=CHC₆H₅)Cl(CO)(BTD)(PPh₃)₂] (5)

Ethynylbenzene (25 μL , 0.236 mmol) was added to a dichloromethane solution (10 mL) of $[\text{RuHCl}(\text{CO})(\text{PPh}_3)_3]$ (150 mg, 0.158 mmol) to give a dark red solution. BTD (32 mg, 0.235 mmol) was then added and the solution was left to stir for 1 hour at room temperature. EtOH (20 mL) was added and dichloromethane was slowly removed under vacuum to yield a bright red crystalline product, which was filtered and washed with EtOH (2 x 10 mL) and petroleum ether (20 mL). Yield: 125 mg (85 %). IR ($\nu_{\max}/\text{cm}^{-1}$): 1917 (CO), 1481, 1433, 1090, 738, 689. NMR δ_{H} (CD_2Cl_2): 5.82 (1H, d, $J_{\text{HH}} = 16.0$ Hz, H β), 6.91 (2H, d, $J_{\text{HH}} = 7.3$ Hz, CPh), 6.98 (1H, t, $J_{\text{HH}} = 7.3$ Hz, CPh), 7.14 – 7.20 (12H + 2H, m, PPh + CPh), 7.30 (6H, m, PPh), 7.46 –

7.51 (12H, m, PPh), 7.54 (2H, m, BT D), 7.95 (2H, m, BT D), 8.70 (1H, dt, $J_{\text{HH}} = 16.0$ Hz, $J_{\text{HP}} = 3.0$ Hz, H α); δ_{P} (CD₂Cl₂) 27.0 (s, PPh₃). MS (ES +ve) m/z 839 ($\text{M}^+ - \text{BT D} + 2\text{Na}$, 34%). Elemental analysis. Found: C, 65.9; H, 4.5. C₅₁H₄₁ClN₂OP₂RuS requires C, 66.0; H, 4.5%.

[Ru(CH=CHNap-2)Cl(CO)(BT D)(PPh₃)₂] (6)

[RuHCl(CO)(PPh₃)₃] (117 mg, 0.123 mmol) and 2-ethynyl naphthalene (21 mg, 0.138 mmol) were dissolved in dichloromethane (15 mL) and a dichloromethane solution (5 mL) of 2,1,3-benzothiadiazole (25 mg, 0.184 mmol) was added. The resulting orange solution was stirred for 1 hour at room temperature. Addition of methanol (20 mL) followed by slow reduction of the solvent volume, resulted in a bright orange crystalline solid, which was washed with cold methanol (10 mL) and petroleum ether (10 mL) and dried. Yield: 87 mg (72%). IR ($\nu_{\text{max}}/\text{cm}^{-1}$) 1925 (CO), 1550, 1483, 1433 (C-N), 1090, 979, 923 cm^{-1} ; ¹H NMR δ_{H} (CD₂Cl₂) 6.00 (1H, d, $J_{\text{HH}} = 16.3$ Hz, H β), 7.13 – 7.56 (30H + 4H, m, PPh₃ + Nap), 7.64 (1H, d, $J_{\text{HH}} = 8.6$ Hz, Nap), 7.70 (1H, d, $J_{\text{HH}} = 8.6$ Hz, Nap), 7.73 (1H, d, $J_{\text{HH}} = 8.6$ Hz, Nap), 7.96 (2H, m, BT D), 8.89 (1H, dt, $J_{\text{HH}} = 16.3$, $J_{\text{HP}} = 3.1$ Hz, H α); δ_{P} (CD₂Cl₂) 26.9 (s, PPh₃) ppm. MS (ES +ve) m/z 889 ($\text{M}^+ - \text{BT D} + 2\text{Na}$, 80%); Elemental analysis. Found: C 67.4, H 4.5, N 3.0. C₅₅H₄₃ClN₂OP₂RuS requires C 67.5, H 4.4, N 2.9 %.

[Ru(CH=CHNap-2)Cl(CO)₂(PPh₃)₂] (6 CO)

Carbon monoxide was bubbled through a dichloromethane solution (10 mL) of **6** (30 mg, 0.031 mmol) until the solution became colourless. Addition of methanol (7 mL) followed by slow reduction of the solvent volume, resulted in the precipitation of a colourless solid, which was washed with cold methanol (10 mL) and petroleum ether (10 mL) and dried. Yield: 25 mg (93%). IR ($\nu_{\text{max}}/\text{cm}^{-1}$) 2026 (CO), 1963 (CO), 1481 (C-N), 1433, 1187, 1091, 998, 859. NMR δ_{H} (CD₂Cl₂) 6.09 (1H, d, $J_{\text{HH}} = 18.0$ Hz, H β), 7.19 (1H, s, Nap), 7.53 – 7.47, 7.73 (30H + 5H, m x 2, PPh₃ + Nap), 7.66 (1H, d, $J_{\text{HH}} = 8.2$ Hz, Nap), 7.79 (1H, dt, $J_{\text{HH}} = 18.0$ Hz, $J_{\text{HP}} = 3.5$ Hz, H α); δ_{P} (CD₂Cl₂) 24.1 (s, PPh₃) ppm. MS (ES +ve): m/z 871 (M^+ , 100%); Elemental analysis. Found: C 65.1, H 4.0. C₅₀H₃₉ClO₂P₂Ru·0.75CH₂Cl₂ requires C 65.3, H 4.4%.

[Ru(CH=CHNap-2-OMe-6)Cl(CO)(BTD)(PPh₃)₂] (7)

[RuHCl(CO)(PPh₃)₃] (100 mg, 0.105 mmol) and 2-ethynyl-6-methoxynaphthalene (21 mg, 0.115 mmol) were dissolved in dichloromethane (10 mL) and a dichloromethane solution (5 mL) of 2,1,3-benzothiadiazole (21 mg, 0.154 mmol) was added. The resulting purple solution was stirred for 1 hour at room temperature and then filtered through Celite. Addition of ethanol (15 mL) followed by slow reduction of the solvent volume, resulted in the formation of a purple crystalline solid, which was washed with cold ethanol (5 mL) and diethyl ether (5 mL) and dried. Yield: 91 mg (86%). IR ($\nu_{\max}/\text{cm}^{-1}$) 1929 (CO), 1600, 1549, 1432 (C-N), 1197, 1090, 1031, 855. NMR δ_{H} (CD₂Cl₂) 3.92 (3H, s, OMe), 5.95 (1H, d, $J_{\text{HH}} = 15.8$ Hz, H β), 7.08 (2H, s, Nap), 7.20, 7.31, 7.51 (30H + 3H, m x 3, PPh₃ + Nap), 7.56 (2H, m, BTD), 7.60 (1H, d, $J_{\text{HH}} = 9.8$ Hz, Nap), 7.96 (2H, m, BTD), 8.75 (1H, dt, $J_{\text{HH}} = 15.8$ Hz, $J_{\text{HP}} = 3.1$ Hz, H α); δ_{P} (CD₂Cl₂) 27.0 (s, PPh₃). MS (ES +ve): m/z 873 (M⁺ – BTD, 100%), 974 (M⁺ – Cl, 50%); Elemental analysis. Found: C 61.5, H 4.6, N 2.7. C₅₆H₄₅ClN₂O₂P₂RuS·1.25CH₂Cl₂ requires C 61.7, H 4.3, N 2.5 %.

[Ru(CH=CHNap-2-OMe-6)Cl(CO)₂(PPh₃)₂] (7 CO)

Carbon monoxide was bubbled through a dichloromethane solution (10 mL) of **7** (45 mg, 0.045 mmol) until the initial purple solution becomes pale yellow. Addition of ethanol (20 mL) followed by slow reduction of the solvent volume, resulted in the precipitation of a yellow solid, which was washed with cold ethanol (10 mL) and diethyl ether (10 mL) and dried. Yield: 38 mg (94%). IR ($\nu_{\max}/\text{cm}^{-1}$) 2025 (CO), 1965 (CO), 1596, 1480, 1433, 1263, 1236, 1160, 1091, 1031, 998. NMR δ_{H} (CD₂Cl₂) 3.93 (3H, s, OMe), 6.05 (1H, d, $J_{\text{HH}} = 18.0$ Hz, H β), 7.08 – 7.18 (4H, m, Nap), 7.37 – 7.47 (18H + 1H, m, PPh₃ + Nap), 7.57 (1H, $J_{\text{HH}} = 8.5$ Hz, Nap), 7.63 (1H, $J_{\text{HH}} = 8.5$ Hz, Nap), 7.68 (1H, dt, $J_{\text{HH}} = 18.0$ Hz, $J_{\text{HP}} = 3.6$ Hz, H α), 7.72 – 7.76 (12H, m, PPh₃). δ_{P} (CD₂Cl₂) 24.0 (s, PPh₃). MS (ES +ve): m/z 921 (M⁺ + Na, 8%). Elemental analysis. Found: C 67.9, H 4.7. C₅₁H₄₁ClO₃P₂Ru requires C 68.0, H 4.6 %.

[Ru(CH=CHPhen-9)Cl(CO)(BTD)(PPh₃)₂] (8)

[RuHCl(CO)(PPh₃)₃] (500 mg, 0.525 mmol) and 9-ethynylphenanthrene (120 mg, 0.593 mmol) were dissolved in dichloromethane (15 mL) and treated with a

dichloromethane solution (5 mL) of 2,1,3-benzothiadiazole (143 mg, 1.050 mmol). The resulting red solution was stirred for 2 hours at room temperature. Addition of ethanol (20 mL) followed by slow reduction of the solvent volume resulted in a dark orange crystalline solid, which was washed with cold ethanol (10 mL) and diethyl ether (10 mL) and dried. Yield: 455 mg (84%). IR ($\nu_{\max}/\text{cm}^{-1}$) 1911 (CO), 1545, 1481, 1431 (C-N), 1092, 833, 740. NMR δ_{H} (CD_2Cl_2) 6.71 (1H, d, $J_{\text{HH}} = 15.4$ Hz, H β), 7.12 (1H, s, Phen), 7.21 (12H, m, PPh $_3$), 7.33 (6H, m, PPh $_3$), 7.44 (1H, m, Phen), 7.53–7.58 (12H + 5H + 2H, m, PPh $_3$ + Phen + BTD), 7.98 (2H, s, BTD), 8.59–8.62 (1H, m, Phen), 8.67 (1H, d, $J_{\text{HH}} = 8.1$ Hz, Phen), 8.91 (1H, dt, $J_{\text{HH}} = 15.4$ Hz, $J_{\text{HP}} = 2.9$ Hz, H α). δ_{P} (CD_2Cl_2) 27.0 (s, PPh $_3$) ppm. MS (ES +ve): m/z 939 ($\text{M}^+ - \text{BTD} + 2\text{Na}$, 42%). Elemental analysis. Found: C 68.8, H 4.3, N 2.7. $\text{C}_{59}\text{H}_{45}\text{ClN}_2\text{OP}_2\text{RuS}$ requires C 68.9, H 4.4, N 2.7%.

[Ru(CH=CHPhen-9)Cl(CO) $_2$ (PPh $_3$) $_2$] (8 CO)

Carbon monoxide was bubbled through a dichloromethane solution (10 mL) of **8** (100 mg, 0.097 mmol) until the dark orange solution became yellow. Addition of methanol (7 mL) followed by slow reduction of the solvent volume resulted in the precipitation of a colourless solid, which was washed with cold methanol (10 mL) and diethyl ether (10 mL) and dried. Yield: 87 mg (98%). IR ($\nu_{\max}/\text{cm}^{-1}$) 2038 (CO), 1972 (CO), 1547, 1483, 1435 (C-N), 1190, 1170, 1090, 1000, 801. NMR δ_{H} (CD_2Cl_2) 6.84 (1H, dt, 1H, $J_{\text{HH}} = 17.5$ Hz, $J_{\text{HP}} = 2.1$ Hz, H β), 7.01 (1H, s, Phen), 7.38–7.50 (18H + 1H, m, PPh $_3$ + Phen), 7.57–7.73 (5H, m, Phen), 7.80–7.84 (12H, m, PPh $_3$), 7.96 (1H, dt, $J_{\text{HH}} = 17.5$ Hz, $J_{\text{HP}} = 3.6$ Hz, H α), 8.63–8.65 (1H, m, Phen), 8.71 (1H, d, $J_{\text{HH}} = 8.1$ Hz, Phen). δ_{P} (CD_2Cl_2) 23.1 (s, PPh $_3$). MS (ES +ve): m/z 942 ($\text{M}^+ + \text{Na}$, 6%), 926 ($\text{M}^+ - \text{Cl} + \text{Na}$, 100%). Elemental analysis. Found: C 66.2, H 4.6. $\text{C}_{54}\text{H}_{41}\text{ClO}_2\text{P}_2\text{Ru}\cdot\text{CH}_2\text{Cl}_2$ requires C 65.7, H 4.3%.

Silica gel immobilisation of the vinyl complexes 1-8

Each vinyl complex (0.007-0.022 mmol) was dissolved in a minimum volume of CHCl_3 . An excess (5 mmol) of silica (particle size 40-63 μm) was added to the coloured solution and the resulting mixture was stirred at room temperature for

five minutes. After removal of the solvent on a rotary evaporator, the solid was left to stand for one hour at room temperature prior to its use (see Figure S4).

2. Crystallography

The dichloromethane solvent molecule included in the structure of **5·CO** was found to be disordered. Two orientations were identified of approximately 86 and 14% occupancy. The geometries of these orientations were optimized, the thermal parameters of adjacent atoms were restrained to be similar, and only the non-hydrogen atoms of the major occupancy orientation were refined anisotropically (those of the minor occupancy orientation were refined isotropically).

Crystal data for 4: C₅₂H₄₃ClN₂OOsP₂S·CH₂Cl₂, *M* = 1116.46, triclinic, *P*-1 (no. 2), *a* = 11.8215(3), *b* = 13.0465(4), *c* = 15.3904(4) Å, α = 92.606(2), β = 99.286(2), γ = 91.790(2)°, *V* = 2338.33(11) Å³, *Z* = 2, *D*_c = 1.586 g cm⁻³, μ (Mo-K α) = 3.053 mm⁻¹, *T* = 173 K, red blocky needles, Oxford Diffraction Xcalibur 3 diffractometer; 10837 independent measured reflections (*R*_{int} = 0.0201), *F*² refinement,⁵⁶ *R*₁(obs) = 0.0232, *wR*₂(all) = 0.0501, 9915 independent observed absorption-corrected reflections [$|F_o| > 4\sigma(|F_o|)$], 2 θ_{\max} = 59°], 570 parameters. CCDC 1011581.

Crystal data for 6: C₅₅H₄₃ClN₂OP₂RuS·CHCl₃, *M* = 1097.80, monoclinic, *P*₂₁/*n* (no. 14), *a* = 16.1844(4), *b* = 15.5180(4), *c* = 19.9196(5) Å, β = 96.285(3)°, *V* = 4972.8(2) Å³, *Z* = 4, *D*_c = 1.466 g cm⁻³, μ (Mo-K α) = 0.679 mm⁻¹, *T* = 173 K, red blocks, Agilent Xcalibur 3E diffractometer; 9846 independent measured reflections (*R*_{int} = 0.0287), *F*² refinement,⁵⁶ *R*₁(obs) = 0.0452, *wR*₂(all) = 0.1199, 7621 independent observed absorption-corrected reflections [$|F_o| > 4\sigma(|F_o|)$], 2 θ_{\max} = 56°], 604 parameters. CCDC 1048863.

Crystal data for 5·CO: C₄₆H₃₇ClO₂P₂Ru·CH₂Cl₂, *M* = 905.14, monoclinic, *P*₂₁/*n* (no. 14), *a* = 10.13508(17), *b* = 18.4651(3), *c* = 22.6080(5) Å, β = 97.2599(18)°, *V* = 4197.06(14) Å³, *Z* = 4, *D*_c = 1.432 g cm⁻³, μ (Cu-K α) = 5.798 mm⁻¹, *T* = 173 K,

colourless needles, Oxford Diffraction Xcalibur PX Ultra diffractometer; 8157 independent measured reflections ($R_{\text{int}} = 0.0479$), F^2 refinement,⁵⁶ $R_1(\text{obs}) = 0.0625$, $wR_2(\text{all}) = 0.1657$, 7081 independent observed absorption-corrected reflections [$|F_o| > 4\sigma(|F_o|)$], $2\theta_{\text{max}} = 145^\circ$, 509 parameters. CCDC 1011582.

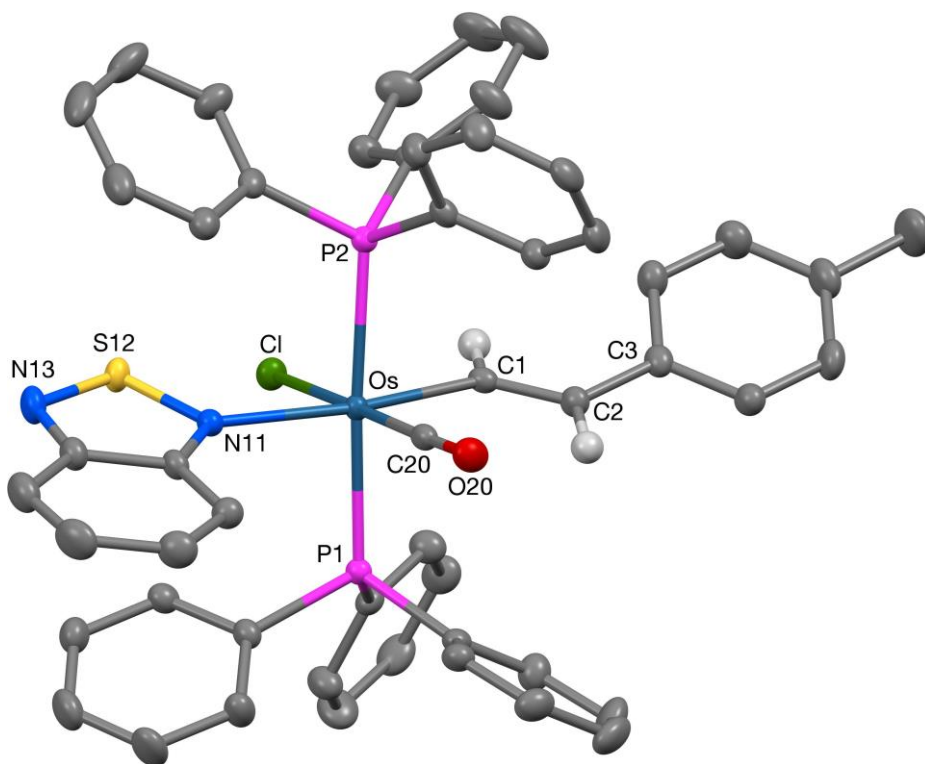


Figure S1. Crystal structure of $[\text{Os}(\text{CH}=\text{CHC}_6\text{H}_4\text{Me-4})\text{Cl}(\text{CO})(\text{BTD})(\text{PPh}_3)_2]$ (**4**) with 50% probability ellipsoids.

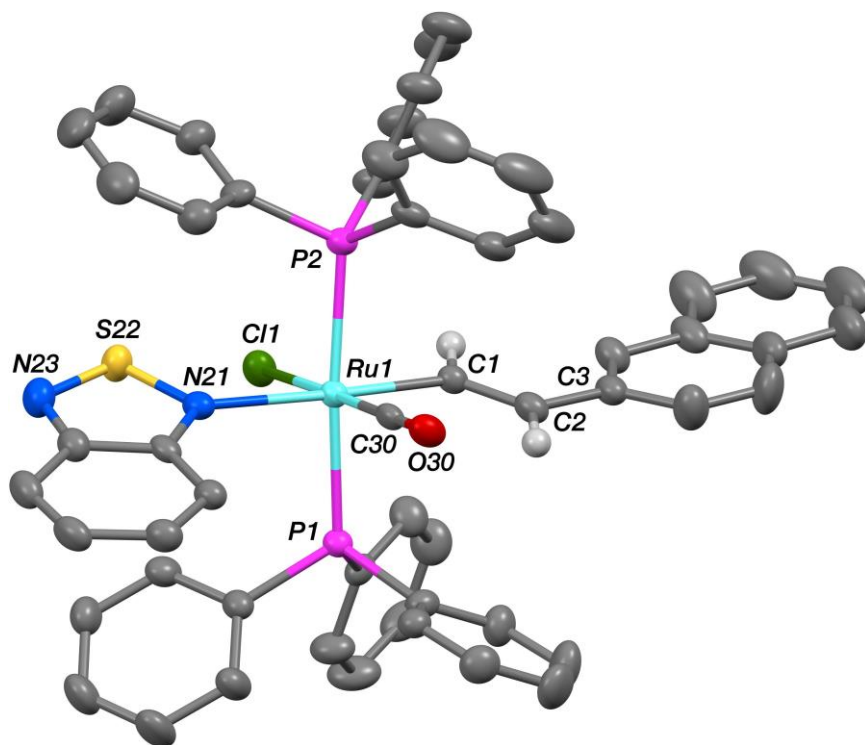


Figure S2. Crystal structure of [Ru(CH=CHNap-2)Cl(CO)(BTD)(PPh₃)₂] (**6**) with 50% probability ellipsoids.

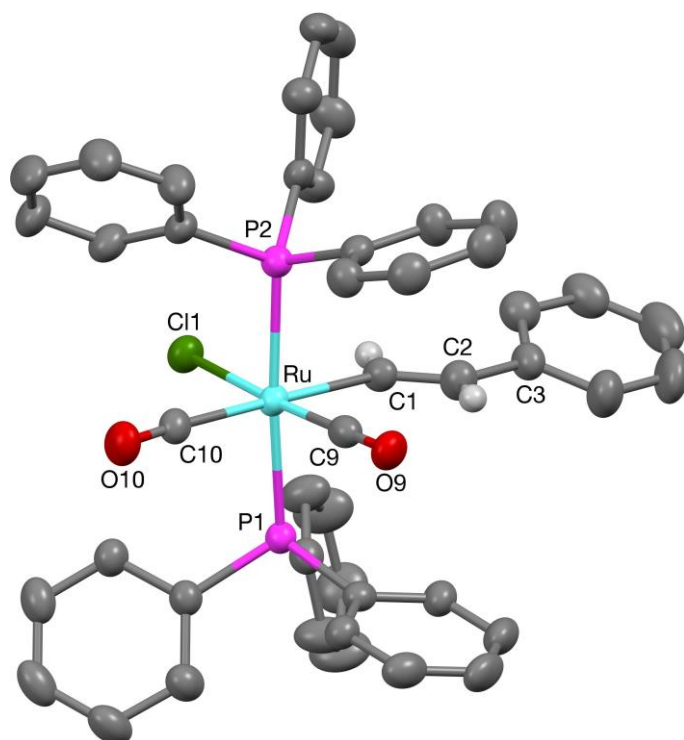


Figure S3. Crystal structure of $[\text{Ru}(\text{CH}=\text{CHC}_6\text{H}_5)\text{Cl}(\text{CO})_2(\text{PPh}_3)_2]$ (**5-CO**) with 50% probability ellipsoids.

3. Carbon monoxide sensing studies



Figure S4. Left: the colour of ruthenium and osmium complexes **1-8**; right: the colour of **1-8** on silica.

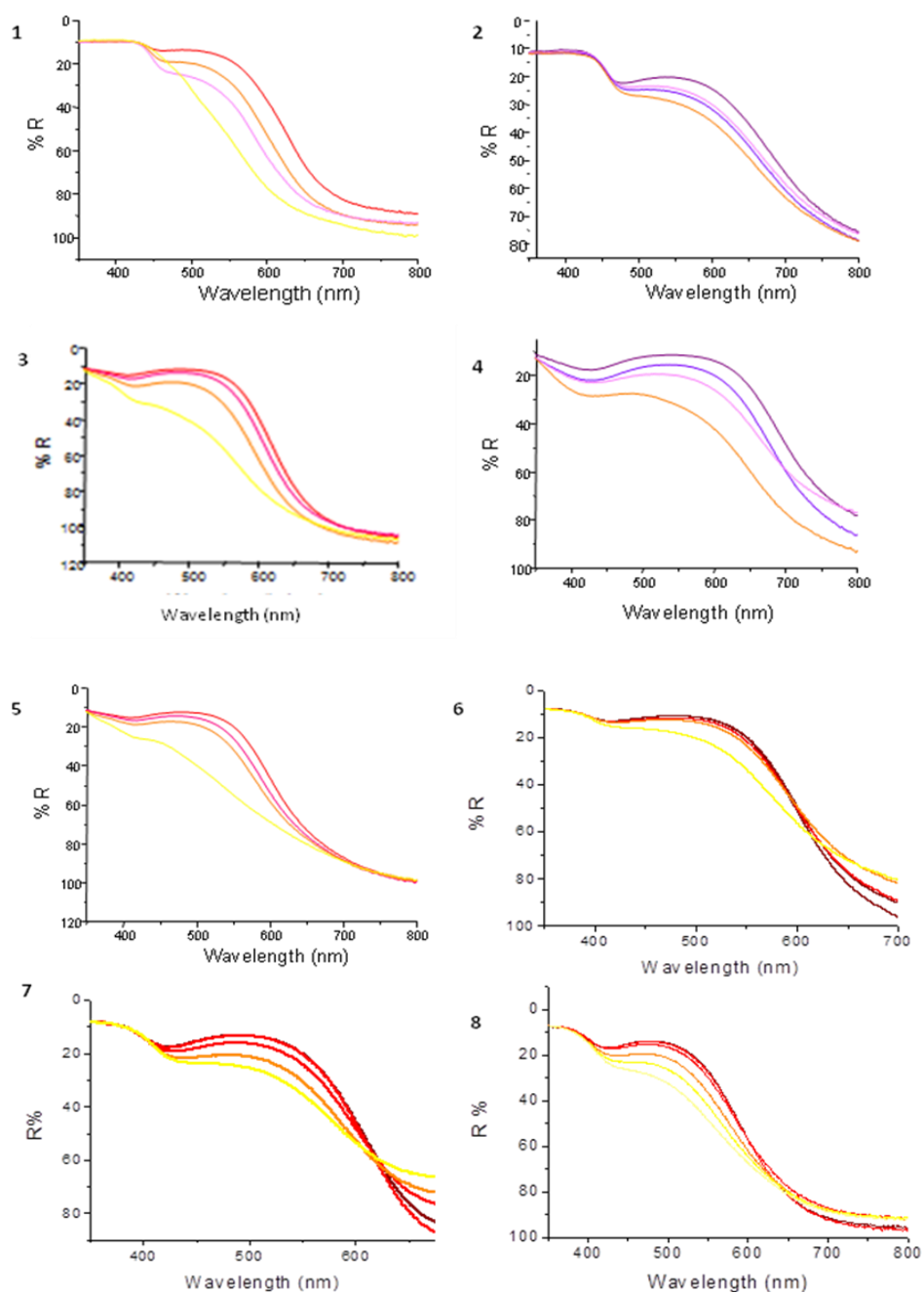


Figure S5. Spectroscopic changes of complexes **1-8** on silica upon exposure to increasing concentrations of CO (0.0001 to 250 ppm).

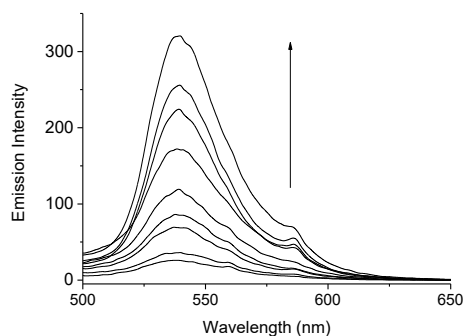


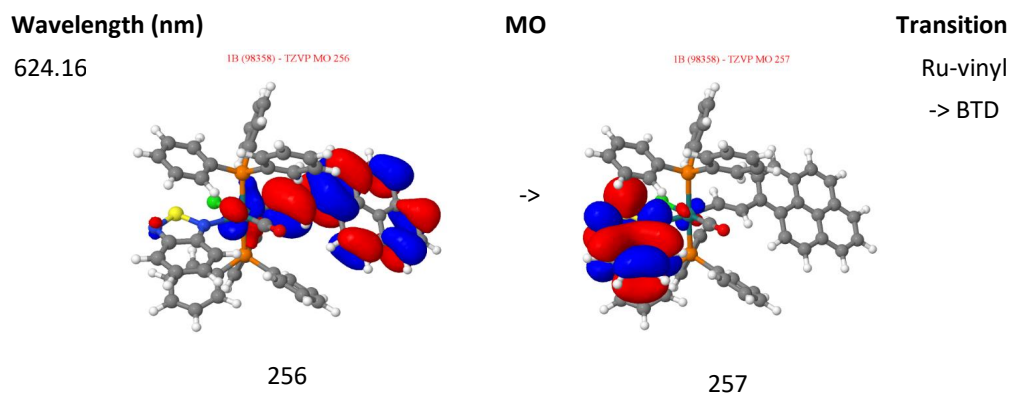
Figure S6. Emission response of complex **8** in chloroform solution upon exposure to increasing concentrations of CO (1.0×10^{-7} to 500 ppm).

4. DFT Studies

Table S1. Calculated bond lengths in Å for complexes **1**, **1·CO**, **5**, **5·CO**, **6** and **6·CO**.

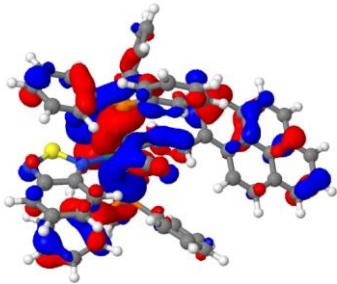
Model	Ru-N or Ru-CO _(added CO)	Ru-P(3)	Ru-P(4)	Ru-Cl	Ru-CO	Ru-C ₁	C ₁ -C ₂
1	2.28483	2.45321	2.43757	2.54494	1.82511	2.05145	1.34432
5	2.28418	2.44656	2.43375	2.54531	1.82544	2.05911	1.34255
6	2.28459	2.44885	2.43105	2.54620	1.82519	2.05455	1.34265
1·CO	1.96983	2.46679	2.44448	2.53908	1.85638	2.11228	1.34186
5·CO	1.96822	2.46190	2.44099	2.54352	1.85638	2.11463	1.33957
6·CO	1.96849	2.46320	2.44023	2.54344	1.85637	2.11296	1.33987

Table S2. Molecular orbitals for Compound **1**



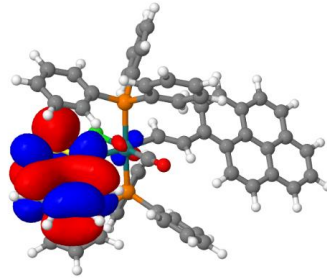
420.79

1B (98358) - TZVP MO 254



254

1B (98358) - TZVP MO 257

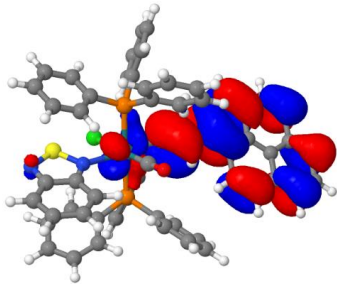


257

Ru-
phosphine
-> BTD

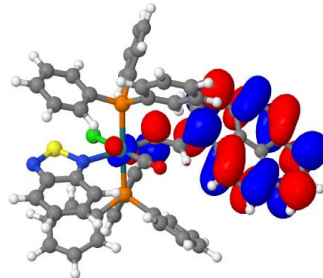
414.86

1B (98358) - TZVP MO 256



256

1B (98358) - TZVP MO 258

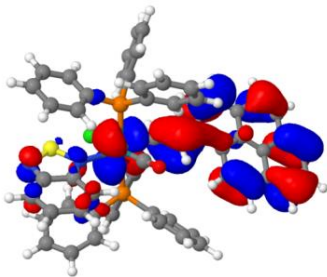


258

Ru-vinyl π
-> π^*

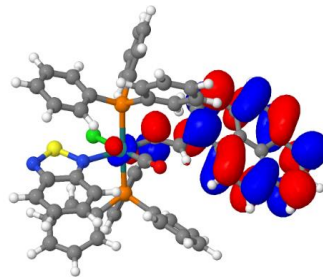
320.65

1B (98358) - TZVP MO 255



255

1B (98358) - TZVP MO 258

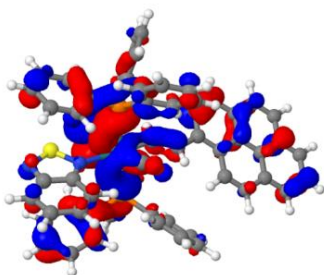


258

Ru-vinyl π
-> π^*

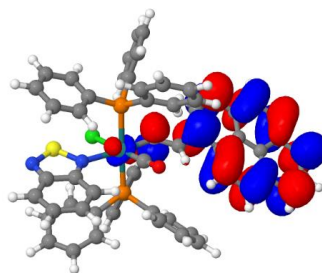
302.90

1B (98358) - TZVP MO 254



254

1B (98358) - TZVP MO 258

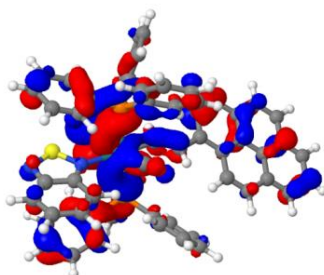


258

Ru-
phosphine
-> Ru-vinyl

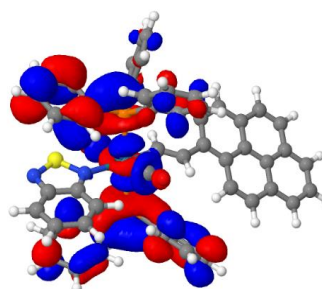
280.68

1B (98358) - TZVP MO 254



254

1B (98358) - TZVP MO 259

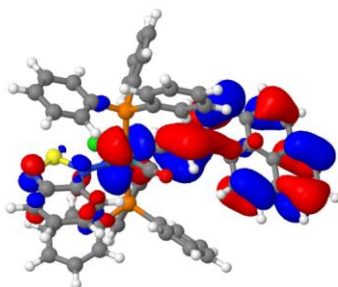


259

Ru-
phosphine
 $\pi \rightarrow \pi^*$

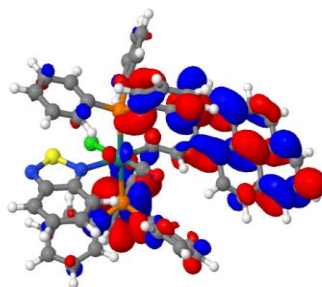
272.83

1B (98358) - TZVP MO 255



255

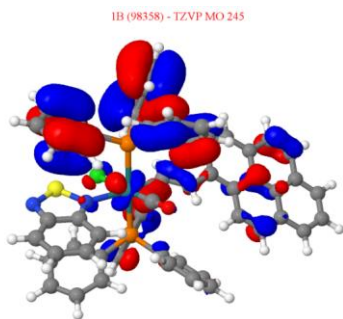
1B (98358) - TZVP MO 262



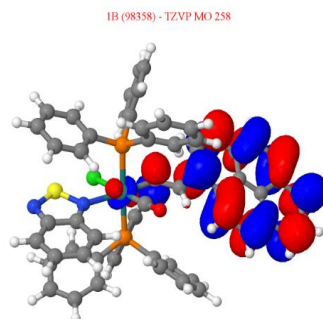
262

Ru-vinyl
-> vinyl π^*

250.11



245



258

Ru-vinyl
-> Ru-
phosphine

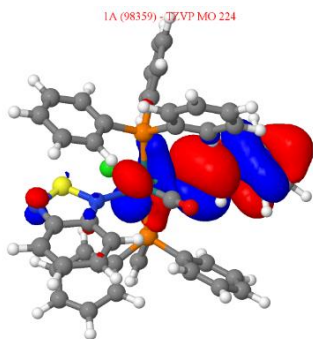
Table S3. Molecular orbitals for Compound 5

Wavelength (nm)

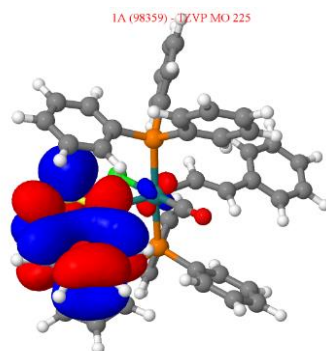
MO

Transition

575.57



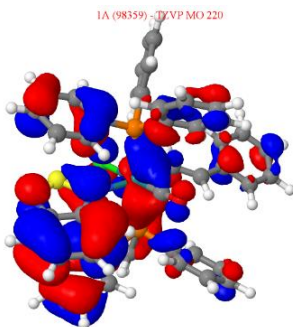
224



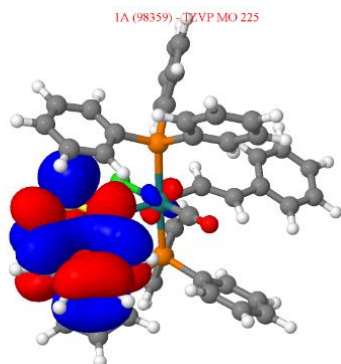
225

Ru-vinyl
-> BTD

355.47



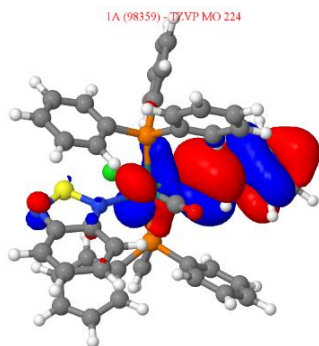
220



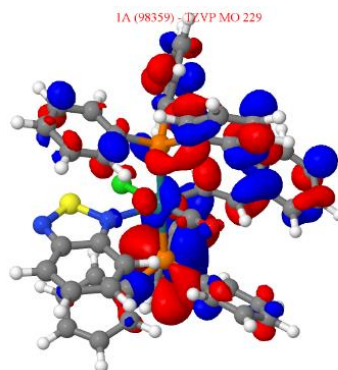
225

BTD π
-> π^*

329.74



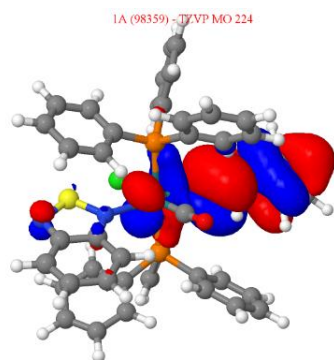
224



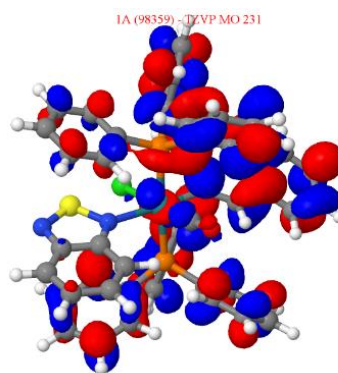
229

Ru-vinyl
->
phosphine

307.82



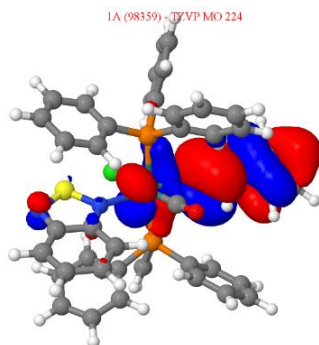
224



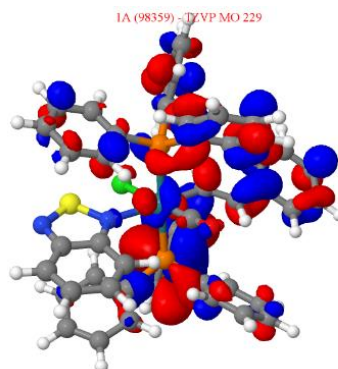
231

Ru-vinyl
->
phosphine

299.95



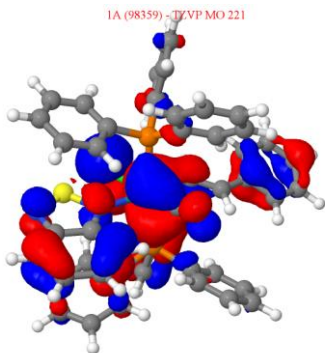
224



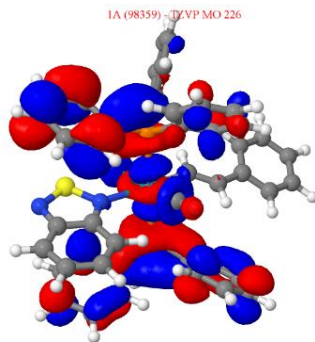
229

Ru-vinyl
->
phosphine

285.5



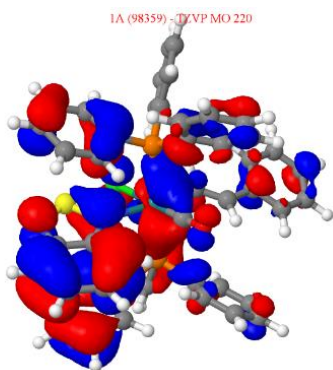
221



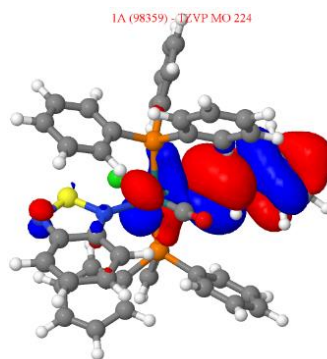
226

Ru-BTD
->
phosphine

259.66



220



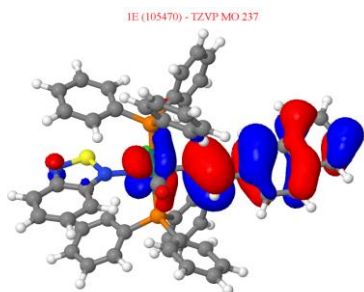
226

Ru-BTD ->
phosphine

Table S4: Molecular orbitals for Compound 6

Wavelength (nm)

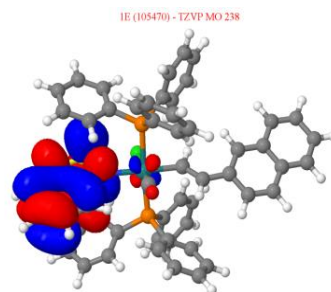
584.72



237

MO

->



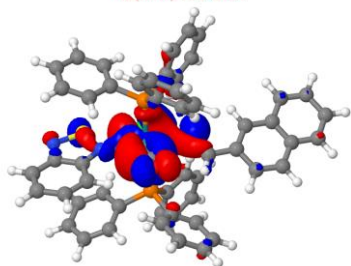
238

Transition

Ru-vinyl
-> BTDA

417.69

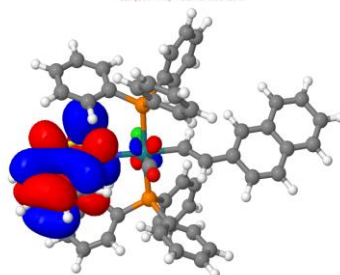
1E (105470) - TZVP MO 234



234

1E (105470) - TZVP MO 238

->

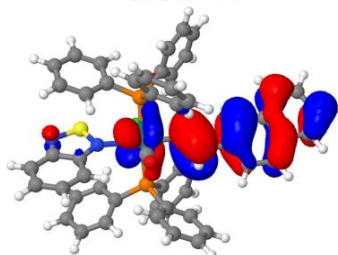


238

Ru ->
BTD

359.20

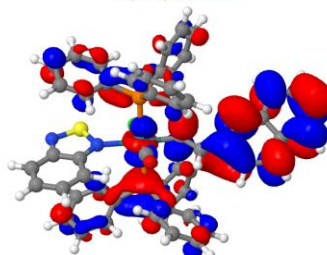
1E (105470) - TZVP MO 237



237

1E (105470) - TZVP MO 240

->

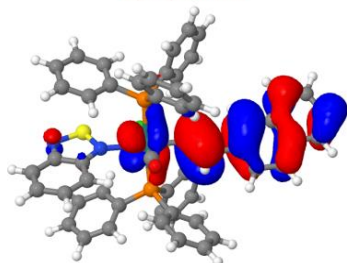


240

Ru-vinyl
 $\pi \rightarrow$ Vinyl
 π^*

310.41

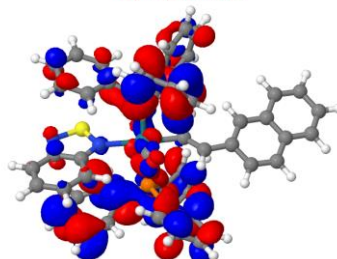
1E (105470) - TZVP MO 237



237

1E (105470) - TZVP MO 245

->

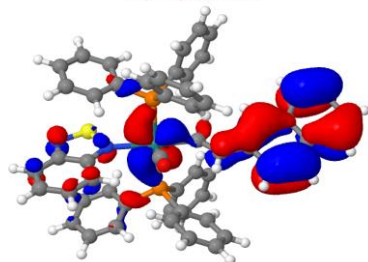


245

Ru-vinyl
 \rightarrow Metal
P (LMTC)

286.45

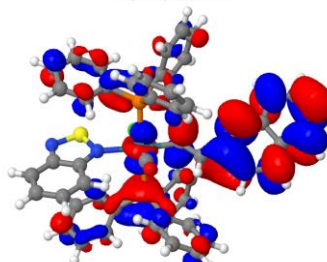
1E (105470) - TZVP MO 236



236

1E (105470) - TZVP MO 240

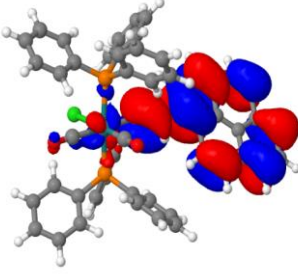
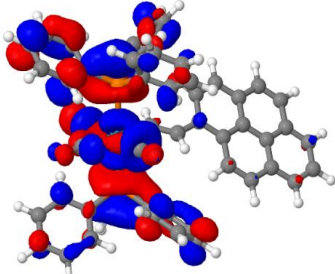
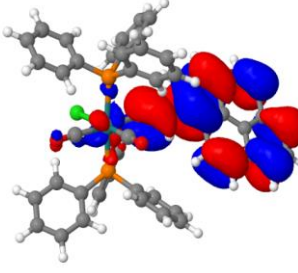
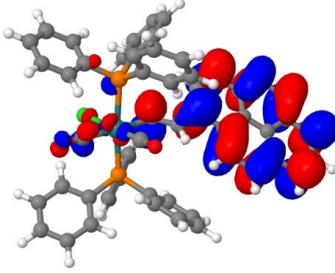
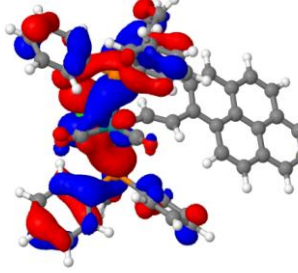
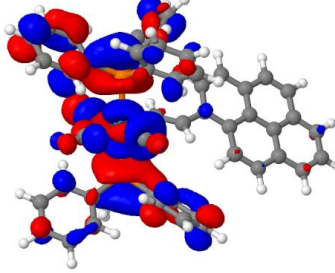
->



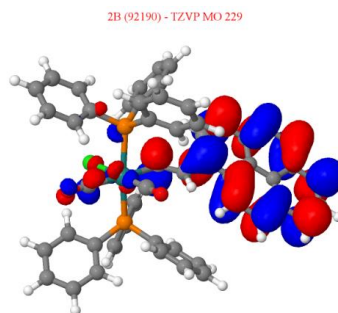
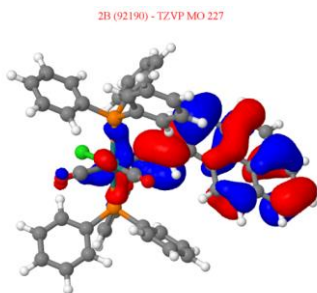
240

Ru-vinyl
 $\pi \rightarrow$ Ru-
Vinyl π^*

Table S5. Molecular orbitals for Compound 1-CO

Wavelength (nm)	MO	Transition
409.53	<p>2B (92190) - TZVP MO 228</p>  <p>228</p>	<p>2B (92190) - TZVP MO 230</p>  <p>230</p> <p>Ligand -> metal P (LMCT)</p>
398.18	<p>2B (92190) - TZVP MO 228</p>  <p>228</p>	<p>2B (92190) - TZVP MO 229</p>  <p>229</p> <p>Ligand π -> π^*</p>
323.76	<p>2B (92190) - TZVP MO 226</p>  <p>226</p>	<p>2B (92190) - TZVP MO 230</p>  <p>230</p> <p>Metal P -> Metal P</p>

301.57

Ligand π
→ π^*

291.64

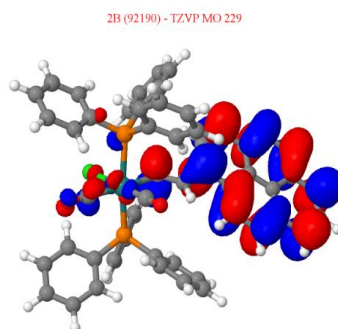
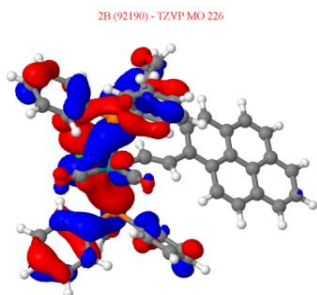
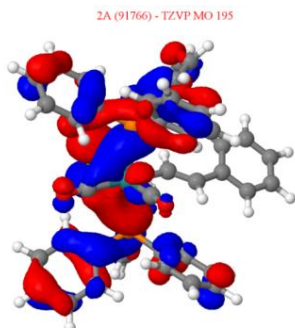
Ligand
→
Metal P
(LMCT)

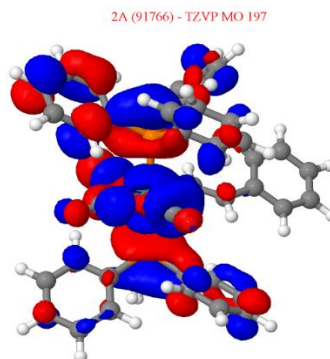
Table S6. Molecular orbitals for Compound 5-CO

Wavelength (nm)

322.38



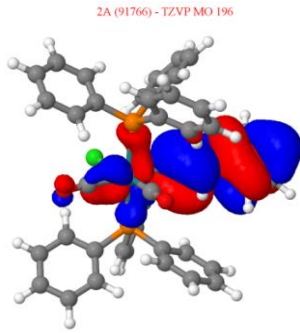
MO



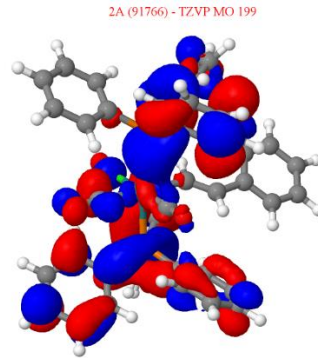
Transition

Metal P
→ Metal
P

313.9



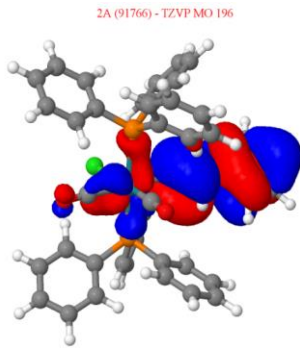
196



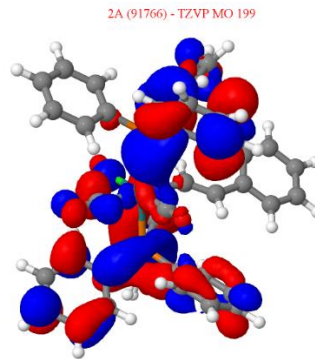
199

Metal
ligand
-> Metal
P

310.6



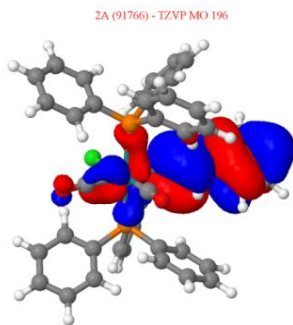
196



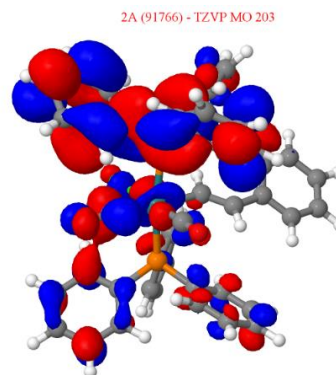
199

Metal
ligand
-> Metal
P

291.34



196

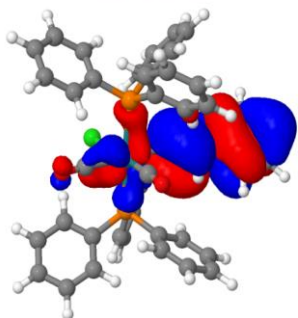


203

Metal
ligand
-> Metal
P

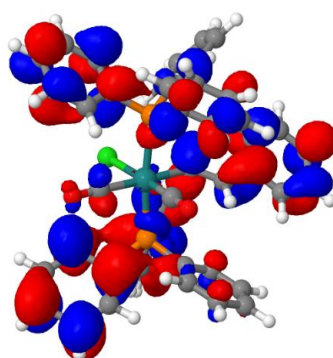
278.46

2A (91766) - TZVP MO 196



196

2A (91766) - TZVP MO 205

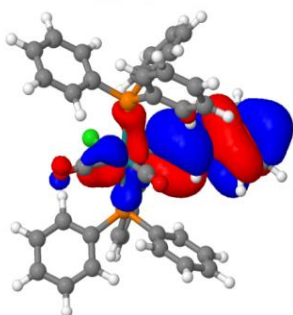


205

Metal
ligand
-> Metal
P

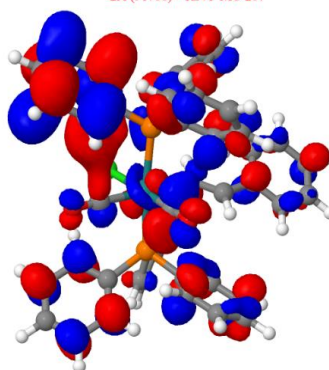
267.77

2A (91766) - TZVP MO 196



196

2A (91766) - TZVP MO 207

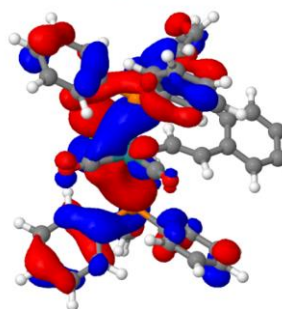


207

Metal
ligand
-> Metal
P

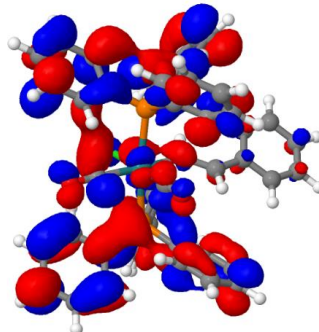
252.22

2A (91766) - TZVP MO 195



195

2A (91766) - TZVP MO 202



202

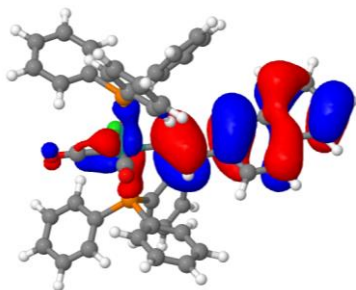
Metal
ligand
-> Metal
P

Table S7: Molecular orbitals for Compound 6.CO

Wavelength (nm)	MO	Transition
337.85 2E (104805) - TZVP MO 209	2E (104805) - TZVP MO 211	Ligand π -> π^*
323.15 2E (104805) - TZVP MO 207	2E (104805) - TZVP MO 210	Metal P (LMTC) -> Metal P (LMTC)
291.82 2E (104805) - TZVP MO 205	2E (104805) - TZVP MO 210	Metal P (LMTC) -> Metal P (LMTC)

277.03

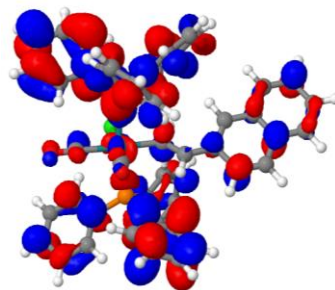
2E (104805) - TZVP MO 209



209

->

2E (104805) - TZVP MO 219

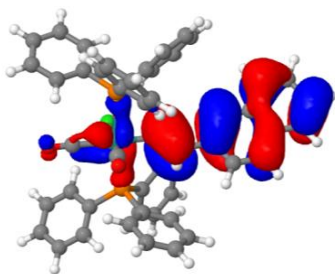


219

Ligand π
-> Metal
P (LMTC)

274.37

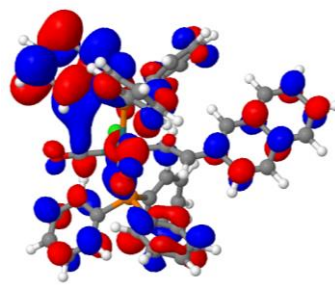
2E (104805) - TZVP MO 209



209

->

2E (104805) - TZVP MO 221

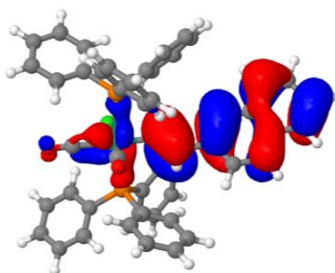


221

Ligand π
-> Metal
P (LMTC)

270.63

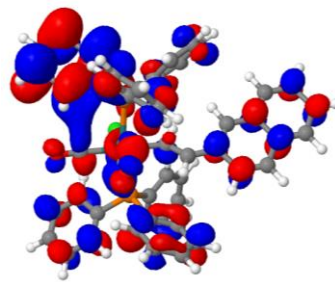
2E (104805) - TZVP MO 209



209

->

2E (104805) - TZVP MO 221



221

Ligand π
-> Metal
P (LMTC)

5. Calculated UV-Vis Spectra

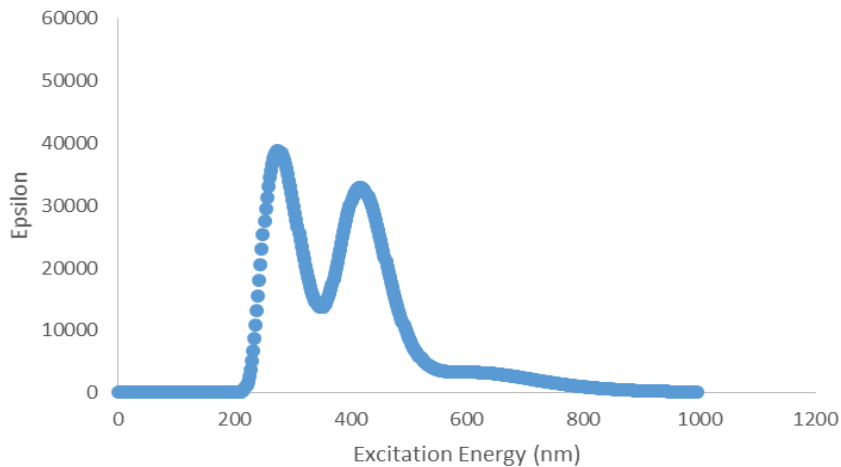


Figure S7. Calculated UV-Vis spectrum for compound **1**

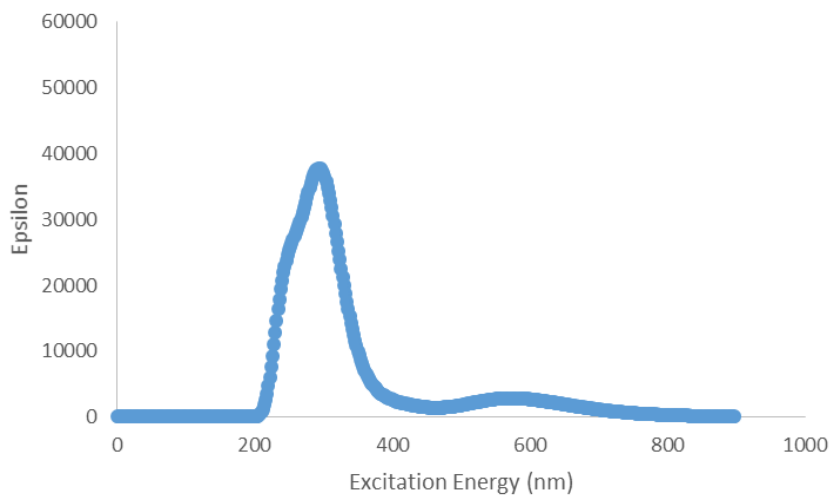


Figure S8. Calculated UV-Vis spectrum for compound **5**

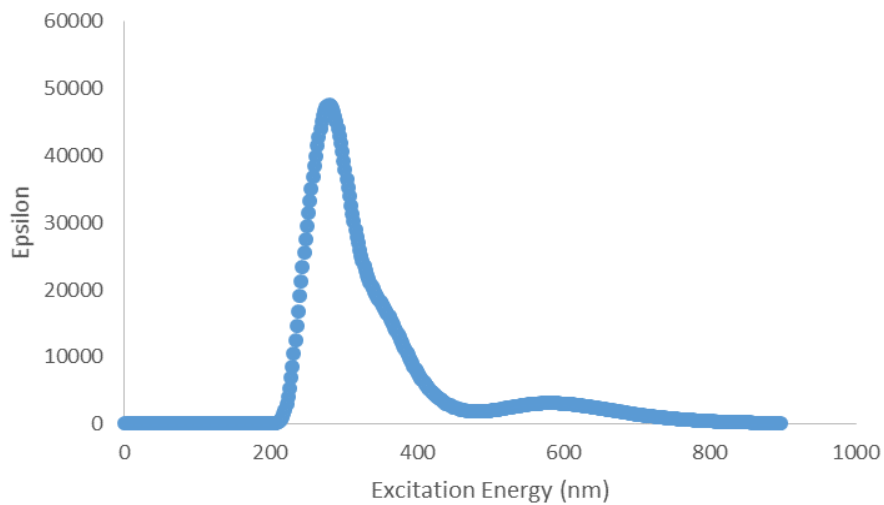


Figure S9: Calculated UV-Vis spectrum for compound **6**

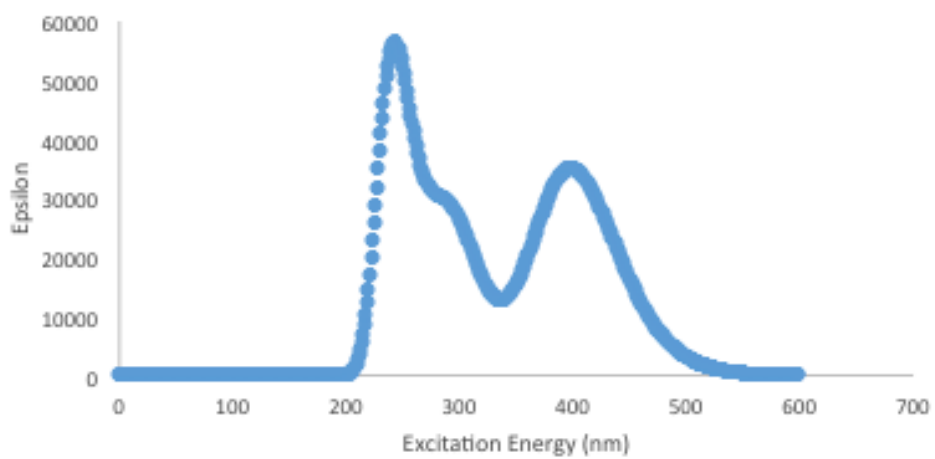


Figure S10. Calculated UV-Vis spectrum for compound **1-CO**

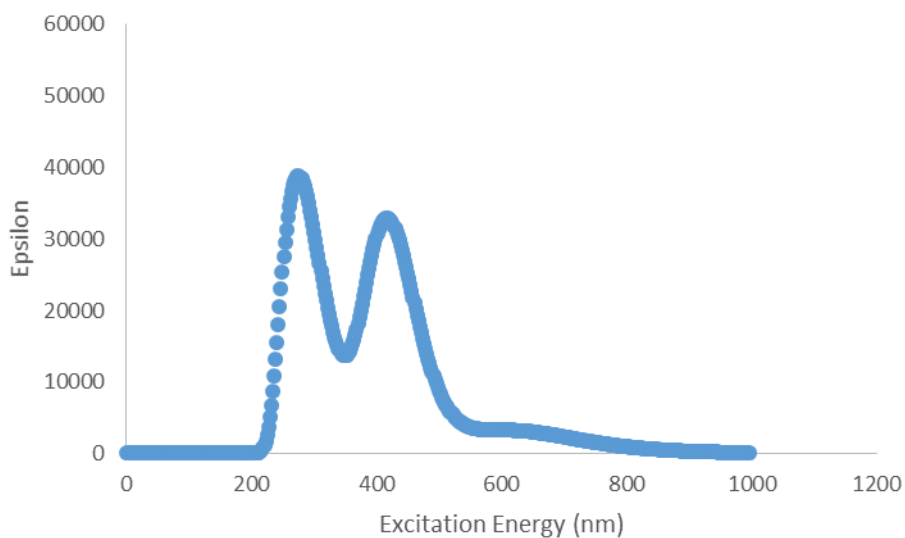


Figure S11. Calculated UV-Vis spectrum for compound **5-CO**

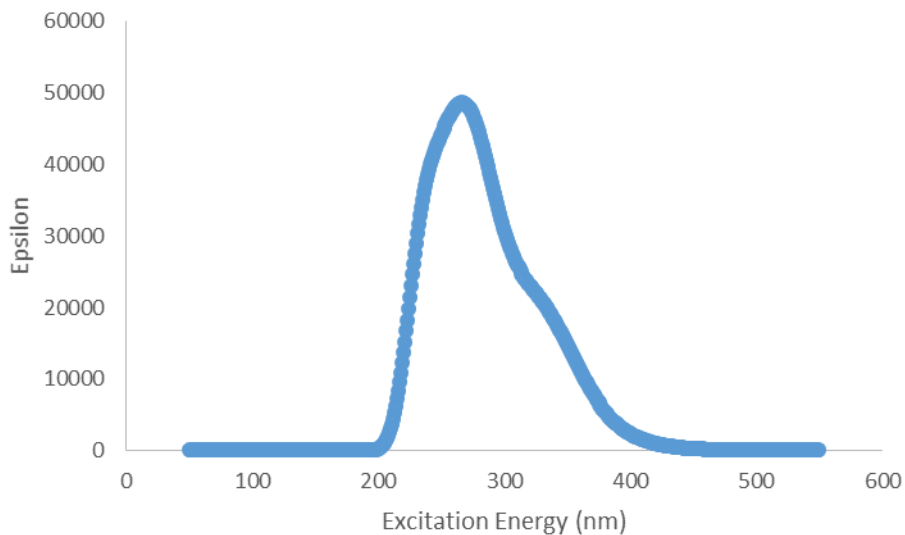


Figure S12: Calculated UV-Vis spectrum for compound **6-CO**

Comparisons of calculated spectra

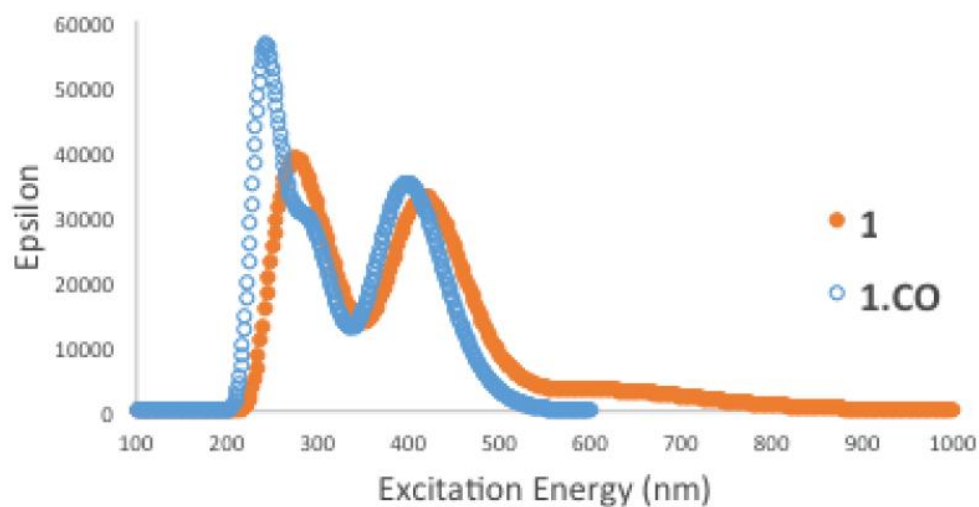


Figure S13. Comparison of calculated UV-Vis spectra for compounds **1** and **1.CO**

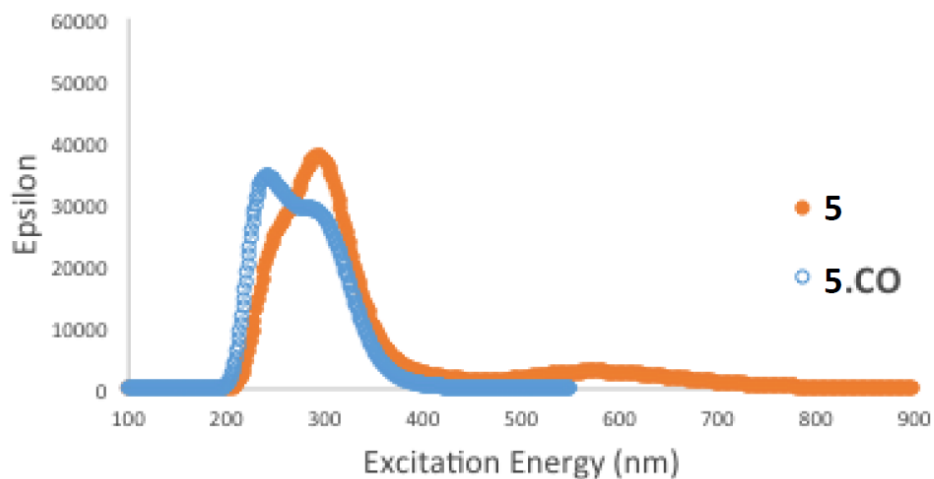


Figure S14. Comparison of calculated UV-Vis spectra for compounds **5** and **5.CO**

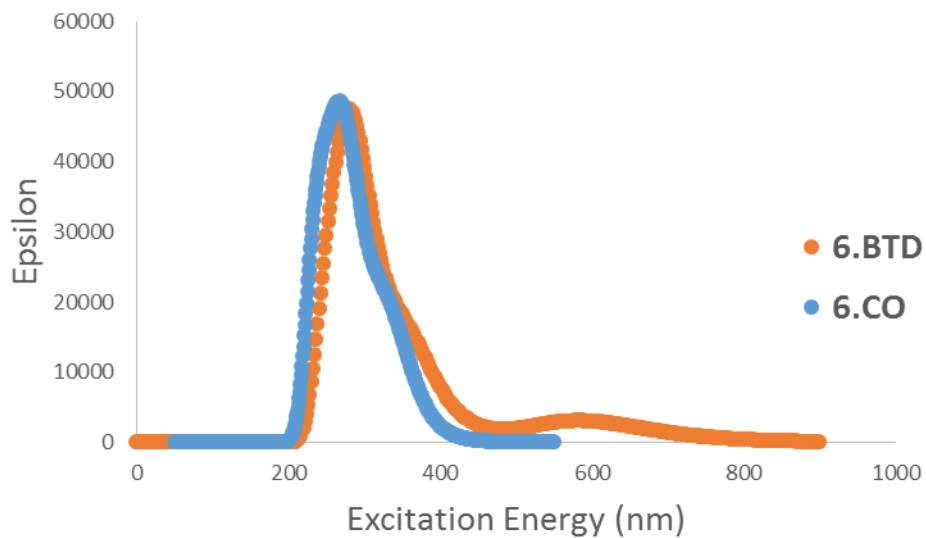


Figure S15. Comparison of calculated UV-Vis spectra for compounds 6 and 6-CO

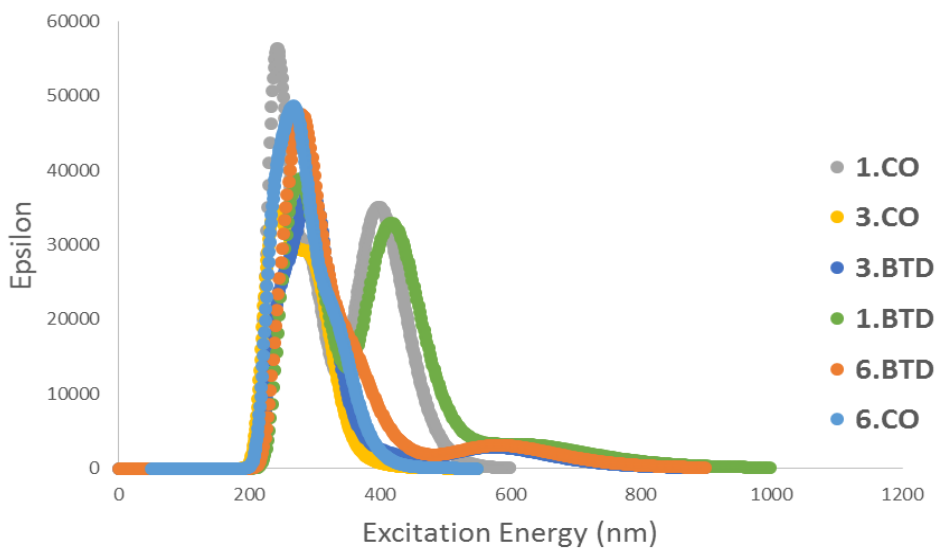


Figure S16. Comparison of calculated UV-Vis spectra for compounds 1, 1-CO, 5, 5-CO, 6 and 6-CO.

References

- S1 K. R. Laing, W. R. Roper, *J. Chem. Soc. A* **1970**, 2149-2153.
- S2 A. F. Hill, J. D. E. T. Wilton-Ely, *J. Chem. Soc., Dalton Trans.* **1999**, 3501-3510.
- S3 R. B. Bedford, A. F. Hill, C. Jones, A. J. P. White, D. J. Williams, J. D. E. T. Wilton-Ely, *Organometallics* **1998**, *17*, 4744-4753.
- S4 H. Loumrhari, J. Ros, M. R. Torres, A. Santos, A. M. Echavarren, *J. Organomet. Chem.* **1991**, *411*, 255-261.
- S5 M. E. Moragues, A. Toscani, F. Sancenón, R. Martínez-Máñez, A. J. P. White, J. D. E. T. Wilton-Ely, *J. Am. Chem. Soc.* **2014**, *136*, 11930-11933.
- S6 (a) SHELXTL, Bruker AXS, Madison, WI; (b) SHELX-97, G.M. Sheldrick, *Acta Cryst.*, **2008**, *A64*, 112-122; (c) SHELX-2013, <http://shelx.uni-ac.gwdg.de/SHELX/index.php>

3.4. Highly sensitive and selective molecular probes for chromo-fluorogenic sensing of carbon monoxide in air, aqueous solution and living cells

***Highly sensitive and selective molecular probes
for chromo-fluorogenic sensing of carbon
monoxide in air, aqueous solution and living cells***

*Anita Toscani,^{a+} Cristina Marín-Hernández,^{b,c,d+} Jonathan A.
Robson,^a Elvin Chua,^a Paul Dingwall,^a Andrew J. P. White,^a
Félix Sancenón,^{b,c,d} Cristina de la Torre,^{b,c,d} Ramón Martínez-
Máñez,^{*,b,c,d} and James D. E. T. Wilton-Ely.^{*,a}*

^a Department of Chemistry, Imperial College London, SW7 2AZ, London, UK

^b Instituto Interuniversitario de Investigación de Reconocimiento Molecular y
Desarrollo Tecnológico (IDM), Universidad de Valencia, Universidad Politécnica de
Valencia. Spain.

^c Departamento de Química, Universidad Politécnica de Valencia, Camino de Vera
s/n, E-46022 Valencia, Spain.

^d CIBER de Bioingeniería, Biomateriales y Nanomedicina (CIBER-BBN).

⁺ These authors contributed equally.

Submitted: October, 2017

3.4.1. Abstract

A new series of vinyl complexes $[\text{Ru}(\text{CH}=\text{CHR})\text{Cl}(\text{CO})(\text{TBTD})(\text{PPh}_3)_2]$ ($\text{R} = \text{aryl}$, $\text{TBTD} = 5\text{-}(3\text{-thienyl})\text{-}2,1,3\text{-benzothiadiazole}$) has been prepared and applied to the highly sensitive and selective detection of carbon monoxide in both solution and air. Depending on the vinyl substituent, chromogenic and fluorogenic responses signalled the presence of this invisible, odourless, tasteless and toxic gas. Adsorbing the complexes on silica produced colorimetric probes for the 'naked eye' detection of CO in the gas phase with a limit of detection as low as 8 ppm in some cases, while the release of the TBTD fluorophore allowed detection as low as 1 ppb through the fluorescence response. Structural data for key species before and after addition of carbon monoxide were obtained by single X-ray diffraction techniques. The photophysical behaviour was explored computationally using TD-DFT experiments. The systems were also shown to be selective for CO over all other gases tested, including water vapour and common organic solvents. By introducing a poly(ethylene)glycol chain to the vinyl functionality, water solubility was achieved and these non-cytotoxic complexes were employed in the sensing of CO in HeLa cells, offering a simple and rapid system for sensing this gasotransmitter in this challenging medium.

3.4.2. Introduction

Optical sensors offer many benefits for the sensing of a wide range of analytes both in solution and in the gas phase.¹ In many applications, their low cost, portability and simplicity of use make them excellent alternatives to methods requiring expensive instrumentation. The selective detection of gases which are toxic at low concentrations is an area which has been explored increasingly over the last 20 years. The detection of carbon monoxide is a particular challenge due to its lack of colour, smell and taste, coupled with its common presence in domestic and work settings. The presence of CO in domestic and work environments is frequently due to the incomplete combustion of gas, oil or solid fuels by improperly maintained appliances in poorly ventilated spaces.

Concentrations of 300 ppm CO are considered toxic and prolonged exposure can lead to loss of consciousness and death,² as indicated by the 40 people who

die from CO poisoning in the UK every year.³ It is a concern that the symptoms are often misdiagnosed as those of common viral infections. However, even much lower (sub-toxic) concentrations of CO (30-50 ppm) have been implicated in long-term neurological damage and other health impacts, suggesting that there is also a role for CO detectors that are able to monitor low levels of the gas.

Traditionally, routine CO detection has been achieved using electrochemical cells, solid-state sensors and thermocouples. Most current commercial CO detectors are based on semiconductor metal oxide technology but have to be sited carefully in environments where water vapour (steam) or particulates (smoke) are generated, such as kitchens and bathrooms. False alarms can be triggered by the presence of these species or solvents (cleaning products, hairspray) or fuels (e.g., in automotive workshops). This has led to an increasing interest in the development of chromogenic sensor systems based on chemical probes, which are able to selectively detect the presence of carbon monoxide in air at low concentrations.

Over the past two decades, interest in CO detection has also intensified due to a very different role for this gas. This was the discovery that CO is an important signalling molecule (gasotransmitter) produced endogenously during the haem catabolism and is implicated in vasodilatation, neurotransmission, anti-inflammatory and anti-apoptotic processes.⁴ Since the elucidation of the benign role of carbon monoxide, the therapeutic potential of this molecule is starting to be harnessed. The direct use of CO gas through inhalation is problematic for obvious reasons and this has led to the development of CO-releasing molecules (CORMs and PhotoCORMs)⁵ that are able to release CO in a controlled manner via hydrolysis or photoactivation. The growth of interest in CO as a gasotransmitter or as a therapeutic agent has led to attempts to develop luminescent chemosensors capable of monitoring and quantifying the production or generation of CO within a cellular environment.¹ However, despite this attention, only a small number of systems capable of the fluorogenic detection of CO in cells and tissues have been reported.

The majority of the probes developed for the optical sensing of CO, both for detection in air or in cells, are based on metal complexes, as they possess many

promising attributes suited to the design of chromo- or fluorogenic probes.⁶ The tuning of steric and/or electronic properties of a metal complex provides the subtle control needed to control selectivity and reactivity of the metal towards CO.⁷ In these metal complexes, the sensing mechanism is intrinsically related to the reactivity of the metal centre towards carbon monoxide and in many cases detection is achieved by direct coordination of CO to the metal. The binding of CO to the metal centre can occur at a vacant coordination site or through the displacement of a labile ligand. Many of these developments are covered in recent reviews.¹

The immobilisation of molecular probes on various supports (e.g., silica, titania, zirconia, cellulose strips) has been exploited in the design of simple, low-cost, systems, such as cellulose strips, which offer a clear, visible colour change on contact with CO. In addition, this approach provides a simple means to interface these systems (especially chromogenic ones) with optoelectronic devices⁸ that could be used as alternatives to those available commercially.

The results presented here describe a system which combines chromogenic and fluorogenic responses to carbon monoxide, allied to extremely high sensitivity and selectivity for CO over other potential interferents. Furthermore, the flexibility of design allows a water solubilising moiety or a tether for nanoparticle attachment to be added in a simple manner. Using this approach, the sensing of CO in air and in aqueous solution is described along with the extension of this detection to the challenges of the cellular environment.

3.4.3. Results and discussion

Our most recent work in this area is based on the exceptional reactivity of the bright red-orange $[\text{Ru}(\text{CH}=\text{CHPyr}-1)\text{Cl}(\text{CO})(\text{BTD})(\text{PPh}_3)_2]$ (Pyr = pyrenyl; BTD = 2,1,3-benothiadiazole)⁹ compound and related vinyl complexes of ruthenium and osmium.¹⁰ The exchange of the BTD ligand for CO leads to formation of the intense yellow complex, $[\text{Ru}(\text{CH}=\text{CHPyr}-1)\text{Cl}(\text{CO})_2(\text{PPh}_3)_2]$. The change in colour during its process allows the concentration of CO to be determined in solution and in the solid state (on either silica or cellulose strips). The clear colour change allows amounts as low as 5 ppb to be detected by the naked eye. The

fluorescence of the pyrenyl substituent is quenched through conjugation with the metal-BTD unit. However, displacement of the BTD ligand by CO (Figure 3.4.1, mechanism **A**) revives this fluorescence without any significant structural change in the RuCH=CHPyr-1 unit. This turn-on fluorescence response (36-fold compared to the precursor) allows a detection limit as low as 1 ppb to be achieved.

In this report, an alternative approach is employed in order to exploit the facile installation of the vinyl unit for other purposes (solubility tuning, tethering to nanoparticle surfaces). This chromogenic response is similar to mechanism **A** (bright red precursor to paler dicarbonyl product) but the fluorescence revival in mechanism **B** (Figure 3.4.1) is due to displacement of the fluorophore from the metal centre, removing quenching through the heavy atom effect.

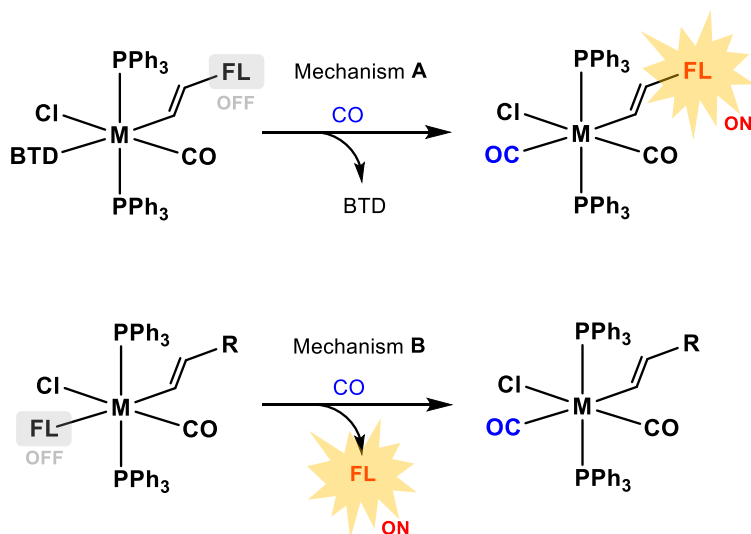


Figure 3.4.1. Schematic representation of two sensing mechanisms.

The success of the CO sensing behaviour displayed by the ruthenium and osmium vinyl complexes $[M(\text{CH}=\text{CHR})\text{Cl}(\text{CO})(\text{BTD})(\text{PPh}_3)_2]$ relies substantially on the properties of the BTD ligand, which enhance the vibrancy of the colour in the probe complexes as well as acting as a sufficiently good ligand to resist exchange

with potentially coordinating interferents, such as SO_2 , NO_x , N_2 , MeCN, H_2O , MeOH, EtOH and other solvent species,^{9,10} thus giving the system its selectivity for CO over other species potentially present. The BTD ligand also plays a key role in the quenching effect when $\text{R} = \text{Pyr-1}$ (mechanism **A**), however, this is no longer relevant in mechanism **B**.

So, in order to achieve sensing via mechanism **B** without compromising the exceptional properties afforded by the BTD complexes, a new highly fluorescent labile ligand was needed. Considerable searching of the literature revealed a notable lack of suitable small N-donor fluorescent compounds which could bind sufficiently well to the metal centre, while being selectively displaced by CO over other species. It became clear that the properties of BTD as a ligand were close to ideal and so it was decided to prepare a novel benzothiadiazole moiety with fluorescent properties. In fact, 2,1,3-benzothiadiazoles are members of a relatively prominent class of photoluminescent compounds and have been considered as potential staining agents for cellular organelles in fluorescence microscopy.¹¹ Usually characterised by emissions above ca. 500 nm and by reasonable quantum yields (0.20 – 0.65), these compounds are indeed very promising candidates for biological applications. It was challenging to find variants which would allow complexation to the metal without encountering steric hindrance issues due to the influence of the relatively large cone angle of triphenylphosphine, in particular.

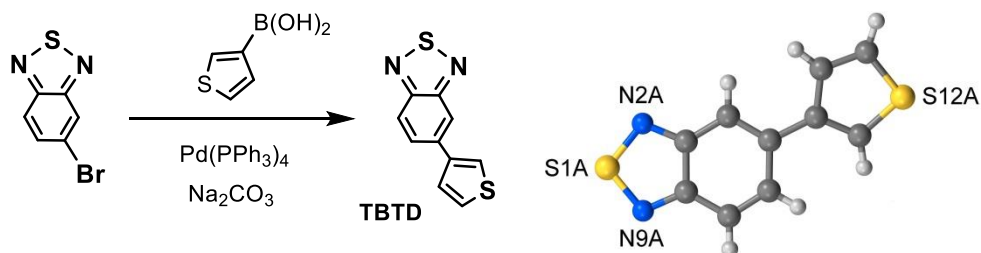


Figure 3.4.2. Synthesis of the 5-(3-thienyl)-2,1,3-benzothiadiazole (TBTD) ligand and its crystal structure.

For these reasons, a new monosubstituted (and therefore less bulky) 5-(3-thienyl)-2,1,3-benzothiadiazole (TBTD) ligand was synthesised and its photophysical and ligand properties tested. The preparation of TBTD was achieved via a Suzuki coupling between 5-bromo-2,1,3-benzothiadiazole and 3-thienylboronic acid, as shown in Figure 3.4.2. The product was obtained in modest yield and was fully characterised using ^1H and $^{13}\text{C}\{^1\text{H}\}$ NMR spectroscopy, mass spectrometry and elemental analysis.

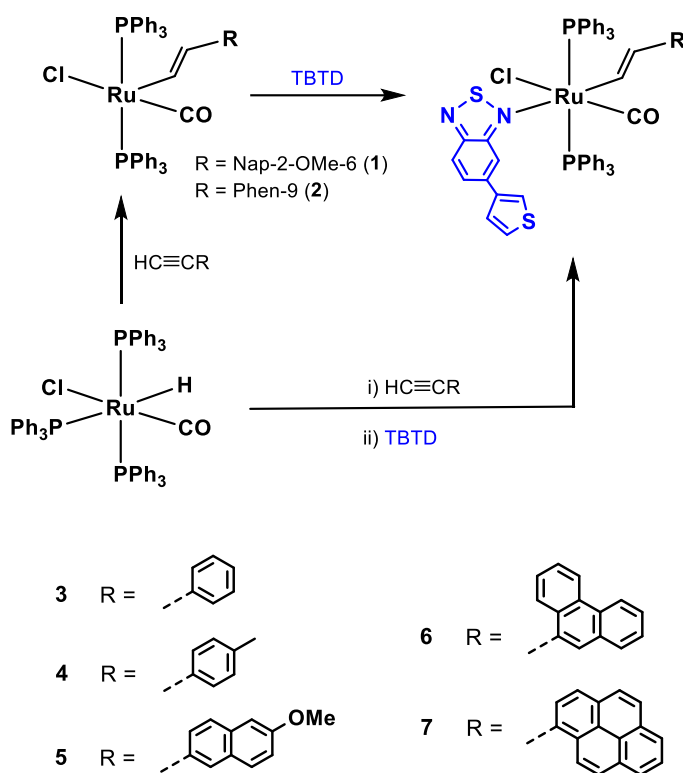
Single crystals suitable for X-ray diffraction were grown via vapour diffusion of hexane onto a solution of the compound in chloroform (Figure 3.4.2). The compound crystallised with two independent molecules (Figures S3-1 and S3-2), with torsion angles across the BTD-thiophene bonds of *ca.* 22.8 and 19.1° respectively.

The bright yellow compound is very soluble in common organic solvents (dichloromethane, chloroform, acetonitrile, ethanol) and moderately soluble in methanol and water. The blue-green broad emission, typical of the thienyl group in position 5 of the BTD unit, is subject to a hypsochromic shift ($\lambda_{\text{em}} = 430 \text{ nm}$) in non-polar organic solvents (Figure S3-1, Supporting Information). The photophysical characterisation included the measurement of the quantum yield ($\Phi = 0.26$), as described in the Supporting Information.

Given the successful use of $[\text{RuHCl}(\text{CO})(\text{BTD})(\text{PPh}_3)_2]^{12}$ as a precursor to the ruthenium vinyl complexes $[\text{Ru}(\text{CH}=\text{CHR})\text{Cl}(\text{CO})(\text{BTD})(\text{PPh}_3)_2]^{13}$ synthesis of the direct TBTD analogue, $[\text{RuHCl}(\text{CO})(\text{TBTD})(\text{PPh}_3)_2]$ was attempted through exchange of PPh_3 in $[\text{RuHCl}(\text{CO})(\text{PPh}_3)_3]$ with TBTD. However, two isomers were formed, giving rise to closely spaced singlet resonances in the $^{31}\text{P}\{^1\text{H}\}$ NMR spectrum at 44.6 and 45.3 ppm in approximately a 1:1 ratio. This hypothesis is also confirmed by the presence of two superimposed triplets at around -7 ppm in the ^1H NMR spectrum. These compounds proved intractable through recrystallization or column chromatography. While the complexes, $[\text{Ru}(\text{CH}=\text{CHR})\text{Cl}(\text{CO})(\text{BTD})(\text{PPh}_3)_2]$, all show a *trans* disposition for the vinyl and BTD ligands (an aspect that is key to the fluorescence quenching mechanism), the crystal structure of $[\text{RuHCl}(\text{CO})(\text{BTD})(\text{PPh}_3)_2]$ displays a mutually *cis* arrangement between the hydride and the BTD ligands.¹² Unlike 2,1,3-benzothiadiazole (BTD) itself, the TBTD ligand

is unsymmetrical and so coordination could be envisaged through either of the two nitrogen donors of the thiadiazole ring. It is not clear which of these isomers (Figure S2-1) form but the difficulty in separation led to investigation of an alternative route to TBTD vinyl complexes via the known 5-coordinate compounds $[\text{Ru}(\text{CH}=\text{CHR})\text{Cl}(\text{CO})(\text{PPh}_3)_2]$.¹⁴

First reported by Santos and co-workers in 1986, the complex $[\text{Ru}(\text{CH}=\text{CHPh})\text{Cl}(\text{CO})(\text{PPh}_3)_2]$ was prepared according to this method.^{14a} The procedures described in later reports were used to synthesise $[\text{Ru}(\text{CH}=\text{CHR})\text{Cl}(\text{CO})(\text{PPh}_3)_2]$ ($\text{R} = \text{C}_6\text{H}_4\text{Me-4}$,^{14b} Pyr-1^{14c}). In addition, a series of new 5-coordinate compounds $[\text{Ru}(\text{CH}=\text{CHR})\text{Cl}(\text{CO})(\text{PPh}_3)_2]$ ($\text{R} = \text{Nap-2-OMe-6}$ (**1**), Phen-9 (**2**)) were also prepared using an analogous route (Scheme 3.4.1) in almost quantitative yield. Further details are provided in the Supporting Information.



Scheme 3.4.1. Synthesis of a series of ruthenium vinyl complexes bearing the TBTD ligand.

Addition of a slight excess of TBTD to a dichloromethane solution of $[\text{Ru}(\text{CH}=\text{CHR})\text{Cl}(\text{CO})(\text{PPh}_3)_2]$ led to the formation of $[\text{Ru}(\text{CH}=\text{CHR})\text{Cl}(\text{CO})(\text{TBTD})(\text{PPh}_3)_2]$ ($\text{R} = \text{Ph}$ (**3**), $\text{C}_6\text{H}_4\text{Me}$ -4 (**4**), Nap-2-OMe-6 (**5**), Phen-9 (**6**), Pyr-1 (**7**)) in yields between 72-85%. A singlet in the $^{31}\text{P}\{^1\text{H}\}$ NMR spectrum for **4** at 26.2 ppm indicated an arrangement with mutual *trans* triphenylphosphine ligands in the product, while the presence of a doublet of triplets at 8.61 ppm ($J_{\text{HH}} = 16.2$ Hz, $J_{\text{HP}} = 3.1$ Hz) for the H_α proton in the ^1H NMR spectrum confirmed retention of the vinyl ligand. In addition, this spectrum also showed new resonances at 7.58 (2H), 7.75 (1H), 7.87 (2H), 8.27 (1H) ppm for the TBTD ligands. The remaining data are in good agreement with the proposed formulation (Scheme 3.4.1).

It was also found that a one-pot route could be employed, in which the alkyne and the TBTD ligand could be added sequentially to $[\text{RuHCl}(\text{CO})(\text{PPh}_3)_3]$ (Scheme 3.4.1), though there is little improvement in overall yield.

Given the isomers encountered with $[\text{RuHCl}(\text{CO})(\text{TBTD})(\text{PPh}_3)_2]$, it is noteworthy that both ^1H and $^{31}\text{P}\{^1\text{H}\}$ NMR spectra revealed the formation of only one isomer for TBTD complexes **3** - **8**, thus confirming the success of this synthetic strategy. Although steric considerations would suggest that it would be more favourable for the thienyl group of the TBTD to be orientated away from the ruthenium centre, this could not be confirmed unambiguously from spectroscopic data. Single crystals of compounds **6** and **7** were obtained and structural determinations were carried out by X-ray diffraction (Figures 3.4.3 and 3.4.4).

In both crystal structures, the TBTD ligand is coordinated to the ruthenium through the nitrogen in position 3 (not 1) and the aromatic groups of the vinyl substituent are found in a tilted orientation with respect to the plane occupied by the TBTD, the torsion angles about the C2–C3 bonds being *ca.* 31.3 and 23.4° in **6** and **7**, respectively. The coordination mode the TBTD ligand is thus somewhat surprising as it appears not to minimise the steric interactions with the rest of the ligand set. Rationalisation of this arrangement is not straightforward, though it is worth noting that the observed coordination mode does provide a greater conjugation between the thienyl group and the metal centre. When comparing

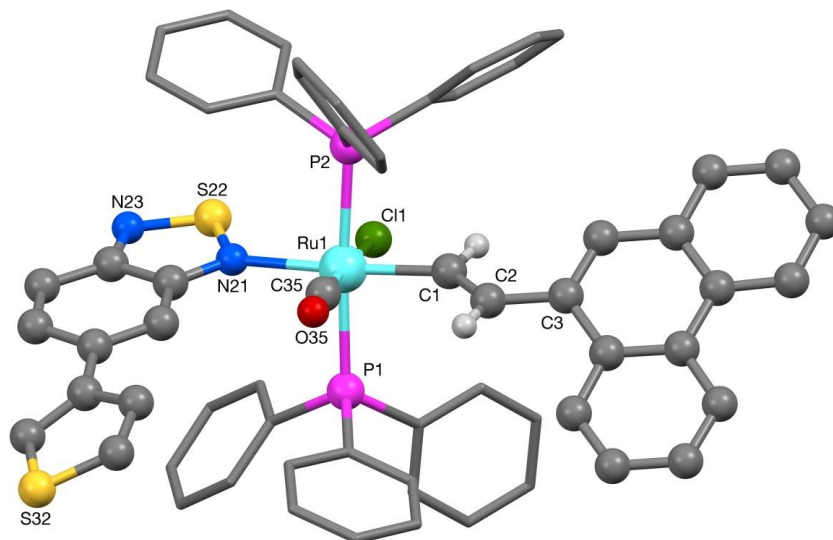


Figure 3.4.3. Crystal structure of compound **6**. Selected bond lengths (Å), bond angles (°) and torsion angles (°): Ru(1)-C(35) 1.824(3), Ru(1)-C(1) 2.055(3), Ru(1)-N(21) 2.235(3), Ru(1)-P(1) 2.3998(8), Ru(1)-P(2) 2.4204(8), Ru(1)-Cl(1) 2.4657(8), C(1)-C(2) 1.335(5); P(1)-Ru(1)-P(2) 176.25(3), Ru(1)-C(1)-C(2) 134.2(2).

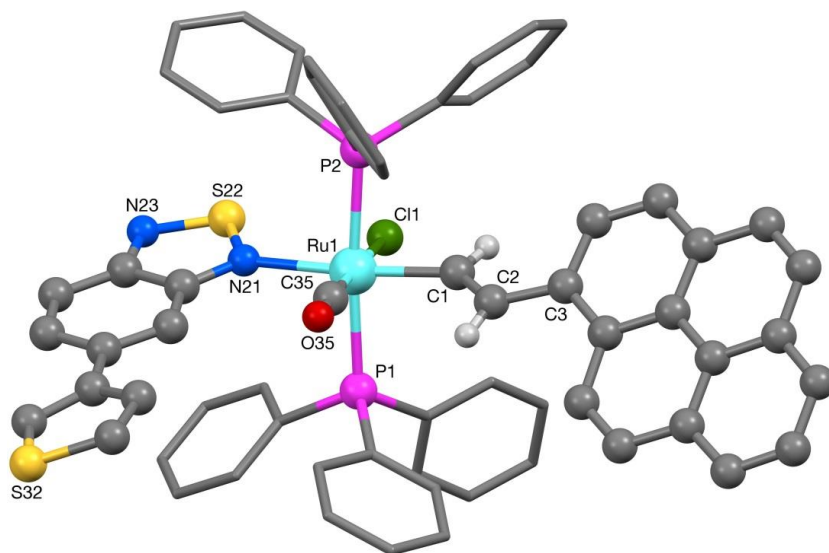
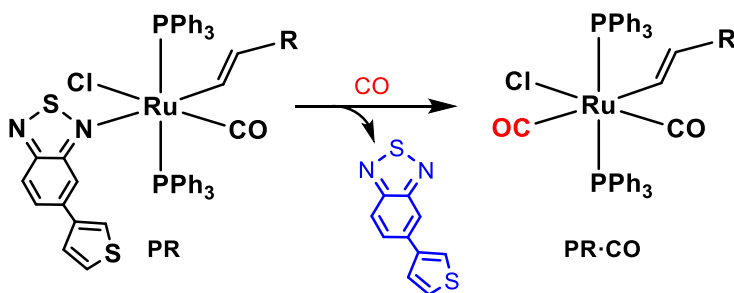


Figure 3.4.4. Crystal structure of compound **7**. Selected bond lengths (Å), bond angles (°) and torsion angles (°): Ru(1)-C(35) 1.830(3), Ru(1)-C(1) 2.054(2), Ru(1)-N(21) 2.241(2), Ru(1)-P(1) 2.3943(8), Ru(1)-P(2) 2.4198(7), Ru(1)-Cl(1) 2.4673(7), C(1)-C(2) 1.337(3); P(1)-Ru(1)-P(2) 175.03(3), Ru(1)-C(1)-C(2) 132.8(2).

the crystallographic features of compound **7** with its BTd analogue, $[\text{Ru}(\text{CH}=\text{CHPyr-1})\text{Cl}(\text{CO})(\text{BTd})(\text{PPh}_3)_2]$,⁹ there is no significant difference between the Ru–N bond lengths in the two complexes. This suggests that, despite the presence of the thienyl group, the TBTD ligand is equally tightly bound to the ruthenium, which bodes well for similarly selective behaviour towards CO over other species.

In order to investigate the reactivity of **3** – **7** with carbon monoxide, the CO adducts were prepared using pure CO (Scheme 3.4.2).



Scheme 3.4.2. Reaction of the probes **3** - **7** with carbon monoxide.

In each case, reaction with CO was rapid in dichloromethane solution, with quantitative conversion being observed within 5 seconds (50 mg scale). This was monitored through the colour changes, with the deep red solution becoming pale orange for all compounds. All the mononuclear dicarbonyl complexes (**3**·CO - **7**·CO) have been characterised previously, either by others^{15,16} or in our previous work on the probes $[\text{M}(\text{CH}=\text{CHR})\text{Cl}(\text{CO})(\text{BTd})(\text{PPh}_3)_2]$.^{9,10} Single crystals of **6**·CO were grown by slow diffusion of ethanol into a dichloromethane solution of the complex. A structural determination was undertaken (Figure 3.4.5), complementing the structure of the TBTD precursor (**6**) described above (Figure 3.4.2). These data for the probe before and after exposure to CO were of particular use in determining the fit of actual structural characteristics with the DFT studies (*vide infra*).

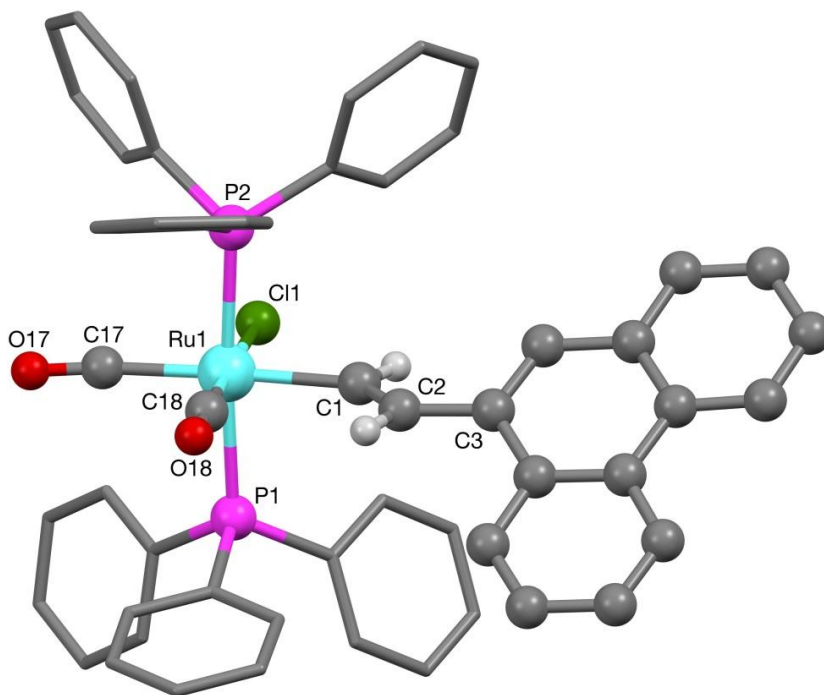


Figure 3.4.5. Crystal structure of compound **6·CO**. Selected bond lengths (Å), bond angles (°) and torsion angles (°): Ru(1)-C(18) 1.849(3), Ru(1)-C(17) 1.965(3), Ru(1)-C(1) 2.120(3), Ru(1)-P(1) 2.4011(6), Ru(1)-P(2) 2.4112(6), Ru(1)-Cl(1) 2.4703(6), C(1)-C(2) 1.334(3), P(1)-Ru(1)-P(2) 175.83(2), C(2)-C(1)-Ru(1) 130.76(19).

Probe complexes **3** - **7** proved very stable both in air and in solution, showing no signs of degradation even after months (as solids). There was no indication of a greater tendency towards dissociation of the TBTD unit compared to the less bulky BTD ligand.

Chromo-fluorogenic detection of CO in air

Once characterisation was complete, the luminescence and colour response of the TBTD probes were tested using spectrophotometric techniques in the presence of increasing levels of CO. Of particular interest was the evaluation of the displacement fluorescence sensing mechanism (Figure 3.4.1, **B**), compared to

the probes $[M(\text{CH}=\text{CHR})\text{Cl}(\text{CO})(\text{BTD})(\text{PPh}_3)_2]$, in which the fluorophore is retained throughout (Figure 3.4.1, **A**).

While all complexes reacted rapidly with CO in dichloromethane or chloroform solution, any viable probe for sensing CO in air would need to operate in the solid state. For this reason, all the complexes were immobilised on standard laboratory grade silica by dissolving the probe in a minimum volume of chloroform and then adding 10 mass equivalents of silica. After stirring, rotary evaporation provided the brightly coloured solid, which was used in the CO measurements after standing for an hour at room temperature.

The chromogenic response of $[\text{Ru}(\text{CH}=\text{CHC}_6\text{H}_4\text{Me-4})\text{Cl}(\text{CO})(\text{TBTD})(\text{PPh}_3)_2]$ (**4**) towards different concentrations of CO gas was carried out directly in the solid state, using the probe supported on silica gel and studied with diffuse reflectance spectroscopy. The UV-Vis measurements show a clear increase in the percentage reflectance (%R) as the CO concentration is increased from 0 ppm to 2000 ppm (Figure 3.4.6).

Using a graphical method, the detection limit of **4** using this method was determined to be 1.4 ppm. In addition, compound **4** (on silica) shows a striking change in colour from red to light yellow when exposed to increasing concentrations of CO (Figure 3.4.6b).

However, as a result of the markedly less dramatic colour modulations, the limit of detection values were found to be at least 10 times higher than the BTD family of probes, $[\text{Ru}(\text{CH}=\text{CHR})\text{Cl}(\text{CO})(\text{BTD})(\text{PPh}_3)_2]$.^{9,10} This poor colour response is likely to be due to the intrinsic optical properties of the TBTD ligand, as the bright yellow colour of this 2,1,3-benzothiadiazole derivative impacts on the optical properties in the visible region. Nevertheless, both spectrophotometric and naked-eye detection limits are suitable for the detection of the onset of toxic levels of CO (50 ppm) through to very high and toxic levels of the gas (exposure to 2000 ppm causes death within a few minutes).

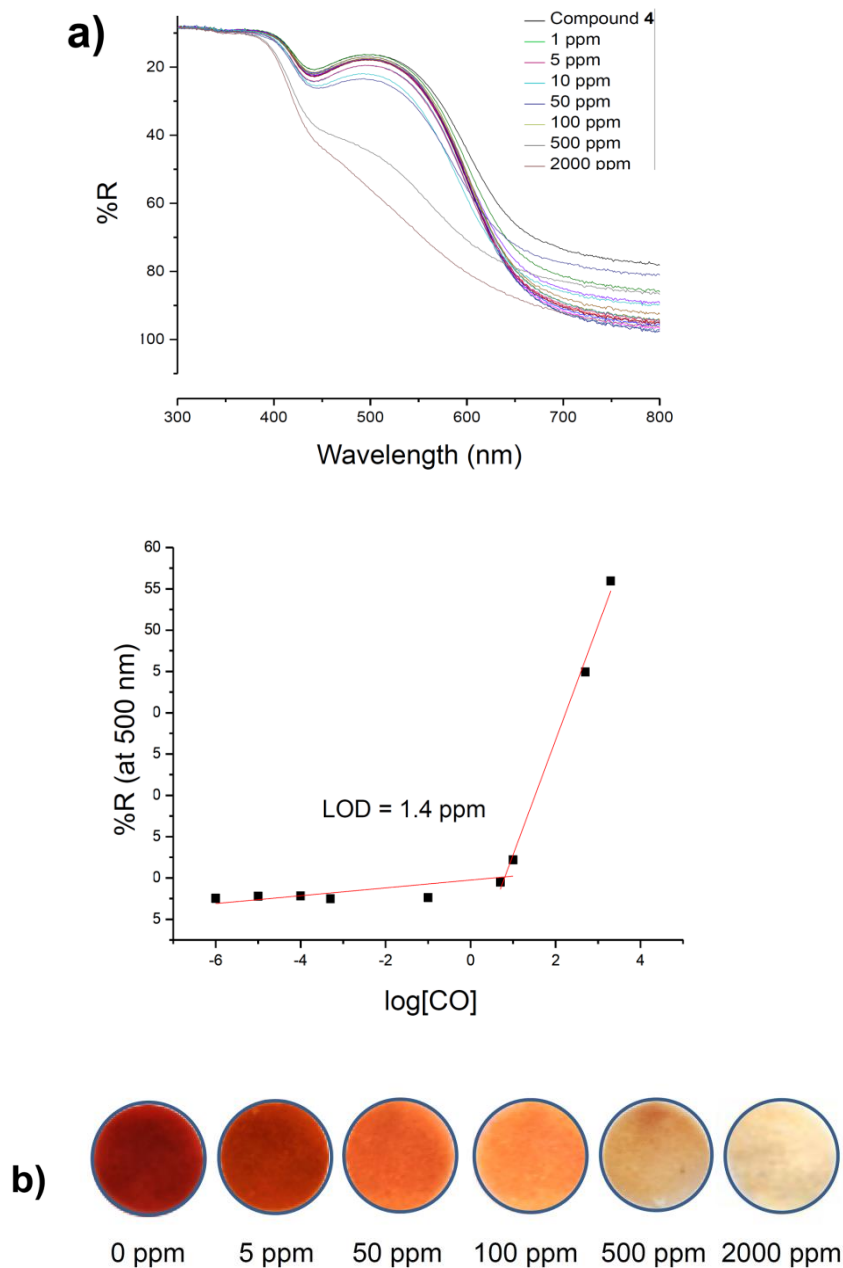


Figure 3.4.6. a) Change in percentage reflectance of silica supported **4** at varying CO concentrations (left) and determination of the detection limit (right) from the absorbance values at 500 nm; b) Colour changes displayed by silica supported compound **4** with increasing CO concentrations.

In contrast to these modest chromogenic results, the fluorogenic response in solution was found to be much more impressive (about 1 ppb for both **3** and **4**), which is comparable or even slightly superior to the BTB probes (Figure 3.4.7). The enhancement of the solid state fluorescence intensity of the silica-adsorbed compounds was also significant.

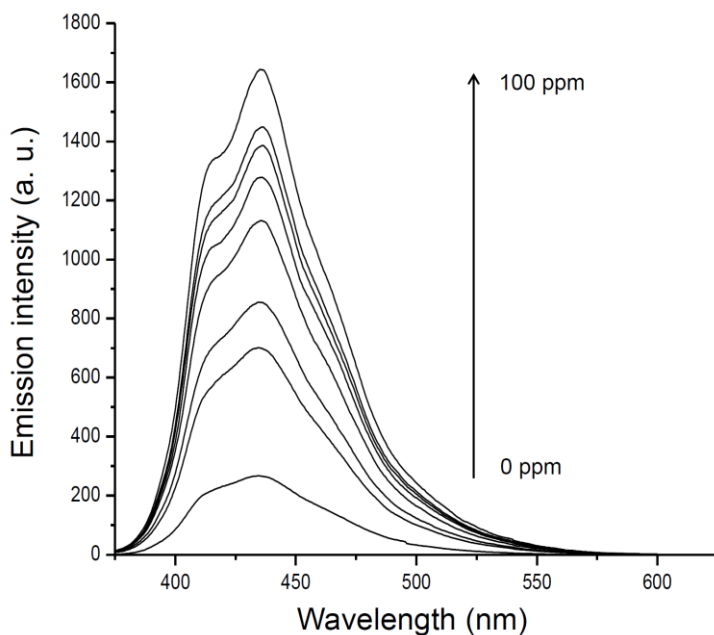


Figure 3.4.7. Plot showing an 8-fold turn-on fluorescence response ($\lambda_{\text{exc}} = 352 \text{ nm}$) of a dichloromethane solution of compound **4** at increasing concentrations of CO ($\lambda_{\text{max}} = 435 \text{ nm}$).

When adsorbed on silica, probe **4** gives rise to a typically sharp emission band in the fluorescence emission spectra in the presence of air containing 0 to 2000 ppm of CO delivering a limit of detection (LOD) of 9.9 ppm.

By exploiting the exceptional reactivity of these probes with carbon monoxide, it was found that complexes $[\text{Ru}(\text{CH}=\text{CHPh})\text{Cl}(\text{CO})(\text{TBTD})(\text{PPh}_3)_2]$ (**3**) and $[\text{Ru}(\text{CH}=\text{CHC}_6\text{H}_4\text{Me-4})\text{Cl}(\text{CO})(\text{TBTD})(\text{PPh}_3)_2]$ (**4**) display similar luminescence behaviours, which are intrinsically connected to their structural characteristics

and, most importantly, are determined solely by the presence of the TBTD fluorophore. As expected, quantum yield measurements confirmed that the fluorescence of free TBTD ($\Phi = 0.26$) is partially quenched when attached to the ruthenium centre ($\Phi = 0.047$ for complex **4** in ethanol). This quenching process is attributed to the heavy-atom effect, in which a high-atomic number element induces enhancement of non-radiative intercombination transitions via spin-orbit coupling. Ultimately, this results in the deactivation of the radiative photon decay, thus depleting the fluorescent intensity and lifetime in the metal-ligand complex (**PR**).

When the probe is exposed to increasing concentrations of CO, the formation of the dicarbonyl species **PR·CO** takes place alongside the displacement of the TBTD ligand. The release of the fluorophore in solution produces the fluorescence turn-on response and enables the detection of CO. Compound **3** displays an analogous behaviour to complex **4**, as the quantum yield of the probe is enhanced from 0.08 to 0.2 at 100 ppm of CO.

Whilst the complexes **3** and **4** bear only a single fluorophore (the TBTD ligand), the complexes $[\text{Ru}(\text{CH}=\text{CHR})\text{Cl}(\text{CO})(\text{TBTD})(\text{PPh}_3)_2]$ ($\text{R} = \text{Nap-2-OMe-6}$ (**5**), Phen-9 (**6**), Pyr-1 (**7**)) bear two separate fluorophores as they possess a fluorescent vinyl substituent in addition to the TBTD unit. The presence of these two fluorophores will dramatically affect the fluorogenic response of the probes, as the reaction with CO will lead to activation of the fluorescence response in both the **PR·CO** probe complex as well as the liberated (and hence unquenched) TBTD group. Moreover, it was considered that this double fluorophore response could be harnessed to enable the ratiometric detection of CO. This detection mode is based on the ratio between the two fluorescence intensities and is particularly important in fluorescence imaging as it permits the analysis and correction of artifacts due to photobleaching and changes in focusing.

In order for this approach to function, the fluorophores (TBTD and vinyl substituent) must exhibit different and independent emission changes, so that the displacement of the TBTD ligand and the formation of the fluorescent dicarbonyl species can be monitored independently. In this way, the ratios of the two emission intensities $I_{\text{TBTD}}/I_{\text{PR·CO}}$ will be proportional to the concentration of CO.

However, preliminary measurements revealed that the fluorescence emission of the TBTD partially or, for complexes **6** and **7**, completely overlaps with the emission of the vinyl substituent (phenanthrenyl/pyrenyl), thus preventing discrimination between the signals. The ratiometric approach for the detection of CO was not pursued further with these particular complexes. Standard spectrophotometric characterisation of **5** – **7** was carried out but neither the colour changes nor the fluorescence enhancements were found to offer significant improvements over the probes bearing a single fluorophore (**3** and **4**).

Despite the less pronounced chromogenic behaviour of the TBTD probes, CO levels far below the onset of toxic levels can be easily detected. Fluorogenic detection of CO using the TBTD series is equally sensitive to that displayed by the BTD series of probes.^{9,10}

The selectivity of the probes for CO was screened against a range of gases (N₂, O₂, Ar, CO₂, NO_x), solvents and volatile organic compounds (water, acetone, chloroform, ethanol, toluene, hexane, formaldehyde, acetonitrile). The interferents tested in detail are ones which could reasonably exist at substantial levels in domestic or commercial environments (Supporting Information). This revealed an excellent tolerance for all but the highest concentrations of these species. The probe [Ru(CH=CHPh)Cl(CO)(TBTD)(PPh₃)₂] (**3**) showed exceptional resilience even in the presence of concentrations of up to 7240 ppm NO_x and 4570 ppm MeCN, at which point spectral changes started to appear. However, these values need to be viewed in context of the concentrations considered toxic for NO_x (TWA 5 ppm) and MeCN (TWA 40 ppm).

Detection of CO in living cells

Despite its toxic reputation, recent studies indicate that CO is a very important biological signalling molecule (gasotransmitter), which is actually produced endogenously during the haem catabolism and is implicated in vasodilatation, neurotransmission, anti-inflammatory and anti-apoptotic processes.⁴ In order to unravel the biochemistry of CO within biological systems, researchers have been investigating fluorescence imaging and sensing as potential techniques to detect and monitor the presence of carbon monoxide in living cells.¹

Additional impetus to achieving this goal has been provided by the increasing interest in the use of CO as a therapeutic agent. Although CO can be administered medically by inhalation, far more control is achieved through the use of carbon monoxide releasing molecules (CO-RMs or PhotoCORMs), which are able to release CO in a controlled manner via hydrolysis or photoactivation.⁵ In order to support the development of CO-RMs and probe the gasotransmitter function of CO, a new research field has emerged, based on the detection of CO in living cells. To date, only a handful of chemodosimeters able to detect CO in cells have been reported so far and these all suffer from various drawbacks, such as poor signal-to-noise ratio, slow response times and lack of reversibility.

Various approaches have been explored with the first successful systems being reported in 2012.^{17,18} He and co-workers developed a haem-based genetically-encoded fluorescent protein (COSer) capable of the selective imaging of CO in cells.¹⁷ While promising, the use of yellow fluorescent protein for the response is problematic due to the autofluorescence of other proteins, which limits the relative fluorescence enhancement observed. The generation of the COSer probe is also beyond the expertise available in most laboratories. In contrast, Chang and co-workers¹⁸ reported a structurally simpler and synthetically more accessible probe based on a palladium-BODIPY complex (COP-1), which undergoes a selective palladium-mediated carbonylation of the borondipyrromethane difluoride (BODIPY) ligand to release the fluorescent BODIPY unit. The fluorescence of this ligand, partially quenched via the heavy-atom effect of the palladium centre, undergoes a 10-fold fluorescence enhancement when the ligand is released in solution. The probe shows a detection limit as low as 28 ppb CO after being incubated with 50 μM [RuCl(glycinate)(CO)₂] (CORM-3). When HEK293T cells were incubated with CORM-3 (5 or 50 μM) and treated with COP-1 (1 μM), a significant and dose-dependent increase in the intracellular fluorescence was observed. Importantly, these probes were shown to be nontoxic and displayed a good selectivity for CO over other species commonly found in cells (H₂S, glutathione, NO, O₂, CN⁻ and imidazole). Another cyclometallated palladium complex has been reported bearing a carbazole-coumarin-fused unit (CC-CO) for the imaging of carbon monoxide in living tissues.¹⁹ The highly conjugated push-

and-pull system present in this chemosensor possesses very attractive two-photon fluorescence electronic properties which can be applied to the imaging of CO in HeLa, MCF-7 and MKN-28 cells in the presence of $[\text{Ru}_2\text{Cl}_4(\text{CO})_6]$ (CORM-2). More recently, the palladium-catalysed intramolecular cyclisation and elimination reaction of a coumarin fluorogenic probe (PCO-1) has been employed to selectively detect CO in aqueous media.²⁰ The luminescence of the organic probe is initially quenched by the presence of a carbamate bond ($\Phi = 0.0034$), but after incubation with the palladium species and CO, a highly fluorescent 7-hydroxycoumarin is generated ($\Phi = 0.4467$) and released into the aqueous medium, resulting in a strong emission at 460 nm. The response was found to be highly selective towards CO over other biologically relevant species (NO, H₂S, NaOCl, H₂O₂, O₂ and other sulfur and nitrogen containing small molecules). Finally, the probe was found to be non-toxic in human lung carcinoma cells within a 4 hour incubation period.

Although the probes described above display an undoubted ability to detect CO in biological systems, further research is still urgently required in order to address the intrinsic drawbacks of each system. Deficiencies of these systems include synthetic complexity (and hence reduced accessibility), delayed fluorescence response times (typically 40-60 mins in the palladium-based systems) and the reduced fluorescence turn-on response of some of the probes (especially in aqueous solution). Moreover, it would be helpful to avoid the use of potentially cytotoxic unligated heavy metal salts if possible. In addition, to the immediate fluorescence response required (with reduced incubation time), the real-time tracking of CO in living cells also demands a high signal-to-noise ratio (SNR). Good SNR is a crucial aspect in optical imaging, since the image quality and sharpness depend on this parameter. Although protein-based sensors, like COSer, represent excellent biocompatibility and selectivity towards the analyte, small-molecule fluorescent probes offer the benefits of higher SNR (with respect to the protein background fluorescence), improved membrane permeability and unique potential for structure-property tuning.²¹⁻²³

From consideration of the exceptional results obtained for the detection of CO in air,^{9,10} it was clear that ruthenium(II) and osmium(II) vinyl complexes offer many

of the desired characteristics for the sensing of carbon monoxide in cells. The immediate fluorogenic response, the outstanding emission enhancement and the exceptional sensitivity and selectivity make these compounds strong candidates for this application. However, the very low solubility of these complexes in water prevented them being applied directly to the sensing of CO in aqueous systems.

It should be noted that, to date, no probe for CO in cells has been reported based on a sensing mechanism in which the CO analyte coordinates directly to the metal centre.

Various different strategies have been applied in order to achieve solubility in highly polar solvents, such as aqueous solution. In the case of metal complexes, the simplest solution is often the modification of the ancillary ligands (those not involved in the primary function) coordinated to the metal centre. As has been demonstrated widely,²⁴ the replacement of triarylphosphine ligands with sulfonated triphenylphosphine ligands can achieve solubility in water.

The mono-sulfonated triphenylphosphine sodium salt $\text{Ph}_2\text{P}(m\text{-C}_6\text{H}_4\text{SO}_3\text{Na})$ (TPPMS) was prepared and investigated. Although multiple sulfonation increases the water solubility, it was anticipated that trisulfonation could change the character of the phosphine too radically and risk compromising a system successfully applied to CO detection.^{24c} However, using the precursor $[\text{RuHCl}(\text{CO})(\text{TPPMS})_3]$ failed to generate the desired TBTD vinyl complexes in sufficient purity. The products were also found to be somewhat unstable in solution, spontaneously losing TBTD after an hour in solution. The same was observed when $[\text{Ru}(\text{CH}=\text{CHC}_6\text{H}_4\text{Me-4})\text{Cl}(\text{CO})(\text{PPh}_3)_2]$ was used as the starting point for the synthesis of $[\text{Ru}(\text{CH}=\text{CHC}_6\text{H}_4\text{Me-4})\text{Cl}(\text{CO})(\text{TBTD})(\text{TPPMS})_2]$.

Further experiments explored other less bulky water-soluble phosphines, such as the tris(hydroxymethyl)phosphine (THP)²⁵ and 1,3,5-triaza-7-phosphaadamantane (PTA)²⁶ as alternatives to TPPMS. However, initial investigation revealed similar issues to those described above. It was thus clear that these water soluble variants do not display the same stability in aqueous media that characterise their triphenylphosphine analogues. These findings led to other approaches being explored to render the probes suitable for use in aqueous systems. One of the conclusions drawn from the study of water-soluble

phosphines is that both the stability and reactivity of the transition metal probes towards CO are intimately related to their ancillary ligands. The successful sensing response described above for the TBTD complexes **3** - **7** relies to some degree on the balance of steric and electronic effects provided by the ligand set containing two triphenylphosphine ligands, a chloride and a carbonyl ligand. Due to its facile introduction through hydrometallation and the structural flexibility afforded by the huge array of known terminal alkynes, it was sought to introduce water solubility through the vinyl ligand.

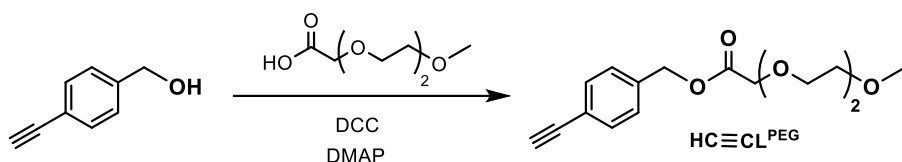
Hydrophilic alkynes bearing highly polar functional groups (amides, carboxylic acids, hydroxyl substituents), or ionic groups (sulfonate, ammonium, phosphonate), are relatively inexpensive starting materials and are relatively common substrates for 'click chemistry' approaches to biological²⁷ systems. Although hydrophilic alkynes thus appear to be ideally suited to this study, the intrinsic nucleophilicity of their polar groups towards transition metals needs to be taken into account. Several studies have shown the preference of ruthenium and osmium triphenylphosphine hydride complexes to react with nucleophilic oxygen-, nitrogen- and sulfur-donor groups, even in presence of terminal alkynes.^{28,29} Thus, when both functionalities are present on the same ligand, the alkyne insertion seems often to be less favoured compared to coordination of the other donors, especially when a bidentate chelate results.^{29,30}

For these reasons, terminal alkynes were designed to possess hydrophilic properties combined with an absence of nucleophilic character. The inexpensive 4-ethynylbenzyl alcohol was thus coupled to a polyethylene glycol (PEG) chain via a simple esterification reaction. Ligand $\text{HC}\equiv\text{CL}^{\text{PEG}}$ was prepared following a Steglich esterification protocol (Scheme 3.4.3) in dry dichloromethane, using *N,N'*-dicyclohexylcarbodiimide (DCC) and 4-dimethylaminopyridine (DMAP).

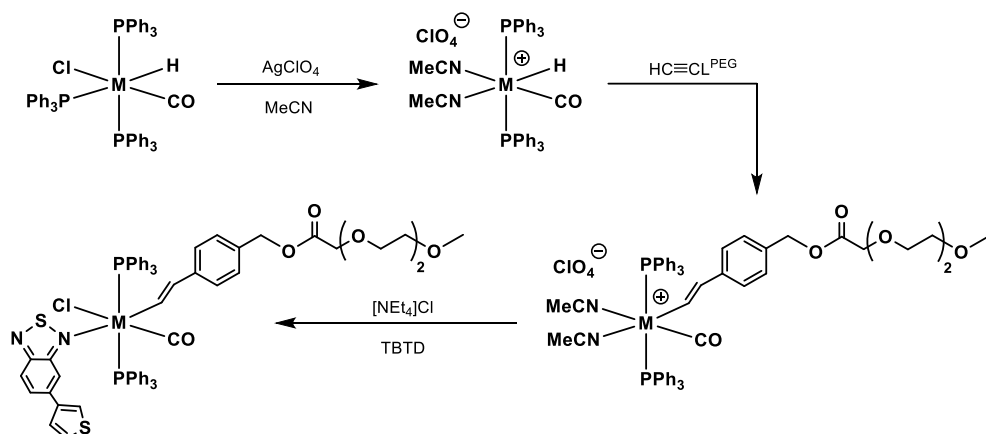
The optimised reaction involves the slow addition of the 4-ethynylbenzyl alcohol to the other reagents over a 1 hour period followed by stirring for 12 h. The $\text{HC}\equiv\text{CL}^{\text{PEG}}$ ligand was fully characterised using NMR and IR spectroscopy, as well as mass spectrometry and elemental analysis.

The preparation of the ruthenium probe $[\text{Ru}(\text{CH}=\text{CHL}^{\text{PEG}})\text{Cl}(\text{CO})(\text{TBTD})(\text{PPh}_3)_2]$ (**8**) was first attempted from $[\text{RuHCl}(\text{CO})(\text{PPh}_3)_3]$ followed by the addition of the

TBTD ligand, as had been employed previously (*vide infra*). However, the need for repeated purification of the complex led to a low yield and so an alternative strategy was adopted. This approach (Scheme 3.4.4) involves generating $[M(\text{CH}=\text{CHL}^{\text{PEG}})(\text{CO})(\text{NCMe})_2(\text{PPh}_3)_2]^+$ from $[M\text{H}(\text{CO})(\text{NCMe})_2(\text{PPh}_3)_2]^+$ which can then be treated with a chloride source and the TBTD ligand to yield the desired products $[M(\text{CH}=\text{CHL}^{\text{PEG}})\text{Cl}(\text{CO})(\text{TBTD})(\text{PPh}_3)_2]$ ($M = \text{Ru}$ (**8**), Os (**9**)) in reasonably high yields (84% for **8** and 75% for **9**). New features were observed in the ^1H NMR spectrum at 3.29 (OMe), 3.46-3.70, 4.17, 5.08 (all OCH_2) and 6.92 (C_6H_4) ppm for the L^{PEG} substituent along with resonances at 6.08 (H_β) and 9.36 (H_α) ppm for the vinyl unit in **9**.



Scheme 3.4.3. Synthesis of water-soluble alkyne, $\text{HC}\equiv\text{CL}^{\text{PEG}}$.



Scheme 3.4.4. Preparation of water-soluble TBTD analogues. $M = \text{Ru}$ (**8**), Os (**9**).

By bubbling CO through methanol solutions of **8** and **9**, the dicarbonyl derivatives **8·CO** and **9·CO** were obtained and isolated as off-white solids. These were characterised using NMR and IR spectroscopy, mass spectrometry and elemental analysis.

Once the probes had been prepared and fully characterised, their solubility in water was tested. Due to the presence of the more hydrophilic vinyl ligand MCH=CHL^{PEG}, the water solubility of these probes was found to be significantly improved over complexes **3** - **7**. While 10⁻⁵ M solutions were stable over 24 h in phosphate buffered saline (PBS) aqueous solutions (pH 7.4), the formation of a fine precipitate was observed in much more concentrated solutions after some hours. However, by first dissolving the probes in acetone and then re-suspending them in the PBS solutions, stability was substantially improved.

PBS solutions of probes **8** and **9** (10⁻⁵ M, 0.1% acetone) were prepared and used in fluorescence titrations with CO (Figure 3.4.8). Both probes show an immediate and distinctive fluorescence enhancement due to the revival of the fluorescence of the TBTD ligand in solution, once dissociated from the quenching effect of the metal centre. As with the other vinyl complexes discussed herein, the displacement of the labile ligand produces an increase of the fluorescence emission, resulting in detection limits of approximately 1 ppb of CO. To confirm that the fluorescence enhancement resulted from the displacement of TBTD by CO rather than the instability of the complexes, the fluorescence spectra were run every 5 minutes in the presence and absence of CO over a 1 hour period. As no fluorescence enhancement was observed in the absence of CO, it can be concluded that the fluorescence response results from the presence of this gas in solution and not due to spontaneous release of the TBTD ligand in aqueous solution (e.g., through displacement by water molecules).

Although the cellular matrix is hard to reproduce, increasing concentrations of amino acids and heteroaromatic compounds (tryptophan, imidazole, etc.) were added to aqueous solutions of probes **8** and **9** in 20 µL aliquots, whilst the emission intensity was monitored. This experiment positively confirmed the selectivity of the probes towards CO as no increase in the TBTD luminescence was observed after the addition of these compounds (Figures 3.4.9 and S6-5).

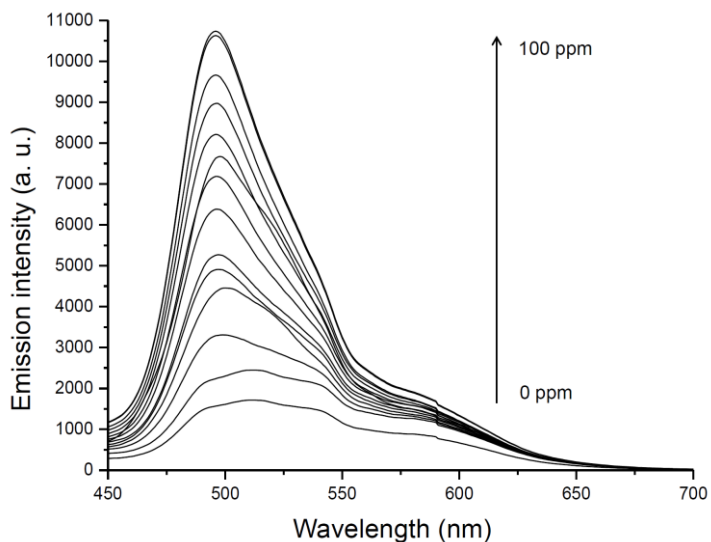


Figure 3.4.8. An 11-fold turn-on emission fluorescence was observed in the CO titration experiment using the probe $[\text{Os}(\text{CH}=\text{CHL}^{\text{PEG}})\text{Cl}(\text{CO})(\text{TBTD})(\text{PPh}_3)_2]$ (**9**) when 0 to 100 ppm of CO was bubbled through the PBS solution.

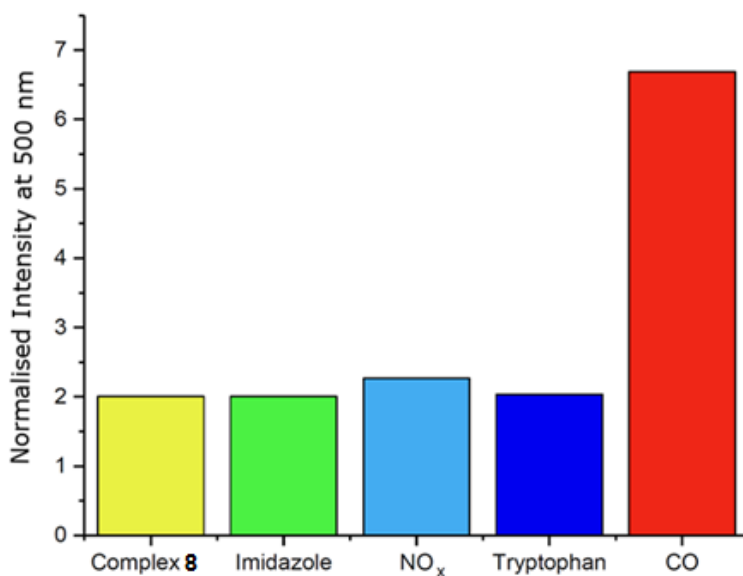


Figure 3.4.9. Normalised emission intensity ($\lambda_{\text{exc}} = 355 \text{ nm}$) of probe **8** in PBS (10^{-4} M) in the presence of various interferents (10^{-4} M imidazole, 10^{-4} M tryptophan, 50 ppm NO_x) and 200 ppm CO. Experimental details in Supporting Information (Figure S6-5).

These experiments successfully demonstrated the potential of complexes **8** and **9** for sensing CO in cells: The probes are a) sufficiently soluble in water, b) remarkably selective for CO, producing a remarkable fluorescence enhancement and c) emissive at higher wavelength than the range typical of protein emissions (250-400 nm). As discussed above, the three properties listed above are vitally important when designing probes for single-molecule imaging in cells and, in for these probes, they are all fulfilled. Before testing the fluorescence response of probes **8** and **9** in cells, their cytotoxicity was tested on the HeLa cervical cancer cell line using an MTT assay (Figure 3.4.10).

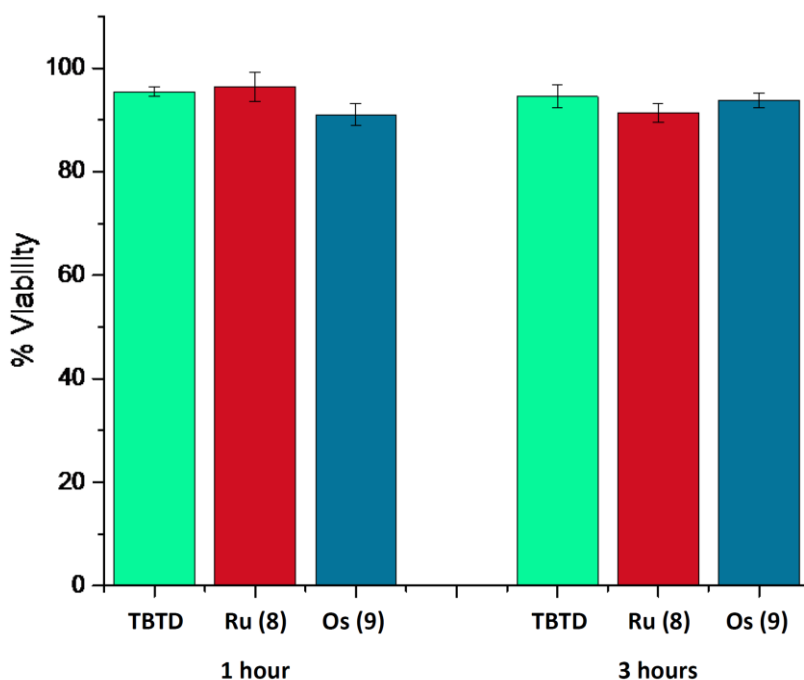


Figure 3.4.10. Percentage viability of HeLa cells with the TBTD ligand, $[\text{Ru}(\text{CH}=\text{CHL}^{\text{PEG}})\text{Cl}(\text{CO})(\text{TBTD})(\text{PPh}_3)_2]$ (**8**) and $[\text{Os}(\text{CH}=\text{CHL}^{\text{PEG}})\text{Cl}(\text{CO})(\text{TBTD})(\text{PPh}_3)_2]$ (**9**) at a concentration of 200 μM after 1 and 3 hours (data for 24 and 72 h, see Supporting Information, Figure S7-1).

The MTT assay reveals that all three compounds (TBTD, **8**, **9**) to be non-toxic at all concentrations tested (up to 200 μM) after incubations of 1 and 3 hours. After 24 hours, the cells show a lower degree of proliferation (80%) at high probe concentrations in comparison to shorter incubation times (further details provided in Supporting Information). Since the imaging of CO in cells would be completed within approximately 2 to 3 hours, these viability results suggest that there would be no significant cytotoxic effect from the probes themselves.

On the basis of these encouraging results, the probes $[\text{Ru}(\text{CH}=\text{CHL}^{\text{PEG}})\text{Cl}(\text{CO})(\text{TBTD})(\text{PPh}_3)_2]$ (**8**) and $[\text{Os}(\text{CH}=\text{CHL}^{\text{PEG}})\text{Cl}(\text{CO})(\text{TBTD})(\text{PPh}_3)_2]$ (**9**) were evaluated for the visualisation of changes in CO levels in live cells using confocal microscopy. The first challenge was to detect and quantify the levels of endogenous CO present in the cells. Thus, HeLa cells were incubated with the probes **8** and **9** (50 μM) and examined using the confocal microscope over a 1 hour period. According to the limit of detection determined from the CO titration experiments described above, any concentration of CO above 1 μM should be visible using the microscope, however, no clear fluorescence emission was observed (Figure 3.4.11). Although somewhat disappointing, this does confirm that the probes appear highly stable in the cellular medium as no release of the TBTD ligand was observed during the 3 hour measurement window. Incubation with TBTD on its own (100 μM) led to a distinct blue fluorescence.

In order to boost the amount of CO present in the cells, they were incubated with the well-known CO-releasing molecule, CORM-3 (50 μM) for 30 mins prior to imaging. This resulted in the blue emission of the TBTD ligand becoming visible as the CO generated triggers the release of the fluorescent TBTD ligand and the formation of the dicarbonyl complex **8**•CO. The experiment was also performed with the osmium analogue (**9**) and these images are included in Figure 3.4.11. Overall, these results show that, while purely endogenous CO cannot be determined, higher levels of CO produced by incubation with CORM-3 are visible through the fluorescence of the released TBTD ligand.

The detection of purely endogenous CO has also not been achieved in previous reports and so many leading studies^{18,20} used incubation with CORM-3 to test the ability of probes to detect the higher concentrations of CO released. In contrast to

this earlier work, however, HeLa cells incubated with CORM-3 for 30 mins exhibited the blue emission of the released TBTD ligand only a few minutes after addition of probes **8** or **9** with a remarkable dose-dependent emission increase. This should be compared with the slow response (60 mins) of the leading molecular probe reported by Chang.¹⁸ It can be seen that the higher the concentration of CORM-3 (and therefore CO) present, the higher the corresponding emission intensities that are measured. Despite these promising results, the release of TBTD can only be observed at relatively high concentrations of CORM-3 (above 50 μM), which are significantly higher than the expected levels of endogenous CO produced in cells.

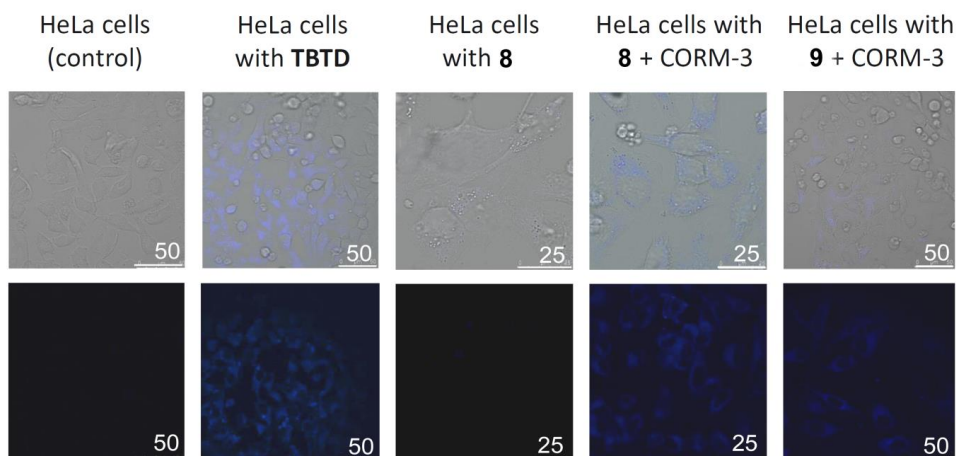


Figure 3.4.11. Microscopy images show HeLa cells in transmitted light (above) and confocal modes (below). Images show HeLa cells incubated only with TBTD (100 μM), only with probe **8** (50 μM) and with probe **8** and **9** (50 μM) with added CORM-3 (50 μM). Scales are in μm .

The low intensity of the emission observed is not only dependent on the fluorophore but is also related to the microscope settings. The lowest operating excitable wavelength of the confocal microscope used for this study was 405 nm, which is approximately 50 nm higher than the ideal excitation wavelength of the TBTD ligand. This resulted in only partial excitation of the fluorophore by the laser and therefore resulted in a lower degree of emission. Lower wavelength

excitation sources (350-370 nm) offered by wide-field microscopes equipped with suitable filters for selecting the optimal excitation wavelength will be employed in future experiments. It is hoped that this will lead to a much stronger emission, allowing the detection of endogenous CO.

Overall, the measured emission seems to be localised only in the cytoplasm, although this could not be ascertained unambiguously as common nuclei- and organelle-staining agents (e.g. DAPI or Hoescht stains) are also detected in the blue channel. Moreover, it is currently not clear whether the levels of endogenous CO cannot be visualised as a consequence of intrinsic limitations of the probes or due to the sub-optimal microscope settings. This will be elucidated in further work on these probes as part of the ongoing programme.

Crystallography

The complexes **6**, **7** and **6-CO** all adopt a slightly distorted octahedral structure [*cis*-interligand angles for **6** are between 83.55(7)-93.13(7)°]. In the complexes bearing the TBTD ligand, it is immediately noted that this ligand bonds to the metal through nitrogen N21 of the ligand, causing the thienyl unit to be closer to the phosphine ligands than if bonded through the other N-donor (N23). In the free ligand (TBTD, which exists as two independent units, hence two values for each bond), the S-N bond of the coordinated nitrogen [1.612(3) / 1.613(3) Å] lengthens on attachment to the metal [N(21)-S(22) 1.640(3) Å in **6**], while the C-N bond involving the N-donor does not change [N(21)-C(29) 1.352(4) in **6**]. The bond data for the vinyl ligand are largely unremarkable and compare well to previous related structures.^{9,10} However, it is worth noting the relatively long C=C bond length of the vinyl ligands [1.337(3) Å for compound **7**] compared to this distance in organic alkenes, which are typical around 1.21 Å.³² This elongation in the complexes can be attributed to the significant back-donation from the ruthenium d-orbitals into the π* orbitals of the C=C bonds.

The comparison of the crystal structures of the TBTD compounds, **6** and **7** with those of the BTD analogues^{9,10} shows no significant differences in both the bond lengths and bond angles of the ligands to the ruthenium centre. This suggests that the addition of the thienyl group to the BTD ligand does not affect the structure of

the metal complex and hence, the reactivity of the complex would be expected to remain similar. These structural data also proved very useful for the DFT modelling studies (*vide infra*).

Since structural data were obtained for both **6** and **6·CO**, the impact on the structure of the exchange of TBTD and CO ligands can be examined. Some reorganisation is apparent compared to the structure of **6**, with *cis*-interligand angles [87.13(6)-93.08(8)°] showing a narrower range and closer to the idealised 90° value. The impact of displacing the TBTD ligand with CO is most obvious in the Ru(1)-C(1) bond distance of the vinyl ligand, which increases from 2.055(3) Å in **6** to 2.120(3) Å in **6·CO**. With two carbonyl ligands in **6·CO**, the relative (*trans*) influence of the vinyl and chloride ligands can be seen with the ligand [Ru(1)-C(18) 1.849(3) Å] opposite the vinyl being substantially longer than the carbonyl resulting from CO addition [Ru(1)-C(17) 1.965(3) Å].

Computational studies

Using a DFT approach, three ruthenium vinyl complexes were modelled containing either a tolyl (**4**) or pyrenyl (**7**) moiety on the vinyl ligand as both the thienyl-BTD compounds (**4** and **7**) and CO bound (**4·CO** and **7·CO**) complexes. The compound **7·CO** had already been modelled in our earlier study.

The strong colours of the TBTD and BTD complexes originate from the HOMO-LUMO transition between the aromatic vinyl group and the TBTD chromophore, at approximately 634 nm for [Ru(CH=CHPyr-1)Cl(CO)(TBTD)(PPh₃)₂] (**7**), 607 nm for [Ru(CH=CHTol)Cl(CO)(TBTD)(PPh₃)₂] (**4**), 624 nm for [Ru(CH=CHPyr-1)Cl(CO)(BTD)(PPh₃)₂] (**7**) and 576 nm for [Ru(CH=CHPyr-1)Cl(CO)(BTD)(PPh₃)₂] (**7·CO**). As reported previously, all compounds lose this >500 nm transition upon coordination of CO and loss of TBTD or BTD.

Comparison of the predicted UV-Vis Spectra for compounds **7** and **7·CO** (Figure 3.4.12) shows little difference other than a slight increase in the intensity of the **7** spectra as well as a slight redshift of the coloured HOMO-LUMO transition, from 624 to 635 nm. Examining the molecular orbitals of **7** (in Table S8-1) the thienyl group can be seen participating in almost all important molecular orbitals, giving

an explanation for the redshift as well as increase in intensity of the compound fluorescence.

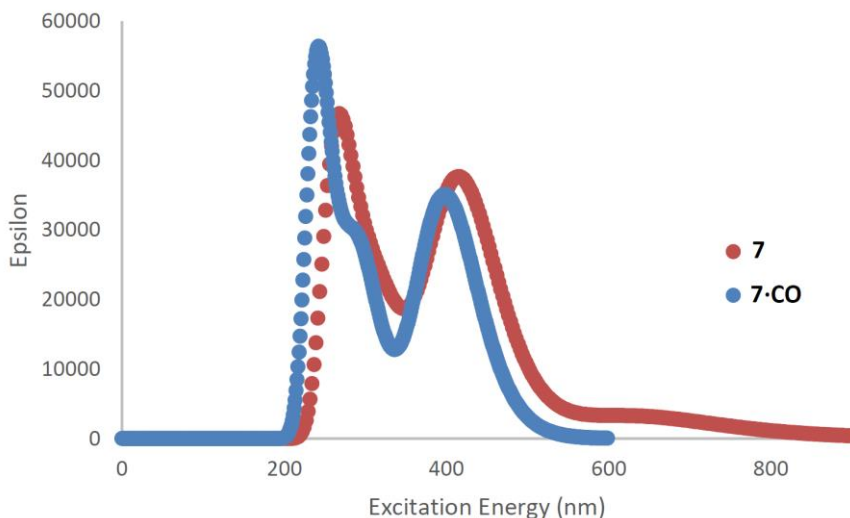


Figure 3.4.12. Comparison of calculated UV-Vis spectra of compounds $[\text{Ru}(\text{CH}=\text{CHPyr}-1)\text{Cl}(\text{CO})(\text{TBTD})(\text{PPh}_3)_2]$ (**7**) and $[\text{Ru}(\text{CH}=\text{CHPyr}-1)\text{Cl}(\text{CO})_2(\text{PPh}_3)_2]$ (**7·CO**).

In comparing predicted UV-Vis spectra for of $[\text{Ru}(\text{CH}=\text{CHTol})\text{Cl}(\text{CO})(\text{TBTD})(\text{PPh}_3)_2]$ (**4**) and $[\text{Ru}(\text{CH}=\text{CHPh})\text{Cl}(\text{CO})(\text{BTD})(\text{PPh}_3)_2]$ (**PhBTD**), shown in Figure 3.4.13, a similar increase in intensity and HOMO-LUMO redshift (575 to 607 nm) is observed with the presence of the thienyl group. Unlike for the pyrenylvinyl ligand, a new region of excitation at ca. 400 nm can be seen for **4**. Examining the molecular orbitals (Table S8-1), these new excitations can be attributed to the thienyl group.

The frontier orbitals have the characteristic of a push-pull system, with the pull ligand (vinyl) contributing to the HOMO and the push ligand (TBTD/BTD) contributing to the LUMO, each with some contribution from the metal. Qualitatively, the push of the TBTD system is greater than that of BTD alone. In addition, the push-pull characteristics between the two ligands are greater for the relatively electron poor tolylvinyl moiety (in comparison to the pyrenylvinyl derivative).

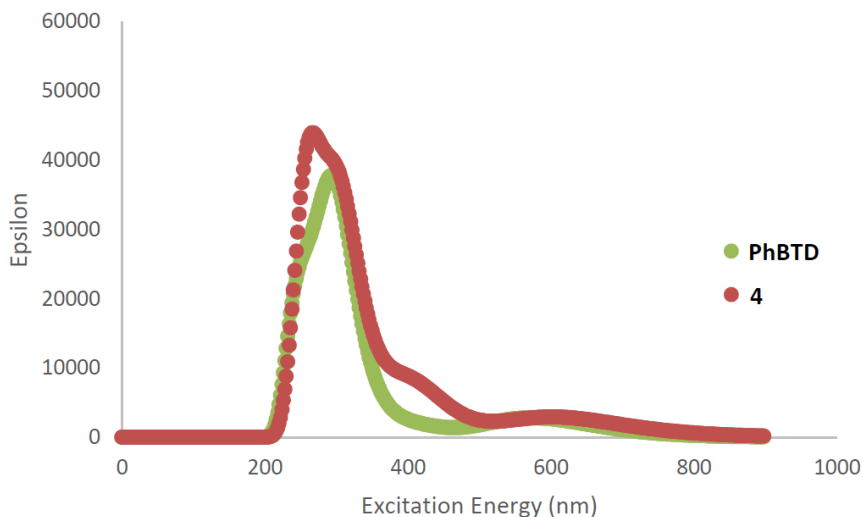


Figure 3.4.13. Comparison of calculated UV-Vis spectra of compounds $[\text{Ru}(\text{CH}=\text{CHTol})\text{Cl}(\text{CO})(\text{TBTD})(\text{PPh}_3)_2]$ (**4**) and $[\text{Ru}(\text{CH}=\text{CHPh})\text{Cl}(\text{CO})(\text{BTd})(\text{PPh}_3)_2]$ (**PhBTd**).

3.4.4. Conclusions

Only a few systems capable of dual chromo-fluorogenic sensing of carbon monoxide are known, with the most successful examples based on rhodium⁸ and ruthenium^{9,10} originating in our own laboratories. However, due to their solubility, these systems are not suited to use in aqueous media, precluding their application to sensing in cells. In contrast, systems based on palladium catalysed carbonylations¹⁸⁻²⁰ have proved effective in terms of solubility and sensitivity but have drawbacks such as relatively slow response times and potential cytotoxicity of the palladium species used.^{1a,21-23} Alternative, genetically-encoded approaches¹⁷ also suffer from the specialised synthetic protocol used and the signal to noise limitations due to background (auto)fluorescence of the proteins present. Therefore, new probes are needed which are straightforward to prepare and use and which display good sensitivity and selectivity towards CO in the challenging environment (for coordination compounds) of the cell.

In order to address these challenges, the new fluorescent ligand, **TBTD**, has been prepared and used to generate a series of probes of general formula

$[M(CH=CHR)Cl(CO)(TBTD)(PPh_3)_2]$ ($M = Ru, Os$). Two examples were structurally characterised, including a phenanthrenyl example, for which a structure of the corresponding dicarbonyl product after CO addition was also obtained. These structural data helped inform DFT calculations used to probe the sensing mechanism. The **TBTD** probes perform reasonably well, displaying chromogenic sensing behaviour comparable to the related BTD series.^{9,10} In contrast to the previous design, the incorporation of the fluorophore as the displaced ligand on CO coordination allows the substituent to the vinyl group to be modified to provide greater solubility in aqueous media through PEGylation. Using this approach, the sensing of CO in aqueous buffer solution is described along with the extension of this detection system to the challenges of the cellular environment. The suitability of the PEGylated probes for sensing in cells was screened using a cytotoxicity assay with HeLa cells, revealing them to be non-toxic. The carbon monoxide released by 50 μ M CORM-3 was successfully detected (apparently within the cell) through the blue emission of the released **TBTD** ligand after only a few minutes. This rapid, dose-dependent response illustrates the advantage of a sensing mechanism based on a direct displacement reaction of the CO with the metal centre, as opposed to fluorophore release through a carbonylation mechanism, which depends on metal-mediated catalysis at room temperature. The excitation wavelength of the confocal microscope used in this study was around 50 nm higher than the ideal excitation wavelength of the **TBTD** ligand. A better match of excitation to the fluorophore could enhance the magnitude of emission substantially. This will be explored in future experiments and could lead to the detection of endogenous CO through a stronger emission response.

3.4.5. Acknowledgements

The authors wish to express their gratitude to the Spanish Government (project MAT2012-38429-C04) and Generalitat Valenciana (project PROMETEOII/2014/047) for their support. C.M-H. thanks the Spanish Ministry of Economy and Competitiveness for her grant. The Leverhulme Trust is gratefully acknowledged for a studentship to A.T. (RPG-2012-634). The Imperial College

Global Engagements fund and the Santander Mobility Award Scheme is thanked by J.D.E.T.W.-E. for provision of travel grants.

Keywords

Sensing, carbon monoxide, ruthenium, osmium, alkenyl.

3.4.6. References

- 1 a) C. Marín-Hernández, A. Toscani, F. Sancenón, J. D. E. T. Wilton-Ely and R. Martínez-Máñez, *Chem. Commun.*, 2016, **52**, 5902-5911; b) M. Strianese and C. Pellecchia, *Coord. Chem. Rev.*, 2016, **318**, 16–28.
- 2 a) J. J. McGrath, *Inhalation Toxicology (Carbon Monoxide)*, 2nd ed. CRC, Boca Raton, 2006, p. 695; b) L. J. Wilkinson, *Molecules of Death (Carbon Monoxide—the Silent Killer)*, 2nd ed. Imperial College Press., London, 2007, 37; c) Waring, Steventon and Mitchell, *Molecules of Death*, Imperial College Press, London, 2007; d) R. Kalescky, E. Kraka and D. Cremer, *J. Phys. Chem. A*, 2013, **117**, 8981-8995
- 3 Carbon monoxide poisoning, NHS Choices, <http://www.nhs.uk/conditions/carbon-monoxide-poisoning/pages/introduction.aspx>.
- 4 R. Motterlini, L. Otterbein, *Nature Rev.*, 2010, **9**, 728-743; b) S. H. Heinemann, . Hoshi, M. Westerhausen, A. Schiller, *Chem. Commun.* 2014, **50**, 3644-3660; c) L. D. Prockop and R. I. Chichkova, *J. Neurol. Sci.*, 2007, **262**, 122–30.
- 5 a) S. García-Gallego and G. J. L. Bernardes, *Angew. Chem. Int. Ed.*, 2014, **53**, 9712-9721; b) B. E. Mann, *Organometallics*, 2012, **31**, 5728-5735.
- 6 K. K.-W. Lo and S. P.-Y. Li, *RSC Adv.*, 2014, **4**, 10560–10585.
- 7 C. W. Rogers and M. O. Wolf, *Coord. Chem. Rev.*, 2002, 233–234, 341–350.
- 8 a) J. Esteban, J. V. Ros-Lis, R. Martínez-Máñez, M. D. Marcos, M. E. Moragues, J. Soto and F. Sancenón, *Angew. Chem., Int. Ed.*, 2010, **49**, 4934-4937; b) M. E. Moragues, J. Esteban, J. V. Ros-Lis, R. Martínez-Máñez, M. D. Marcos, M. Martínez, J. Soto and F. Sancenón, *J. Am. Chem. Soc.*, 2011, **133**, 15762-15772; c) M. E. Moragues, R. Montes-Robles, J. Vicente Ros-Lis, M. Alcañiz, J. Ibáñez, T. Pardo and R. Martínez-Mañez, *Sens. Actuators B*, 2014, **191**, 257-263.
- 9 M. E. Moragues, A. Toscani, F. Sancenón, R. Martínez-Máñez, A. J. P. White and J. D. E. T. Wilton-Ely, *J. Am. Chem. Soc.*, 2014, **136**, 11930-11933.

- 10 A. Toscani, C. Marín-Hernández, M. E. Moragues, F. Sancenón, P. Dingwall, N. J. Brown, R. Martínez-Mañez, A. J. P. White and J. D. E. T. Wilton-Ely, *Chem. Eur. J.*, 2015, **21**, 14529-14538.
- 11 B. A. D. Neto, P. H. P. R. Carvalho, D. C. B. D. Santos, C. C. Gatto, L. M. Ramos, N. M. d. Vasconcelos, J. R. Correa, M. B.; Costa, H. C. B. de Oliveira, R. G., Silva, *RSC Advances* 2012, **2**, 1524-1532.
- 12 N. W. Alcock, A. F. Hill, M. S. Roe, *J. Chem. Soc., Dalton Trans.*, 1999, 1737-1740.
- 13 M. C. J. Harris, A. F. Hill, *Organometallics*, 1991, **10**, 3903-3906.
- 14 a) M. R. Torres, A. Vegas, A. Santos, J. Ros, *J. Organomet. Chem.*, 1986, **309**, 169-177; b) J. Maurer, M. Linseis, B. Sarkar, B. Schwederski, M. Niemayer, W. Kaim, S. Zális, C. Anson, M. Zabel, R. F. Winter, *J. Am. Chem. Soc.*, 2008, **130**, 259-268.
- 15 A. F. Hill, J. D. E. T. Wilton-Ely, *J. Chem. Soc., Dalton Trans.*, 1998, 3501-3510.
- 16 H. Loumrhari, J. Ros, M. R. Torres, A. Santos, A. M. Echavarren, *J. Organomet. Chem.*, 1991, **411**, 255-261.
- 17 J. Wang, J. Karpus, B. S. Zhao, Z. Luo, P. R. Chen and C. He, *Angew. Chem. Int. Ed.*, 2012, **51**, 9652-9656
- 18 B. W. Michel, A. R. Lippert and C. J. Chang, *J. Am. Chem. Soc.*, 2012, **134**, 15668-15671.
- 19 K. Zheng, W. Lin, L. Tan, H. Chen and H. Cui, *Chem. Sci.*, 2014, **5**, 3439-3448.
- 20 S. Pal, M. Mukherjee, B. Sen, S. K. Mandal, S. Lohar, P. Chattopadhyay and K. Dhara, *Chem. Commun.*, 2015, **51**, 4410-4413
- 21 K. K.-W. Lo and S. P.-Y. Li, *RSC Advances*, 2014, **4**, 10560-10585.
- 22 M.-L. Yeung and V.-W. Yam, in *Luminescent and Photoactive Transition Metal Complexes as Biomolecular Probes and Cellular Reagents*, ed. K. K.-W. Lo, Springer Berlin Heidelberg, 2015, vol. 165, pp. 109-129.
- 23 L. Yuan, W. Lin, L. Tan, K. Zheng and W. Huang, *Angew. Chem. Int. Ed.*, 2013, **52**, 1628-1630.
- 24 a) N. Pinault and D. W. Bruce, *Coord. Chem. Rev.*, 2003, **241**, 1-25; b) A. Andriollo, A. Bolívar, F. A. López and D. E. Páez, *Inorg. Chim. Acta*, 1995, **238**, 187-192; c) N. Fey, A. C. Tshipis, S. E. Harris, J. N. Harvey, A. G. Orpen, R. A., Mansson, *Chem. – A Eur. J.*, 2006, **12**, 291; d) D. J. Darensbourg and C. J. Bischoff, *Inorg. Chem.*, 1993, **32**, 47-53; e) E. Fache, C. Santini, F. Senocq and J. M. Basset, *J. Mol. Cat.*, 1992, **72**, 337-350; f) M. Saoud, A. Romerosa and M. Peruzzini, *Organometallics*, 2000, **19**, 4005-4007.
- 25 B. R. James and F. Lorenzini, *Coord. Chem. Rev.*, 2010, **254**, 420-430.
- 26 A. D. Phillips, L. Gonsalvi, A. Romerosa, F. Vizza and M. Peruzzini, *Coord. Chem. Rev.*, 2004, **248**, 955-993.

Chapter 3

- 27 a) J.-F. Lutz and Z. Zarafshani, *Adv. Drug Deliv. Rev.*, 2008, **60**, 958-970; b) H. C. Kolb and K. B. Sharpless, *Drug Discov. Today*, 2003, **8**, 1128-1137.
- 28 V. L. Hurtubise, J. M. McArdle, S. Naeem, A. Toscani, A. J. P. White, N. J. Long and J. D. E. T. Wilton-Ely, *Inorg. Chem.*, 2014, **53**, 11740-11748.
- 29 Y. H. Lin, L. Duclaux, F. González de Rivera, A. L. Thompson and J. D. E. T. Wilton-Ely, *Eur. J. Inorg. Chem.*, 2014, 2065-2072.
- 30 P. Patel, S. Naeem, A. J. P. White and J. D. E. T. Wilton-Ely, *RSC Adv.*, 2012, **2**, 999-1008.
- 31 T. L. Riss, R. A. Moravec, A. L. Niles, H. A. Benink, T. J. Worzella, and L. Minor, *Assay Guidance Manual [Internet]*, 2013, <http://www.ncbi.nlm.nih.gov/books/NBK144065/>.
- 32 F. H. Allen, O. Kennard, D. G. Watson, L. Brammer, A. G. Orpen, R. Taylor, *J. Chem. Soc., Perkin Trans.* 1987, S1.

SUPPORTING INFORMATION

Highly sensitive and selective molecular probes for chromo-fluorogenic sensing of carbon monoxide in air, aqueous solution and living cells

Anita Toscani, Cristina Marín-Hernández, Jonathan A. Robson, Elvin Chua,
Paul Dingwall, Andrew J. P. White, Félix Sancenón, Cristina de la Torre,
Ramón Martínez-Máñez,* and James D. E. T. Wilton-Ely.*

S1. General considerations regarding starting materials and equipment

The compounds $[\text{RuHCl}(\text{CO})(\text{PPh}_3)_3]$,^{S1} $[\text{RuHCl}(\text{CO})(\text{BTD})(\text{PPh}_3)_3]$,^{S2} $[\text{OsHCl}(\text{CO})(\text{PPh}_3)_3]$,^{S3} $[\text{RuH}(\text{NCMe})_2(\text{CO})(\text{PPh}_3)_2]\text{BF}_4$,^{S4} $[\text{OsH}(\text{NCMe})_2(\text{CO})(\text{PPh}_3)_2]\text{ClO}_4$,^{S4} $[\text{OsHCl}(\text{CO})(\text{BTD})(\text{PPh}_3)_2]$,^{S5} $[\text{Ru}(\text{CH}=\text{CHPh})\text{Cl}(\text{CO})(\text{PPh}_3)_2]$,^{S6} $[\text{Ru}(\text{CH}=\text{CHC}_6\text{H}_4\text{Me-4})\text{Cl}(\text{CO})(\text{PPh}_3)_2]$,^{S7} $[\text{Ru}(\text{CH}=\text{CHPyr-1})\text{Cl}(\text{CO})(\text{PPh}_3)_2]$,^{S8} $[\text{Ru}(\text{CH}=\text{CHPh})\text{Cl}(\text{CO})_2(\text{PPh}_3)_2]$ (**3•CO**),^{S9} $[\text{Ru}(\text{CH}=\text{CHC}_6\text{H}_4\text{Me-4})\text{Cl}(\text{CO})_2(\text{PPh}_3)_2]$ (**4•CO**),^{S10} $[\text{Ru}(\text{CH}=\text{CHNap-2-OMe-6})\text{Cl}(\text{CO})_2(\text{PPh}_3)_2]$ (**5•CO**),^{S10} $[\text{Ru}(\text{CH}=\text{CHPhen-9})\text{Cl}(\text{CO})_2(\text{PPh}_3)_2]$ (**6•CO**),^{S10} $[\text{Ru}(\text{CH}=\text{CHPyr-1})\text{Cl}(\text{CO})_2(\text{PPh}_3)_2]$ (**7•CO**),^{S10,S11} were prepared according to published procedures. The ligand $\text{HC}\equiv\text{CL}^{\text{PEG}}$ was prepared using an adapted literature procedure.^{S12}

All other chemicals and solvents were purchased from Alfa-Aesar, Sigma-Aldrich and VWR and were used without further purification, unless otherwise stated. Solvents used for UV-Vis and fluorescence measurements were thoroughly degassed with nitrogen before use. All experiments and manipulations of compounds were conducted in air, unless otherwise specified. The commercially-available carbon monoxide lecture bottle (N3.7, purity 99.97%, with a CONCOA 302 – 2322 – CGA180 single-stage regulator) and sulfur dioxide lecture bottle (N3.7, purity 99.9%) were purchased from CK Special Gases Limited and were used for the titration experiments. The gases used as interferents in this work were generated *in situ* according to standard protocols (see Section S4). These procedures provided materials of sufficient purity for synthetic and spectroscopic purposes. All moisture and oxygen sensitive compounds were prepared using standard Schlenk line and cannula techniques. Solvent mixtures are volume/volume mixtures. Solvents used in the reactions of oxygen and moisture sensitive compounds were dried and degassed according to standard techniques. Toluene was dried by passage through a column containing 3 Å molecular sieves. Triethylamine was distilled under nitrogen over calcium hydride after passing through 4 Å molecular sieves. Petroleum ether refers to the fraction boiling in the range 40-60 °C. Waters LCT Premier ES-ToF (ESI) and a Micromass Autospec Premier (LSIMS) spectrometer were used for electrospray and high-resolution

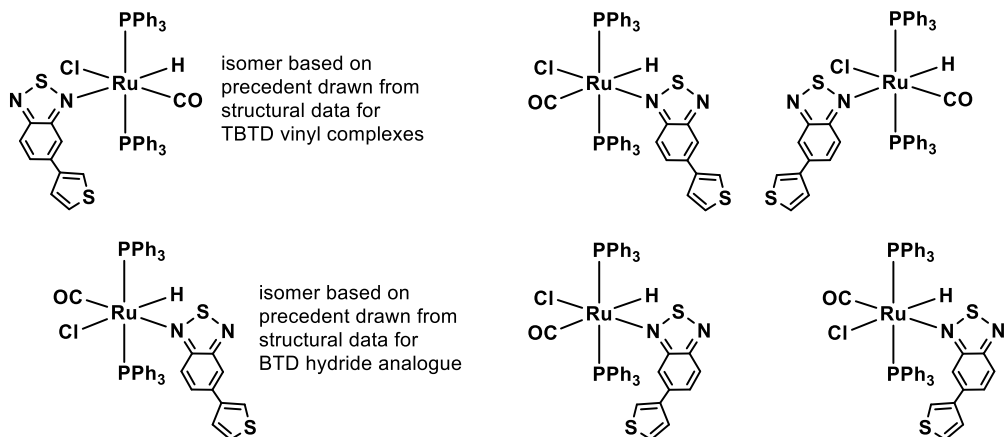
mass spectra (accurate mass mode). Further mass spectra analyses were performed at the Servei d'Espectrometria de Masses of the Universitat de València, Spain, on a Quadrupole time of flight (QqTOF) 5600 system (Applied Biosystems-MDS Sciex) spectrometer for high resolution mass spectra. The HRMS was operated in positive mode under the following conditions: Gas1 35 psi, GS2 35, CUR 25, temperature 450 °C, ion spray, voltage 5500 V. Standard FTIR spectra were measured using a Perkin Elmer Spectrum GX spectrometer. UV-Vis spectra were recorded with a Perkin Elmer Lambda-20 (Imperial College) and a Jasco V-650 (Polytechnic University of Valencia) spectrophotometer equipped with a diffuse reflectance sphere (model ISV-722) for diffuse reflectance. In the latter case, measurements were conducted at room temperature over a wavelength range of 350-800 nm with 1 nm wavelength step. Fluorescence measurements in solution were carried out using a Jasco FP-8500 (Polytechnic University of Valencia) and Agilent (Varian) Cary Eclipse (Imperial College London) spectrofluorimeters. Fluorescence measurements on solids were carried out with a Jasco FP-8500 (Polytechnic University of Valencia) fitted with a powder sample cell block (model JASCO FPA-810). Fluorescence lifetimes were measured at the Polytechnic University of Valencia using a EasyLife™ fluorescence lifetime fluorimeter equipped with a 340 nm NanoLED pulsed diode (nanosecond excitation pulses – spectral bandwidth of 2 – 10 nm). Fluorescence quantum yields Φ were determined by the comparative method^{S13} using [Ru(bpy)₃]²⁺ and perylene as fluorescence standards. For the experiments with the gases, a gas mixer was connected to carbon monoxide and argon cylinders to afford CO/Ar mixtures at different ratios. The gases were purged at different flow rates (0 – 200 mL/min). Carbon monoxide concentrations were measured using an ambient carbon monoxide analyzer (Testo 315-2 model 0632 0317), properly validated with an ISO calibration certificate issued by Instrumentos Testo, Cabrilis (Spain). NMR spectroscopy was performed at 25°C using a Bruker AV400 or 500MHz spectrometers at room temperature in CD₂Cl₂ unless otherwise stated. ¹H NMR and ¹³C NMR chemical shifts (δ) were referenced to the residual non-deuterated solvent signal and the ¹³C signal of the deuterated solvent respectively. The deuterated solvents were all purchased from Sigma Aldrich. ³¹P{¹H} NMR chemical

shifts were referenced externally to H_3PO_4 85% in H_2O respectively and were all proton decoupled. NMR spectra for air sensitive compounds were recorded under a nitrogen atmosphere with suitable Young's tap NMR tube.

S2. Experimental details for new compounds

5-(3-thienyl)-2,1,3-benzothiadiazole (TBTD)

Under nitrogen, 5-Bromo-2,1,3-Benzothiadiazole (300 mg, 1.395 mmol) and $[\text{Pd}(\text{PPh}_3)_4]$ (240 mg, 0.208 mmol) were dissolved in dry, degassed 1,4-dioxane (25 mL) and the resulting yellow solution was stirred at room temperature for 15 min. Initially, the yellow solution became first red and then orange after few minutes. A degassed, aqueous solution of Na_2CO_3 (10 mL, 2.0 mol L^{-1}) was then added, and the resulting orange suspension was heated at reflux for 10 min. After the addition of 3-thienylboronic acid (210 mg, 1.640 mmol) in 1,4-dioxane (10 mL), the mixture was left to stir at reflux for 24 h. The resulting brown solution was cooled and washed with deionised water (3 x 30 mL), dried over Na_2SO_4 and filtered. The pale brown solution was freed of volatiles under vacuum. Silica column chromatography (98% petroleum ether, 2% ethyl acetate) was then performed to purify the oily brown crude product to afford a bright yellow solid (140 mg, 46%). IR ($\nu_{\text{max}}/\text{cm}^{-1}$): 3096, 1608, 1516, 1387, 1259, 1019, 821, 776. ^1H NMR (CDCl_3): δ_{H} 7.50 (dd, $J_{\text{HH}} = 5.1, 2.9$ Hz, 1H, thienyl-CH), 7.55 (dd, $J_{\text{HH}} = 5.1, 1.4$ Hz, 1H, thienyl-CH), 7.68 (m, 1H, thienyl-CH), 7.94 (dd, $J_{\text{HH}} = 9.1, 1.7$ Hz, 1H, C_6H_3 -CH), 8.05 (d, $J_{\text{HH}} = 9.1$ Hz, 1H, C_6H_3 -CH), 8.20 (m, 1H, C_6H_3 -CH) ppm. $^{13}\text{C}\{^1\text{H}\}$ NMR (CDCl_3): δ_{C} 155.5, 154.1, 140.7, 136.9 (s x 4, C-quaternary), 129.7, 127.1, 126.3, 122.4, 121.6, 117.3 (s x 6, C-H) ppm. MS (ES +ve) m/z (abundance): 218 (100) $[\text{M}]^+$. Calculated for $\text{C}_{10}\text{H}_6\text{N}_2\text{S}_2$: C 55.0, H 2.8, N 12.8%. Found: C 55.2, H 2.7, N 12.7%.

[RuHCl(CO)(TBTD)(PPh₃)₂] – mixture of two isomers**Figure S2-1.** Possible isomers for [RuHCl(CO)(TBTD)(PPh₃)₂].**[Ru(CH=CHNap-2-OMe-6)Cl(CO)(PPh₃)₂] (1)**

[RuHCl(CO)(PPh₃)₃] (95.3 mg, 0.100 mmol) was dissolved in dichloromethane (20 mL) and treated with 2-ethynyl-6-methoxynaphthalene (20.0 mg, 0.110 mmol) to form a bright red solution. After stirring at room temperature for 15 min, the solvent was removed under vacuum. The resulting powder was suspended in diethyl ether (10 mL) and triturated for a few minutes in an ultrasound bath. The resulting pale red product was collected by filtration, washed with diethyl ether (20 mL) and dried (85.5 mg, 98%). IR ($\nu_{\max}/\text{cm}^{-1}$): 2976, 1921 (CO), 1629, 1600 (C=C), 1563, 1434, 1091. ¹H NMR (CD₂Cl₂): δ_{H} 3.91 (s, 3H, OMe), 5.75 (dt, $J_{\text{HH}} = 14.3$ Hz, $J_{\text{HP}} = 1.9$ Hz, 1H, H β), 5.75 (dt, $J_{\text{HH}} = 14.3$ Hz, $J_{\text{HP}} = 1.9$ Hz, 1H, H β), 6.98 – 7.17 (m, 4H, naphthyl), 7.29 – 7.81 (m, 30H + 2H, PPh₃ + naphthyl), 8.44 (dt, $J_{\text{HH}} = 14.3$ Hz, $J_{\text{HP}} = \text{unresolved}$, 1H, H α) ppm. ³¹P{¹H} NMR (CD₂Cl₂): δ_{P} 29.5 (s, PPh₃) ppm. MS (ES +ve) m/z (abundance): 878 (100) [M]⁺. Calculated for C₅₀H₄₁ClO₂P₂Ru: C 68.8, H 4.7%. Found: C 68.7, H 4.8%.

[Ru(CH=CHPhen-9)Cl(CO)(PPh₃)₂] (2)

[RuHCl(CO)(PPh₃)₃] (500 mg, 0.525 mmol) was dissolved in dichloromethane (20 mL) and treated with 9-ethynylphenanthrene (140 mg, 0.690 mmol) to form a bright red solution. After stirring at room temperature for 15 min, the solvent was removed under vacuum. The resulting powder was suspended in diethyl ether (10 mL) and triturated for a few minutes in an ultrasound bath and the orange product was then collected by filtration. It was washed with diethyl ether (20 mL) and dried (450 mg, 96%). IR ($\nu_{\max}/\text{cm}^{-1}$): 2974, 1934 (CO), 1555 (C=C), 1480, 1433, 1093. ¹H NMR (CD₂Cl₂): δ_{H} 6.54 (dt, $J_{\text{HH}} = 12.8$ Hz, $J_{\text{HP}} = \text{unresolved}$, 1H, H β), 6.89 (s, 1H, phenanthrenyl), 7.41 – 7.71 (m, 30H + 6H, PPh₃ + phenanthrenyl), 8.54 (dt, $J_{\text{HH}} = 12.8$ Hz, $J_{\text{HP}} = 2.1$ Hz, 1H, H α), 8.58 – 8.62 (m, 1H, phenanthrenyl), 8.66 (d, $J_{\text{HH}} = 8.2$ Hz, 1H, phenanthrenyl) ppm. ³¹P{¹H} NMR (CD₂Cl₂): δ_{P} 30.9 (s, PPh₃) ppm. MS (ES +ve) m/z (abundance): 898 (100) [M]⁺. Calculated for C₅₃H₄₁ClOP₂Ru: C 71.3, H 4.6%. Found: C 71.2, H 4.5%.

[Ru(CH=CHPh)Cl(CO)(TBTD)(PPh₃)₂] (3)

A dichloromethane solution (10 mL) of [Ru(CH=CHPh)Cl(CO)(PPh₃)₂] (50.0 mg, 0.063 mmol) was treated with a slight excess of TBTD (15.1 mg, 0.069 mmol), and the reaction mixture was stirred at room temperature for 30 min. The solvent was removed under vacuum and the resulting red product was triturated with petroleum ether (10 mL) for 10 min and then filtered. The resulting bright red solid was washed with more petroleum ether (3 mL) and dried (44.2 mg, 69%). IR ($\nu_{\max}/\text{cm}^{-1}$): 2918, 1908 (CO), 1609, 1579 (C=C), 1481, 1433, 1090. ¹H NMR (CD₂Cl₂): δ_{H} 5.89 (d, $J_{\text{HH}} = 16.1$ Hz, 1H, H β), 6.93 (d, $J_{\text{HH}} = 7.3$ Hz, 2H, *o*-C₆H₅), 6.99 (t, $J_{\text{HH}} = 7.3$ Hz, 1H, *p*-C₆H₅), 7.17, 7.29, 7.49 (m, 30H + 2H, PPh₃ + *m*-C₆H₅), 7.59 (m, 2H, TBTD), 7.75 (t, $J_{\text{HH}} = 2.1$ Hz, 1H, TBTD), 7.88 (s, 2H, TBTD), 8.27 (s(br), 1H, TBTD), 8.73 (dt, $J_{\text{HH}} = 16.1$ Hz, $J_{\text{HP}} = 3.0$ Hz, 1H, H α) ppm. ³¹P{¹H} NMR (CD₂Cl₂): δ_{P} 26.3 (s, PPh₃) ppm. MS (ES +ve) m/z (abundance): 1068 (2) [M + H₂O + K]⁺, 798 (100) [M – TBTD]⁺. Calculated for C₅₅H₄₃ClN₂OP₂RuS₂: C 65.4, H 4.3, N 2.8%. Found: C 65.3, H 4.2, N 2.9%.

[Ru(CH=CHC₆H₄Me-4)Cl(CO)(TBTD)(PPh₃)₂] (4)

A dichloromethane solution (10 mL) of [Ru(CH=CHC₆H₄Me-4)Cl(CO)(PPh₃)₂] (75.0 mg, 0.093 mmol), was treated with a slight excess of TBTD (22.3 mg, 0.102 mmol), and the reaction mixture was stirred at room temperature for 30 min. All solvent was subsequently removed under vacuum and petroleum ether (10 mL) was added. The crude product was triturated for 10 min. and filtered to yield an orange solid (80.4 mg, 84%). IR ($\nu_{\max}/\text{cm}^{-1}$): 2955, 1909 (CO), 1608, 1572 (C=C), 1481, 1432, 1090. ¹H NMR (CD₂Cl₂): δ_{H} 2.29 (s, 3H, CH₃), 5.83 (d, $J_{\text{HH}} = 16.2$ Hz, 1H, H _{β}), 6.84, 6.99 (AB, 2 x 2H, $J_{\text{AB}} = 7.7$ Hz, C₆H₄), 7.16, 7.29, 7.49 (m x 3, 30H, C₆H₅), 7.58 (m, 2H, TBTD), 7.75 (t, $J_{\text{HH}} = 2.1$ Hz, 1H, TBTD), 7.87 (s, 2H, TBTD), 8.27 (s(br), 1H, TBTD), 8.61 (dt, $J_{\text{HH}} = 16.2$ Hz, $J_{\text{HP}} = 3.1$ Hz, 1H, H _{α}) ppm. ¹³C{¹H} NMR (CD₂Cl₂): δ_{C} 204.5 (t, CO, $J_{\text{PC}} = 14.1$ Hz), 155.1, 154.1 (s x 2, quaternary^{TBTD}), 150.4 (t, C _{α} , $J_{\text{PC}} = 13.1$ Hz), 140.7 (s, quaternary^{TBTD}), 138.6 (s, C _{β}), 138.3 (s, C¹-C₆H₄), 136.8 (s, quaternary^{TBTD}), 134.4 (t^v, *o/m*-C₆H₅, $J_{\text{PC}} = 5.0$ Hz), 133.9 (s, C⁴-C₆H₄), 132.4 (t^v, *ipso*-C₆H₅, $J_{\text{PC}} = 20.9$ Hz), 129.9 (s, *p*-C₆H₅), 129.2 (s, C-H^{TBTD}), 129.0 (s, C^{2,6}-C₆H₄), 127.8 (t^v, *o/m*-C₆H₅, $J_{\text{PC}} = 4.3$ Hz), 127.7 (s, C-H^{TBTD}), 126.4 (s, C-H^{TBTD}), 124.4 (s, C^{2,6}-C₆H₄), 123.0 (s, C-H^{TBTD}), 122.1 (s(br), C-H^{TBTD}), 117.0 (s, C-H^{TBTD}), 21.0 (s, CH₃) ppm. ³¹P{¹H} NMR (CD₂Cl₂): δ_{P} 26.2 (s, PPh₃) ppm. MS (ES +ve) *m/z* (abundance): 1024 (3) [M]⁺, 812 (100) [M – TBTD]⁺. Calculated for C₅₆H₄₅ClN₂OP₂RuS₂: C 65.6, H 4.4, N 2.7%. Found: C 65.5, H 4.3, N 2.8%.

[Ru(CH=CHNap-2-OMe-6)Cl(CO)(TBTD)(PPh₃)₂] (5)

A dichloromethane solution (10 mL) of [Ru(CH=CHNap-2-OMe-6)Cl(CO)(PPh₃)₂] (50.0 mg, 0.057 mmol), was treated with a slight excess of TBTD (13.7 mg, 0.063 mmol), and the reaction mixture was stirred at room temperature for 30 min. The solvent was removed under vacuum and diethyl ether (10 mL) was added to the crude product. The resulting red solid was triturated for 10 min. and then filtered and dried (44.7 mg, 72%). IR ($\nu_{\max}/\text{cm}^{-1}$): 2935, 1925 (CO), 1601, 1552 (C=C), 1432, 1089. ¹H NMR (CD₂Cl₂): δ_{H} 3.92 (s, 3H, OMe), 6.01 (d, $J_{\text{HH}} = 16.1$ Hz, 1H, H _{β}), 7.06 (m, 3H, naphthyl), 7.18 (m, 12H, PPh₃), 7.24 (d, $J_{\text{HH}} = 7.8$ Hz 1H, naphthyl), 7.30, 7.52 (m x 2, 18H + 1H, PPh₃ + naphthyl), 7.57 – 7.62 (m, 2H + 1H, TBTD + naphthyl), 7.76 (t, $J_{\text{HH}} = 2.1$ Hz, 1H, TBTD), 7.88 (s, 2H, TBTD), 8.28 (s(br), 1H,

TBTD), 8.78 (dt, $J_{\text{HH}} = 16.1$ Hz, $J_{\text{HP}} = 3.2$ Hz, 1H, H α) ppm. $^{31}\text{P}\{^1\text{H}\}$ NMR (CD_2Cl_2): δ_{P} 26.3 (s, PPh_3) ppm. MS (ES +ve) m/z (abundance): 1085 (5) $[\text{M} - \text{CO} + \text{Na}]^+$, 878 (100) $[\text{M} - \text{TBTD}]^+$. Calculated for $\text{C}_{60}\text{H}_{47}\text{ClN}_2\text{O}_2\text{P}_2\text{RuS}_2$: C 66.1, H 4.3, N 2.6%. Found: C 66.0, H 4.2, N 2.7%.

[Ru(CH=CHPhen-9)Cl(CO)(TBTD)(PPh₃)₂] (6)

A dichloromethane solution (10 mL) of $[\text{Ru}(\text{CH}=\text{CHPhen-9})\text{Cl}(\text{CO})(\text{PPh}_3)_2]$ (50.0 mg, 0.056 mmol) was treated with a slight excess of TBTD (13.4 mg, 0.061 mmol). The reaction mixture was then stirred at room temperature for 30 min. The solvent was removed under vacuum and diethyl ether (10 mL) was added to the crude product. The resulting red solid was triturated for 10 min. and then filtered and dried (41.0 mg, 66%). IR ($\nu_{\text{max}}/\text{cm}^{-1}$): 2972, 1912 (CO), 1609, 1544 (C=C), 1481, 1432, 1089. ^1H NMR (CD_2Cl_2): δ_{H} 6.85 (d, $J_{\text{HH}} = 15.5$ Hz, 1H, H β), 7.15 (s, 1H, phenanthrenyl), 7.20, 7.33 (m x 2, 18H, PPh_3), 7.45 (m, 1H, phenanthrenyl), 7.54 – 7.67 (m, 12H + 4H + 2H, PPh_3 + phenanthrenyl + TBTD), 7.77 (m, 1H, TBTD), 7.89 (m, 2H, TBTD), 8.30 (s(br), 1H, TBTD), 8.61 (m, 1H, phenanthrenyl), 8.68 (d, $J_{\text{HH}} = 7.9$ Hz, 1H, phenanthrenyl), 8.93 (dt, $J_{\text{HH}} = 15.5$ Hz, $J_{\text{HP}} = 3.1$ Hz, 1H, H α) ppm. $^{31}\text{P}\{^1\text{H}\}$ NMR (CD_2Cl_2): δ_{P} 26.6 (s, PPh_3) ppm. MS (ES +ve) m/z (abundance): 1111 (5) $[\text{M}]^+$. Calculated for $\text{C}_{63}\text{H}_{47}\text{ClN}_2\text{OP}_2\text{RuS}_2 \cdot 0.25\text{CH}_2\text{Cl}_2$: C 67.1, H 4.2, N 2.5%. Found: C 67.2, H 4.1, N 2.9%.

[Ru(CH=CHPyr-1)Cl(CO)(TBTD)(PPh₃)₂] (7)

A dichloromethane solution (10 mL) of $[\text{Ru}(\text{CH}=\text{CHPyr-1})\text{Cl}(\text{CO})(\text{PPh}_3)_2]$ (75.0 mg, 0.081 mmol), was treated with a slight excess of TBTD (19.6 mg, 0.090 mmol) and the reaction mixture was stirred at room temperature for 30 min. The solvent was removed under vacuum and diethyl ether (10 mL) was added to the crude product. The resulting orange solid was triturated for 10 min. and then filtered and dried (76.0 mg, 82%). IR ($\nu_{\text{max}}/\text{cm}^{-1}$): 3056, 1920 (CO), 1607, 1555 (C=C), 1481, 1432, 1089. ^1H NMR (CD_2Cl_2): δ_{H} 7.17 (m, 12H + 1H, PPh_3 + H β), 7.30 (m, 6H, PPh_3), 7.54 – 7.59 (m, 12H, PPh_3), 7.63 (m, 2H, TBTD), 7.78 (m, 1H, TBTD), 7.82 – 7.87 (m, 2H, pyrenyl), 7.90 (s, 2H, TBTD), 7.92 – 8.02 (m, 5H, pyrenyl), 8.12 (d, $J_{\text{HH}} = 8.0$ Hz,

2H, pyrenyl), 8.33 (s(br), 1H, TBTD), 9.22 (dt, $J_{\text{HH}} = 16.0$ Hz, $J_{\text{HP}} = 3.1$ Hz, 1H, H α) ppm. $^{31}\text{P}\{^1\text{H}\}$ NMR (CD_2Cl_2): δ_{P} 26.2 (s, PPh_3) ppm. MS (ES +ve) m/z (abundance): 1157 (2) $[\text{M} + \text{Na}]^+$, 922 (100) $[\text{M} - \text{TBTD}]^+$. Calculated for $\text{C}_{65}\text{H}_{47}\text{ClN}_2\text{OP}_2\text{RuS}_2$: C 68.8, H 4.2, N 2.5%. Found: C 68.7, H 4.1, N 2.6%.

4-ethynylbenzyl-O-[2-(2-Methoxyethoxy)ethoxy]ethanoate ($\text{HC}\equiv\text{CL}^{\text{PEG}}$)

Under a nitrogen atmosphere, 2-[2-(2-methoxyethoxy)ethoxy]acetic acid (623 μL , 723 mg, 4.06 mmol) was dissolved in dry, degassed dichloromethane (25 mL) and the solution was cooled to 0 °C with an ice bath. *N,N'*-dicyclohexylcarbodiimide [DCC] (838 mg, 4.06 mmol) was added as a dichloromethane solution (10 mL). A second dichloromethane (25 mL) solution of 4-ethynylbenzyl alcohol (537 mg, 4.06 mmol) and 4-dimethylaminopyridine [DMAP] (94 mg, 0.77 mmol) was slowly added dropwise via a cannula, resulting in a cloudy yellow mixture. After the addition, the reaction mixture was stirred for 1 hour at 0 °C and then at room temperature overnight. Successively, the mixture was filtered through Celite in order to remove the resulting insoluble salts and the yellow filtrate was freed of volatiles under vacuum to provide a pale yellow oil (405 mg, 34%). IR ($\nu_{\text{max}}/\text{cm}^{-1}$): 1752 (CO), 1196, 1104, 847, 821. ^1H NMR (CDCl_3): δ_{H} 3.11 (s, $\text{C}\equiv\text{CH}$), 3.39 (s, 3H, OMe), 3.56, 3.66, 3.71, 3.77 (m x 4, 4 x 2H, OCH_2), 4.23 (s, 2H, $\text{OCH}_2\text{C}_6\text{H}_4$), 5.19 (s, 2H, $\text{C}(=\text{O})\text{CH}_2$), 7.33, 7.50 (AB, $J_{\text{AB}} = 8.0$ Hz, 4H, C_6H_4) ppm. $^{13}\text{C}\{^1\text{H}\}$ NMR (CDCl_3): δ_{C} 170.3 (s, C=O), 136.1 (s, $\text{C}^{1/4}\text{-C}_6\text{H}_4$) 132.3, 128.2 (s x 2, $\text{C}^{2/3}\text{-C}_6\text{H}_4$), 122.2 (s, $\text{C}^{1/4}\text{-C}_6\text{H}_4$), 83.2 (s, $\text{HC}\equiv\text{C}$), 77.8 (s, $\text{HC}\equiv\text{C}$), 71.9, 70.9, 70.7, 70.6 (s x 4, OCH_2), 68.7 ($\text{C}(=\text{O})\text{CH}_2$), 65.9 (s, $\text{OCH}_2\text{C}_6\text{H}_4$), 59.1 (OCH_3) ppm. MS (ES +ve) m/z (abundance): 293 (10) $[\text{M} + \text{H}]^+$, 310 (70) $[\text{M} + \text{H}_2\text{O}]^+$, 315 (100) $[\text{M} + \text{Na}]^+$. HRMS: 315.1208 (calculated), 312.1200 (found) corresponding to $\text{C}_{16}\text{H}_{20}\text{O}_5\text{Na}$. Calculated for $\text{C}_{16}\text{H}_{20}\text{O}_5$: C 65.7, H 6.9%. Found: C 65.8, H 6.7%.

$[\text{Ru}(\text{CH}=\text{CHL}^{\text{PEG}})\text{Cl}(\text{CO})(\text{TBTD})(\text{PPh}_3)_2]$ (8)

Under nitrogen, $[\text{RuH}(\text{CO})(\text{NCMe})_2(\text{PPh}_3)_2]\text{BF}_4$ (120 mg, 0.146 mmol) was dissolved in dry, degassed dichloromethane (10 mL). To this was added $\text{HC}\equiv\text{CL}^{\text{PEG}}$ (54 μL , 50 mg, 0.17 mmol) and the resulting pale yellow solution was stirred for 10 min. Then, $[\text{Et}_4\text{N}]\text{Cl}$ (37 mg, 0.22 mmol) was added as a methanolic solution (3 mL)

and the mixture was vigorously stirred for 15 minutes at 40 °C. All solvent was removed under reduced pressure (vacuum line) and dry, degassed dichloromethane (5 mL) was then added to dissolve the orange solid. In order to remove insoluble inorganic salts, the bright orange solution was filtered by cannula and a dry, degassed dichloromethane (5 mL) solution of TBTD (37 mg, 0.17 mmol) was added to afford a dark red solution, which was stirred for 15 min. at room temperature. The solvent was removed under vacuum and the red solid was recrystallised from a mixture of diethyl ether (3 mL) and petroleum ether (4 mL), filtered and dried (148 mg, 84%). IR ($\nu_{\max}/\text{cm}^{-1}$): 1946 (CO), 1750 (C=O), 1463, 1482, 1434, 1086, 849, 790. ^1H NMR (acetone- d_6): δ_{H} 3.29 (s, 3H, OMe), 3.53, 3.57, 3.62, 3.70 (m x 4, 4 x 2H, OCH₂), 4.18 (s, 2H, OCH₂C₆H₄), 5.07 (s, 2H, C(=O)CH₂O), 5.94 (d, $J_{\text{HH}} = 16.3$ Hz, 1H, H β), 6.90 (d, $J_{\text{HH}} = 7.8$ Hz, 2H, C₆H₄), 7.18 (m, 12H, C₆H₅), 7.30 (m, 6H + 2H, C₆H₅ + C₆H₄), 7.54 (m, 12H, C₆H₅), 7.71 – 7.77 (m, 2H, TBTD), 7.96 (s(br), 1H, TBTD), 8.07 – 8.13 (m, 2H, TBTD), 8.38 (s(br), 1H, TBTD), 8.88 (dt, $J_{\text{HH}} = 16.3$ Hz, $J_{\text{HP}} = 3.3$ Hz, 1H, H α) ppm. $^{31}\text{P}\{^1\text{H}\}$ NMR (Acetone- d_6): δ_{P} 25.4 (s, PPh₃) ppm. MS (ES +ve) m/z (abundance): 1218 (3) [M + H₂O]⁺, 988 (100) [M – TBTD]⁺. Calculated for C₆₃H₅₇ClN₂O₆P₂RuS₂: C 63.0, H 4.8, N 2.3%. Found: C 62.9, H 4.7, N 2.4%.

[Os(CH=CHL^{PEG})Cl(CO)(TBTD)(PPh₃)₂] (9)

Under nitrogen, [OsH(CO)(NCMe)₂(PPh₃)₂]ClO₄ (50 mg, 0.054 mmol) was dissolved in dry, degassed dichloromethane (10 mL) and treated with HC≡CL^{PEG} (18 μL , 17 mg, 0.058 mmol) and the pale yellow solution was stirred for 10 mins. A methanolic solution (3 mL) of [Et₄N]Cl (13 mg, 0.079 mmol) was added and the mixture vigorously stirred for 15 mins at 40 °C. All solvent was removed under vacuum and dry, degassed dichloromethane (5 mL) was then added to dissolve the orange solid. The resulting bright orange solution was filtered using a cannula to remove inorganic salts. To this filtrate, a dichloromethane (5 mL) solution of TBTD (13.5 mg, 0.062 mmol) was added to afford a dark red solution, which was stirred for 15 min at room temperature. All solvent was removed under vacuum and a red solid was recrystallised by addition of a mixture of diethyl ether (3 mL) and petroleum ether (4 mL) to a solution of the crude product in a minimum

volume of acetone. This was then filtered and dried (52 mg, 75%). IR ($\nu_{\max}/\text{cm}^{-1}$): 1901 (CO), 1745 (C=O), 1481, 1433, 1187, 1090, 849, 785. ^1H NMR (acetone- d_6): δ_{H} 3.29 (s, 3H, OMe), 3.48, 3.59, 3.62, 3.70 (m x 4, 4 x 2H, OCH₂), 4.17 (s, 2H, OCH₂C₆H₄), 5.08 (s, 2H, C(=O)CH₂O), 6.08 (d, $J_{\text{HH}} = 16.9$ Hz, 1H, H β), 6.92 (d, $J_{\text{HH}} = 7.9$ Hz, 2H, C₆H₄), 7.15 – 7.67 (m, 30H + 2H, C₆H₅ + C₆H₄), 7.92 (m, 2H, TBTD), 8.08 (m, 2H, TBTD), 8.15 (m, 1H, TBTD), 8.52 (s(br), 1H, TBTD), 9.36 (dt, $J_{\text{HH}} = 16.9$ Hz, J_{HP} unresolved, 1H, H α) ppm. $^{31}\text{P}\{^1\text{H}\}$ NMR (acetone- d_6): $\delta_{\text{P}} -2.3$ (s, PPh₃) ppm. MS (ES +ve) m/z (abundance): 1328 (5) [M + K]⁺. Calculated for C₆₃H₅₇ClN₂O₆OsP₂S₂: C 58.7, H 4.5, N 2.2%. Found: C 59.1, H 4.7, N 2.5%.

[Ru(CH=CHL^{PEG})Cl(CO)₂(PPh₃)₂] (8 CO)

Compound **8 CO** was prepared by treating an acetone solution (5 mL) of **8** (20.0 mg, 0.017 mmol) with carbon monoxide until the dark red solution became pale yellow. After the complete removal of the solvent under vacuum, the compound was dissolved in the minimum amount of acetone, followed by the addition of a diethyl ether (1 mL) and petroleum ether (4 mL) which resulted in the precipitation of an off-white solid, which was washed with cold petroleum ether (5 mL) and dried. Yield: 15.7 mg (93%). IR ($\nu_{\max}/\text{cm}^{-1}$): 2029 (CO), 1968 (CO), 1751 (C=O), 1482, 1434, 1191, 1092, 1027, 998. ^1H NMR (acetone- d_6): δ_{H} 3.29 (s, 3H, OMe), 3.48, 3.58, 3.64, 3.71 (m x 4, 4 x 2H, OCH₂), 4.19 (s, 2H, OCH₂C₆H₄), 5.10 (s, 2H, C(=O)CH₂O), 5.96 (d, $J_{\text{HH}} = 18.0$ Hz, 1H, H β), 6.86, 7.19 (AB, $J_{\text{AB}} = 7.9$ Hz, 4H, C₆H₄), 7.40 – 7.49 (m, 18H, C₆H₅), 7.74 – 7.79 (m, 12H, C₆H₅), 7.80 (dt, $J_{\text{HH}} = 18.0$ Hz, $J_{\text{HP}} = 3.5$ Hz, 1H, H α) ppm. $^{31}\text{P}\{^1\text{H}\}$ NMR (acetone- d_6): $\delta_{\text{P}} 23.0$ (s, PPh₃) ppm. MS (ES +ve) m/z (abundance): 1016 (100) [M – Cl + MeCN]⁺. Calculated for C₅₄H₅₁ClO₇RuP₂: C 64.2, H 5.1%. Found: C 64.3, H 5.2%.

[Os(CH=CHL^{PEG})Cl(CO)₂(PPh₃)₂] (9 CO)

Compound **9 CO** was prepared by treating an acetone solution (5 mL) of **9** (15.0 mg, 0.017 mmol) with carbon monoxide until the dark red solution became pale yellow. After the complete removal of the solvent under vacuum, the crude product was dissolved in the minimum amount of acetone, followed by addition of diethyl ether (1 mL) and petroleum ether (4 mL) which resulted in the

precipitation of an off-white solid, which was washed with cold petroleum ether (5 mL) and dried. Yield: 12.0 mg (94%). IR ($\nu_{\max}/\text{cm}^{-1}$): 2018 (CO), 1947 (CO), 1750 (C=O), 1482, 1463, 1434. ^1H NMR (acetone- d_6): δ_{H} 3.29 (s, 3H, OMe), 3.48, 3.59, 3.63, 3.70 (m x 4, 4 x 2H, OCH₂), 4.19 (s, 2H, OCH₂C₆H₄), 5.10 (s, 2H, C(=O)CH₂O), 6.08 (dt, $J_{\text{HH}} = 18.5$ Hz, $J_{\text{HP}} = 2.3$ Hz, 1H, H β), 6.84, 7.19 (AB, $J_{\text{AB}} = 7.9$ Hz, 4H, C₆H₄), 7.41 – 7.49 (m, 18H, C₆H₅), 7.69 – 7.74 (m, 12H, C₆H₅), 7.76 (dt, $J_{\text{HH}} = 18.5$ Hz, $J_{\text{HP}} = 3.5$ Hz, 1H, H α) ppm. $^{31}\text{P}\{^1\text{H}\}$ NMR (acetone- d_6): $\delta_{\text{P}} -8.1$ (s, PPh₃) ppm. MS (ES +ve) m/z (abundance): 1101 (25) [M + H]⁺, 1118 (100) [M + H₂O]⁺. Calculated for C₅₄H₅₁ClO₇OsP₂: C 59.0, H 4.7%. Found: C 59.1, H 4.6%.

Silica gel immobilisation of the vinyl complexes

Each ruthenium vinyl complex was dissolved in a minimum volume of CHCl₃. An excess of silica (particle size 40-63 μm , silica gel for chromatographic use) was added to the coloured solution in a 1:10 (complex:silica) mass ratio and the resulting suspension was stirred at room temperature for five minutes. After removal of the solvent on a rotary evaporator, the solid was recovered and left to stand for one hour at room temperature prior use.

S3. Crystallographic details

The X-ray crystal structure of TBTD

Crystal data for TBTD: C₁₀H₆N₂S₂, $M = 218.29$, monoclinic, $P2_1/c$ (no. 14), $a = 11.3068(9)$, $b = 7.0845(5)$, $c = 23.268(2)$ Å, $\beta = 96.544(8)^\circ$, $V = 1851.7(3)$ Å³, $Z = 8$ (two independent molecules), $D_c = 1.566$ g cm⁻³, $\mu(\text{Mo-K}\alpha) = 0.528$ mm⁻¹, $T = 173$ K, pale yellow blocky needles, Agilent Xcalibur 3 E diffractometer; 3736 independent measured reflections ($R_{\text{int}} = 0.0236$), F^2 refinement,^{S14} $R_1(\text{obs}) = 0.0513$, $wR_2(\text{all}) = 0.1283$, 2900 independent observed absorption-corrected reflections [$|F_o| > 4\sigma(|F_o|)$], $2\theta_{\text{max}} = 56^\circ$], 295 parameters. CCDC 1498392.

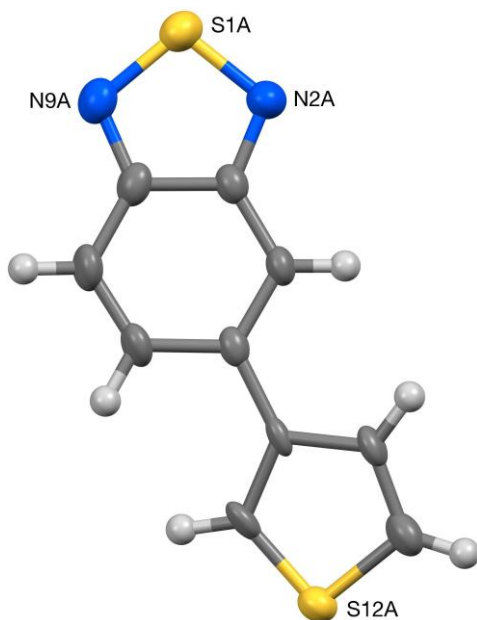


Fig. S3-1. The structure of one (TBTD-A) of the two independent molecules present in the crystal of TBTD (50% probability ellipsoids).

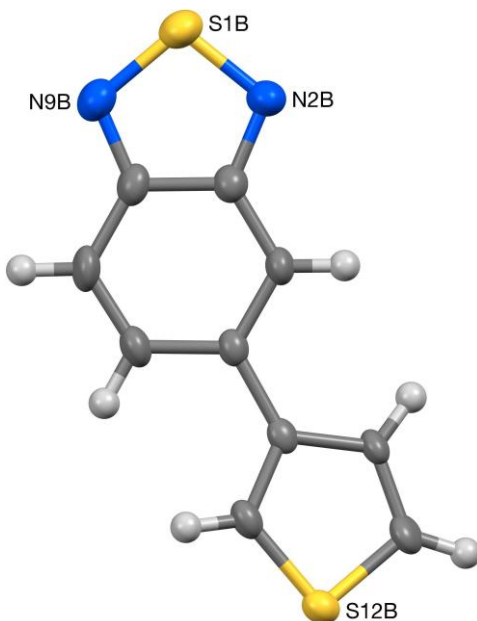


Fig. S3-2. The structure of one (TBTD-B) of the two independent molecules present in the crystal of TBTD (50% probability ellipsoids).

The crystal structure of **TBTD** was found to contain two independent molecules (**TBTD-A** and **TBTD-B**), and in each molecule the C10-based thiophene unit was found to be disordered. In both instances two orientations were identified, of *ca.* 64:36 and 88:12% occupancy for molecules **A** and **B** respectively. The geometries of all four orientations were optimised, the thermal parameters of adjacent atoms were restrained to be similar, and only the non-hydrogen atoms of the major occupancy orientations were refined anisotropically (those of the minor occupancy orientations were refined isotropically).

The X-ray crystal structure of Compound 6

Crystal data for 6: $C_{63}H_{47}ClN_2OP_2RuS_2 \cdot 3(CH_2Cl_2)$, $M = 1365.38$, triclinic, $P-1$ (no. 2), $a = 12.1009(4)$, $b = 14.7925(6)$, $c = 17.7731(5)$ Å, $\alpha = 76.557(3)$, $\beta = 82.335(2)$, $\gamma = 85.440(3)^\circ$, $V = 3062.73(18)$ Å³, $Z = 2$, $D_c = 1.481$ g cm⁻³, $\mu(\text{Cu-K}\alpha) = 6.367$ mm⁻¹, $T = 173$ K, red blocks, Agilent Xcalibur PX Ultra A diffractometer; 11722 independent measured reflections ($R_{\text{int}} = 0.0248$), F^2 refinement, $R_1(\text{obs}) = 0.0433$, $wR_2(\text{all}) = 0.1210$, 10263 independent observed absorption-corrected reflections [$|F_o| > 4\sigma(|F_o|)$], $2\theta_{\text{max}} = 148^\circ$], 770 parameters. CCDC 1498393.

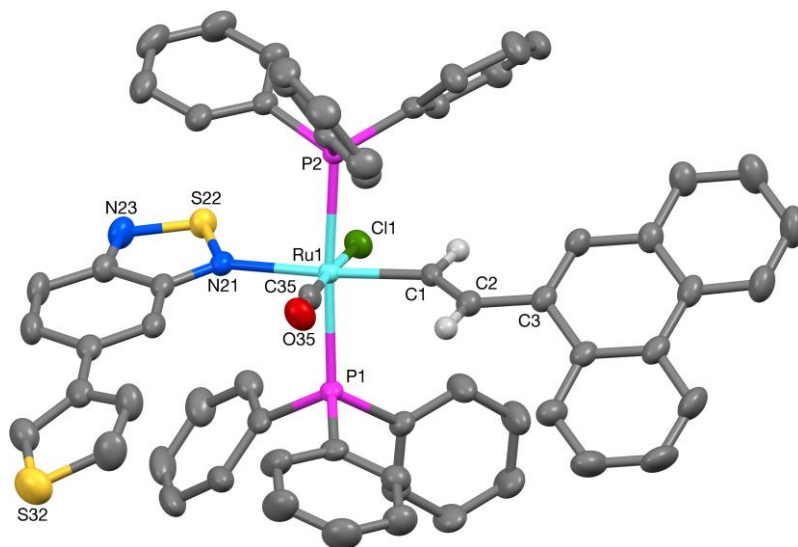


Fig. S3-3. The crystal structure of **6** (50% probability ellipsoids).

The C80- and C90-based dichloromethane solvent molecules in the structure of **6** were both found to be disordered; for the former, two orientations were identified of *ca.* 78 and 22% occupancy, whilst for the latter, three orientations were identified of *ca.* 68, 19 and 13% occupancy. The geometries of all five orientations were optimised, the thermal parameters of adjacent atoms were restrained to be similar, and only the non-hydrogen atoms of the major occupancy orientations were refined anisotropically (those of the minor occupancy orientations were refined isotropically).

The X-ray crystal structure of compound **6-CO**

Crystal data for 6-CO: C₅₄H₄₁ClO₂P₂Ru·CH₂Cl₂, *M* = 1005.25, triclinic, *P*-1 (no. 2), *a* = 10.4363(5), *b* = 14.9450(8), *c* = 15.1451(8) Å, α = 82.763(4), β = 77.136(4), γ = 88.273(4)°, *V* = 2284.6(2) Å³, *Z* = 2, *D*_c = 1.461 g cm⁻³, μ (Mo-K α) = 0.632 mm⁻¹, *T* = 173 K, colourless tabular needles, Agilent Xcalibur 3 E diffractometer; 8946 independent measured reflections (*R*_{int} = 0.0275), *F*² refinement,^{S14} *R*₁(obs) = 0.0348, *wR*₂(all) = 0.0780, 7592 independent observed absorption-corrected reflections [*|F*_o| > 4 σ (*|F*_o|)], 2 θ _{max} = 56°, 569 parameters. CCDC 1498394.

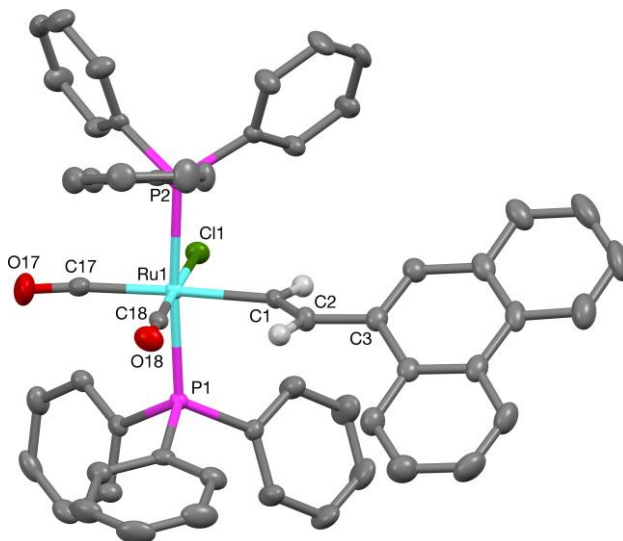


Fig. S3-4. The crystal structure of **6-CO** (50% probability ellipsoids).

The X-ray crystal structure of compound **7**

Crystal data for 7: $C_{65}H_{47}ClN_2OP_2RuS_2 \cdot 2(CH_2Cl_2) \cdot C_2H_6O$, $M = 1350.54$, monoclinic, $P2_1/c$ (no. 14), $a = 17.9954(2)$, $b = 15.62220(17)$, $c = 24.0270(3)$ Å, $\beta = 110.5812(13)^\circ$, $V = 6323.54(14)$ Å³, $Z = 4$, $D_c = 1.419$ g cm⁻³, $\mu(Cu-K\alpha) = 5.414$ mm⁻¹, $T = 173$ K, brown plates, Agilent Xcalibur PX Ultra A diffractometer; 12194 independent measured reflections ($R_{int} = 0.0244$), F^2 refinement,^{S14} $R_1(obs) = 0.0345$, $wR_2(all) = 0.0926$, 10650 independent observed absorption-corrected reflections [$|F_o| > 4\sigma(|F_o|)$], $2\theta_{max} = 148^\circ$, 688 parameters. CCDC 1498395.

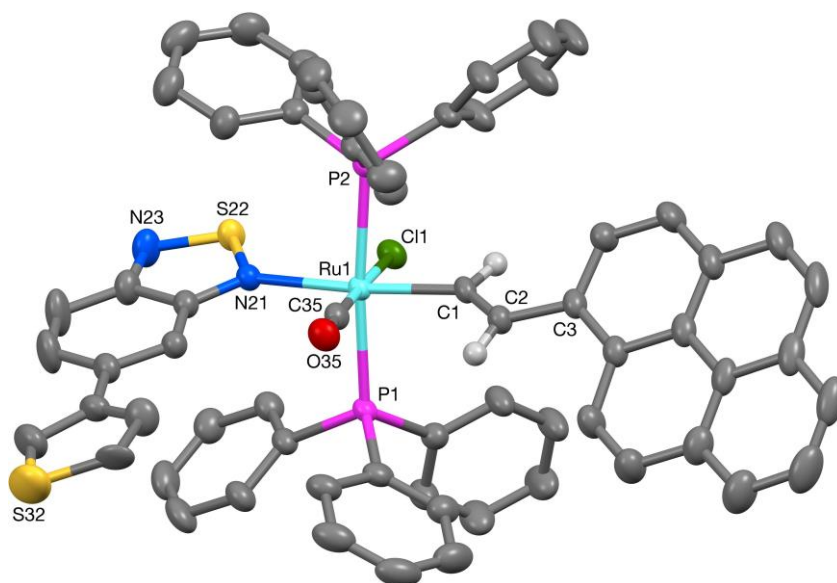


Fig. S3-5. The crystal structure of **7** (50% probability ellipsoids).

The included solvent was found to be highly disordered, and the best approach to handling this diffuse electron density was found to be the SQUEEZE routine of PLATON.^{S14} This suggested a total of 426 electrons per unit cell, equivalent to 106.5 electrons per asymmetric unit. Before the use of SQUEEZE the solvent most resembled a mixture of dichloromethane (CH_2Cl_2 , 42 electrons) and ethanol (C_2H_6O , 26e) with a predominance of the former. 2 dichloromethane molecules and one ethanol molecule corresponds to $(42 \times 2) + 26 = 110$ electrons, so this was used as the solvent present. As a result, the atom list for the asymmetric unit

is low by $2(\text{CH}_2\text{Cl}_2) + (\text{C}_2\text{H}_6\text{O}) = \text{C}_4\text{H}_{10}\text{Cl}_4\text{O}$ (and that for the unit cell low by $\text{C}_{16}\text{H}_{40}\text{Cl}_{16}\text{O}_4$) compared to what is actually presumed to be present.

The C30-based thiophene unit was found to be disordered. Two orientations were identified of *ca.* 60 and 40% occupancy, their geometries were optimised, the thermal parameters of adjacent atoms were restrained to be similar, and only the non-hydrogen atoms of the major occupancy orientation were refined anisotropically (those of the minor occupancy orientation were refined isotropically).

S4. Photophysical characterisation of the TBTD ligand

The photophysical attributes of the new **TBTD** ligand were characterised, including the quantum yield ($\Phi = 0.27$).

The fluorescence Quantum Yields (QYs) of **TBTD** and complex **3** were calculated according to the comparative method^{S13} by employing the following formula:

$$\Phi_X = \Phi_{\text{ST}} \left(\frac{\text{Grad}_X}{\text{Grad}_{\text{ST}}} \right) \left(\frac{\eta_X^2}{\eta_{\text{ST}}^2} \right)$$

where η the refractive index of the solvent and Grad_X and Grad_{ST} are the gradient from the plot of integrated fluorescence intensity vs absorbance for the compound X (**TBTD** or complex **3**) and the standard (ST). The QY of **TBTD** was measured in ethanol solution whereas complex **3** was dissolved in a dichloromethane/ethanol mixture (2:98) at the concentrations of 10^{-5} , 0.9×10^{-5} , 0.8×10^{-5} , 0.5×10^{-5} and 0.3×10^{-5} M.

In order to minimise re-absorption effects,^{S15} the absorbance values in the 10 mm fluorescence cuvette should never exceed 0.1 at the excitation wavelength. Moreover, being the quantum yields measured in the same solvent (ethanol), it was assumed that $\eta_X^2 \approx \eta_{\text{ST}}^2$ and therefore $\eta_X^2 / \eta_{\text{ST}}^2 = 1$. The solutions were thoroughly degassed with nitrogen before use.

The comparative method of Williams *et al.*⁵¹³ is based on the assumption that solutions of different samples with identical absorbance at the same excitation wavelength absorb the same number of photons. Thus, a simple ratio of the integrated fluorescence intensities of the solution of a selected standard and a generic sample (recorded under identical conditions) affords the ratio of the quantum yield values.

The standard sample perylene ($\Phi_{ST} = 0.92$ in ethanol)⁵¹⁶ was chosen because its absorption and emission properties are similar to the samples TBTD and complex **3**. In fact, it absorbs at the excitation wavelength of choice ($\lambda_{exc} = 375$ nm), and emits in a similar spectral region to the **TBTD** and complex **3**. Standard quartz 10 mm path length fluorescence cuvettes (Hellma, 1750 μ L) were used.

From these measurements, the quantum yield for TBTD was calculated to be 0.27, while the corresponding value the complex $[\text{Ru}(\text{CH}=\text{CHC}_6\text{H}_4\text{Me}-4)\text{Cl}(\text{CO})(\text{TBTD})(\text{PPh}_3)_2]$ (**4**) is 0.047.

S5. Carbon monoxide sensing studies

Two cylinders, of CO and Ar, are connected to the gas chamber via a gas mixer, which allows control over the rate of the gas streams (Fig. S5-1). Into the sealed gas chamber, the ambient CO analyser (Testo, Cabrils) measures the content of CO in ppm and allows different CO/Ar mixtures to be achieved where the CO content is known. From the gas chamber, the gas mixture is passed in a controlled manner to a container from which the aliquots of CO/Ar are taken and used in the CO titration experiments.

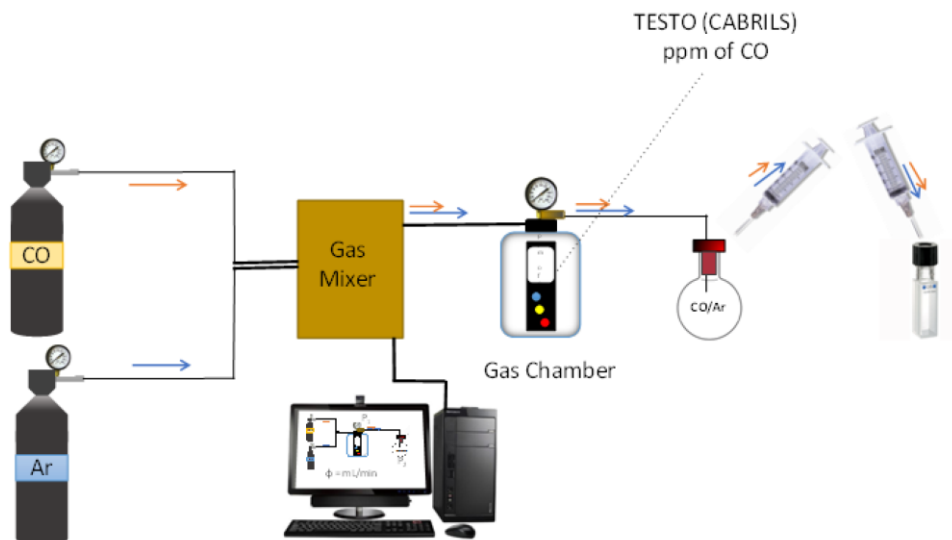


Figure S5-1. Schematic representation of the gas-mixing equipment used to carry out the experiments with carbon monoxide.

Detection limit measurements

Table S5-1. Limits of detection (ppm) for complexes **3** and **4** in the presence of CO. Limits calculated from diffuse reflectance and emission spectra data.

Complex	Limits of detection of CO (ppm)		
	Uv-visible (silica)	Fluorescence (solution)	Fluorescence (silica)
3	21.9	0.001	13.8
4	1.4	0.001	9.9

S6. Interference studies

Gas and vapour generation protocols

The following protocols were used to generate the gases necessary to perform the screening of interferences. For the generation of all gases (except for CO), the reagents were mixed together in a 1000 mL round-bottom flask equipped with a rubber septum.

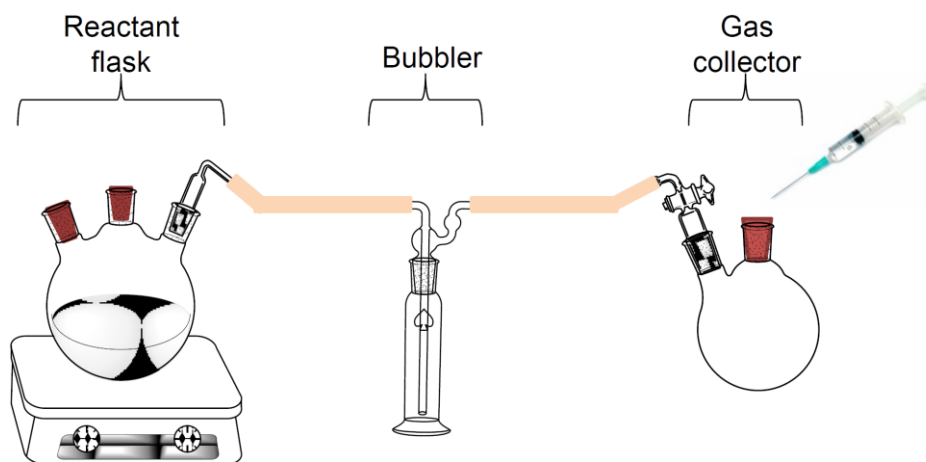


Figure S6-1. Glassware set up for the generation of gases. The reactants are mixed carefully in the reactant flask and the temperature is increased. The generated gases pass through a water-filled bubbler and are then collected into a flask fitted with a rubber septum. Aliquots of gases are collected with the use of a syringe and used in the interferent experiment.

NO_x generation: 0.0692 g (1.0889·mmol) of Cu_(s) [Copper powder] reacts with 1 mL of HNO₃ (69.5%) to generate approximately 53210 ppm of NO₂. In the same manner, 0.3183 g (5.0087·mmol) of Cu_(s) [Copper powder] is reacted with 2.85 mL of HNO₃ (20.85%) under argon atmosphere. Prior to the addition of the acid it is very important that the flask had been flushed with argon for several minutes in order to avoid NO oxidation. In this manner, approximately 81590 ppm of NO are

generated. Although the reaction is conducted in inert atmosphere, some NO_2 may still form.

CO₂ generation: 0.227 g ($2.2729 \cdot 10^{-3}$ mol) of CaCO_3 (s) reacts with 1 mL of HCl (1 M) to generate 55541 ppm of CO_2 .

Volatile organic compound (VOCs) vapours were generated by warming up the VOC to evaporation. A 1000 mL flask fitted with a rubber septum was used. All these manipulations were performed in the fume hood.

Various gases (N_2 , O_2 , Ar, CO_2 , steam) and VOCs (acetone, chloroform, ethanol, toluene, hexane, formaldehyde) were tested as potential interferences up to 30,000 ppm levels but gave no colour change in any of the complexes tested.

The only species which gave rise to a colour change were MeCN and NO_x . The measurements of these compounds were used to determine detection limits for these interferences using the same graphical method used previously (Fig. S6-2).

Table S6-1. Summary of the observed behavior for acetonitrile and NO_x with complexes **3** and **4**. Responses are shown with the concentration (in ppm) necessary to induce a colour change.

Solid	Interferents UV-visible (ppm)	
	acetonitrile	NO_x
3	4570	7240
4	-	794

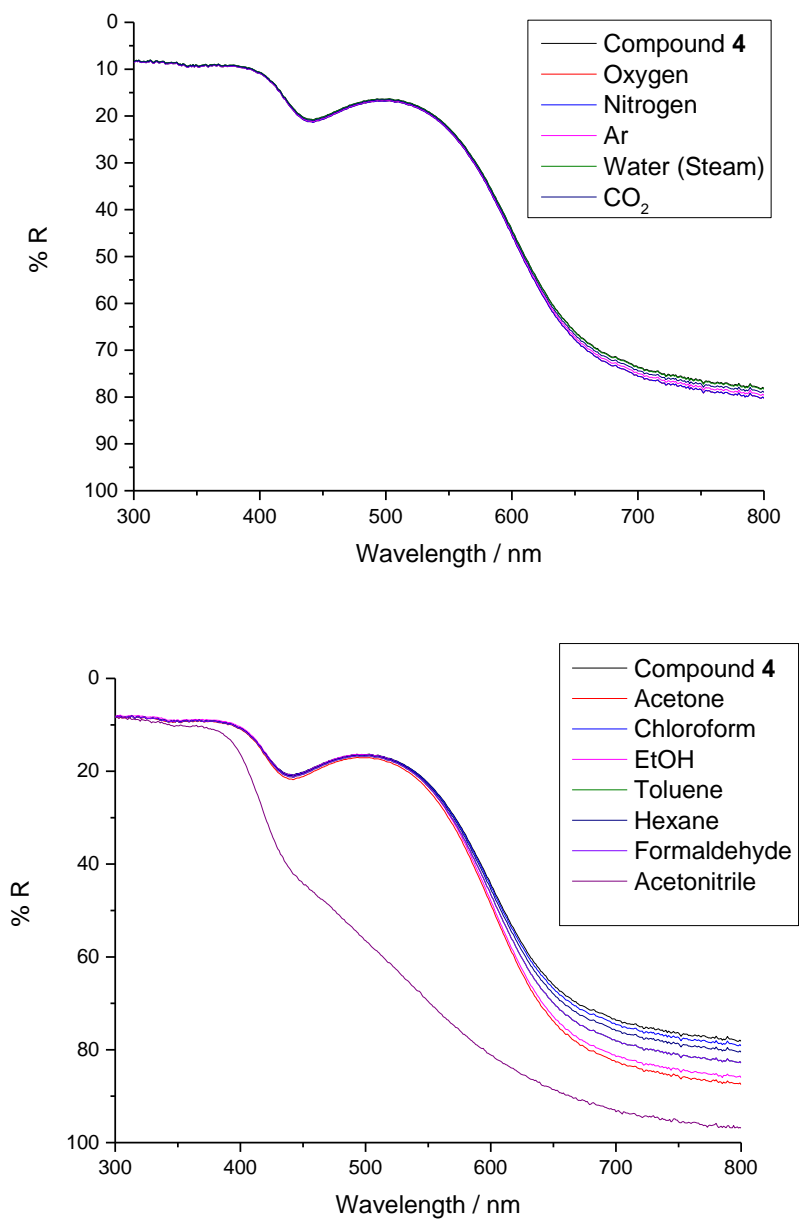


Figure S6-2. Diffuse reflectance measurements for **4** in the presence of various interferents.

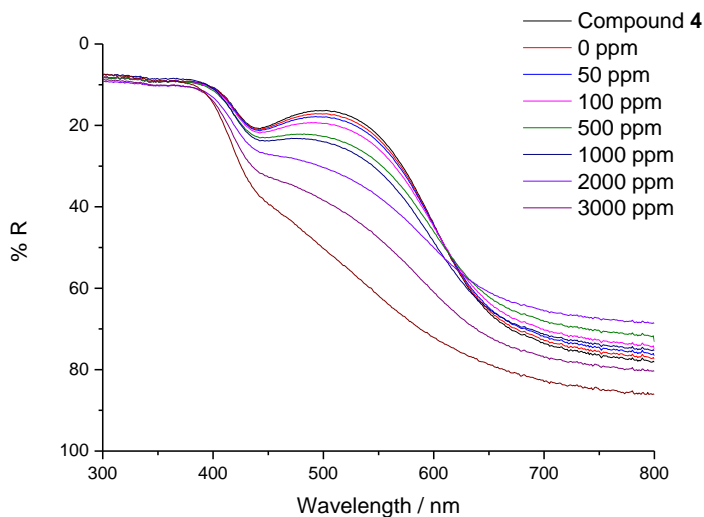


Figure S6-3. Diffuse reflectance spectra for **4** in the presence of increasing concentrations of MeCN (left) and the graphical method to determine the detection limit (right).

In all cases, the quantities of MeCN and NO_x required to cause a colour change were vastly higher than likely to be found in the environments in which the probes described here would be used.

Competition test against various biological components

The fluorescence emission of complex **8** (10^{-4} M solution in 0.1% acetone/PBS solution) was measured in the presence of tryptophan (10^{-4} M) imidazole (10^{-4} M), NO_x (50 ppm) and in the presence of 200 ppm of CO. The variation of the emission intensity in relation to the different biological components is depicted below in Figure S6-5 (and also shown in Figure 11 in the main text). The experiments was performed by adding 20 μ L of 0.15 M solutions of tryptophan and imidazole in PBS buffer to a 10^{-4} M solution of complex 9 (10^{-4} M solution in 0.1% acetone/PBS solution); in the case of NO_x, the gas was generated *in situ* and then bubbled through a solution of the complex without any further purification.

57. Cytotoxicity assay and confocal microscopy

The MTT assay is a colorimetric assay that assesses the reduction of the cell viability (balance between living and dead cells) over time, when the cells are incubated with a compound. This assay involves the reduction of the tetrazolium salt MTT (3-(4,5-dimethylthiazolyl-2)-2,5-diphenyltetrazolium bromide) by mitochondrial dehydrogenase. During this process, the yellow MTT is reduced to the purple formazan by metabolically active cells (living cells), whereas it is not internalised and metabolised by dead cells. The resulting intracellular purple product, which can be spectrophotometrically quantified, indicates the degree of cell viability in the presence of different concentrations of the ruthenium and osmium vinyl probes and the free **TBTD** ligand. The viability test was performed in 96-well plates where the HeLa cells were placed at a density of 15000 cells per well. The cells were incubated with the probes **8** and **9**, as well as the free **TBTD** ligand, at concentrations between 250 and 1 μ M for 1, 3, 24 and 72 hours.

Cervical cancer HeLa cells were kindly donated by Prof. Ed Tate from Imperial College London. The cells were routinely grown in a DMEM (Dulbecco's Modified Eagle Medium), high glucose + GlutaMAXTM medium containing 10% foetal calf serum (FCS), purchased from Gibco[®] by Life TechnologiesTM. The maintenance of the cell culture was carried out according to standard protocols given by the European Collection of Authenticated Cell Cultures (ECACC). For growth inhibition assays, the cells were seeded in 96-well plates (Corning[®] Costar[®], Sigma-Aldrich) and grown for 24 h at 37 °C in a 4 – 10 % CO₂ incubator. Stock solutions of the compounds were prepared by dissolving the compounds (**8**, **9** and **TBTD**) in DMSO (sterile-filtered) to reach a concentration of 10⁻² M. After gently aspirating the cell medium from the wells, different aliquots of these solutions were diluted with the DMEM medium and then added to the wells (200 μ L) to reach final concentrations between 0.5 to 100 μ M. DMSO was also tested as a control and found to produce no effect on the cell viability. After 1, 3, 24 and 72 h incubation, the medium was gently aspirated and replaced with 200 μ L of a solution of (3-(4,5-dimethylthiazol-2-yl)-2,5-diphenyltetrazolium bromide) (MTT) in PBS (2 mg mL⁻¹) was added to each well, and the plates were then incubated for 2 h at 37°C, after which the

absorbance of each well was measured at 580 nm using a 96-well multiwell-plate reader (SpectraMax M2/M2e Microplate Reader from Molecular Devices.) and compared to the values of control cells incubated without compounds. The viability was assessed by fitting the percentage of surviving cells against the complex concentrations using a sigmoidal function (Origin v8).

Cellular internalisation studies were performed using a confocal Leica microscope with a TCS SP2 system and equipped with an acoustic optical beam splitter (AOBS). In the first instance, HeLa cells were incubated for 30 minutes with compounds **8**, **9** and **TBTD** at final concentrations of 50 μM before starting the measurements (this time delay allowed the compounds to enter the cell). In a second instance, HeLa cells were incubated with compounds **8** and **9** (50 μM) in the presence of $[\text{RuCl}(\text{glycinate})(\text{CO})_3]$ (CORM-3) at a concentration of 50 μM . The images were edited with Fiji Macro.

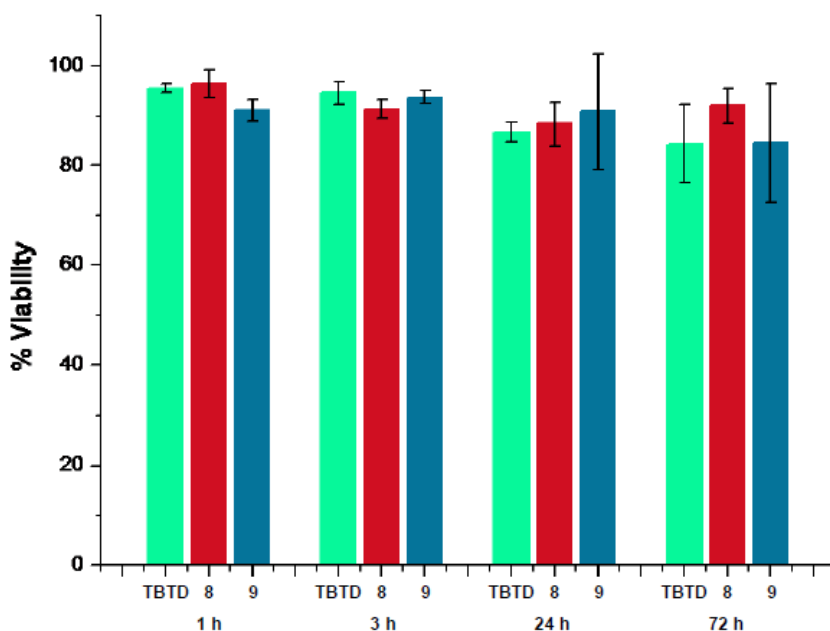


Figure S7-1. Percentage viability of HeLa cells with the **TBTD** ligand, $[\text{Ru}(\text{CH}=\text{CHL}^1)\text{Cl}(\text{CO})(\text{TBTD})(\text{PPh}_3)_2]$ (**9**) and $[\text{Os}(\text{CH}=\text{CHL}^1)\text{Cl}(\text{CO})(\text{TBTD})(\text{PPh}_3)_2]$ (**10**) at a concentration of 200 μM after 1, 3, 24 and 72 hours.

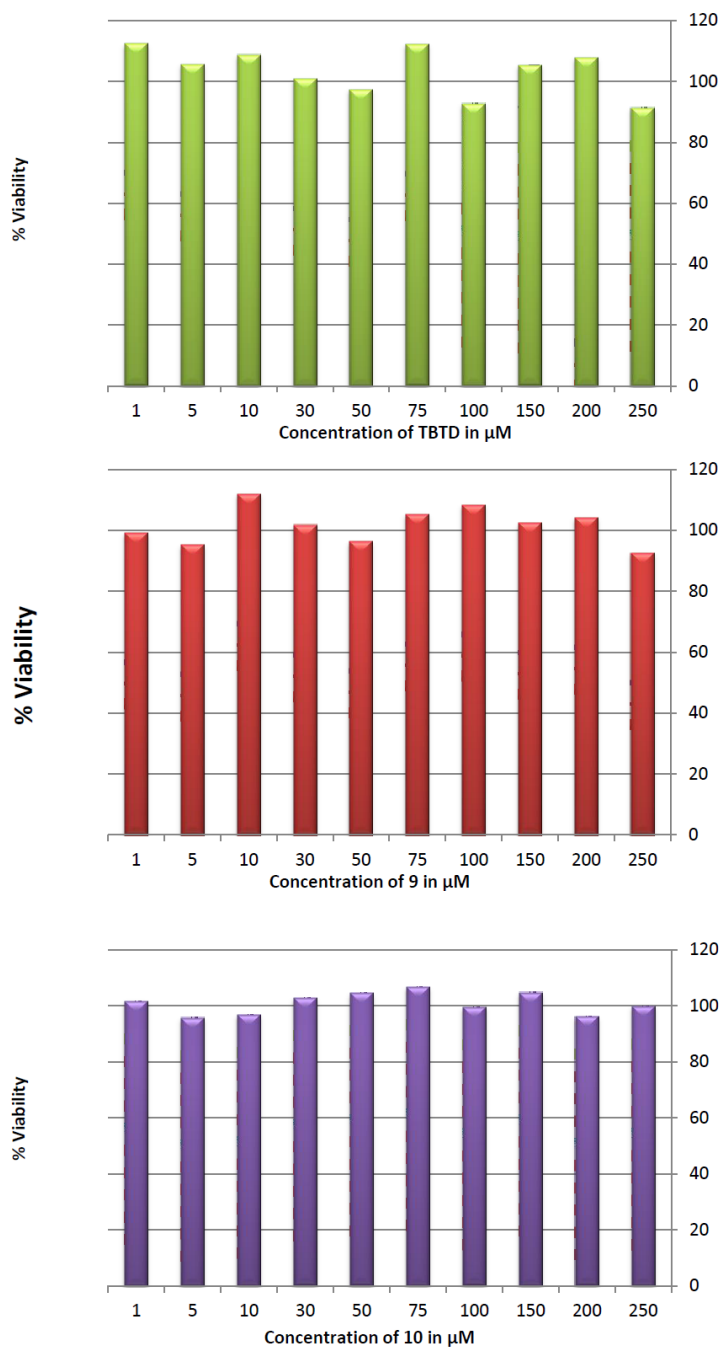


Figure S7-2. Viability of HeLa cells incubated for 1h with **TBTD** (top) and complexes **8** (middle) and **9** (bottom).

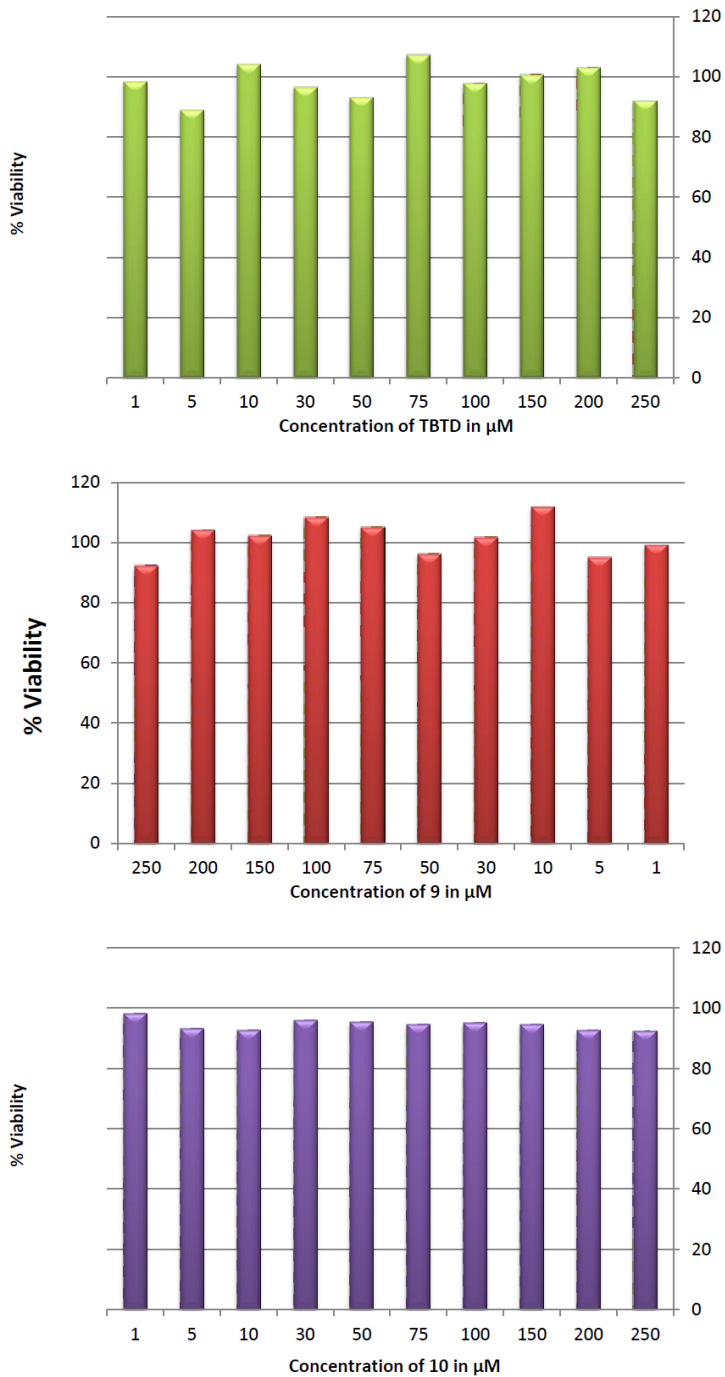


Figure S7-3. Viability of HeLa cells incubated for 3h with **TBTD** (top) and complexes **8** (middle) and **9** (bottom).

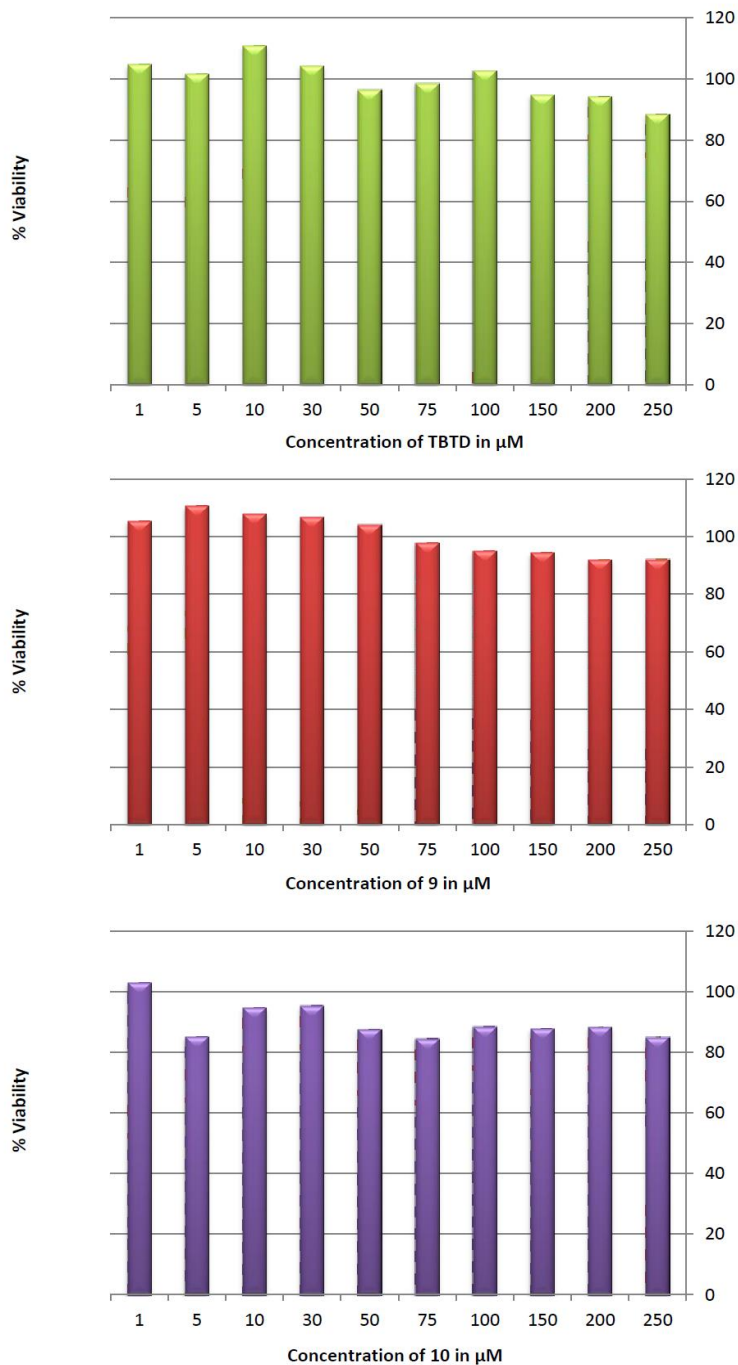


Figure S7-4. Viability of HeLa cells incubated for 24h with **TBTD** (top) and complexes **8** (middle) and **9** (bottom).

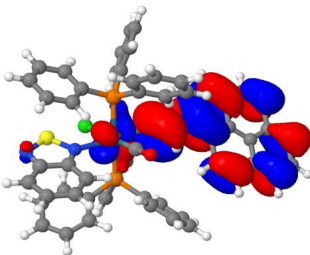
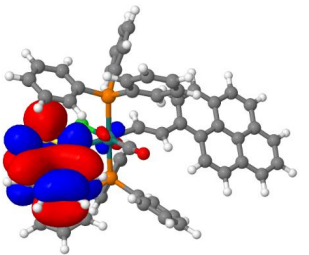
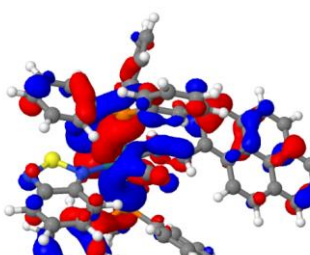
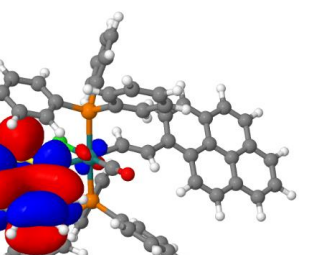
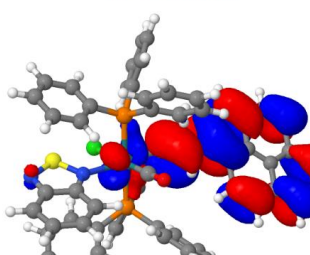
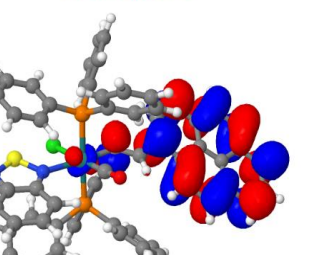
S8. DFT calculations

Computational calculations were performed using the B3LYP functional, dispersion corrections were added using the empirical dispersion keyword and Grimme's D3 procedure.^{S16} MWB28 was used as the pseudo potential and basis set for Ru. Initially, all other atoms were calculated at 6-31G(d) and then refined using the TZVP basis set. Solvent (methanol) was included in all calculations using the CPCM methodology. An ultrafine grid and tight convergence criteria, scf = 9, was employed throughout. TD-DFT calculations were carried out on fully optimised structures for the first 100 states using the same functional and basis sets.

Table S8-1: Calculated bond lengths in Å for complexes **7**, [Ru(CH=CHPyr-1)Cl(CO)(BTD)(PPh₃)₂] (**PyrBTD**), **4**, [Ru(CH=CHPh)Cl(CO)(BTD)(PPh₃)₂] (**PhBTD**), **7•CO** and **4•CO**; The Ru-CO refers to the carbonyl trans to vinyl ligand originating from added CO.

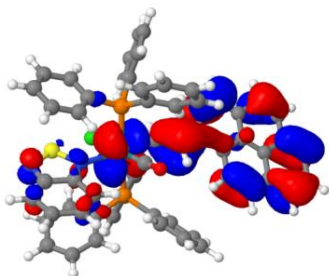
Model	Ru-N or Ru-CO	Ru-P(3)	Ru-P(4)	Ru-Cl	Ru-CO	Ru-C ₁	C ₁ -C ₂
7	2.27869	2.45235	2.43842	2.54678	1.82509	2.05162	1.34447
PyrBTD	2.28483	2.45321	2.43757	2.54494	1.82511	2.05145	1.34432
4	2.28026	2.44371	2.43721	2.54736	2.98286	2.06022	1.34237
PhBTD	2.28418	2.44656	2.43375	2.54531	1.82544	2.05911	1.34255
7•CO	1.96983	2.46679	2.44448	2.53908	1.85638	2.11228	1.34186
4•CO	1.96781	2.46216	2.43981	2.54467	1.85590	2.11568	1.33958

Table S8-2: Molecular orbitals for [Ru(CH=CHPyr-1)Cl(CO)(BTD)(PPh₃)₂] (PyrBTD)

Wavelength (nm)	MO	Transition	
624.16	<p>IB (98358) - TZVP MO 256</p>  <p>256</p>	<p>IB (98358) - TZVP MO 257</p>  <p>257</p>	<p>Ru-vinyl -> BTD</p>
420.79	<p>IB (98358) - TZVP MO 254</p>  <p>254</p>	<p>IB (98358) - TZVP MO 257</p>  <p>257</p>	<p>Ru-phosphine -> BTD</p>
414.86	<p>IB (98358) - TZVP MO 256</p>  <p>256</p>	<p>IB (98358) - TZVP MO 258</p>  <p>258</p>	<p>Ru-vinyl π -> π^*</p>

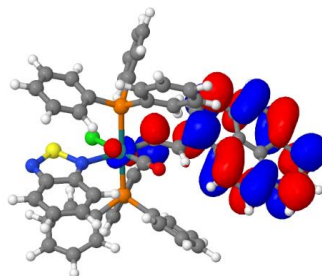
320.65

1B (98358) - TZVP MO 255



255

1B (98358) - TZVP MO 258

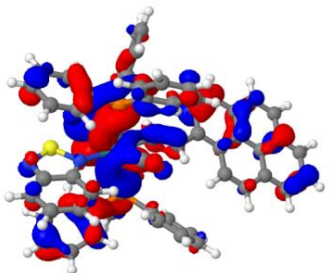


258

Ru-vinyl π
-> π^*

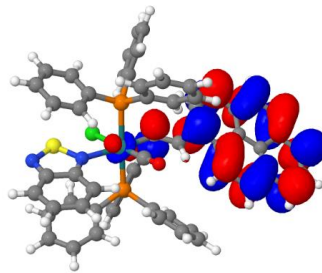
302.90

1B (98358) - TZVP MO 254



254

1B (98358) - TZVP MO 258

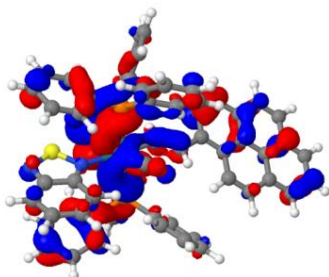


258

Ru-phosphine
-> Ru-vinyl

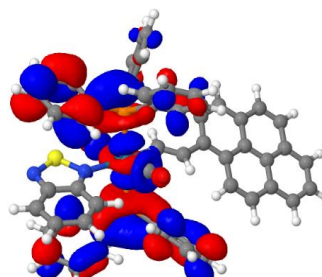
280.68

1B (98358) - TZVP MO 254



254

1B (98358) - TZVP MO 259

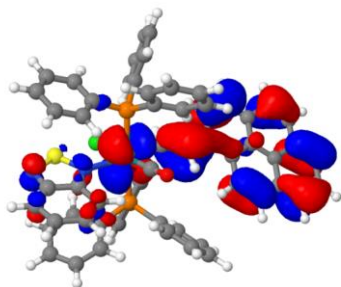


259

Ru-phosphine
 π -> π^*

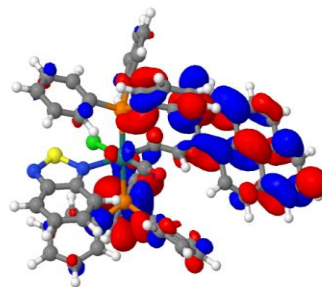
272.83

1B (98358) - TZVP MO 255



255

1B (98358) - TZVP MO 262

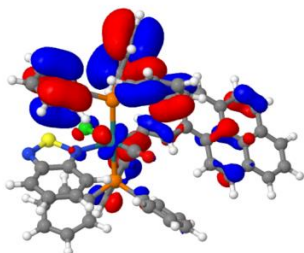


262

Ru-vinyl
-> vinyl π^*

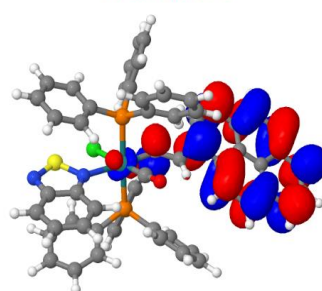
250.11

1B (98358) - TZVP MO 245



245

1B (98358) - TZVP MO 258



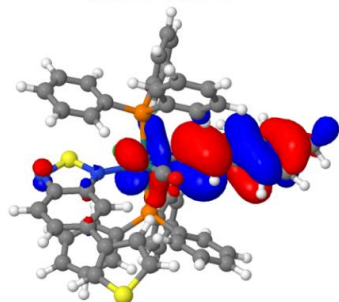
258

Ru-vinyl
-> Ru-
phosphine**Table S8-3:** Molecular orbitals for compound $[\text{Ru}(\text{CH}=\text{CHToI})\text{Cl}(\text{CO})(\text{TBTD})(\text{PPh}_3)_2]$ (**4**)**Wavelength (nm)****MO****Transition**

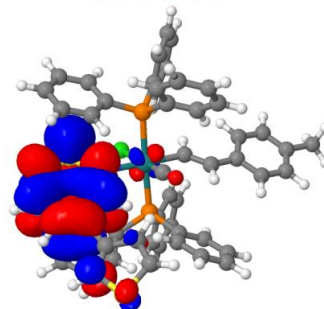
607.04

1C (104807) - TZVP MO 249

1C (104807) - TZVP MO 250



→



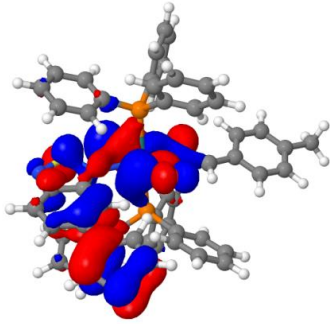
249

250

Ligand
→ TBTD

425.20

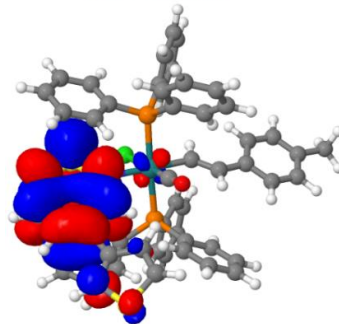
IC (104807) - TZVP MO 247



247



IC (104807) - TZVP MO 250



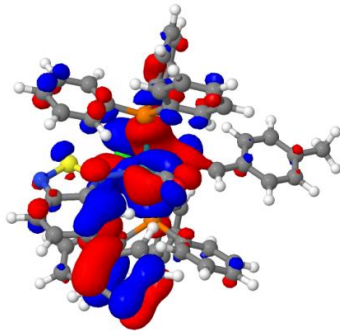
250

TBTD π \rightarrow

TBTD π^*

397.63

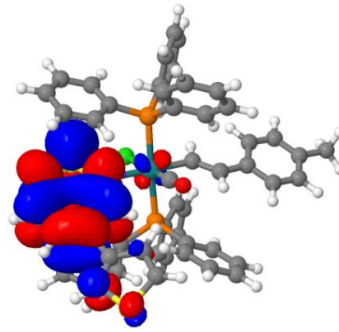
IC (104807) - TZVP MO 246



246



IC (104807) - TZVP MO 250



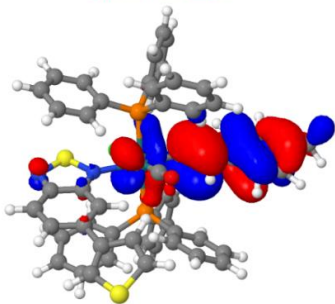
250

Phosphine

\rightarrow TBTD π

302.33

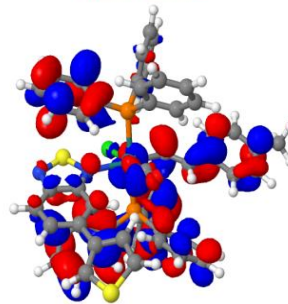
IC (104807) - TZVP MO 249



249



IC (104807) - TZVP MO 261



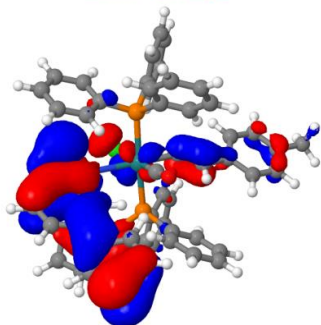
261

Ligand \rightarrow

phosphine

263.65

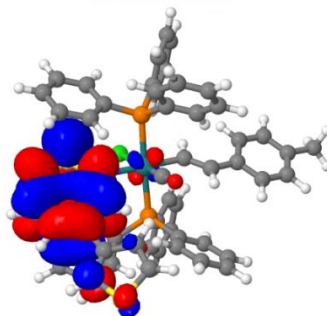
IC (104807) - TZVP MO 226



226

→

IC (104807) - TZVP MO 250



250

TBTD-Vinyl

→ TBTD

Table S8-4: Molecular orbitals for compound $[\text{Ru}(\text{CH}=\text{CHPyr-1})\text{Cl}(\text{CO})(\text{TBTD})(\text{PPh}_3)_2]$ (7)

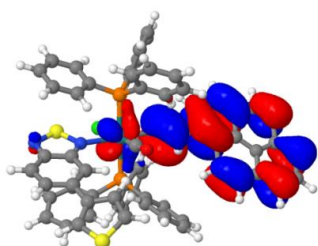
Wavelength (nm)

MO

Transition

635.62

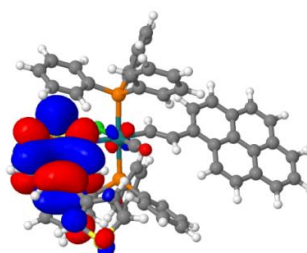
ID (105018) - TZVP MO 277



277

→

ID (105018) - TZVP MO 278



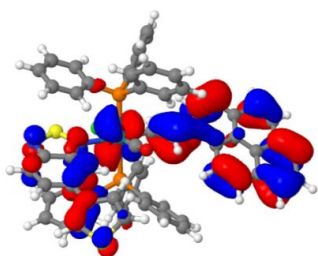
278

Ru-vinyl

→ TBTD

450.53

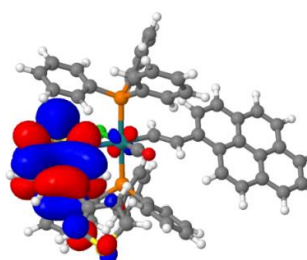
ID (105018) - TZVP MO 276



276

→

ID (105018) - TZVP MO 278



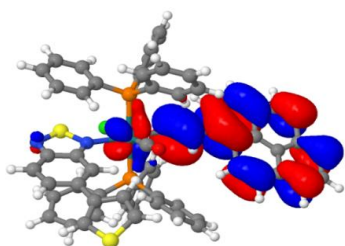
278

TBTD

 $\pi \rightarrow \pi^*$

415.66

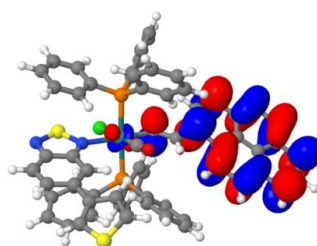
ID (105018) - TZVP MO 277



277

→

ID (105018) - TZVP MO 279

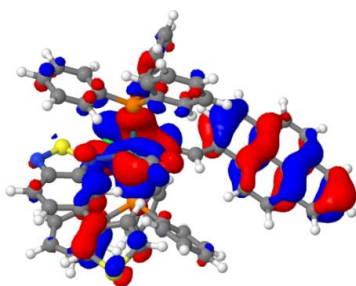


279

Ru-vinyl
→
phosphine

390.67

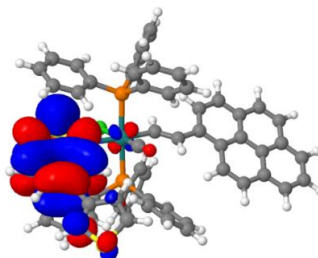
ID (105018) - TZVP MO 273



273

→

ID (105018) - TZVP MO 278

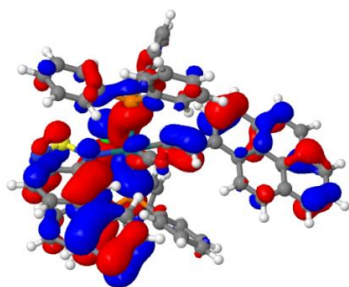


278

Ru-vinyl
→
phosphine

303.25

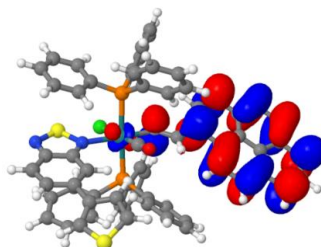
ID (105018) - TZVP MO 275



275

→

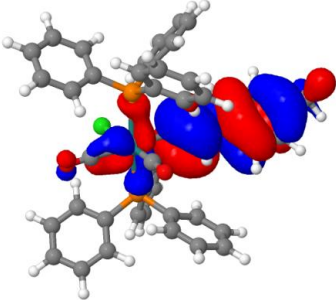
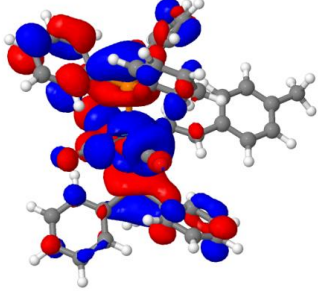
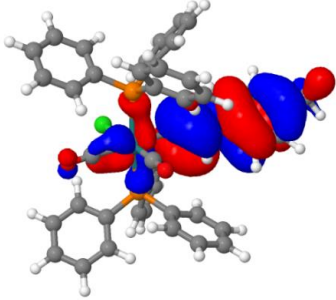
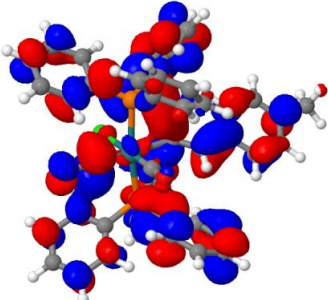
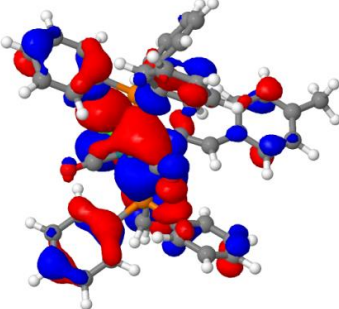
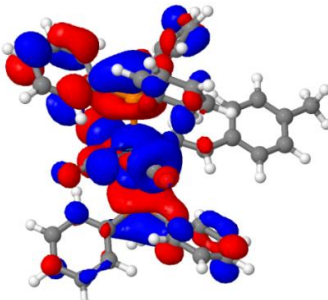
ID (105018) - TZVP MO 279



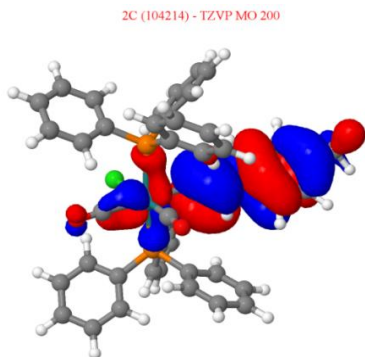
279

Ru-vinyl
→
phosphine

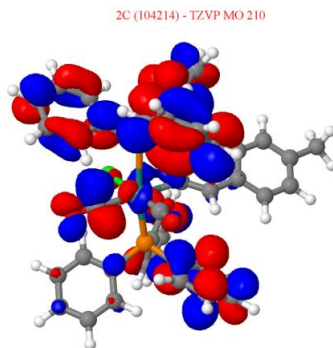
Table S8-5: Molecular orbitals for compound [Ru(CH=CHTol)Cl(CO)₂(PPh₃)₂] (**4**·CO)

Wavelength (nm)	MO	Transition	
386.62	<p>2C (104214) - TZVP MO 200</p>  <p>200</p>	<p>2C (104214) - TZVP MO 201</p>  <p>201</p>	Ligand → Metal- phosphine (LMCT)
318.73	<p>2C (104214) - TZVP MO 200</p>  <p>200</p>	<p>2C (104214) - TZVP MO 202</p>  <p>202</p>	Ligand → Metal- phosphine (LMCT)
294.57	<p>2C (104214) - TZVP MO 197</p>  <p>197</p>	<p>2C (104214) - TZVP MO 201</p>  <p>201</p>	Metal Phosphine →Metal phosphine

284.37



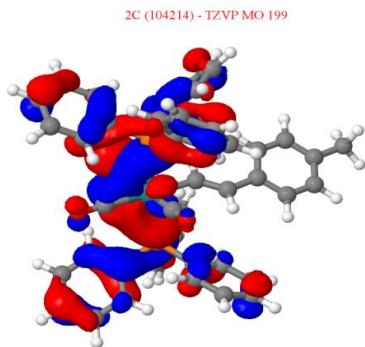
200



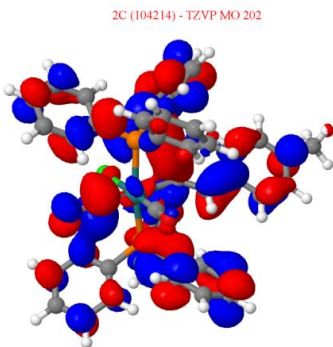
210

Ligand →
Metal-
phosphine
(LMCT)

269.16



199



202

Metal-
Phosphine
→
Metal-
phosphine

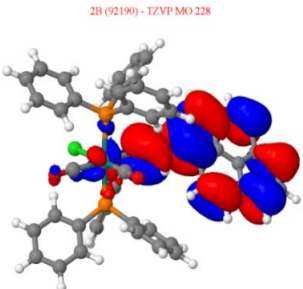
Table S8-6: Molecular orbitals for compound $[\text{Ru}(\text{CH}=\text{CHPyr}-1)\text{Cl}(\text{CO})_2(\text{PPh}_3)_2]$ (**7·CO**)

Wavelength (nm)

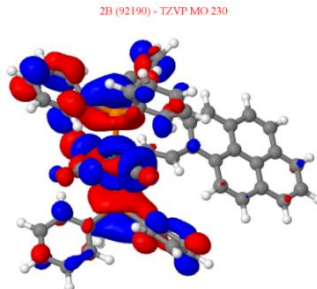
MO

Transition

409.53



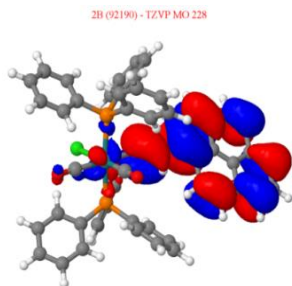
228



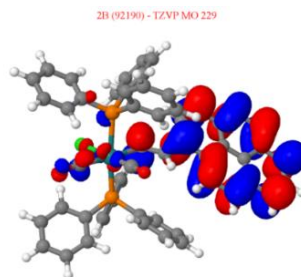
230

Ligand
→
Metal-
phosphine
(LMCT)

398.18



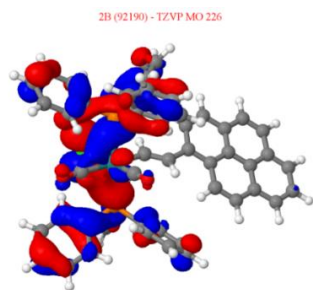
228



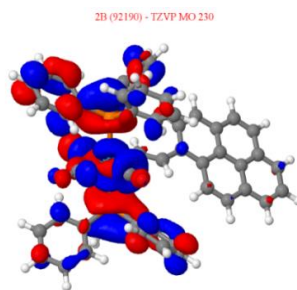
229

Ligand π
→ π^*

323.76



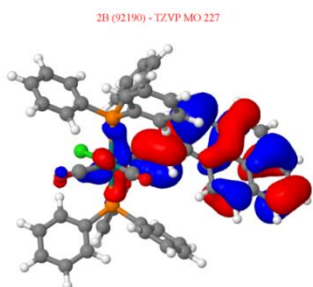
226



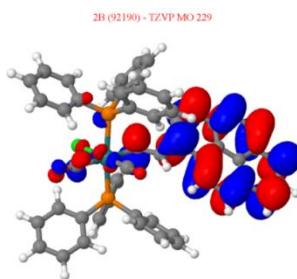
230

Metal
phosphine
→
Metal
phosphine

301.57



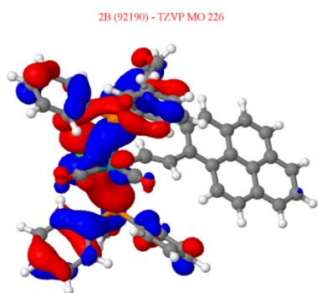
227



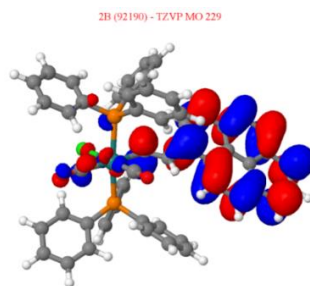
229

Ligand π
→ π^*

291.64



226



229

Ligand
→ Metal-
phosphine
(LMCT)

Calculated UV-Vis Spectra

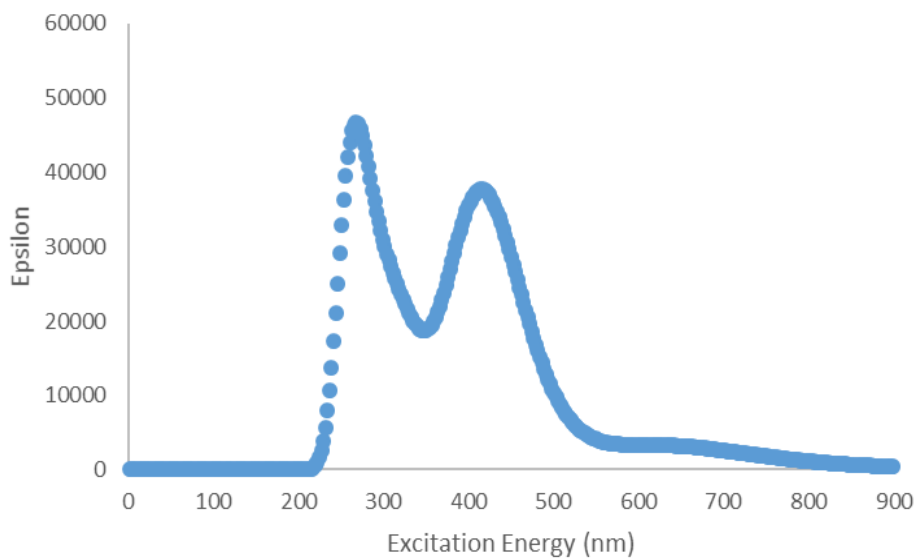


Figure S8-1: UV-Vis spectra for $[\text{Ru}(\text{CH}=\text{CHPyr-1})\text{Cl}(\text{CO})(\text{TBTD})(\text{PPh}_3)_2]$ (**7**)

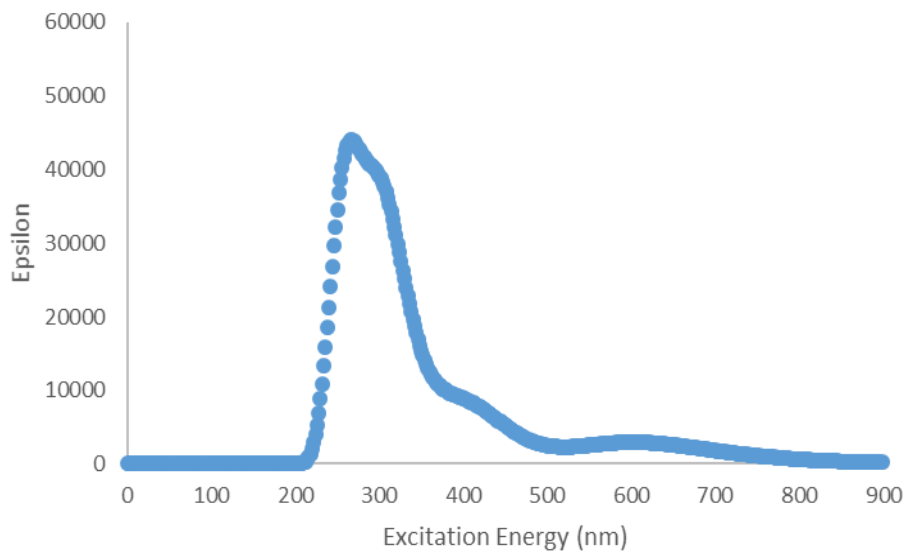


Figure S8-2: UV-Vis Spectra for [Ru(CH=CHTol)Cl(CO)(TBTD)(PPh₃)₂] (**4**)

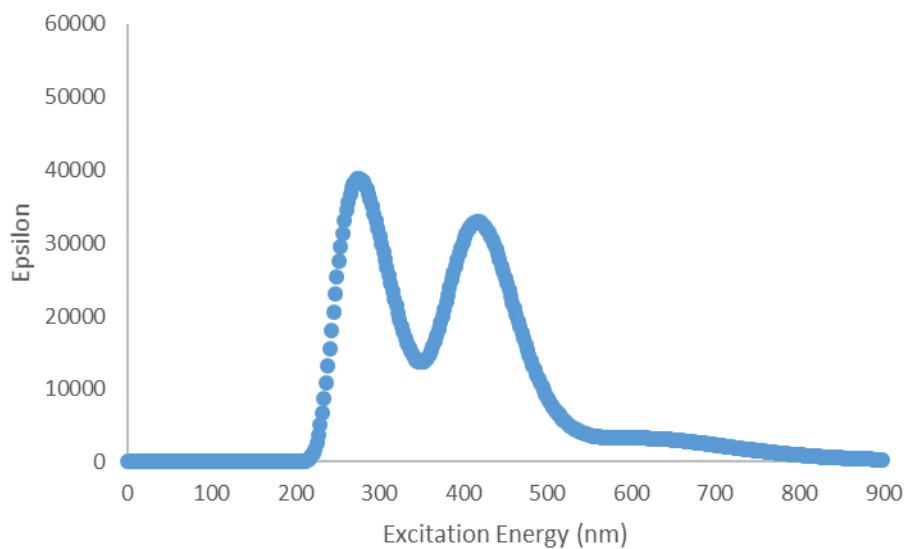


Figure S8-3: UV-Vis spectra for [Ru(CH=CHPyr-1)Cl(CO)(BTD)(PPh₃)₂] (**PyrBTD**)

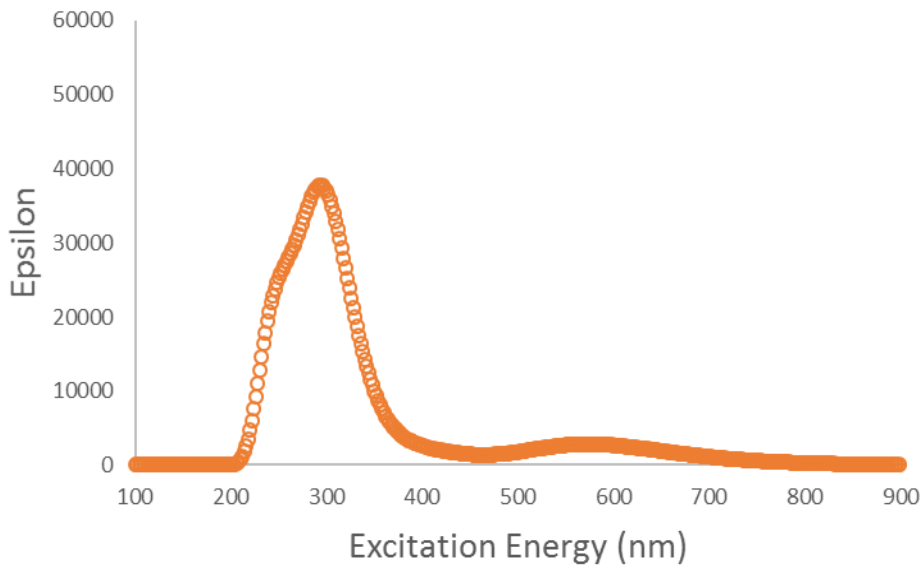


Figure S8-4: UV-Vis spectra for [Ru(CH=CHPh)Cl(CO)(BTD)(PPh₃)₂] (**PhBTD**)

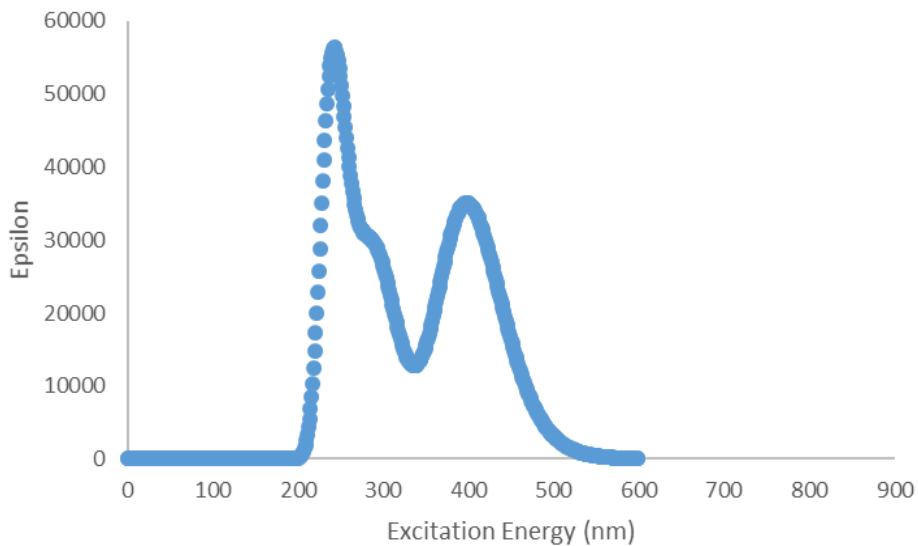


Figure S8-5: UV-Vis Spectra for [Ru(CH=CHPyr-1)Cl(CO)₂(PPh₃)₂] (**7-CO**)

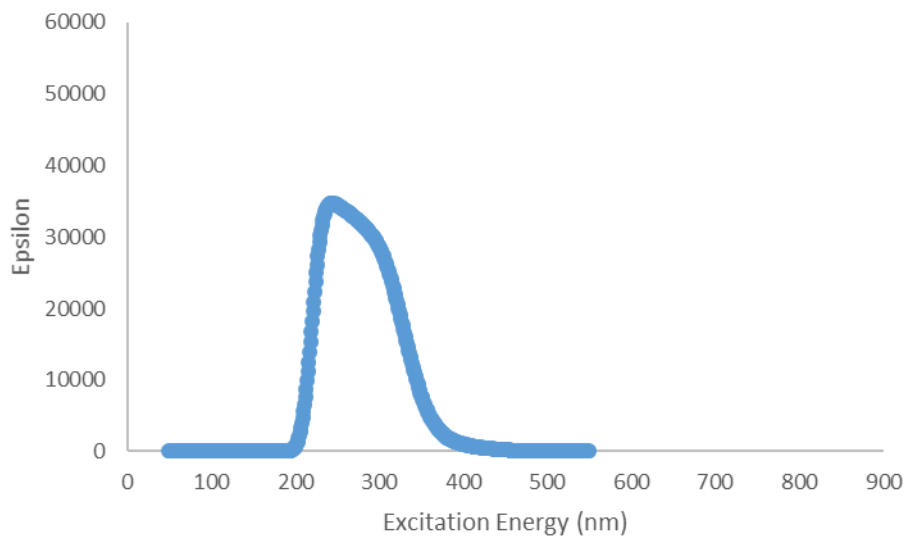


Figure S8-6: UV-Vis spectra for [Ru(CH=CHTol)Cl(CO)₂(PPh₃)₂] (**4-CO**)

Comparison of Calculated Spectra

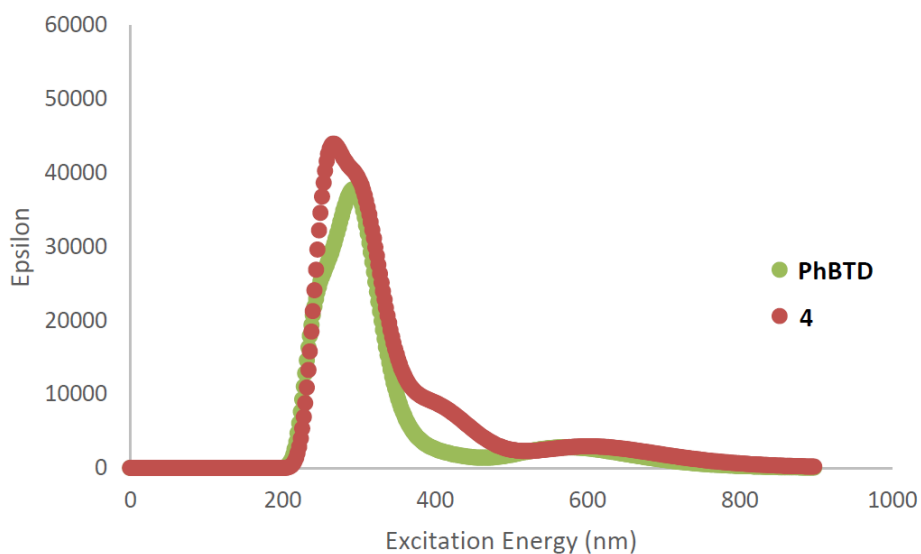


Figure S8-7: Comparison of calculated UV-Vis spectra of compounds [Ru(CH=CHTol)Cl(CO)(TBTD)(PPh₃)₂] (**4**) and [Ru(CH=CHPh)Cl(CO)(BTD)(PPh₃)₂] (**PhBTD**).

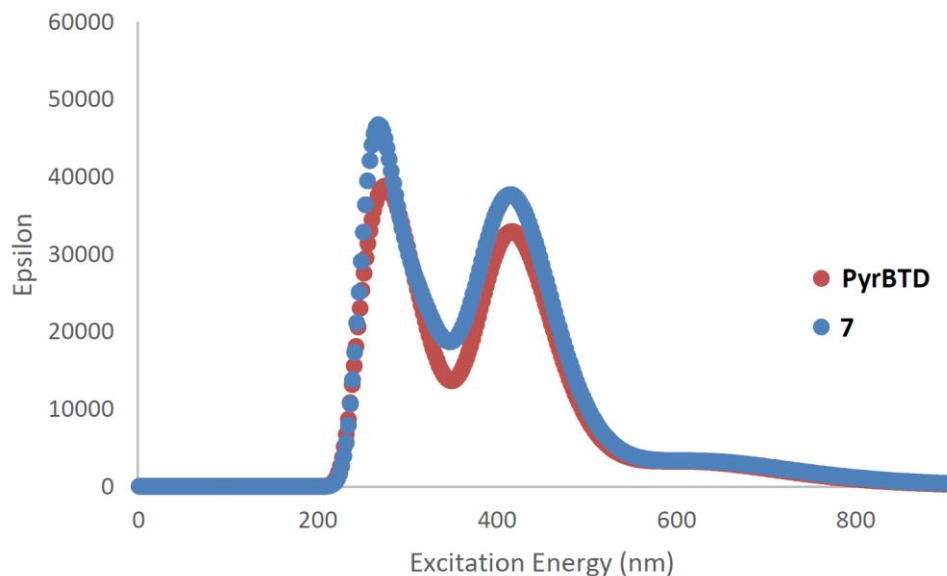


Figure S8-8: Comparison of calculated UV-Vis spectra of compounds $[\text{Ru}(\text{CH}=\text{CHPyr}-1)\text{Cl}(\text{CO})(\text{TBTD})(\text{PPh}_3)_2]$ (**7**) and $[\text{Ru}(\text{CH}=\text{CHPyr}-1)\text{Cl}(\text{CO})(\text{BTD})(\text{PPh}_3)_2]$ (**PyrBTD**).

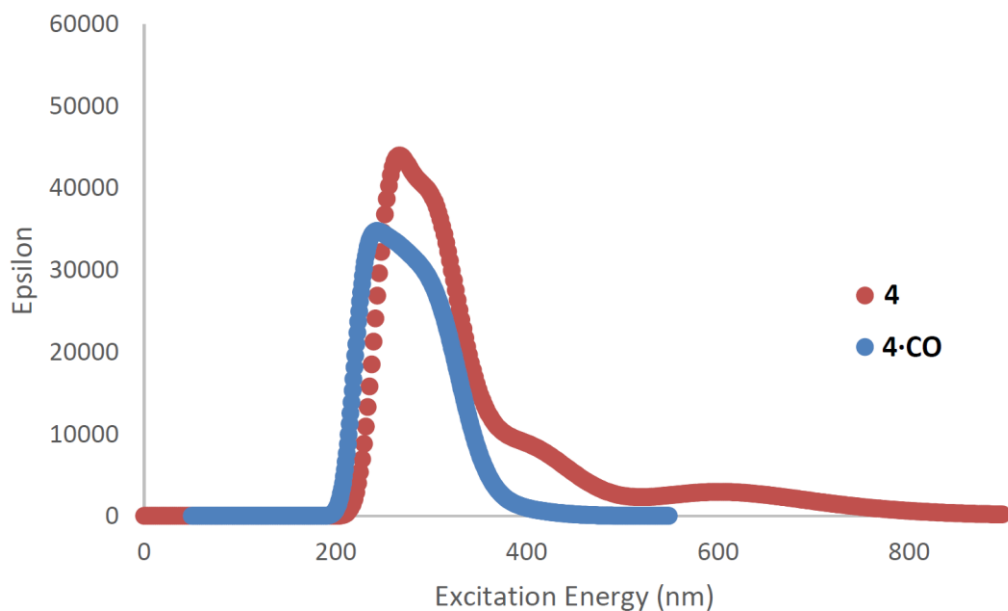


Figure S8-9: Comparison of calculated UV-Vis spectra of compounds $[\text{Ru}(\text{CH}=\text{CHTol})\text{Cl}(\text{CO})(\text{TBTD})(\text{PPh}_3)_2]$ (**4**) and $[\text{Ru}(\text{CH}=\text{CHTol})\text{Cl}(\text{CO})_2(\text{PPh}_3)_2]$ (**4-CO**).

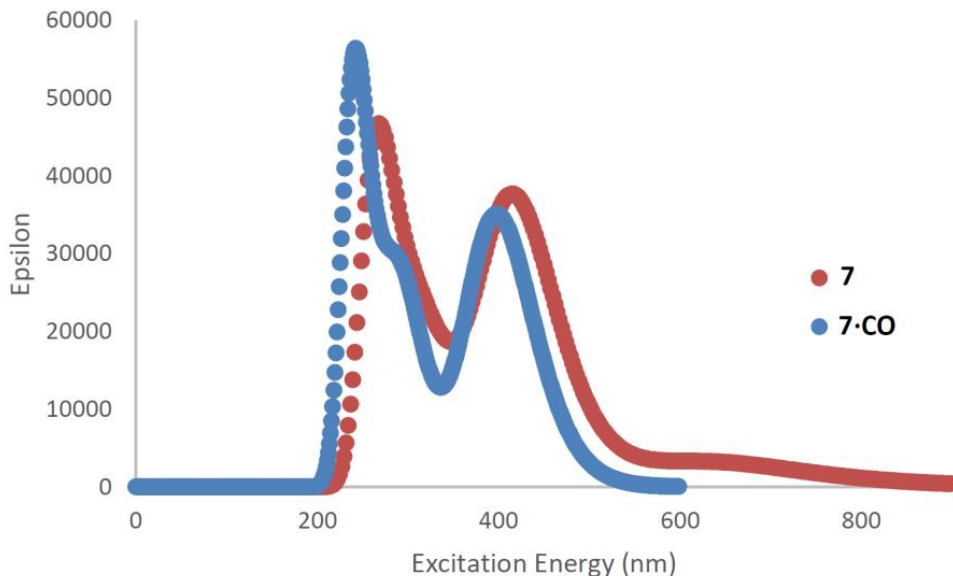


Figure S8-10: Comparison of calculated UV-Vis spectra of compounds $[\text{Ru}(\text{CH}=\text{CHPyr}-1)\text{Cl}(\text{CO})(\text{TBTD})(\text{PPh}_3)_2]$ (**7**) and $[\text{Ru}(\text{CH}=\text{CHPyr}-1)\text{Cl}(\text{CO})_2(\text{PPh}_3)_2]$ (**7-CO**).

S9. References

- S1 K. R. Laing, W. R. Roper, *J. Chem. Soc. A* **1970**, 2149-2153.
- S2 N. W. Alcock, A. F. Hill, M. S. Roe, *J. Chem. Soc., Dalton Trans.*, 1999, 1737-1740.
- S3 L. Vaska, *J. Am. Chem. Soc.*, 1964, **86**, 1943.
- S4 B. E. Cavit, K. R. Grundy and W. R. Roper, *J. Chem. Soc., Chem. Commun.*, 1972, 60.
- S5 A. F. Hill, J. D. E. T. Wilton-Ely, *J. Chem. Soc., Dalton Trans.* **1998**, 3501-3510.
- S6 M. R. Torres, A. Vegas, A. Santos, J. Ros, *J. Organomet. Chem.*, 1986, **309**, 169-177
- S7 J. D. Farmer, W. Y. Man, M. A. Fox, D. S. Yufit, J. A. K. Howard, A. F. Hill and P. J. Low, *J. Organomet. Chem.*, 2012, **721-722**, 173-185.
- S8 J. Maurer, M. Linseis, B. Sarkar, B. Schwederski, M. Niemayer, W. Kaim, S. Zálíř, C. Anson, M. Zabel, R. F. Winter, *J. Am. Chem. Soc.*, 2008, **130**, 259-268.
- S9 H. Loumrhari, J. Ros, M. R. Torres, A. Santos, A. M. Echavarren, *J. Organomet. Chem.* 1991, **411**, 255-261.

- S10 A. Toscani, C. Marín-Hernández, M. E. Moragues, F. Sancenón, P. Dingwall, N. J. Brown, R. Martínez-Máñez, A. J. P. White and J. D. E. T. Wilton-Ely, *Chem. Eur. J.*, 2015, **21**, 14529-14538.
- S11 M. E. Moragues, A. Toscani, F. Sancenón, R. Martínez-Máñez, A. J. P. White and J. D. E. T. Wilton-Ely, *J. Am. Chem. Soc.*, 2014, **136**, 11930-11933.
- S12 A. Martí, A. M. Costero, P. Gaviña and M. Parra, *Chem. Commun.*, 2015, **51**, 3077–3079.
- S13 A. T. R. Williams, S. A. Winfield and J. N. Miller, *Analyst*, 1983, **108**, 1067.
- S14 (a) SHELXTL, Bruker AXS, Madison, WI; (b) SHELX-97, G. M. Sheldrick, *Acta Cryst.*, 2008, **A64**, 112-122; (c) SHELX-2013, G. M. Sheldrick, *Acta Cryst.*, 2015, **C71**, 3-8; d) A. L. Spek (2003, 2009) PLATON, A Multipurpose Crystallographic Tool, Utrecht University, Utrecht, The Netherlands. See also A. L. Spek, *Acta Cryst.*, 2015, **C71**, 9-18.
- S15 S. Dhimi, A. J. de Mello, G. Rumbles, S. M. Bishop, D. Phillips and A. Beeby, *Photochem. Photobiol.*, 1995, **61**, 341.
- S16 A. M. Brouwer, *Pure Appl. Chem.*, 2011, **83**, 2213–2228.
- S16 S. Grimme, J. Antony, S. Ehrlich and H. Krieg, *J. Chem. Phys.* 2010, **132**, 154104

3.5. Conclusions

Taking into account the high toxicity of CO and its common presence in urban and indoor environments, the detection of this gas in air is crucial for home and workplace safety. Moreover, due to its important role as biological signalling molecule, biomedical research has required efficient and easy to handle probes to detect CO in cells and in tissues. Bearing in mind these facts, and pursuing the development of sensory materials for the sensitive and selective optical detection of CO both in solution and in air, the following conclusions can be drawn from this chapter:

- A collection of vinyl ruthenium(II) and osmium(II) complexes bearing 2,1,3-benzothiadiazole (BTD) are prepared and characterized. Chloroform solutions of the complexes underwent remarkable color changes when CO is bubbled. Also, significant emission enhancements are observed due to coordination of CO and displacement of BTD fluorophore. Besides, the adsorption of the complexes on silica yielded solids that presented remarkable color changes that allowed a naked eye detection of CO in gas phase. The observed response is quite selective to CO and low detection limits (5 ppb) are achieved.
- A family of vinyl ruthenium(II) and osmium(II) complexes bearing 5-(3-thienyl)-2,1,3-benzothiadiazole (TBTD) are synthesized and characterized. The prepared complexes allowed the selective and sensitive detection of CO in solution and in gas phase by colour and emission changes. The color and fluorescence modulations are assigned to a displacement of TBTD fluorophore upon CO coordination with the metal center.
- Also, two new ruthenium(II) and osmium(II) complexes bearing TBTD fluorophores and a poly(ethylene)glycol chain into the vinyl functionality are prepared. Both complexes are able to detect CO in water (through color and emission changes) and in HeLa cells.

The combination of sensitivity, selectivity, simple synthesis and low cost make the systems described here a very attractive and efficient chemosensors for the detection of this poisonous gas.

Encouraged to keep the biological importance of CO in mind and considering the potential use of carbon monoxide for therapeutic applications, our current studies are focused on the improving the development of water-soluble transition metal complexes able to detect and determine CO in biological and cellular media.

4. General Conclusions

Taking into account the importance of detecting some target species such as anions, cations and CO, this PhD thesis has been focused on the design and synthesis of chromo-fluorogenic sensors for the sensitive and selective detection of these chemicals.

In chapter 2, the use of imidazoanthraquinone and imidazoquinoline probes for the selective and sensitive detection of anions and cations was evaluated. At this respect, of all the anions tested, only fluoride induced remarkable UV-visible and emission changes due to deprotonation processes active with both types of probes. The optical response of both families of probes toward metal cations is unselective. However, the imidazoanthraquinone probes yielded color and emission changes only in the presence of trivalent metal cations.

In chapter 3, a collection of vinyl ruthenium(II) and osmium(II) complexes bearing 2,1,3-benzothiadiazole (BTD) and 5-(3-thienyl)-2,1,3-benzothiadiazole (TBTD) were prepared and characterized. The prepared complexes showed a marked optical (chromo and fluorogenic) sensitive (with limits of detections as low as 5 ppb) and selective response toward CO in chloroform and water solution and in gas phase (when adsorbed onto a silica support). Besides, detection of CO in HeLa cells was achieved when the complexes were derivatized with poly(ethylene)glycol chains.

Considering the importance of detecting ions and neutral molecules (as CO), this PhD thesis has continued the study on how to design efficient systems for sensing applications. Current studies are focused on detecting anions and cations in a very selective and sensitive way in aqueous solution and improving the systems to recognize CO in biological samples.

*Gracias al Ministerio de Economía y Competitividad por la beca
concedida para realizar esta tesis doctoral.*